

**THE DUAL ROLES OF WNT SIGNALING: DIRECTING CELL FATE
AND TISSUE MORPHOGENESIS DURING EARLY MOUSE DEVELOPMENT**

by

James Patrick Mahaffey

A Dissertation

Presented to the Faculty of the Louis V. Gerstner, Jr.

Graduate School of Biomedical Sciences,

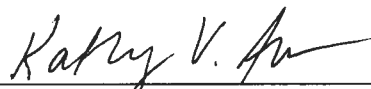
Memorial Sloan-Kettering Cancer Center

in Partial Fulfillment of the Requirements for the Degree of

Doctor of Philosophy

New York, NY

September, 2013



Kathryn V. Anderson, PhD
Dissertation Mentor



Date

© 2013 James Patrick Mahaffey

To Jim, Amy, Jenny, Nicci, and above all Jack

ABSTRACT

From day e5.5 to e8.5 the mouse embryo undergoes dramatic changes as it develops from a single layer, cup shaped epithelial sheet to a complex body plan with three germ layers, a beating heart, and three defined embryonic axes. These changes require intercellular cell signaling events to both specify unique cell fates and to construct the architecture of the embryo. Studying loss of function mutations that cause early embryo lethality has allowed for the genetic dissection of the cell signaling pathways that govern these two critical aspects of early mouse embryogenesis. The decades of experiments have revealed that signaling from only a handful of different genetic pathways generates these remarkable changes in the early mouse embryo, highlighting the importance of tight regulation of the time and place that these pathways are active. This makes the early mouse embryo an ideal model system to study cell-cell signaling, as the lessons learned from mouse development can provide insight into human diseases that are caused by a misregulation of these same pathways.

One pathway that stands out as a key regulator of early mouse development is the Wnt pathway, as the two arms of this pathway can direct cell fate specification and tissue morphogenesis. The canonical Wnt pathway is one of the most studied molecular signaling cascades as it directs cell fate decisions in a myriad of contexts including embryonic development, adult tissue homeostasis, and cancer. Despite a wealth of biochemical and genetic data, it remains unclear how the canonical Wnt pathway, working primarily through a single transcription factor can function in such varying contexts. Here I will show

that Axin, a key regulator of Wnt pathway activation, can promote or inhibit Wnt signaling in a cell specific manner during gastrulation and neural patterning.

The non-canonical Wnt/planar cell polarity pathway, a separate and distinct arm of Wnt signaling, is also a key intercellular signaling pathway required for normal mouse development. The planar cell polarity pathway does not directly contribute to cell fate decisions in the early mouse embryo; rather it plays a key role in the morphogenesis of many embryonic structures. Non-canonical Wnt signaling serves as a molecular compass for the cells in the embryo and directs the uniform orientation of every cell within an epithelium. I will show genetic and molecular data that reveals a role for dynamic rearrangement of the actin cytoskeleton in the establishment of planar polarity. Through these experiments I uncovered a previously unappreciated step in the trafficking of planar cell polarity proteins that is required for their activity. Together two projects further our understanding of how the Wnt pathway is regulated during mouse development and can contribute to both cell fate decisions and pattern formation.

VITAE

James P. Mahaffey began his scientific career in the laboratory of James W. Mahaffey at North Carolina State University while a student at W.G. Enloe High School in Raleigh, NC. James' first project in his father's lab was to investigate if the RNAi pathway that was recently discovered in *C. elegans* was evolutionarily conserved. This work led to his first ever publication. After graduating high school, James continued to work in his father's lab, studying the regulation of body plan formation by the HOX family transcription factors. This work led to another authorship, and sparked an interest in academic research.

At The University of North Carolina at Chapel Hill, James began work on his undergraduate thesis project in the laboratory of Dr. Mark Peifer. James worked under the tutelage Dr. Julie Gates investigating the role of *Enabled* in *Drosophila* development. During the course of this project James developed a love for microscopy and studying morphogenesis, and was named a Barry M. Goldwater Scholar. After the acceptance of his senior thesis in 2006, and with two more papers in the process of publication, James graduated from UNC with a Bachelor of Science with Distinction in Biology, *Highest Honors*.

James began graduate school at the Louis V. Gerstner, Jr. Graduate School of Biomedical Sciences at MSKCC in 2006, as part of the first class of the program. As predicted by Dr. Peifer at his college graduation, he "joined the dark side" in 2007 when he began a new phase of his career, studying developmental biology in *Mus musculus*, as a member of Dr. Kathryn Anderson's group.

ACKNOWLEDGEMENTS

First and foremost I want to thank my thesis advisor, Dr. Kathryn Anderson. When I first joined the lab, Kathryn gave me a single piece of paper, which simply consisted of bullet point ideas for potential projects I should start. Sadly, I fear I only truly accomplished one of her bullet points, but this set the tone for my dissertation research: Kathryn set the overarching goals, but gave me the freedom to pursue the experimental design on my own. She allowed me to develop my own assays, and to start new procedures that the lab had not used before (even if she wasn't the biggest fan of drug-treating embryos at first). The best part about my six years in the lab was Kathryn's excitement over new data, funny looking embryos, and even bands on a Western blot. Her passion for her work is infectious, and that, more than anything else I have learned in her lab, is what I hope to take with me through the rest of my career.

Along with Kathryn, I have to thank the other faculty at MSKCC who helped guide me through this process. At the top of this list are my committee members Dr. Alan Hall and Dr. Anna-Katerina Hadjantonakis, who have provided support and important insights into my research throughout my graduate studies. In addition, I would like to thank Dr. Mary Baylies for serving as my thesis defense chairperson. I also want to thank Dr. Jennifer Zallen who helped me interpret my data and design new experiments.

This work would never have been completed without the help of so many others at MSKCC. I have to especially thank all the members of the Anderson lab for helpful discussion and insights during lab meetings, and for making the lab a

great place to work each and every day. I would like to particularly acknowledge Angela Parrish, Joaquim Grego-Bessa and Hisham Bazzi for all their help with my two projects, and for all the afternoon Champion's League games. I also have to thank John Maciejowski for being a running partner, a drinking buddy, a helpful biochemist, a person who listened to ideas, and most of all a friend.

Without the love and support of my family, I would not have made it this far. My father got me started in this business, and is, and will always be my inspiration as a scientist, and more importantly as a father and a man. My mother I cannot thank enough for her unyielding love and support. Above all I am thankful for all that my wife, Nicole has done for me. Nicole put up with years of midnight dissections and the resulting cranky mornings, suffered through paper submissions and revisions, and all the other stresses that come with graduate school, and through it all has always been my rock. I have to thank her most of all for Jack, who is the best thing that has ever happened in my life.

TABLE OF CONTENTS

LIST OF FIGURES	xiii
LIST OF ABBREVIATIONS	xv
CHAPTER ONE	1
1 INTRODUCTION	1
1.1 The canonical Wnt/β-catenin signaling pathway	2
1.1.1 Canonical Wnt signaling in early mouse development.....	3
Wnt signaling in the inner cell mass and embryonic stem cells	5
Formation of the anterior-posterior axis	6
The primitive streak	10
1.1.2 The β -catenin destruction complex	12
1.1.3 Activation of canonical Wnt signaling	15
Wnt ligands	15
Wnt receptors	17
The destruction complex at the membrane	21
β -catenin/TCF dependent transcription	25
Wnt pathway self-regulation	26
1.1.4 The <i>Axin2</i> ^{canp} mutation	27
1.2 The non-canonical Wnt/planar cell polarity pathway	32
1.2.1 Planar cell polarity in vertebrate development	34
Morphogenesis	35
Left-right asymmetry	39

1.2.2	Establishment of planar cell polarity.....	44
	Establishing global planar polarity	44
	Establishing planar cell polarity within an individual cell.....	52
1.2.3	Embryonic phenotypes of the <i>Van12^{Lp}</i> mutant mouse	55
CHAPTER TWO		58
2	MATERIALS AND METHODS	58
2.1	Mapping and genotyping	58
2.1.1	Mouse strains.....	58
2.2	Phenotypic characterization.....	61
2.2.1	Immunofluorescence and microscopy.....	63
2.2.2	Embryo culture	65
2.2.3	Embryonic stem cell culture	67
2.3	Data analysis and statistics.....	67
2.3.1	Image analysis	67
CHAPTER THREE		70
3	AXIN PROMOTES CANONICAL WNT SIGNALING IN THE LATE PRIMITIVE STREAK	70
3.1	IWR-1-treated embryos phenocopy <i>Axin2^{canp}</i> mutants.....	72
3.1.1	Elevated Wnt signaling in response to IWR-1 is ligand dependent..	76
3.1.2	Wnt pathway regulation in embryonic stem cells	81
3.2	GSK3β is required to activate Wnt signaling in the late streak.....	82
3.2.1	Proteasome inhibition promotes Wnt signaling in the late streak.....	87
3.3	Discussion.....	89

CHAPTER FOUR	101
4 PLANAR POLARITY CONTROLS CONVERGENT EXTENSION AND LEFT- RIGHT PATTERNING IN THE EARLY MOUSE EMBRYO	101
4.1 The cellular basis of neural tube closure	103
4.2 <i>Cofilin1</i> enhances the <i>Vangl2</i>^{L^P} phenotype	107
4.2.1 Convergent extension of the midline	114
4.2.2 Cofilin1 and PCP signaling cooperate to orient nodal cilia.....	117
4.3 Discussion	125
CHAPTER FIVE	129
5 ACTIN DYNAMICS ARE REQUIRED FOR PCP SIGNALING IN THE MOUSE EMBRYO	129
5.1 <i>Cofilin1</i> and <i>Vangl2</i> are required for the localization of <i>Celsr1</i>	130
5.1.1 Cofilin1 regulation in <i>Vangl2</i> ^{L^P} embryos	131
5.1.2 Loss of cofilin activity is sufficient to disrupt planar polarity	137
Actin dynamics are required for the initiation, but not maintenance, of planar polarity	138
Wnt ligands are required for planar cell polarity signaling	144
PCP signaling in the node does not require the primary cilium	145
5.2 Jasplakinolide inhibits vesicle trafficking of PCP proteins	146
5.2.1 Actin severing is required for the coordinated localization of Rab11 and PCP proteins to the plasma membrane	152
5.3 Discussion	154
CHAPTER SIX	157

6	PROTEIN VIRILIZER HOMOLOGUE.....	157
6.1	Introduction.....	159
6.1.1	ENU mutagenesis	160
6.1.2	Virilizer in <i>Drosophila</i>	162
6.2	The <i>2-seam</i> mutation.....	164
6.2.1	<i>2-seam</i> is an allele of <i>Protein virilizer homologue</i>	164
6.2.2	The <i>2-seam</i> embryonic phenotype.....	168
6.3	Discussion.....	172
CHAPTER SEVEN		178
7	SUMMARY AND FUTURE DIRECTIONS	178
7.1	Canonical Wnt signaling	179
7.1.1	Localization of stabilized Axin in the head versus primitive streak.	182
7.1.2	The environment of late streak.....	184
7.1.3	Adult tissue homeostasis	186
7.2	Non-canonical Wnt signaling	188
7.2.1	Trafficking core PCP proteins to the apical membrane	189
7.2.2	Planar cell polarity signaling and cilia orientation.....	191
7.2.3	Non-canonical Wnt signaling regulates convergent extension.....	195
REFERENCES		198

LIST OF FIGURES

Figure 1.1: Regulation of canonical Wnt signaling.	4
Figure 1.2: <i>Axin2^{canp}</i> disrupts morphogenesis and slows protein turnover.	29
Figure 1.3: Reduced canonical Wnt activity in <i>Axin2^{canp}</i> mutants.	30
Figure 1.4: Wnt signaling in the primitive streak of <i>Axin2^{canp}</i> embryos.	31
Figure 1.5: The orientation of planar cell polarity in an epithelial sheet.	33
Figure 1.6: Mechanisms of convergent extension.	36
Figure 1.7: The asymmetrical distribution of the core PCP proteins.	45
Figure 1.8: Non-cell-autonomous phenotypes of PCP mutant clones.	47
Figure 2.1: Embryo culture time-lines.	66
Figure 3.1: Tankyrase inhibition alters Wnt signaling in wild-type embryos.	74
Figure 3.2: IWR-1 stabilizes Axin1 and increases LRP6 phosphorylation.	77
Figure 3.3: Stabilized Axin requires ligand to increase <i>TOPGAL</i> expression.	80
Figure 3.4: IWR-1 inhibits Wnt signaling in embryonic stem cells.	83
Figure 3.5: CHIR99021 inhibits Wnt signaling in the late primitive streak.	85
Figure 3.6: MG132 increases Wnt signaling in the primitive streak.	90
Figure 3.7: The tissue specific roles of Axin and GSK3 β in the Wnt pathway.	96
Figure 4.1: The changes in cellular architecture during neural tube closure.	106
Figure 4.2: Genetic interaction between <i>Vangl2^{Lp}</i> and <i>Cfl1^{C5}</i> at e9.5.	111
Figure 4.3: Planar polarity is disrupted in <i>Cfl1^{tm1wit}</i> <i>Vangl2^{Lp}</i> double mutants. ...	112
Figure 4.4: <i>Cfl1^{C5}</i> enhances the CE defect in the <i>Vangl2^{Lp}</i> notochord.	116
Figure 4.5: Left-right asymmetry defects in <i>Vangl2^{Lp}</i> <i>Cfl1^{C5}</i> double mutants. ...	118

Figure 4.6: Nodal cilia are not polarized in <i>Vangl2^{Lp} Cfl1^{C5}</i> double mutants.....	120
Figure 4.7: Peripheral node cilia are not planar polarized.	123
Figure 4.8: Node cilia are centered along the mediolateral axis of node cells. .	126
Figure 5.1: Celsr1 is not planar polarized in <i>Vangl2^{Lp} Cfl1^{C5}</i> double mutants. ..	132
Figure 5.2: Membrane association of Celsr1 and Rab11	133
Figure 5.3: Apical-basal polarity in nodes with reduced Cofilin activity.	134
Figure 5.4. Cofilin1 regulation in <i>Vangl2^{Lp}</i> mutant embryos	136
Figure 5.5: Vangl2 and Celsr1 localization in <i>Cfl1^{C5} Dstn^{corn1/+}</i> mutants.....	139
Figure 5.6: Jasplakinolide and IWP-2 disrupt planar polarity signaling.	140
Figure 5.7: Celsr1 and pMLC2 are planar polarized in the axial midline.	141
Figure 5.8: Jasplakinolide does not cause Vangl2 accumulation in the Golgi... ..	142
Figure 5.9: Planar cell polarity is normal in the node of <i>Ift88^{-/-}</i> mutant embryos.	147
Figure 5.10: Vesicles containing Celsr1 do not colocalize with Rab8 or Rab5.. ..	150
Figure 5.11: Jasplakinolide causes Celsr1 accumulation in endosomes.	151
Figure 5.12: Membrane associated Rab11 and Celsr1 require dynamic actin.. ..	153
Figure 6.1: Embryonic phenotype of homozygous <i>Pvh^{2sm}</i> mutants.....	158
Figure 6.2: ENU mutagenesis screen.....	161
Figure 6.3: The <i>2-seam</i> phenotype.	165
Figure 6.4: Mapping and cloning the TO1 allele.....	167
Figure 6.5: Primitive streak defects in <i>2-seam</i> mutants.....	169
Figure 6.6: <i>2-seam</i> phenotypes at e6.5.....	171
Figure 6.7: Extraembryonic ectoderm is present in <i>2-seam</i> mutants.	173

LIST OF ABBREVIATIONS

- 2sm:** *2-seam* (*Pvh* allele)
- ADF:** Actin depolymerizing factor
- AP:** Anterior-posterior
- APC:** Adenomatous polyposis coli
- AVE:** Anterior visceral endoderm
- BMP:** Bone morphogenetic protein
- Canp:** *Canopus* (*Axin2* allele)
- CE:** Convergent extension
- Cfl1:** Cofilin1
- CHIR:** CHIR99021
- CK1:** Casein kinase 1
- Dstn:** Destrin
- Dvl:** Dishevelled
- EEA1:** Early endosome antigen 1
- ENU:** N-ethyl N-nitrosourea
- ER:** Endoplasmic reticulum
- ES:** Embryonic stem
- F-actin:** Filamentous actin
- FGF:** Fibroblast growth factor
- Fl(2)d:** Female-lethal-2-D
- Fmi:** Flamingo

FRAP: Fluorescence recovery after photobleaching

Fzd: Frizzled

GFP: Green fluorescent protein

GSK3 β : Glycogen synthase kinase 3 β

ICM: Inner cell mass

Lp: *Looptail* (*Vangl2* allele)

LRP: Lipoprotein receptor-related protein

LWR: Length-to-width ration

MAPK: Mitogen-activated protein kinase

Mb: Megabases

PARP: Poly-ADP-ribose polymerase

PCP: Planar cell polarity

Pkd2: Polycystin-2

pMLC2: phosphorylated-Myosin light chain 2

PP2A: protein phosphatase 2A

PSM: Presomitic mesoderm

Pvh: Protein virilizer-homologue

ROCK: Rho-associated protein kinase

SEM: Scanning electron microscopy

SNP: Single nucleotide polymorphism

Sxl: Sex-lethal

T: Brachyury

TBD: Tankyrase-binding domain

TCF: T cell factor

Vang: van Gogh (also Strabismus)

Vangl: van Gogh-like

Wnt: Wingless/integration-1

WTAP: Wilms' tumor 1-associating protein

WT-1: Wilms' tumor suppressor gene-1

β Gal: β -galactosidase

β TrCP: β -transducin repeats-containing protein

CHAPTER ONE

1 INTRODUCTION

The Wingless/integration-1 (Wnt) signaling pathway has been the subject of intense investigation for over 30 years due to its innumerable roles in development and disease; in many model organisms it appears that every cell in the adult has responded to Wnt ligands at some point during development. It was subsequently revealed that components of the canonical Wnt signaling cascade are also involved in a separate pathway that controls tissue polarity, hereafter referred to as the non-canonical Wnt/planar cell polarity pathway, redoubling the interest in the field. While there are around 20 different *Wnt* ligands in the mouse genome and an ever-growing number of Wnt receptors, our understanding of how the Wnt pathway can generate a multitude of different cellular responses is still murky. In adult tissues the Wnt pathway plays an essential role in tissue homeostasis, but mutations that cause excess Wnt signaling can lead to diseases such as colon and ovarian cancer. This has prompted a search to find small molecule inhibitors of Wnt signaling that could be used as targeted therapeutics for these malignancies. The work presented in this thesis aims to address outstanding questions in the regulation of both the canonical and non-canonical Wnt signaling pathways. Using the mouse embryo as a model system I show that small molecule inhibitors of canonical Wnt signaling suppressed or promoted Wnt-dependent transcription in different tissues. While these findings

may cast doubt on the efficacy of these putative therapeutic agents, they also gave new insights into the intricacies of Wnt signal transduction. In a separate set of experiments I defined the embryonic phenotypes associated with planar cell polarity mutants at the cellular level, and in doing so identified a previously overlooked step in the establishment of the non-canonical Wnt signaling pathway.

1.1 The canonical Wnt/ β -catenin signaling pathway

The canonical Wnt/ β -catenin signaling pathway is one of the few evolutionarily conserved signaling cascades that mediates cell-cell communication during embryonic development and adult tissue homeostasis (Chakrabarti et al., 1992; Jue et al., 1992; Peifer et al., 1991). During vertebrate development, the Wnt pathway plays a critical role in the establishment of the anterior-posterior axis, along with a myriad of functions in early organogenesis (Liu et al., 1999b; MacDonald et al., 2009; Yamaguchi, 2001). In addition to these roles in development, many tissues including the intestine, hematopoietic system and hair follicles, require Wnt/ β -catenin signaling to maintain adult stem cells (DasGupta and Fuchs, 1999; Korinek et al., 1998; Reya et al., 2003). Proper regulation of Wnt signaling during stem cell self-renewal is important as mutations that aberrantly activate Wnt signaling can lead to disease states in humans, most notably colorectal cancers (Miyoshi et al., 1992). For this reason, there is an ongoing effort to discover small molecules that inhibit the Wnt pathway. However, for these drugs to be effective in patients, it is important to

fully elucidate the roles of all the proteins involved in this pathway, first to make sure the right drug targets are being identified, and second, to prevent unintended consequences of these novel small molecules.

The predominant biological activity of canonical Wnt signaling is to change the transcriptional output of the signal-receiving cell. Thus, all aspects of canonical Wnt pathway regulation converge on the transcriptional activator β -catenin, and its nuclear availability. In the absence of Wnt ligand, cytoplasmic β -catenin levels are kept at low levels by the β -catenin destruction complex. In the presence of ligand, this destruction complex is inactivated, allowing β -catenin to accumulate and ultimately translocate to the nucleus, where it can interact with T cell factor (TCF) family transcription factors and activate gene transcription (Figure 1.1A; Brunner et al., 1997).

1.1.1 Canonical Wnt signaling in early mouse development

The canonical Wnt/ β -catenin signaling pathway is an important regulator of early embryonic cell fate decisions in all vertebrates. At the earliest stages of development Wnt signaling is required for the establishment of embryonic body axes and the formation of the mesendodermal germ layers. During zebrafish and *Xenopus* development Wnt signaling plays an integral role in the induction of the dorso-ventral body axis, and the ectopic expression of *Wnt1* can induce a secondary anterior-posterior axis (McMahon and Moon, 1989; Schneider et al., 1996). While these studies have revealed common roles for canonical Wnt signaling in early vertebrate embryogenesis, fish and frogs are both externally

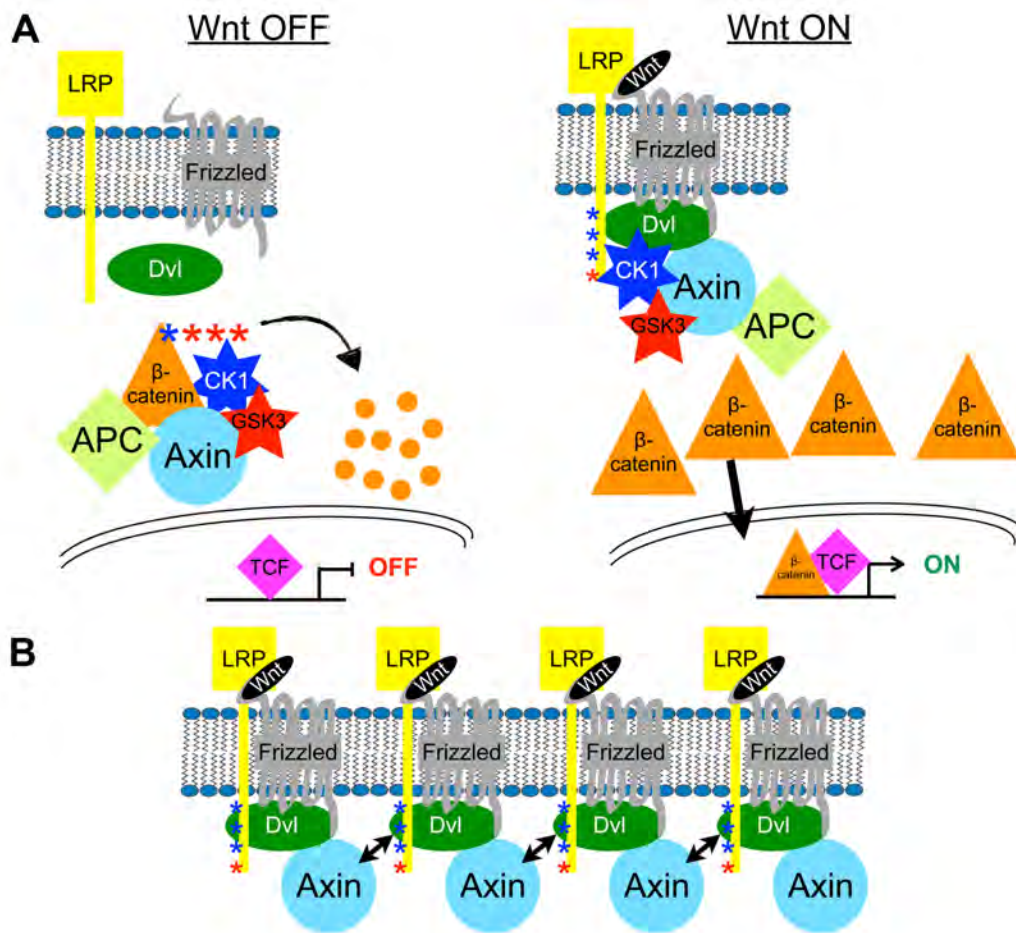


Figure 1.1: Regulation of canonical Wnt signaling.

(A) The destruction complex, consisting of Axin, APC, GSK3 β and CK1 α , degrades cytoplasmic β -catenin in the absence of Wnt ligand keeping Wnt target genes inactive. N-terminal phosphorylation by CK1 α and GSK3 β targets β -catenin for poly-ubiquitination by β TrCP. The presence of Wnt ligands causes a dimerization of Frizzled and LRP5/6 at the membrane, activating Dishevelled, which binds Axin and brings the destruction complex to the membrane. At the membrane CK1 α and GSK3 β phosphorylate and bind to the cytoplasmic tail of LRP5/6, further inhibiting the destruction complex. This allows β -catenin to accumulate and eventually enter the nucleus where it binds TCF/LEF family transcription factors turning on Wnt target gene expression. (B) At the membrane interactions between the DIX domains of Axin and Dishevelled cause receptor clustering in response to Wnt ligand. This aggregation of the active signaling complex may facilitate Wnt signaling by quickly shifting the ratio of cytoplasmic and membrane destruction complexes in response to Wnt ligand.

developing model systems, which deposit signaling factors that control early developmental decisions in a spatially restricted manner in the oocyte. In contrast, the early stages of mammalian development require cell-cell communication from zygotically transcribed genes; therefore, the early mouse embryo is an important model system to study Wnt pathway regulation.

Wnt signaling in the inner cell mass and embryonic stem cells

The preimplantation mouse embryo is comprised of two different cell types: the inner cell mass (ICM), which will give rise to the embryo proper, and the surrounding trophectoderm, which interacts with the uterus and initiates implantation. Both of these cell types express *Wnt* ligands along with all the components of the canonical Wnt signaling cascade (Kemp et al., 2005). Additionally, it was shown that exogenous green fluorescent protein (GFP)-tagged β -catenin was found in the nucleus of cells of the ICM, but not the trophectoderm (Wang et al., 2004). This led to the hypothesis that Wnt signaling was responsible for the delineation of these two cell types in the preimplantation embryo. However, later experiments found that a commonly used Wnt reporter was not expressed in the preimplantation embryo, and also showed that non-degradable forms of β -catenin, which should activate Wnt signaling in all cells, did not block the formation of the trophectoderm or cause any other phenotypes in the preimplantation embryo (Kemler et al., 2004). This belied the previous model and suggested that Wnt signaling had no role in the earliest stages of mouse development, despite the expression of multiple Wnt ligands at this stage.

Embryonic stem (ES) cells are derived from cells of the ICM, and can be

grown indefinitely in culture where they remain undifferentiated and retain their ability to contribute to all three germ layers. The maintenance of undifferentiated ES cells in culture requires Wnt signaling, either through the addition of Wnt ligand or small molecules that stabilize β -catenin to the culture medium (Sokol, 2011). Therefore, at least in an *ex vivo* setting, cells of the ICM require a Wnt stimulus, as the removal of Wnt agonists promotes differentiation of these cells. In most cells Wnt signaling triggers the accumulation of β -catenin in the nucleus, where it interacts with *TCF* family transcription factors and activates gene transcription. This paradigm does not hold true in ES cells, where the *β -catenin* mutants lacking the N-terminal transactivation domain are still capable of maintaining pluripotency in response to Wnt agonists (Wray et al., 2011). N-terminally truncated *β -catenin* remains active in ES cell maintenance, as it is still capable of interacting with Tcf3, which represses genes required for pluripotency, including *Oct4* and *Nanog* (Berge et al., 2011; Wray et al., 2011). Thus, Wnt signaling in ES cells functions solely to remove Tcf3 from the DNA, and does not require active transcription. Wnt signaling is also required for the maintenance of stem cells in adult tissues; however, it is unclear in these contexts whether pluripotency requires active β -catenin/TCF transcription or if follows the same paradigm as embryonic stem cells.

Formation of the anterior-posterior axis

After implantation, at embryonic day 5.5 (e5.5) the cells of the ICM have differentiated into two distinct cell types: the visceral endoderm and the epiblast. The cells of the epiblast will contribute to the all three germ layers of the embryo,

including germ cells, while the visceral endoderm gives rise to extraembryonic structures such as the yolk sac, as well as contributing, in part, to the embryonic endodermal lineage (Kwon et al., 2008). The delineation of the epiblast and visceral endoderm cells types is first seen prior to implantation at e4.5 when the surface layer of the ICM, cells facing the blastocoel, were found to be restricted to visceral endoderm fates in cell transplantation experiments (Gardner, 1982). The formation of the primitive endoderm, and subsequently the visceral endoderm, does not appear to require Wnt signaling as the visceral endoderm is formed in both embryos that are homozygous mutant for *β-catenin* and embryos expressing non-degradable forms of *β-catenin* (Huelsenken et al., 2000; Kemler et al., 2004).

At e5.5 the epiblast has grown distally, away from the polar trophectoderm, and become a cup-shaped epithelium, the apical side of which faces the newly formed proamniotic cavity, while the basal side is surrounded by the visceral endoderm. The epiblast and the surrounding visceral endoderm at e5.5 are radially symmetric, as no embryonic body axes have yet been established. However, there is a proximal distal axis, as the epiblast is adjacent to the polar trophectoderm proximally and the visceral endoderm distally. While Wnt signaling is not necessary for the formation of the primitive endoderm, it does play a critical role in the patterning of the visceral endoderm at e5.5 along the proximal-distal axis.

The cells at the distal tip of the visceral endoderm are the first cells to break the radial symmetry of e5.5 embryo, as they actively migrate proximally

along what will become the anterior side of the embryo, and stop at the embryonic/extra-embryonic border (Srinivas et al., 2004). These cells, also referred to as the anterior visceral endoderm (AVE), are marked by the expression of *Hhex*, *Hesx1*, *Otx2*, *Lefty*, *Cer11* and *Sfrp5*. The expression of these genes is important for the migratory behavior of these cells and signaling events during the formation of the neural ectoderm in the underlying epiblast by blocking the formation of the primitive streak (Levine and Brivanlou, 2007; Lu et al., 2001). Wnt signaling is required to fully specify the AVE as β -catenin mutant embryos fail to express *Hhex* and *Hesx1* in the distal visceral endoderm. Some markers of AVE are present in these embryos including *Cer11*; however, the *Cer11*⁺ cells fail to migrate and remain at the distal tip of the embryo in the absence of β -catenin (Huelsenken et al., 2000).

Canonical Wnt signaling is not required in the visceral endoderm to specify the AVE, as anterior-posterior axis formation and mesoderm specification were normal in chimeras with a wild type epiblast and β -catenin mutant visceral endoderm (Huelsenken et al., 2000). Wnt signaling in the distal epiblast appears to be required for the expression *Cripto*. *Cripto* is a TGF β receptor, required for Nodal signaling, and thus, is required for AVE formation. *Cripto* homozygous mutants also fail to fully specify the AVE similar to β -catenin mutants (Morkel et al., 2003; Varlet et al., 1997). While the *Cripto* enhancer has binding sites for β -catenin/TCF, and *Cripto* is overexpressed in embryos with stabilized β -catenin (Morkel et al., 2003), *Cripto* is a transmembrane receptor, not a signaling molecule. Therefore, β -catenin mutant visceral endoderm cells would also fail to

express *Cripto*. This suggests that a combination of Wnt and Nodal signaling in the epiblast is required for the formation of the AVE in the adjacent visceral endoderm. Alternatively it has been proposed that signals from the proximal extraembryonic ectoderm inhibit AVE formation, and that epiblast growth defects in the β -*catenin* and *Cripto* mutants cause the distal visceral endoderm to remain within the range of these inhibitory signals, accounting for the loss of AVE in these mutants (Rossant and Tam, 2009).

While the Wnt pathway is important for the specification of AVE cell fates, blocking Wnt signaling is necessary for proper AVE migration. This suggests a complex role for Wnt signaling in the specification and subsequent migration of the AVE. Wnt signaling appears to be required for the expression of *Hhex* and *Hesx1* in the distal visceral endoderm. Since these cells are not properly specified in the absence of β -*catenin* they fail to migrate. However, after cells at the distal tip of the embryo have adopted an AVE fate, Wnt signaling is inhibited by the expression of *Dkk1*, which antagonizes Wnt signaling by blocking the co-receptor LRP6. Although other classic markers of the AVE are expressed in the AVE in *Otx2* mutants, *Dkk1* is not, causing a failure of AVE migration (Zakin et al., 2000). When *Dkk1* was knocked into the *Otx2* locus AVE migration was restored, suggesting that blocking further Wnt signaling in the AVE is necessary for anterior migration (Kimura-Yoshida et al., 2005). Wnt ligands may act as chemorepellents during AVE migration as ectopic Wnt3a, locally administered by placing a ligand soaked bead next to an e5.5 embryo was able to redirect migrating AVE cells (Kimura-Yoshida et al., 2005). However, while Wnt3 ligand is

asymmetrically expressed on the future posterior side of the embryo at e5.5, *Wnt3* is not required for AVE migration (Liu et al., 1999b; Rivera-Pérez and Magnuson, 2005), suggesting that blocking the Wnt pathway is a permissive signal for AVE migration, not instructive.

The primitive streak

The first break in the radial symmetry of the epiblast is the formation of the primitive streak opposite to the AVE at the embryonic/extraembryonic border on the posterior side of the embryo. This event is distinguished morphologically by the epithelial-mesenchymal transition of epiblast cells, which delaminate from the epiblast and migrate around the embryo and adopt mesendodermal fates. The formation of the primitive streak is concurrent with the polarized expression of *Brachyury* in the posterior of the epiblast, which requires Wnt signaling for its expression. Wnt signaling is necessary and sufficient to induce primitive streak formation, as *Wnt3* mutants fail to express *Brachyury*, and embryos expressing non-degradable forms of *β-catenin* display a streak phenotype in the entire epiblast (Kemler et al., 2004; Liu et al., 1999b). Despite the polarized expression of *Wnt3* in the proximal posterior visceral endoderm at e5.5 (Rivera-Pérez and Magnuson, 2005), the migration of the AVE is also required to restrict the primitive streak to the posterior side of the embryo. This is best demonstrated in embryos that lack the tumor suppressor *Pten* in the visceral endoderm. Although the AVE is properly specified in these mutants, it does not coherently migrate to the anterior side of the embryo, causing axis duplication and the formation of multiple primitive streaks (Bloomekatz et al., 2012). These and other experiments

show that the AVE secretes factors that repress the primitive streak, most notably *Dkk1*, which inhibits the Wnt pathway and the Nodal inhibitors *Lefty* and *Cer11*. While these mutant phenotypes highlight the importance of Wnt signaling in the initiation of the primitive streak, under normal conditions the formation of the streak requires a combination of signaling pathways including Nodal, Bone morphogenetic protein (BMP) and Wnt.

The primitive streak, marked by the expression of *Brachyury*, is present in the mouse embryo from e6.0 to e12.0 and is responsible for generating mesoderm and endoderm cells along the entire anterior-posterior axis of the body. The earliest derivatives of the primitive streak at e6.0 contribute to cardiac and axial mesoderm, which migrate to the most anterior regions of the embryo, while the late streak is primarily responsible for generating paraxial mesoderm, which will contribute to the somites in the trunk and tail bud. Although there are many Wnt ligands present in the primitive streak, it is notable that during this transition *Wnt3* expression is lost and *Wnt3a* starts to be expressed (Yamaguchi, 2001). After the primitive streak is initiated at the proximal side of posterior epiblast, it elongates distally, a process that involves a positive feedback loop between *Wnt3a* and fibroblast growth factor (FGF) signaling pathways (Ciruna and Rossant, 2001). FGF signaling is required for the epithelial-mesenchymal transition of epiblast cells in the streak, but it also appears that *Wnt3a* and *Brachyury* expression are down regulated in the absence of FGF signaling (Boulet and Capecchi, 2012). Thus, while *Wnt3*, Nodal and BMP are required for the initiation of the primitive streak, the elongation and maintenance of the streak

require different Wnt ligands. In this thesis I will present data that suggests that the intracellular regulation of the Wnt pathway is also different in the early and late primitive streak suggesting that different Wnt ligands may have different signaling properties with regards to the activity of the β -catenin destruction complex.

1.1.2 The β -catenin destruction complex

In the absence of Wnt ligands, β -catenin/TCF target genes are not expressed because cytoplasmic and nuclear β -catenin levels are depressed by the constitutive activity of the Axin complex, which degrades newly synthesized β -catenin. This protein complex is also known as the β -catenin destruction complex and is comprised of the scaffold proteins Axin and Adenomatous polyposis coli (APC), the kinases casein kinase 1 (CK1) and glycogen synthase kinase 3 β (GSK3 β), and the E3 ubiquitin ligase β -transducin repeats-containing protein (β TrCP) (Figure 1.1A).

Axin serves as the main scaffold for the destruction complex, having different binding sites for β -catenin, APC, CK1 α and GSK3 β (Fagotto et al., 1999; Itoh et al., 1998; Sobrado et al., 2005; Spink et al., 2000). Axin also appears to be the least abundant protein in the complex and therefore limits the number of destruction complexes in the cell (Lee et al., 2003). The main function of Axin is to bring together newly synthesized β -catenin and the kinases CK1 α and GSK3 β . CK1 α initially phosphorylates β -catenin on serine 45, which primes β -catenin for further GSK3 β -dependent phosphorylation on serines 33, 37 and threonine 41

(Hagen and Vidal-Puig, 2002; Liu et al., 2002; Yost et al., 1996). While these phosphorylation events can occur in the absence of Axin *in vitro*, the scaffolding role of Axin is likely required in the cellular context as it raises the efficiency of these kinases by several orders of magnitude (Dajani et al., 2003). After β -catenin has been phosphorylated at the four sites on its N-terminus, it is a target for ubiquitination by the E3-ligase β TrCP and subsequent proteasomal degradation (Liu et al., 1999a).

APC also has binding sites for β -catenin, in fact, it has the same binding sites as Axin, and *in vitro* it appears to competitively bind β -catenin (Xing et al., 2003). There is evidence that APC has a higher affinity for phosphorylated β -catenin, which has led to the model where APC acts as a ratchet, removing phosphorylated β -catenin from the destruction complex, allowing the complex to be processive (Eklof Spink et al., 2001; Ha et al., 2004). The binding of phosphorylated β -catenin by APC may be a key step in the subsequent β TrCP-mediated ubiquitin ligation reactions as APC also shields β -catenin from protein phosphatase 2A (PP2A). PP2A can also interact with the destruction complex where it promotes β -catenin stability by removing the phosphorylation marks that are required for β TrCP binding and ubiquitination (Ratcliffe et al., 2000; Su et al., 2008; Zhang et al., 2009).

Each component of the destruction complex is integral to reducing nuclear β -catenin levels in the absence of ligand, and mutation of any member of complex can lead aberrant β -catenin/TCF transcription causing early embryo lethality and cancer. Genetically ablating members of the destruction complex, or

overexpressing β -catenin or Wnt ligands in the early embryo causes axis duplication in all vertebrate model systems (Kelly et al., 1995; McMahon and Moon, 1989; Yost et al., 1996; Zeng et al., 1997). Of all the components of the destruction complex, mutations in APC are the especially noteworthy in the context of human disease, as mutations in APC underlie the familial adenomatous polyposis coli syndrome (Miyoshi et al., 1992). In this inherited colorectal cancer syndrome a mutant copy of APC is present in the germline, and the second allele is lost in the tumor (Crabtree et al., 2003), causing tumorigenesis at very early ages in patients from these families. Mutations in APC are also present in the majority of sporadic colon cancers (Rowan et al., 2000). Misregulation of the Wnt pathway can lead to many other types of cancers including melanoma, endometrial cancers and hepatoblastoma (Polakis, 2007). In these cases inactivating mutations in Axin1, Axin2, as well as mutations in and around the phosphorylation and ubiquitination sites of β -catenin were found in different patients presenting with similar diseases, suggesting that aberrant activation of canonical Wnt signaling is a key step in tumorigenesis in these tissues (Taniguchi et al., 2002).

APC mutations are rarely found in tumors outside of the gastrointestinal tract, and only a small percentage of colorectal tumors have mutations in Axin1, Axin2 or β -catenin. This presents a puzzling situation, as each of these mutations ultimately leads to increased nuclear β -catenin, but each has different clinical outcomes. While the underlying mechanism for the differing clinical presentations in patients with mutations in the same pathway remain unknown, mouse models

harboring Wnt pathway mutations also display organ specific tumors: *APC* mutations lead to intestinal polyps, mutations in the GSK3 β phosphorylation sites of *β -catenin* have been found in liver cancers and overexpression of *Wnt1* can cause mammary tumors (Jue et al., 1992; La Coste et al., 1998; Su et al., 1992). Understanding how these mutations cause different malignancies in model systems may help in the development of new therapies and could provide further details into Wnt pathway regulation.

1.1.3 Activation of canonical Wnt signaling

Wnt ligands

Wnt ligands are 350-400 amino acid secreted, cysteine-rich proteins that are conserved from flies to mammals. In the mammalian genome there are 19 Wnt ligands, at least three of which specifically target the non-canonical/planar cell polarity pathway, as described in Section 1.2 (MacDonald et al., 2009). Though Wnt ligands were first described for their non-cell-autonomous functions, in many systems Wnt signaling can also function in an autocrine manner, especially in the self-renewal of embryonic stem cells (Berge et al., 2011). Wnt3a is the best characterized of the Wnt ligands and is most often used to activate the Wnt pathway in cell culture experiments.

Wnt ligands are post-translationally modified by the addition of two lipids and two sugar molecules, which affect the secretion and signaling potential of the protein. The glycosylation of Wnt3a at asparagines 87 and 298 were the first discovered modifications of the ligand and are essential for its secretion

(Komekado et al., 2007; Smolich et al., 1993). These sugar additions also prime the protein for the addition of a palmitate moiety at cysteine 77 (Komekado et al., 2007; Willert et al., 2003). While the palmitoylation of cysteine 77 is not required for ligand secretion, Wnt3a lacking this modification can no longer bind to the Wnt receptors Frizzled and LRP6 and fails to activate the pathway (Komekado et al., 2007). The final post-translational modification discovered in Wnt3a is the addition of a second palmitate to serine 209. The O-acyltransferase Porcupine catalyzes this reaction, and failure to add this moiety caused Wnt3a to be trapped in the endoplasmic reticulum (ER). Recent structural data also suggests that this second palmitoylation facilitates Wnt binding to Fzd (Janda et al., 2012). While all these modifications have only been specifically characterized for Wnt3a, it appears that most (if not all) other Wnt ligands are modified similarly, if not at these exact residues, as all Wnt ligands are extremely hydrophobic.

Porcupine was initially identified as a member of the Wnt pathway in forward genetic screens in *Drosophila*, as it caused a non-cell-autonomous loss of Wnt pathway activity and was epistatic to overexpressed *Wingless* transgenes (Manoukian et al., 1995; van den Heuvel et al., 1993). Recently, a *Porcupine* mutation was recovered in a forward genetic screen in the mouse, and these studies showed that Wnt ligands are not secreted in either ES cells or embryoid bodies in the absence of *Porcupine* (Biechele et al., 2011). Furthermore, Biechele et al. (2011) also showed that IWP-2, a small molecule inhibitor of Porcupine, was able to phenocopy the genetic loss of *Porcupine*. IWP-2 is a pharmacological inhibitor that was found in a screen for novel compounds that

could block Wnt signaling; IWP-2 was part of a class of molecules that specifically blocked Wnt production, but did not interfere with the ability of a cell to respond to exogenous Wnt ligand (Chen et al., 2009). Because there is no evidence that IWP-2 has off target effects, or phenotypes other than in the Wnt pathway in ES cells and embryoid bodies, it suggests that IWP-2 specifically targets Porcupine, making it a powerful compound for manipulating the Wnt pathway *in vivo*.

Wnt receptors

Wnt ligand binding by the signal-receiving cell requires two families of transmembrane receptors: *Frizzled* (*Fzd*) and *Arrow*/Lipoprotein receptor-related protein (*LRP*). The *Frizzled* family of receptors are seven-pass transmembrane proteins with a similar domain structure to G-protein coupled receptors. *Drosophila* Fzd1 has a shared role in canonical and non-canonical Wnt signaling, while *Drosophila* Fzd2 is specific for the β -catenin pathway (Bhanot et al., 1996; Chen and Struhl, 1999; Krasnow and Adler, 1994). In mammals there also appears to be a specification in the receptors for the two different Wnt pathways: Fzd3, Fzd4, Fzd7 and Fzd8 can all activate β -catenin signaling, while only Fzd3 and Fzd6 appear to have a role in the planar cell polarity pathway (Guo et al., 2004; Mikels and Nusse, 2006; Nam et al., 2006; Umbhauer et al., 2000; Wang et al., 2006b; Xu et al., 2004). The fact that *Drosophila* Fzd1 can participate in both β -catenin and planar cell polarity signaling pathways may be due to the fact that ligand binding appears to be dispensable for the non-canonical Wnt pathway in flies. In mammals the two functions of Fzd are likely separated by the specific

Wnt ligands that each family member can bind, and the presence or absence of the Ror2 (promotes planar cell polarity signaling) and LRP5/6 (required for β -catenin signaling) at the membrane (Bryja et al., 2009; Gao et al., 2011; He et al., 2008). There are 10 *Fzd* family members in the mammalian genome, and there is clearly genetic redundancy between the different *Fzd* genes as no individual or double mutant combination results in early embryonic phenotypes that resemble loss of Wnt ligand.

The Wnt co-receptors of the *Arrow/LRP* family are single pass transmembrane proteins that are required for β -catenin signaling. *Drosophila* maternal/zygotic *arrow* mutants phenocopy *wingless* mutants (Wehrli et al., 2000). In mammals *LRP6* is the main co-receptor functioning during embryogenesis, as single mutants have phenotypes indicative of Wnt pathway defects, including a shortened tailbud, and defects in somatogenesis and limb patterning (Pinson et al., 2000). *LRP5* mutants are viable and fertile, but have defects in adult bone homeostasis (Kato et al., 2002). However, there is genetic redundancy between the two murine family members, as *LRP5 LRP6* double mutants phenocopy *Wnt3* mutants (Kelly et al., 2004). Together with the genetic data from *Drosophila*, it is clear that without the Arrow/LRP family of proteins there is no canonical Wnt activity.

The LRP extracellular domain, alone, can bind to Wnt ligands and form a complex with the extracellular domain of Fzd, but the cytoplasmic tail of LRP is required for Wnt target gene activation, as this complex failed to stabilize β -catenin and activate Wnt target genes (Tamai et al., 2000). Conversely, *LRP6*

overexpression in cells that do not express *Fzd* can lead to pathway activation even in the absence of Wnt ligand (Brennan et al., 2004). In a similar experiment Brennan et al. (2004) also found that the *TOPFLASH* Wnt reporter was transcribed at higher levels when only the cytoplasmic domain of *LRP6* was expressed. These results correlate with other findings that suggested that the extracellular domain of LRP6 causes oligomerization of the receptor at the membrane, which is inactive, while monomeric LRP6 protein is constitutively active (Liu et al., 2003). In a set of very elegant experiments Liu et al. (2003) showed that by controlling whether LRP6 was monomeric or in homodimers at the membrane they could modulate Wnt activity. In these experiments the extracellular domain of *LRP6* was replaced with an N-terminal fragment of bacterial DNA Gyrase B, which will dimerize in the presence of coumermycin, an antibiotic with a 1:2 stoichiometry. Using this chimeric protein they were able to show that β -catenin was stabilized in the absence of the drug, and that in a dose dependent manner β -catenin was degraded when coumermycin was added, forcing LRP6 into dimers at the membrane. In accordance with these results it has also been shown that a fusion protein consisting of the Arrow intracellular domain and Dfz2 activates β -catenin signaling independent of ligand (Tolwinski et al., 2003).

Together these data have led to a model in which the cytoplasmic tail of Arrow/LRP is the signal-generating component of the Wnt/Fzd/LRP complex, and in the absence of Wnt ligands LRP is sequestered in inactive homomeric complexes. While overexpressed LRP alone can bind to Wnt ligand, the

LRP/Wnt interaction may be weaker than the interaction between Fzd/Wnt, which is in the 1-10 nM range (Wu and Nusse, 2002). It is also unclear whether Wnt/LRP binding alone can separate LRP monomers from the clusters of the receptor at the membrane. Thus, in this model, Fzd/Wnt binding is required only to free the cytoplasmic tail of LRP, which can transduce a signal that allows for β -catenin stabilization.

While this model fits with the LRP-centric overexpression data, there is also evidence that Fzd can activate the Wnt pathway alone. Activation of the Fzd receptor induces Dishevelled (Dvl) binding to Fzd (Figure 1.1A; Wong et al., 2003). In *Drosophila*, overexpression of *dsh* can activate Wnt target gene expression (Wehrli et al., 2000), but it was not shown in these experiments that the overexpressed *dsh* was interacting with Fzd at the membrane. However, experiments in *Xenopus* egg extracts have also shown that the addition of recombinant Dvl protein is able to activate the Wnt pathway (Salic et al., 2000). In this experimental system there is no Fzd, or LRP, so presumably Dvl can directly interfere with the activity of the cytoplasmic destruction complex. Fzd signaling can also activate the Wnt pathway independent of LRP, as a chimeric protein, consisting of the extracellular domain of β_2 -Androgen Receptor and the intracellular domain of Fzd, can activate Wnt pathway targets in response to Isoproterenol, a ligand of β_2 -Androgen Receptor (Liu et al., 2001). Since Isoproterenol is not a ligand of LRP, the activation of β -catenin in this system was solely dependent on the Dvl/Fzd complex.

Putting together the genetic loss-of-function data with the overexpression

data it appears that *Fzd* and *LRP* are both required for the activation of the Wnt pathway under physiological conditions, but when overexpressed, each is sufficient on its own to achieve ectopic Wnt activation. This leads to a hypothesis in which these two receptors activate the Wnt pathway through parallel molecular pathways, each of which is insufficient to overcome the β -catenin destruction complex under normal conditions. However, either of these parallel pathways can be exploited to activate Wnt target gene expression under specific experimental conditions. Alternatively, these two receptors could work synergistically, targeting the same protein to inhibit the destruction complex. This second hypothesis would predict that the affinity of LRP and Fzd/Dvl for this target protein is low, and only when these two receptors are brought together in the trimeric Wnt/Fzd/LRP complex, is their combined activity sufficient to inhibit the destruction complex.

The destruction complex at the membrane

Wnt ligand binding by Fzd and LRP co-receptors inactivates the destruction complex, allowing stabilization and nuclear translocation of β -catenin. This appears to be achieved through two main mechanisms: the degradation of Axin and the sequestration of the destruction complex to the membrane, or possibly multivesicular endosomes (Cselenyi et al., 2008; Li et al., 2012; Taelman et al., 2010).

Axin, the main scaffolding protein of the destruction complex, has been shown to be degraded in response to Wnt ligands in many different systems (Cselenyi et al., 2008; Lee et al., 2003; Tolwinski et al., 2003). *In vivo*, this is

most apparent in the segmentation of *Drosophila*, where the naked cuticle bands of the epidermis, which are defined by active Wingless signaling, have less Axin protein, compared to the denticles fields that lack Wingless signaling (Tolwinski et al., 2003). Active LRP signaling produces polyubiquitinated Axin, and Axin degradation is blocked by MG132, which inhibits the proteasome, indicating that the Wnt dependent degradation of Axin is mediated by the ubiquitin/proteasome pathway (Cselenyi et al., 2008). Wnt dependent Axin degradation is also distinct from other mechanisms that limit Axin levels in the cell including Tankyrase ribosylation (discussed later) and APC mediated degradation, as the domains of Axin that are required for these interactions are dispensable for Wnt mediated Axin breakdown (Cselenyi et al., 2008). While a decrease in Axin protein, which is thought to be the limiting factor in the destruction complex, could account for the decreased activity of the destruction complex after Wnt stimulation, in cell culture, β -catenin stabilization precedes the decreases in Axin protein (Liu et al., 2005). This suggests that another mechanism of inhibiting the destruction complex must take place upon Wnt activation.

The C-terminus of Axin and the N-terminus of Dishevelled share an 85 amino acid region of homology, termed the DIX domain. This domain has been shown to facilitate homo- and hetero-dimerization of Dvl and Axin, and mutant forms of *Dvl* that lack the DIX domain fail to stabilize β -catenin *in vitro* or *in vivo* (Fagotto et al., 1999; Fukui et al., 2000; Julius et al., 2000; Kishida et al., 1999). Removing the DIX domain from *Axin* also caused Dvl to lose the ability to stabilize β -catenin, despite *Axin*^{ADIX} mutations having no effect on the β -catenin

destruction complex (Kishida et al., 1999). This result suggested, for the first time, that Axin might have a role in stabilization of β -catenin through its interaction with Dvl via their common DIX domain. The interaction between Dvl and Axin can recruit Axin to the Fzd/Dvl complex at the membrane, but this alone cannot account for the inhibition of the β -catenin destruction complex, because Axin at the membrane is still bound GSK3 β , CK1 and β -catenin (Li et al., 2012). Therefore, while the genetic data suggest that the Dvl/Axin interaction is required for β -catenin stabilization, this interaction does not provide a molecular mechanism for this activity, because it appears to simply move the intact destruction complex to the membrane.

The cytoplasmic tail of LRP contains five repeats of the PPPS/TPxS motif, which fits the consensus sequence for GSK3 phosphorylation; this motif is also repeated in β -catenin at the sites of GSK3 phosphorylation. When these sites are mutated in *LRP*, Wnt signaling is blocked (Brennan et al., 2004; Tamai et al., 2000). Upon Wnt ligand binding, both serine (or threonine) residues of this motif in LRP are phosphorylated, which can recruit Axin to LRP (Mao et al., 2001). Based upon the similarity of this motif with the β -catenin phosphorylation sites, it was found that CK1 γ and GSK3 β phosphorylate LRP in a Wnt dependent manner (Davidson et al., 2005; Zeng et al., 2005). In fact the phosphorylation patterns of LRP mirror that of β -catenin, in that GSK3 β first primes LRP for further phosphorylation by CK1 γ at sites flanking this motif (Davidson et al., 2005). The phosphorylation of the PPPS/TPxS motifs of LRP can inhibit GSK3 β phosphorylation of β -catenin and Tau (a non-Wnt related protein) *in vitro*, and

when expressed *in vivo*, this phosphorylated motif activates Wnt pathway targets and can induce a secondary axis in *Xenopus* embryos (Piao et al., 2008; Wu et al., 2009). Thus, while genetically GSK3 β is a negative regulator of the Wnt pathway, as inactivating mutations cause the accumulation of β -catenin, it also functions to phosphorylate LRP, an activity that is absolutely required for pathway activation under normal conditions (Siegfried et al., 1990; Tamai et al., 2000).

Together, the activities of Fzd/Dvl and LRP/GSK3 β form a feed-forward loop that can generate a Wnt 'signalsome' at the membrane (Figure 1.1B; Bilic et al., 2007). In this model, Fzd activation by Wnt ligand triggers the membrane recruitment Axin (and its associated kinases) through the DIX domain of Dvl. At the membrane, GSK3 β and CK1 can phosphorylate the cytoplasmic tail of LRP, which is in a trimeric complex with Fzd and Wnt ligand. The phosphorylation of LRP not only inactivates GSK3 β , but also recruits more Axin to the membrane. Axin can then recruit more Fzd/Wnt/LRP complex through interactions with Dvl or other Axin molecules through the DIX domain. As this pattern repeats, large aggregates of inactive destruction complexes, which are marked by phosphorylated LRP6, accumulate at the membrane (Bilic et al., 2007). In some cell types these aggregates have been reported to be internalized in multivesicular endosomes (Taelman et al., 2010). The sequestration of Wnt signaling clusters was interpreted to be a means of physically removing GSK3 β from cytoplasmic β -catenin, thus playing a positive role in Wnt activation. However, multivesicular endosome can mature into lysosomes and degrade their

contents; therefore, another interpretation of this data would suggest that the observed translocation of the Wnt signalsomes to multivesicular endosomes is a means to turn off Wnt signaling and stop the feed-forward loop of activated Fzd and LRP. To distinguish between these two mechanisms, future experiments will have to examine the time frame in which Wnt signalsomes are incorporated into multivesicular endosomes, and what happens to newly translated β -catenin protein after this time point.

β -catenin/TCF dependent transcription

Stabilized β -catenin activates Wnt target gene expression primarily through interactions with the *TCF/LEF* family of transcription factors (Molenaar et al., 1996; van de Wetering et al., 1997). In the absence of nuclear β -catenin, this family of DNA binding proteins act as transcriptional repressors by promoting histone deacetylation through interactions with Groucho (Cavallo et al., 1998; Chen et al., 1999). β -catenin binding to TCF relieves Groucho mediated repression, as it recruits direct transcriptional activators and components of the SWI/SNF complex that promote chromatin remodeling favorable for transcription (Barker et al., 2001; Takamaru and Moon, 2000). The TCF/LEF family of proteins can all bind to a common consensus sequence (CCTTTGWW), which has been called the Wnt-responsive element. Most Wnt target genes contain multiple copies of this sequence, which is important both for their Wnt dependent activation, and repression in the absence of ligand (Filali et al., 2002; Hatzis et al., 2008).

In the vertebrate genome there are four *TCF/LEF* family genes, and their

specific expression patterns and different isoforms underlie the cell specific transcriptional responses to Wnt ligands (Arce et al., 2006). TCF proteins can also serve as the hubs for crosstalk between Wnt and other signaling pathways; for instance TCF proteins are phosphorylation targets of the mitogen-activated protein kinase (MAPK) pathway, which inhibits target gene expression even in the presence of nuclear β -catenin (Ishitani et al., 1999; Meneghini et al., 1999). While these complexities allow for wide range of responses to nuclear β -catenin, components of the Wnt pathway are common transcriptional targets to all cells that receive Wnt signals (Logan and Nusse, 2004).

Wnt pathway self-regulation

One of the most accurate readouts of Wnt signaling is the transcription of *Axin2* (Aulehla et al., 2003; Jho et al., 2002; Li et al., 2012). Unlike *Axin1*, which is expressed in all cells, *Axin2* is solely expressed in response to β -catenin/TCF activation. The transcription of *Axin2* in response to active Wnt signaling is proposed to play a role in a negative feedback loop that limits Wnt signaling. Newly synthesized *Axin2* can reform the β -catenin destruction complex and restores the overall level of Axin, which is degraded upon Wnt stimulation. *Axin2* shares all of the functional domains of *Axin1* and there are no phenotypes associated with mice expressing *Axin2* transcript from the endogenous *Axin1* locus, demonstrating that *Axin2* can participate in both the β -catenin destruction complex, as well as the membrane associated signalosome complex (Chia and Costantini, 2005). The *Axin2* negative feedback loop may be only one of many pathways that attenuate Wnt signaling during development, as *Axin2* mutant

mice are viable and fertile, though they display defects in skull formation and tooth development (Yu et al., 2005). However, the role of Axin2 in the β -catenin destruction complex is revealed when one or more copies of *Axin1* are removed: *Axin1 Axin2* double mutants are reported to have a much stronger phenotype than *Axin1* single mutants, and *Axin1*^{+/-} *Axin2*^{-/-} compound mutants have brain and skeletal defects not seen in *Axin1* heterozygotes (Dao et al., 2010; Zeng et al., 1997). While, these data demonstrate that Axin2 can function as a scaffold for the destruction complex, there are aspects of *Axin2* biology that remain puzzling. Foremost, if *Axin2* is only transcribed in a cell that has active Wnt signaling, then newly transcribed Axin2 protein could presumably be recruited to the membrane associated signalsome, further promoting Wnt signaling. It has been assumed that Axin2 reforms the destruction complex to attenuate Wnt signaling, but the mechanisms that preclude Axin2 from joining the signalsomes at the membrane are unknown. Therefore, further studies of Axin2 could provide critical clues to what regulates the balance of destruction complex and Wnt signalsome, a key aspect of Wnt signaling that has been long overlooked.

1.1.4 The *Axin2*^{canp} mutation

While mice lacking *Axin2* are viable and fertile (Yu et al., 2005), our lab identified a unique allele of *Axin2*, *canopus* (*canp*) in a forward genetic screen for N-ethyl N-nitrosourea (ENU)-induced recessive mutations that caused morphological defects in midgestation mouse embryos (Qian et al., 2011). All homozygous *Axin2*^{canp} mutants arrest at embryonic day 10.5, but present with

two distinct phenotypes: ~75% displayed cardia bifida and shortened tails, and ~25% had a dorsal tail-like protrusion, a class of mutants referred to as double-tail (Figure 1.2A-C). The *canp* mutation caused a single point mutation, resulting in a V26D missense substitution in an evolutionarily conserved N-terminal motif of Axin2 (Figure 1.2D). The V26D substitution in Axin2 caused an increase of Axin2 protein in embryo lysate, by stabilizing Axin2, which was demonstrated by treating cells expressing *Axin2^{canp}* with cycloheximide (Figure 1.2E-F).

Axin is a key component of the β -catenin destruction complex, and the majority (~75%) of *Axin2^{canp}* mutants displayed phenotypes consistent with decreased Wnt signaling. Thus, it was not surprising that the majority of embryo tissues, including the neural tube, somites and early primitive streak (e7.25) showed decreased expression of the Wnt reporter, *TOPGAL* (Figure 1.3A-F). However, in the late primitive streak (e8.5), there was an unexpected increase *TOPGAL* expression (Figure 1.4A-D). The Wnt target genes *Brachyury (T)* and *Meox1* were also found to be upregulated in the double tail class of mutants, suggesting that this increase in Wnt activity in the *Axin2^{canp}* mutants was not limited to the exogenous *TOPGAL* reporter, as it could be reproduced in classic Wnt target genes (Figure 1.4E-H). Together, these data show that Axin2 protein, which is expressed only after Wnt pathway activation, can play either a positive or and negative role in the Wnt pathway, in a tissue specific manner.

I will present data showing that small molecules that increase cellular Axin levels also reduce or increase Wnt activity in a tissue dependent manner, consistent with the phenotypes in the *Axin2^{canp}* mutants. Further, I will show that

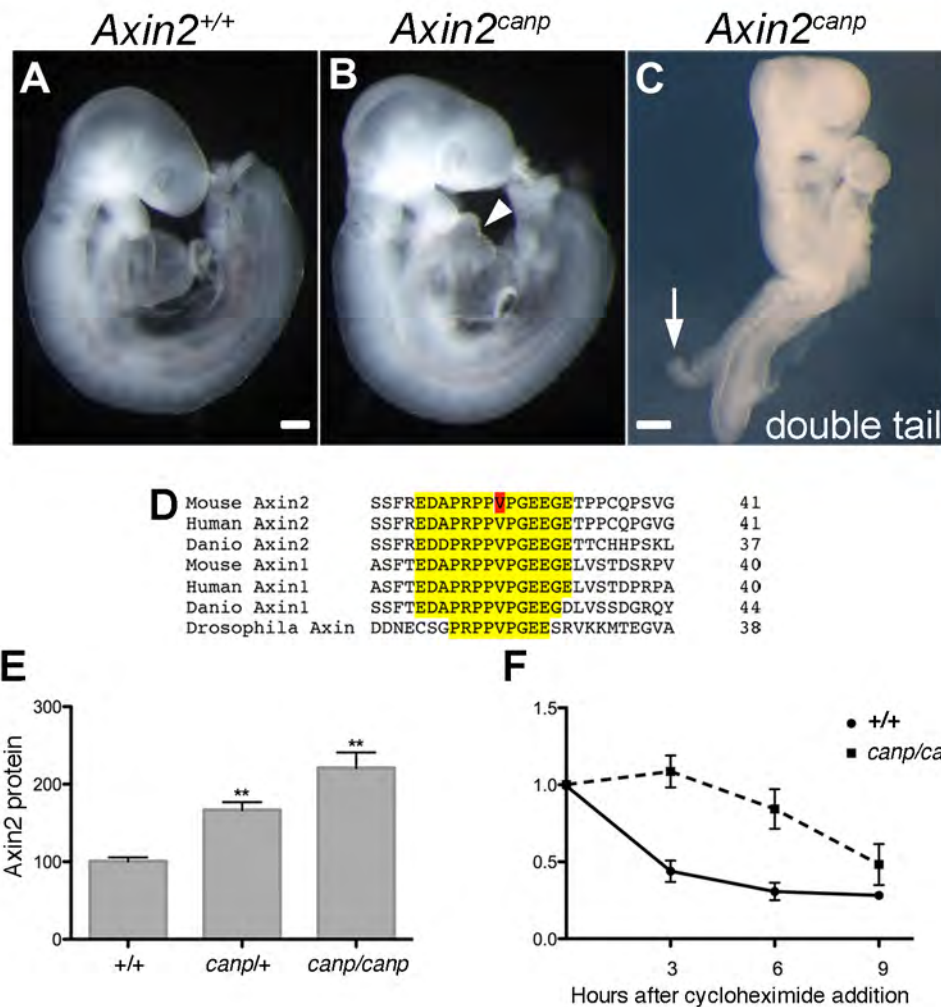


Figure 1.2: *Axin2*^{canp} disrupts morphogenesis and slows protein turnover.

Unlike e9.5 wild-type embryos (**A**), *Axin2*^{canp} mutants have abnormal hearts (arrowhead), slightly shorter tails, and about 30% are exencephalic (**B**). (**C**) An *Axin2*^{canp} embryo of the double tail class, with a short tail-like protrusion on the dorsal side of the embryo (arrow). (**D**) The V26D missense mutation (red) in *Axin2*^{canp} lies in a highly conserved motif in Axin2 (yellow). (**E**) Western blot data from three e9.0 litters showed Axin2 levels were increased 1.6-fold in heterozygous and 2.2-fold in homozygous *Axin2*^{canp} embryos relative to wild type ($P < 0.001$). (**F**) Turnover of Axin2 protein in MEFs. Wild-type and *Axin2*^{canp} homozygous MEFs were cultured with 20 μ g/mL cycloheximide for the indicated number of hours and analyzed by Western blot. The *Axin2*^{canp} mutation increased the half-life of Axin2 from 1.4 h to 4.6 h. Modified from Qian et al., 2011.

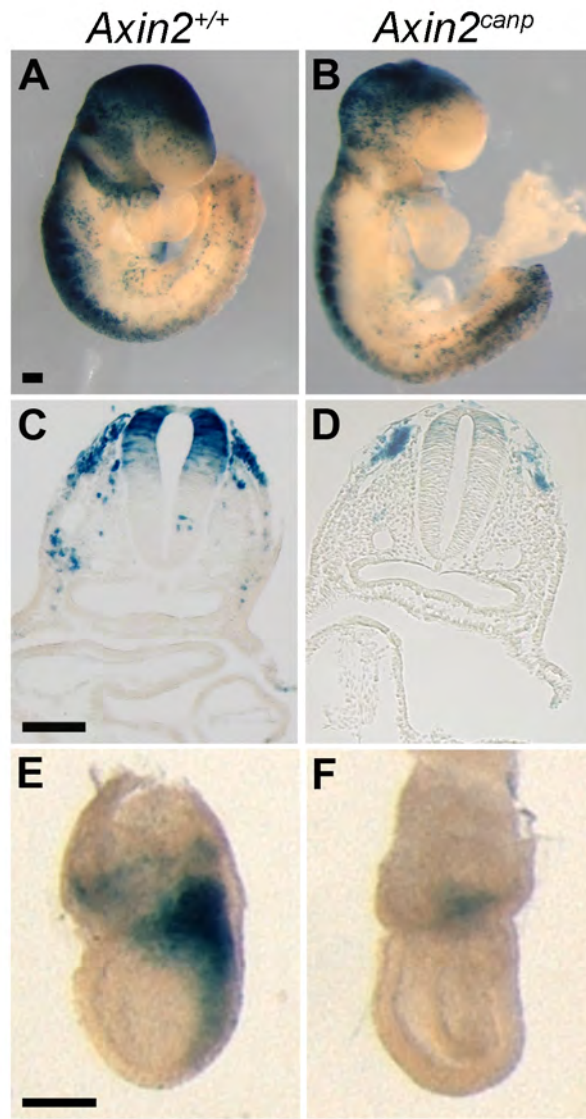


Figure 1.3: Reduced canonical Wnt activity in *Axin2^{canp}* mutants.

Wild type (A, C, E) and homozygous *Axin2^{canp}* mutants (B, D, F) carrying one copy of the TOPGAL reporter transgene, stained for β -galactosidase activity. *Axin2^{canp}* mutants displayed reduced TOPGAL staining at the 16–20 somite stage (A-D) in the brain, branchial arches, dorsal neural tube, and somites. Cross-sections through X-Gal-stained wild-type and homozygous *Axin2^{canp}* embryos at the level of branchial arches (C-D). TOPGAL expression in e7.25 embryos was greatly reduced in the primitive streak in *Axin2^{canp}* embryos (E-F). Modified from Qian et al., 2011.

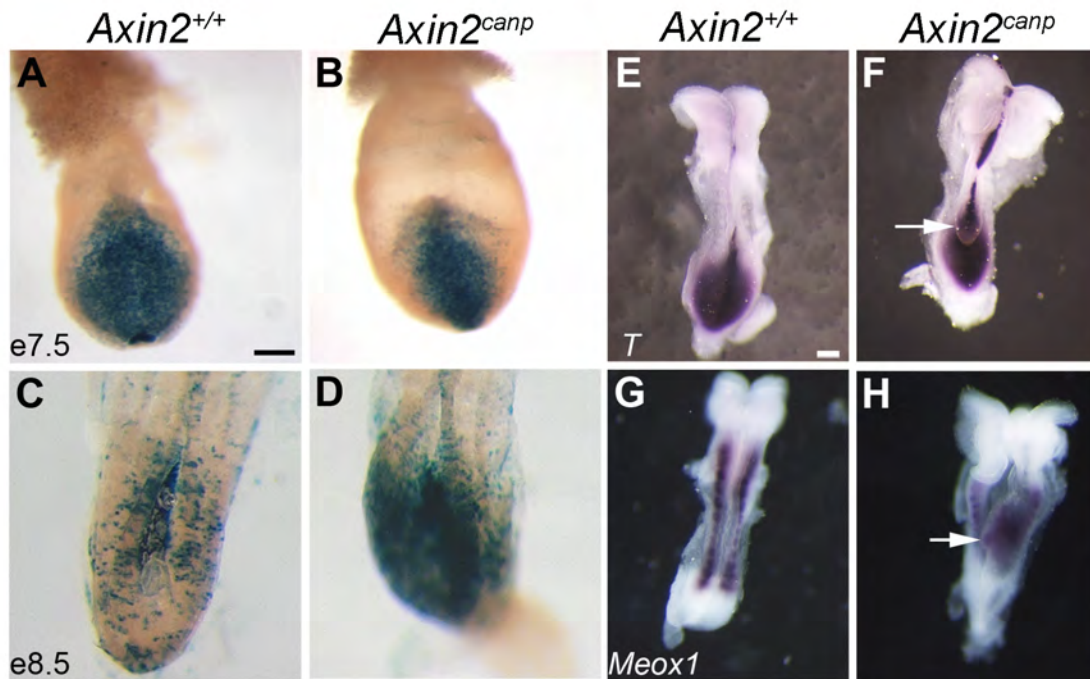


Figure 1.4: Wnt signaling in the primitive streak of *Axin2*^{canp} embryos.

(A–D) Canonical Wnt activity assayed by TOPGAL staining is elevated in the late streak of *Axin2*^{canp} embryos. TOPGAL expression is strong in the wild-type primitive streak of e7.5 embryos (A) and decreases by e8.5. (C). In contrast, TOPGAL activity is reduced in the primitive streak of e7.5 *Axin2*^{canp} embryos (B), but is increased in the tailbud at e8.5 (D). (E–H) Elevated Wnt activity leads to the formation of a duplicated primitive streak in the double-tail class of *Axin2*^{canp} embryos. *Brachyury* (*T*) is expressed in the primitive streak of wild-type embryos (E). In *Axin2*^{canp} double-tail embryos, both a normal-appearing primitive streak and a smaller, dorsal protrusion shaped like a primitive streak express *T* (G, arrow). *Meox1*, expressed in the wild-type somites and presomitic mesoderm (F), is expressed in the dorsal protrusion of the mutant (H, arrow). Modified from Qian et al., 2011.

the increase in Wnt activity is a consequence of increased Axin at the membrane presumably in the LRP/Fzd complex. This data highlights the difficulty in finding small molecules that could serve as cancer therapies by inhibiting the Wnt pathway. Because the components of the β -catenin destruction complex are also present at the membrane where they play an active role in promoting Wnt signaling, small molecules that target these proteins can have both repressive and enhancing effects on the pathway. This work shows that the mouse embryo is an invaluable model to study Wnt signaling, and that through studying Wnt pathway regulation in the embryo we may be able to uncover the factors that cause ectopic Axin to either reform the β -catenin destruction complex or promote signaling at the membrane.

1.2 The non-canonical Wnt/planar cell polarity pathway

Cell polarity is critical for the development and function of all cells in the embryo. Migrating fibroblasts establish a leading and trailing edge to efficiently translocate towards a chemo-attractant, and in epithelial sheets apical-basal polarity is important for determining which side of the cells will interact with the environment. Another important form of epithelial polarity lies in the orientation of the cells within the plane of the epithelium. This aspect of cell polarity, termed planar cell polarity (PCP), orients the cells of an epithelial sheet along an axis that is orthogonal to the apical-basal axis of the individual cell (Figure 1.5). The output of this signaling pathway can be seen in the uniform orientation of cellular processes such as the wing hairs in *Drosophila* or in multicellular structures such

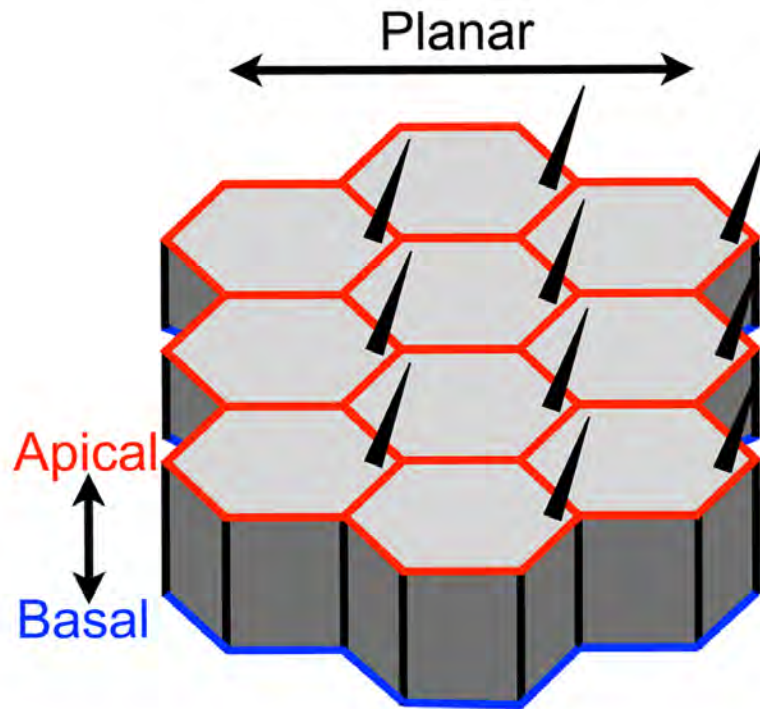


Figure 1.5: The orientation of planar cell polarity in an epithelial sheet.

All epithelial sheets are polarized along the apical-basal axis, evidenced by specific junctional proteins in the apical domain and the deposition of extracellular matrix basally. The cells of the epithelium are also polarized in the plane of the sheet, orthogonal to apical-basal axis, by the non-canonical Wnt/planar cell polarity pathway. This is manifested in the polarized production of cellular appendages such as wing hairs or cilia, which all emanate from a common site in each cell (the right in this cartoon).

as the fur in mice (Devenport and Fuchs, 2008; Vinson and Adler, 1987).

Genetic screens in *Drosophila* identified a core group of proteins, Flamingo (Fmi), van Gogh/Strabismus (Vang), Frizzled (Fzd), Dishevelled (Dvl), Prickle and Diego, whose functions are required to confer planar polarity and uniform cell orientation in the developing eye ommatidia, larval cuticle and wing epithelium (Das et al., 2002; Feiguin et al., 2001; Krasnow and Adler, 1994; Price et al., 2006; Taylor et al., 1998; Theisen et al., 1994; Tree et al., 2002; Usui et al., 1999; Wolff and Rubin, 1998). As planar polarity and Wnt/ β -catenin signaling both require the Wnt receptor Frizzled and its cytoplasmic binding partner Dishevelled, the PCP pathway has also been termed the non-canonical Wnt pathway, though the role of Wnt ligand in planar polarity signaling in *Drosophila* is controversial. The core PCP proteins are conserved throughout evolution in both structure and function (Seifert and Mlodzik, 2007), but are not alone in influencing planar polarity. Other pathways, most notably Fat/Dachsous, also influence global planar polarity. Unlike other signaling pathways, which activate second messengers with post-translational modifications, non-canonical Wnt signaling is achieved through specific interactions between the core PCP proteins that restrict their localization to opposing sides of the cell. At its essence, global planar polarity is achieved within a tissue when there is uniform planar polarity of the core PCP proteins within the individual cells of that tissue.

1.2.1 Planar cell polarity in vertebrate development

In *Drosophila*, the planar cell polarity pathway organizes epithelial sheets

and controls the orientation of specialized actin-based structures, such as wing hairs and larval denticles (Price et al., 2006; Vinson and Adler, 1987). PCP also contributes to the organization and cell fate decisions of the photoreceptors in the developing eye (Das et al., 2002; Wolff and Rubin, 1998). In all of these examples, planar polarity is simply an elaboration on a static epithelium. During vertebrate development the PCP pathway controls two major processes: the orientation of specialized cellular structures and morphogenesis, the active shaping of tissues within the embryo. In both cases the signaling output of the PCP pathway shares the same principles as in *Drosophila*, as changes in cell behavior require the localized activity of Dvl within the cell (Rothbächer et al., 2000; Wallingford et al., 2000).

Morphogenesis

In vertebrate development the PCP pathway contributes to morphogenesis by regulating convergent extension. Convergent extension (CE) is the morphogenetic process through which a tissue gets longer along one axis while also becoming narrower along the orthogonal axis (Figure 1.6A). This tissue reorganization requires cell intercalation and can take place in the absence of cell division (Keller, 2002). Cell intercalation can take place either through a simple neighbor exchange (mediolateral intercalation) or through an intermediate step that requires the formation of multicellular rosette structures (Figure 1.6B-C; Blankenship et al., 2006; Davidson and Keller, 1999). Either way, the cells in a tissue undergoing CE must be uniformly oriented with respect to the medial-lateral axis in order to undergo the stereotyped morphogenic movements.

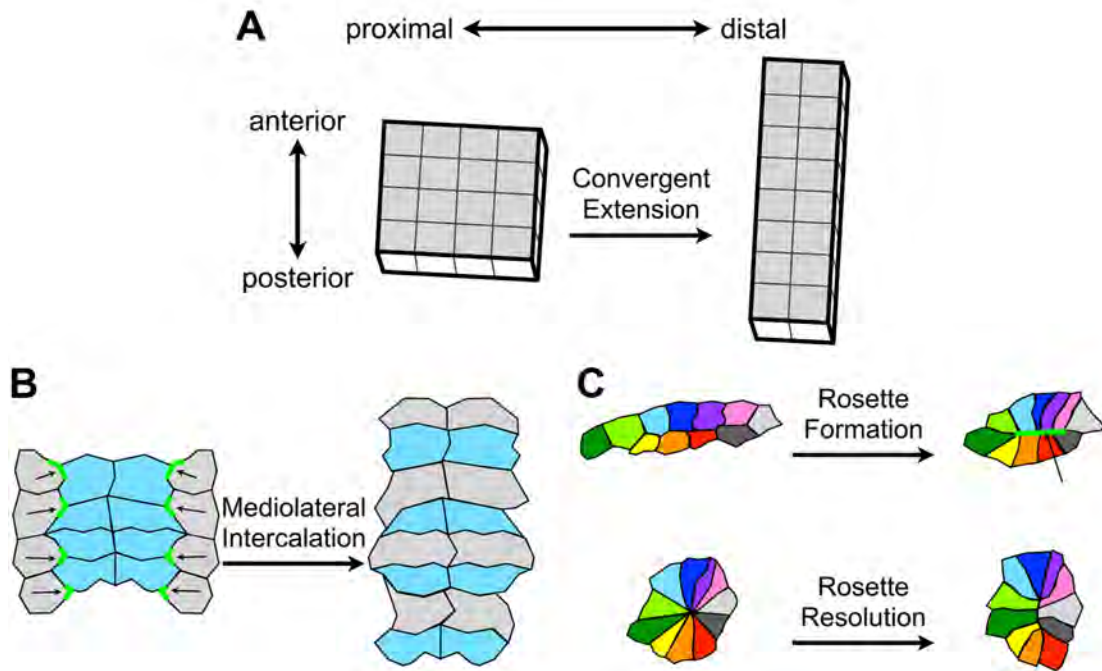


Figure 1.6: Mechanisms of convergent extension.

(A) Convergent extension is a morphogenetic process that elongates a tissue along one axis (anterior-posterior in the cartoon) while narrowing the tissue along the orthogonal axis (proximal-distal). This process involves local neighbor exchange, which has been observed to take place via two distinct mechanisms. (B) In the mediolateral intercalation model cells on the outside of the tissue intercalate between their neighbors elongating the tissue. This process is driven by polarized lamellipodia protrusions, and Myosin accumulations at the sites of intercalation (green). (C) In the rosette model a group of cells converge on a central axis through the contraction of a multicellular Myosin band (green). This generates a multicellular vertex, which later resolves along the axis of elongation. Note that this model also causes neighbor exchange as cells that originally shared a border along the anterior-posterior axis are now separated by many cell diameters (e.g. the red and purple cell)

In *Xenopus* embryos, neural and mesodermal tissues that are undergoing CE movements display polarized lamellipodia protrusions along the mediolateral faces of mediolaterally intercalating cells (Davidson and Keller, 1999; Elul and Keller, 2000; Elul et al., 1997). These protrusions also accumulate Myosin II and are thought to drive the intercalation of neighboring cells medially, lengthening the tissue along the anterior-posterior axis (Figure 1.6B). This cellular behavior has been shown to require both the non-canonical Wnt ligand, Wnt5, and core PCP proteins, including Fzd8 and Dvl (Wallingford and Harland, 2001; Wallingford et al., 2000; Wallingford et al., 2001). However, unlike in *Drosophila*, in this context Dvl protein is not planar polarized within the individual cells, rather, it is uniformly localized to the cell membrane in migrating cells, and cytoplasmic in static cells (Wallingford et al., 2000). The membrane localization of Dvl is crucial for its role in CE, as sequestering Dvl to the mitochondria causes CE defects, accompanied by a failure to activate the GTPases Rho and Rac (Park et al., 2005). Determining how Dvl stimulates planar polarized lamellipodia formation, despite its uniform membrane localization remains to be addressed.

The cellular mechanism of CE of the neural tube in mice may differ from the observations made in *Xenopus*. Unlike in the developing mammalian neural tube, the *Xenopus* neural tube is stratified epithelial sheet, as each cell does not make contacts to both the apical and basal surfaces of the tissue. Therefore, individual cells in *Xenopus* have more plasticity along their mediolateral cell faces to make these directional cellular protrusions. In the mammalian neural tube, each cell has contacts to both the apical surface and basal lamina; therefore the

mediolateral faces of the cell are rigid. Therefore, it seems more likely that the mechanisms of CE in the mammalian neural plate would be based on neighbor exchange through a multicellular rosette intermediate. During this process a large group of cells that are arrayed along the medial-lateral axis of the embryo come together, and then disperse along the anterior-posterior axis. During rosette formation an actin/myosin band forms along the apical membranes of a large group of cells, and as it contracts a common multicellular junction is formed. This rosette structure then resolves along the orthogonal angle (along the anterior-posterior axis), such that cells that were once separated by many cell diameters along the mediolateral axis are now neighbors (narrowing the tissue). At the same time cells were once neighbors are separated by many cell diameters along the anterior-posterior axis (lengthening the tissue) (Figure 1.6C). This process was first described during *Drosophila* germband extension, but since then, it has been proposed to be a method of CE in many other tissues including the chick neural tube and primitive streak (Blankenship et al., 2006; Nishimura et al., 2012; Wagstaff et al., 2008)

Defects in convergent extension are a common phenotype in all vertebrate model systems with mutations in core PCP genes affecting the morphology of many tissues including the neural tube, somites and cochlea (Darken et al., 2002; Greene et al., 1998; Park and Moon, 2002; Wallingford and Harland, 2001; Wang et al., 2005). In all cases, mutations in the PCP pathway lead to tissues that are short along one axis, and wide along the orthogonal axis. The most striking phenotype in these mutants is craniorachischisis, the failure to close the

neural tube from the midbrain-hindbrain junction to the tail (Wallingford, 2005). Craniorachischisis is a hallmark phenotype of PCP mutants in the mouse, including the core PCP genes *van Gogh-like2 (Vangl2)*, the Flamingo homologue *Celsr1*, and *Fzd3 Fzd6* and *Dvl1 Dvl2* double mutants (Curtin et al., 2003; Hamblet et al., 2002; Kibar et al., 2001b; Wang et al., 2006b). This specific defect in neural tube closure is also seen in other mutants, including *Sec24b*, *Scribble*, *Ptk7* and the ubiquitin ligases *Smurf1 Smurf2* double mutants, implicating a role for these proteins in the mammalian PCP pathway (Lu et al., 2004; Merte et al., 2010; Murdoch et al., 2003; Narimatsu et al., 2009; Wansleeben et al., 2010). These observations are important in the context of human disease, as mutations in *Vangl1* have been found in patients born with neural tube defects including spina bifida (Kibar et al., 2007b). Despite the known role of PCP in morphogenesis and CE, and the role of these processes in human disease, no studies have investigated the mechanisms of PCP dependent convergent extension at a cellular level during mammalian development.

Left-right asymmetry

In addition to its role in morphogenesis, the PCP pathway also plays a role in the orientation of specialized cellular structures during vertebrate development. Like in *Drosophila*, some of these specialized structures are actin-based, such as in the stereocilia in the inner ear. Both the auditory and vestibular epithelia in the inner ear produce actin-based stereocilia, which appear as a chevron in each cell, and play a crucial role in hearing and balance in the animal. This chevron pattern of stereocilia is planar polarized, such that the tip of the chevron points

towards the lateral face of the cell. This stereotyped pattern is disrupted in PCP mutants including *Vangl2* and *Celsr1* (Curtin et al., 2003; Montcouquiol et al., 2003). At the molecular level the PCP pathway in the inner ear appears to follow the same principles as the *Drosophila* wing disc: the core PCP proteins are asymmetrically aligned within the cells of the organ of Corti, and the actin-based structures are oriented towards the side of the cell that has membrane-associated Dvl. When any of the core PCP genes are mutated, the orientation of the stereocilia is randomized with respect to neighboring cells (Jones et al., 2008; Montcouquiol et al., 2003; Montcouquiol et al., 2006). Each cell in the organ of Corti also has a planar polarized primary cilium. The relationship between the PCP pathway, the actin-based stereocilia, and the microtubule-based cilium are unclear; it has been shown that mutants lacking a primary cilium also have defects in stereocilia polarity. However, in these mutants there was no defect in the alignment of the PCP proteins at the cell membrane, suggesting that the cilium anchors the stereocilia, and the position of the primary cilium may not be directly influenced by the PCP pathway in this context (Jones et al., 2008).

The PCP pathway can also control the orientation of multicellular structures, such as the fur in mice. In this context the asymmetric membrane association of *Celsr1* and *Vangl2* are critical for the proximally polarized invagination of the forming hair placode, which produces hair follicles that all point distally (Devenport and Fuchs, 2008). Because *Vangl2* is enriched to the distal side of the cell during this process, it is likely that Dvl is enriched to the opposing face of the cell. Therefore it has been hypothesized that effectors of

Dvl, including Rho and Rac, could drive polarized follicle invagination, as these GTPases are key regulators of cell invagination in other systems (Dawes-Hoang et al., 2005).

In both the organ of Corti and developing hair follicles, the PCP pathway appears to orient structures by affecting actin dynamics, most likely through the localized activation of Rho and Rac, similar to what has been reported in *Drosophila*. However, in vertebrate development the PCP pathway has also been reported to have a novel role in controlling the positioning/orientation of the centrosome, which acts as the microtubule-organizing center. Examples of this are seen in the developing kidney tubules and *Xenopus* epidermis where the PCP pathway plays a role in polarized cell division and cilia orientation, respectively (Fischer et al., 2006; Park et al., 2008). By controlling the position of the centrosome in these systems, the PCP pathway affects the morphology of epithelial tissues and global patterning within the embryo.

The primary cilium is a slim microtubule-based organelle, which has recently become the focus of intense study due to its role in the Hedgehog signaling pathway. In an epithelial sheet cilia emanate from the apical side of the cell, and are produced from the apically docked basal body. The basal body is a modified centrosome, and therefore cilia are only present in non-dividing cells (Goetz and Anderson, 2010). Apart from the role in Hedgehog signal transduction, cilia are also important for generating fluid flow. These cilia are termed motile cilia, and are distinct from the primary cilium, as they have a different microtubule structure and additional motor proteins that allow them to

beat in the extracellular environment. Commonly motile cilia are present in multiciliated cells such as the *Xenopus* epidermis and ependymal cells of the brain. PCP signaling is required to produce uniform fluid flow, as it directs the homogeneous orientation of the cilia, with respect to the cell and to each other, in a multiciliated epithelium (Guirao et al., 2010; Hirota et al., 2010; Park et al., 2008). In these examples cilia-generated fluid flow is important for physiology of the specific organs, but motile cilia can also influence global patterning of the embryo.

The late organizer in the mouse, also referred to as the ventral node, is a specialized mesendodermal epithelium that is transiently visible at the distal tip of the e7.5 embryo. The node is a spherical depression of 150-200 mesoderm cells that have reformed into an epithelium and will later give rise to the trunk notochord, which emits signaling molecules that pattern the neural tube. Each node cell contains a single apically docked modified primary cilium, which is motile and critical for the generation of the left-right axis of the embryo. Leftward fluid flow in the node is necessary and sufficient to establish the expression of *Nodal*, *Lefty2* and *Pitx2* in the left lateral plate mesoderm (Nonaka et al., 2002; Nonaka et al., 1998; Nonaka et al., 2005). This leftward fluid flow establishes a left-to-right Ca^+ gradient and the expression of *Nodal* in the endoderm surrounding the node (Tanaka et al., 2005). These signals are then transmitted to the lateral plate mesoderm through gap junctions in the gut endoderm (Viotti et al., 2012). The creation of the initial symmetry breaking fluid flow in the node depends not only on ciliary motility, but also the coherent leftward flow depends

on a repositioning of the cilium from the center to the posterior of each node cell (Hashimoto et al., 2010; Nonaka et al., 2005; Shinohara et al., 2012; Song et al., 2010). Between the early headfold and late headfold stage, nodal cilia move from the center to the posterior side of the cell; then, at early somite stages, they begin to beat, creating the leftward flow (Hashimoto et al., 2010). Thus, the establishment of the left-right axis of the embryo is dependent on each cell in the node producing a planar polarized cilium along the already established anterior-posterior axis.

While there are no defects in left-right asymmetry in any of the single mutants for mouse PCP genes, recent reports have shown that double mutants for *Vangl1 Vangl2* and embryos mutant for five of the six alleles of *Dvl1 Dvl2 Dvl3* have stronger defects in CE, similar to what has been seen in other vertebrates (Hashimoto et al., 2010; Song et al., 2010). These experiments also showed a role for the non-canonical Wnt pathway in the establishment of left-right asymmetry, through the posterior positioning of nodal cilia. While these data provide convincing evidence that the PCP pathway is upstream of polarized cilia, it is unclear how the PCP pathway changes the localization of the centrosome, a microtubule based organelle. To date, the effector proteins downstream of the PCP pathway all govern changes in the actin cytoskeleton. In the mouse node does the PCP pathway directly change the apical microtubule network, or can the actin cytoskeleton regulate the positioning of the primary cilia?

1.2.2 Establishment of planar cell polarity

In the *Drosophila* wing disc it was revealed through biochemical and genetic analysis that the core PCP proteins are present in two distinct complexes that are asymmetrically localized in the apical domain of individual cells along the axis of planar polarity. The van Gogh complex is localized to the apical membrane at the proximal face of the cell and includes the transmembrane proteins Fmi and Vang, along with the cytoplasmic protein Prickle (Strutt and Strutt, 2007; Tree et al., 2002; Usui et al., 1999). At the opposing, distal face of the cell, the Frizzled complex is comprised of the transmembrane proteins Fmi and Fzd, along with the cytoplasmic proteins Dvl and Diego (Figure 1.7A; Axelrod, 2001; Feiguin et al., 2001; Shimada et al., 2001; Strutt, 2001). One way in which the PCP pathway influences cell behavior is by modifying the actin cytoskeleton. The asymmetric alignment of the Fzd and Vang complexes are integral to PCP activity, as they restrict the membrane associated Dvl to one edge of the cell. In the *Drosophila* wing disc this restricts the downstream effectors of Dishevelled – Rac1, RhoA, Rho-associated protein kinase (ROCK) and Myosin II – to the distal side of cell, where the actin-based wing hair is created (Eaton et al., 1996; Strutt et al., 1997; Walters et al., 2006; Winter et al., 2001).

Establishing global planar polarity

The *Drosophila* wing disc is composed of roughly 30,000 cells, and each produces a single, distally polarized, wing hair. Thus, global planar polarity in this

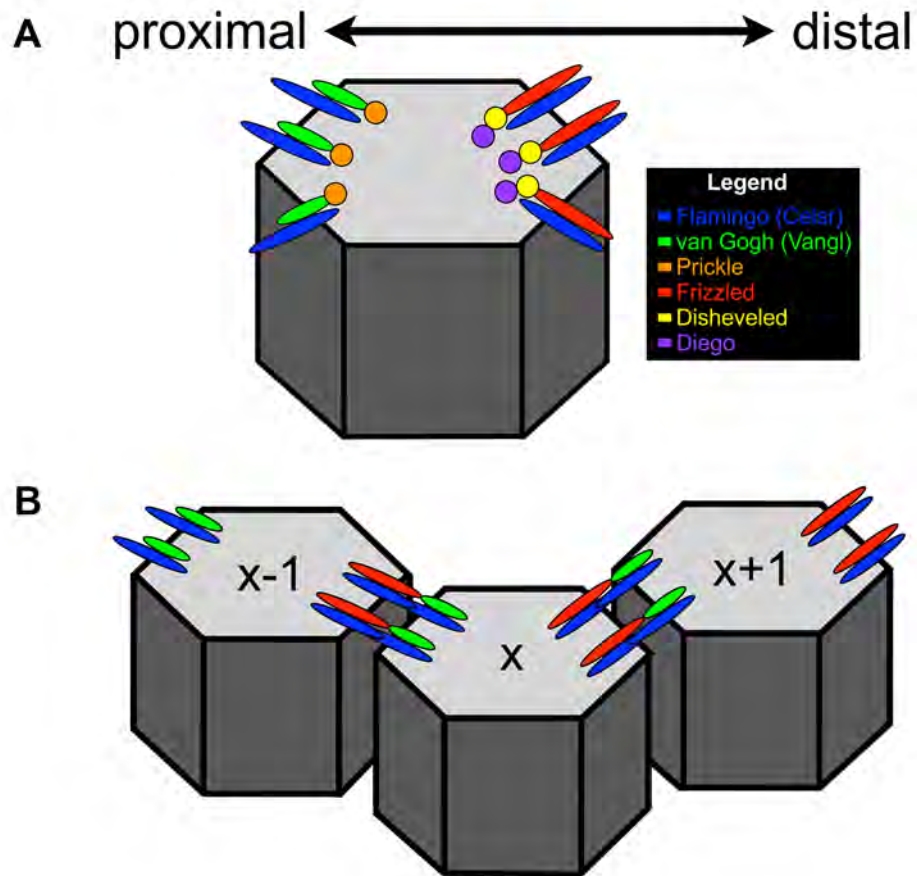


Figure 1.7: The asymmetrical distribution of the core PCP proteins.

(A) The core planar cell polarity proteins are asymmetrically distributed in apical membrane along the axis of tissue polarity. The *Drosophila* wing disc, which is planar polarized along the proximal-distal axis, has van Gogh and Prickle present along the proximal face of the cells while Frizzled, Dishevelled and Diego are restricted to the distal faces. Flamingo is present with both the van Gogh and Frizzled complex. (B) Flamingo is capable of forming homodimers in the extracellular space between two cells. These interactions are favored when one cell is presenting van Gogh and the neighboring cell is presenting Frizzled. The head-to-tail model of non-canonical Wnt signal propagation suggests that when one cell (x) has established the asymmetric distribution of the van Gogh and Frizzled complexes it can orient its neighboring cells to adopt the same orientation through the extracellular interactions between Frizzled/Flamingo and van Gogh/Flamingo.

tissue instructs the same proximal and distal directional cues to both neighboring cells and cells on opposite ends of the tissue. When any of the transmembrane PCP proteins, *Fzd*, *Vang* or *Fmi*, is removed from a patch of cells within the developing wing epithelium there are both cell-autonomous and non-cell-autonomous phenotypes, indicating that uniform planar polarity across the tissue is achieved through intercellular interactions (Adler et al., 1997; Usui et al., 1999). These experiments led to the hypothesis that specific neighbor-to-neighbor interactions can instruct a head-to-tail alignment of the Vang and Fzd complexes between neighboring cells (Strutt, 2002).

In the wing discs of wild-type pupae all wing hairs point distally, and emanate from the distal side of the cell (Figure 1.8A). Clonal patches of cells that are mutant for any of the core PCP genes cause a swirling pattern of the wing hairs within the mutant clone. However mutations in the different PCP genes have different effects on the wild-type cell surrounding that surround the clone. Mutations in *Fzd* cause the neighboring cells to orient wing hairs towards the mutant clone (Figure 1.8B; Vinson and Adler, 1987). In contrast, disrupting *Vang* expression cause the wild-type cells adjacent to the clone to all point their wing hairs away from the mutant cells (Figure 1.8C; Taylor et al., 1998). This suggests that the status of the Fzd complex is key to the non-cell-autonomous effects of PCP mutants, such that wing hairs of neighboring wild-type cells point away from the source of the highest Fzd activity, and towards cells with lower Fzd activity (Adler et al., 1997).

These genetic observations have been clarified by the molecular

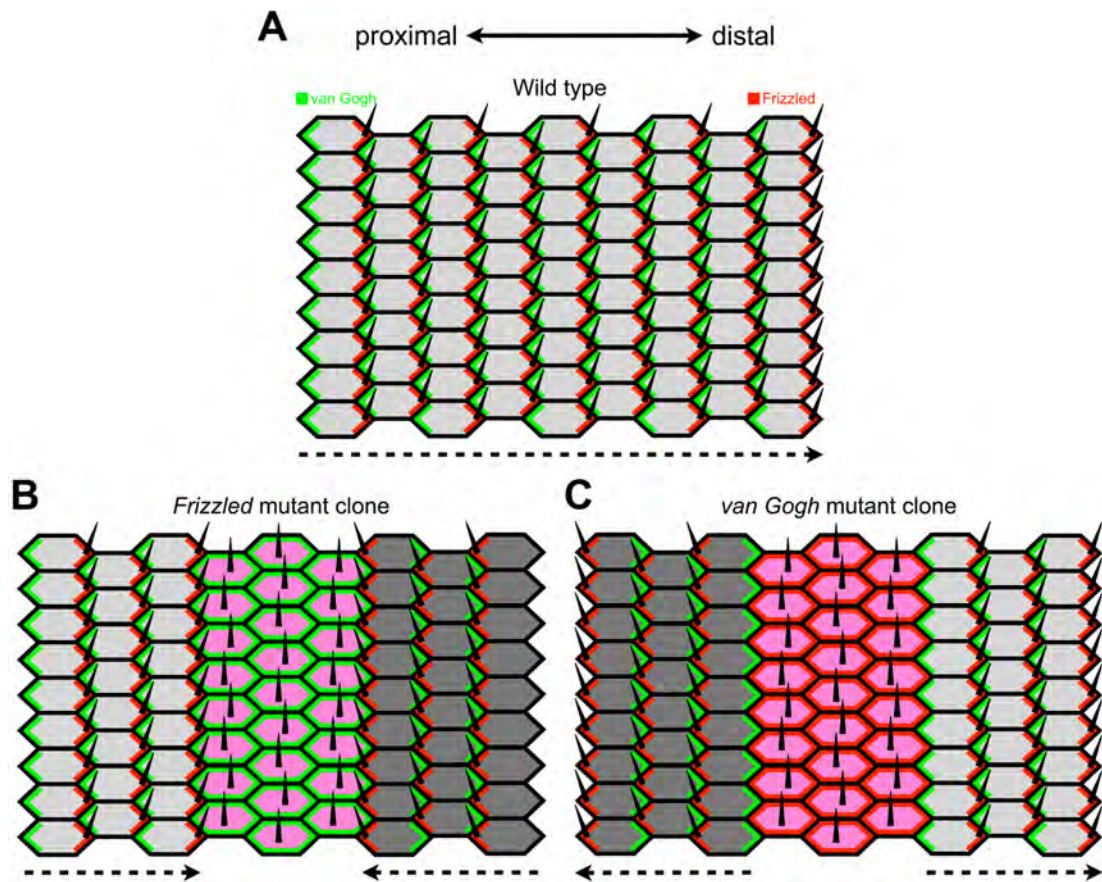


Figure 1.8: Non-cell-autonomous phenotypes of PCP mutant clones.

(A) Cells in the *Drosophila* wing disc have van Gogh (green) and Frizzled (red) segregated to the proximal and distal domains, respectively, and form a wing hair at the distal side of the cell. A dashed arrow indicates the orientation of wing hairs. (B-C) *van Gogh* or *Frizzled* mutant clones (pink cells) have randomly oriented wing hairs (cell-autonomous phenotype). The mutant clones also produce non-cell-autonomous phenotypes in the adjacent wild-type cells (dark grey cells). When *Frizzled* is clonally depleted (B), the mutant cells present van Gogh in the entire apical surface. This causes distally adjacent cells to recruit Frizzled to the proximal domain, as Frizzled/van Gogh complexes in the extracellular space are favored, reorienting the immediately adjacent cells, which then propagate this signal distally to their neighbors. *van Gogh* mutant clones (C) cause a reorientation in their proximal neighbors by uniformly expressing Frizzled, which causes neighboring cells to generate wing hairs that point away (proximal) from the mutant cells.

characterization of the extracellular interactions between the transmembrane components of the PCP pathway. The common component of the two membrane complexes is the protocadherin protein Fmi (Figure 1.7A), the extracellular domain of which may be able to homodimerize between neighboring cells. Fmi is present within an individual cell with Vang proximally and Fzd distally.

Biochemical and genetic data have shown that the extracellular domain of Fzd coimmunoprecipitates with Vang and is required for the non-cell-autonomous phenotypes of *Fzd* overexpressing clones (Strutt and Strutt, 2008; Wu and Mlodzik, 2008). These data suggest that the extracellular homodimeric binding of Fmi may be enhanced when one cell has the Fmi/Vang complex and the immediate adjacent cell has the Fmi/Fzd complex. At the same time, it has been shown in *Drosophila* S2 cells that when two cells express Fmi and Fzd, Flamingo dimerization is blocked. Removing the extracellular domain of Fzd in one or both cells can alleviate this block in homodimeric Fmi binding (Strutt and Strutt, 2008). These data suggest that in the wing disc when one cell has the Fmi/Fzd complex at the membrane it will suppress the Fmi/Fzd complex in the neighboring cell in favor of the Fmi/Vang complex, which will allow for the extracellular binding of neighboring Fmi molecules through its cadherin repeats.

This has led to a model for global PCP establishment known as the head-to-tail model. Once a cell (x) has established the proximal and distal Vang and Fzd complexes (respectively), this influences the neighboring cells to adopt a similar orientation of proximal and distal complexes, such that the distal side of the proximally adjacent cell (x-1) accumulates the Fzd complex, allowing the

interaction of the Fzd/Fmi complex (x-1) with the Vang/Fmi complex of the origin cell (x) in the intercellular space. At the same time the neighboring face (proximal side) of the other distally adjacent cell (x+1) will accumulate the Vang/Fmi complex (Figure 1.7B; Strutt and Strutt, 2005). By this mechanism, the planar polarity of one cell can be transmitted throughout the tissue. This model also predicts the observed phenotypes when either *Vang* or *Fzd* are clonally removed from a patch of cells. Removing either of the proteins causes the other protein to accumulate uniformly along all edges of the cell. Thus, when *Vang* is genetically removed, all neighboring cells are presented with Fzd/Fmi complexes, causing them to accumulate Vang at the side of the cell facing the mutant clone, whether or not this is the cell's true proximal face. This causes cells proximal to the clone to have reversed asymmetry in PCP localization and produce wing hairs on the proximal side of the cell (Figure 1.8C).

While the genetic and molecular data provide a mechanism that supports the head-to-tail model for planar polarity signal propagation, this model would also suggest that when a mutant clone is introduced, the reorientation of polarity of the surrounding wild-type cells would propagate to the ends of the tissue. However, this phenomenon is not found in wing discs harboring patches of mutant cells; while there are effects on the surrounding cells, they are only present in 7-10 rows of cells adjacent to the mutant clone. Further away from the mutant clone, normal planar polarity is restored and all wing hairs point distally. This not only suggests the presence of global signals that establish the domains of proximal and distal planar polarity within the tissue, but also that these global

signals can eventually override the head-to-tail interactions between the Vang and Fzd complexes.

Despite the wealth of data that suggests the presence of a global determinant for planar polarity, no such signal has been specifically defined. One possible mechanism, that relies solely on the non-canonical PCP proteins, would be for a gradient in Fzd activity in the wing disc, such that there was more available membrane Fzd in the proximal domain and less distally. While there is no apparent gradient in *Fzd* gene expression, global wing hair polarity was reversed when ectopic *Fzd* was expressed under a heat-shock promoter, and hot wax was dripped, to locally activate the heat-shock promoter, onto the distal portion of the pupal wing. This resulted in graded *Fzd* expression from the distal to proximal region, and reversed planar polarity in the whole tissue (Adler et al., 1997). While this proved that ectopic *Fzd* could globally regulate wing hair polarity, *Fzd* expression is uniform throughout the wild-type tissue. So in practice, this model would require a second signal that preferentially stabilizes Fzd in the proximal domain. A simple candidate for a molecule that could preferentially stabilize membrane Fzd is Wingless, but there are no apparent PCP defects when multiple *Wingless* genes are clonally removed in the wing disc, suggesting that Wnt ligand is not responsible for generating graded Fzd activity in the wing disc (Chen et al., 2008).

Although the role of Wingless ligands in PCP signaling in the wing disc of *Drosophila* is controversial, there is a clear role for Wnt ligands in the establishment of PCP in vertebrates. In frogs, zebrafish and mice there are

dedicated non-canonical Wnt ligands for the PCP pathway, and these ligands are required for the localized activation of Rho, Rac and Rok2 that control actin dynamics (Habas and He, 2006; Karner et al., 2009; Marlow et al., 2002; Qian et al., 2007; Wallingford et al., 2001). Recent data suggests that these non-canonical Wnt ligands cause the mammalian van Gogh homologue, Vangl2, to interact with the transmembrane protein Ror2, which allows for CK1 dependent phosphorylation of Vangl2 (Gao et al., 2011). Phosphorylated Vangl2 appears to be correlated with active PCP signaling, but the relationship between these phosphorylation marks and interactions between Vangl2 and the other core PCP proteins have yet to be determined.

The Fat/Dachsous pathway is another candidate for a second pathway that could contribute to global planar polarity and rescue the distal orientation of wing hairs in wing discs that harbor clones of cells lacking components of the non-canonical Wnt pathway. Disruptions in Fat signaling lead to defects in wing hair polarity similar to mutations in the core PCP proteins (Adler et al., 1998); but the Fat/Dachsous pathway is clearly distinct from the Vang/Fzd pathway, as ectopic Fat expression can locally rescue planar polarity in a genetic background in which Vang and Fzd are both missing from the membrane (Casal et al., 2006). In wild-type tissues the relationship between Fat/Dachsous and the non-canonical Wnt pathway are still unclear; in the *Drosophila* eye it appears that *Wingless* ligand expression controls *Dachsous* at the poles of the eye disc, and that this can reinforce asymmetries in *Fzd* expression in the developing ommatidia clusters (Yang et al., 2002). Dachsous inhibits Fat; therefore, the

asymmetric expression of *Dachsous* at the pole leads to a higher expression of *Fat* in cells closer to the equator. Clonal analysis has shown that asymmetries in *Fat* expression in the R3/R4 cells are required for *Fzd* signaling. However, in the context of the wing disc and global planar polarity, it is unclear whether this mechanism of crosstalk between the *Fat/Dachsous* and non-canonical Wnt signaling pathways exists. Recent evidence suggests that *Fat* signaling may influence cell division, microtubule polarity and wing disc architecture, and this may indirectly affect *Fzd* signaling (Aigouy et al., 2010; Donoughe and DiNardo, 2011; Harumoto et al., 2010).

The *Fat/Dachsous* pathway in vertebrates does not appear to be as tightly linked to non-canonical Wnt signaling, as is the case in *Drosophila*. *Dchs1* mutant mice do not display classic PCP phenotypes, and *Fat4* and *Dchs1* are primarily expressed in mesenchymal cells. Interestingly, disrupting *Fat/Dachsous* signaling causes a simultaneous shortening and widening in the sternum and vertebrae (Mao et al., 2011), suggesting that *Fat/Dachsous* signaling regulates CE similar to the non-canonical Wnt pathway. Therefore, it appears that in mammalian development *Fat/Dachsous* and non-canonical Wnt signaling are required for planar polarity and morphogenesis in distinct tissues.

Establishing planar cell polarity within an individual cell

While there is strong experimental evidence for the head-to-tail model for organizing the core planar cell polarity proteins, this model relies on at least one cell correctly organizing the *Vang* and *Fzd* complexes first, and then subsequent intracellular interactions establish PCP asymmetries in receiving cells. Therefore,

it has become increasingly important to understand how a single cell can internally establish the correct domains of the Vang and Fzd complexes.

Prior to wing hair formation in the *Drosophila* wing disc, the core PCP proteins are localized to vesicles within the cytoplasm. Vang and Fzd are next deposited into the apical membrane, in a Fmi-dependant process, but not in a planar polarized fashion (Chae et al., 1999; Shimada et al., 2001; Usui et al., 1999). In fact, when either *Vang* or *Fzd* is mutated, Fmi remains symmetrically localized around the entire apical membrane of the cell (Shimada et al., 2001; Usui et al., 1999). Therefore, in *Drosophila* at least, Fmi functions to bring the other transmembrane proteins to the apical surface but plays no role in establishing asymmetries, a process that requires both Vang and Fzd.

The establishment of the asymmetric PCP complexes within the cell could be dependent on the interactions between the cytoplasmic proteins Diego, Prickle and Dvl. Prickle binds Vang, and inhibits any interaction between Vang and Dvl (Bastock et al., 2003; Jenny et al., 2003). Similarly, Diego binds Dvl, inhibiting any interactions with Prickle or Vang (Das et al., 2004; Jenny et al., 2005). Together, these data establish a model where the cytoplasmic Dvl/Fzd complex inhibits any interactions between Vang/Prickle on the opposite side of the cell, and visa versa. However, this maintenance model does not answer how the initial asymmetries are uniformly established within an epithelial sheet when the proteins are first symmetrically deposited on the membrane.

Changes in the architecture of the microtubule and actin cytoskeleton may play a decisive role in establishing the initial asymmetry in the Vang and Fzd

complexes. Prior to wing hair formation, the microtubules in the apical cap of wing epithelial cells become polarized along the proximal-distal axis. At the same time GFP-tagged Fzd was found to be predominantly trafficked to the distal side of the cell (Shimada et al., 2006). This could be the key step in breaking the initial symmetric deposition of the transmembrane PCP proteins, and after this initial break the interactions of Prickle and Diego further refine the localization of the Vang and Fzd complexes to the extreme proximal and distal domains, respectively.

Supporting this model, it was recently shown that the Rab5 effector protein Rabenosyn-5, which is required for the endocytosis and recycling of membrane proteins, is required for the asymmetric localization of Fmi prior to wing hair formation (Mottola et al., 2010). Therefore, it is clear that the transmembrane PCP proteins are internalized after their initial incorporation into the membrane and recycled back to the membrane during the establishment of planar polarity.

The actin cytoskeleton was originally thought to be the target of modifications by the PCP pathway, as key regulators of actin dynamics are downstream of active Dishevelled (e.g. Rac, Rho, Daam and Myosin II). However, data from *Drosophila* suggest that dynamic rearrangements of the actin cytoskeleton are required for apical membrane targeting of the PCP proteins Fzd and Fmi. Cofilin regulates actin dynamics by severing F-actin filaments, an essential step in remodeling the actin cytoskeleton. While loss of *Drosophila* Cofilin, *twinstar*, is embryonic lethal, animals homozygous for a temperature-sensitive allele show PCP phenotypes in the eye and wing when

animals are shifted to the restrictive temperature during development. Cells in the *twinstar* mutant clones do not produce uniformly distal wing hairs, which was attributed to the loss of plasma membrane associated Fzd and Fmi (Blair et al., 2006). Therefore, while PCP pathway dependent modifications of the actin cytoskeleton downstream of Dvl are required for the uniform production of distal wing hairs, these results suggest actin dynamics have a role upstream to the establishment of planar polarity. However, the precise role of the actin cytoskeleton and Cofilin in this process remains an open question.

1.2.3 Embryonic phenotypes of the *Vanl2*^{Lp} mutant mouse

The mouse model of craniorachischisis was first isolated as a dominant, spontaneous mutation known as *looptail* (*Lp*). Heterozygous *Lp* mice have a signature kinked or looped tail and a behavioral phenotype that results from a disruption of the polarized stereociliary bundles in the organ of Corti. Homozygous *Lp* embryos display an open neural tube from the midbrain-hindbrain region to the most caudal regions of the spinal cord, as well as skeletal defects, and die shortly before or at birth (Greene et al., 1998; Musci and Mullen, 1990). Subsequent genetic studies identified *van Gogh-like2*, a mouse homologue of *Drosophila Strabismus/van Gogh*, as the mutated gene in *Lp* mice (Kibar et al., 2001b; Kibar et al., 2003; Murdoch et al., 2001). *Vangl2* encodes 521-amino acid protein, containing four transmembrane domains and an intracellular PDZ-binding motif at its C-terminus. The *Lp* mutant is associated with a missense mutation, S464N, in a conserved amino acid in the C-terminal

cytoplasmic domain. A second allele of *Vangl2*, *Lp^{m1Jus}*, was later recovered in an ENU induced chemical screen (Kibar et al., 2001a). This allele also has a missense mutation, D225E, in the C-terminal cytoplasmic domain. Despite the fact that neither of the two *Lp* alleles directly affects the amino acid sequence of the PDZ-binding motif, both alleles disrupt the interaction of *Vangl2* and *Dvl* *in vitro* (Torban et al., 2004). Subsequent studies have shown that the S464N mutation in *Vangl2^{Lp}* disrupts the interaction of *Vangl2* with the COPII complex member *Sec24b* (Merte et al., 2010; Wansleben et al., 2010), and that *Vangl2* protein harboring the S464N mutation cannot be trafficked from the ER to the Golgi, and therefore cannot contribute to PCP in the embryo.

As in other mouse PCP mutants, *Vangl2^{Lp}* homozygous embryos display craniorachischisis (Musci and Mullen, 1990). Craniorachischisis in these mutants has been attributed to defects in CE, though no experiments have specifically demonstrated the cell behaviors underlying CE in the neural tube, or the cellular defects in *Vangl2^{Lp}* mutants during this process. Convergent extension in other tissues, such as narrowing of the somites and elongation of the notochordal plate, are only mildly affected in *Vangl2* mutants, in contrast to the stronger defects observed in zebrafish mutant or *Xenopus* morpholino knockdown embryos (Darken et al., 2002; Greene et al., 1998; Park and Moon, 2002; Wallingford and Harland, 2002). There are also no defects in left-right asymmetry in the *Vangl2^{Lp}* single mutants. These mild phenotypes in mouse embryos are due to genetic redundancy between *Vangl1* and *Vangl2*, as the CE defects in the axial mesoderm (midline) and somites of *Vangl1 Vangl2* double mutants is

stronger than either mutant alone, and the double mutants also have defects in left-right asymmetry (Song et al., 2010).

The midline is formed from cells that migrate rostrally from the node and eventually lie under the neural plate, inducing the floor plate of the neural tube. Tissue-level analysis has shown that the notochordal plate and floor plate are wider in PCP mutants (Greene et al., 1998; Wang et al., 2006a; Ybot-Gonzalez et al., 2007); in Chapter Four of this thesis I will describe experiments using high resolution imaging that define the cellular basis of PCP-dependent narrowing of the midline. The initiation of left-right asymmetry also depends on planar polarity. The PCP pathway is required for the posterior location of nodal cilia, as the basal bodies of cilia remain at the middle of the cells of the node in *Vangl1 Vangl2* double mutants and the *Dvl1 Dvl2 Dvl3* compound mutants (Hashimoto et al., 2010; Song et al., 2010). The *Vangl2 Cfl1* double mutant embryos had PCP phenotypes as strong as those seen in *Vangl1 Vangl2* double mutants, including short and wide somites, failure of convergent extension of the midline and randomization of left/right asymmetry caused by the failure to properly polarize nodal cilia. In Chapter Five, I will show that Cofilin acts in concert with Vangl2 during the initiation of PCP to control the initial asymmetric localization of the core PCP protein Celsr1 to the apical membrane. Thus, dynamic rearrangements of the actin cytoskeleton are required for the establishment of PCP signaling in the mouse.

CHAPTER TWO

2 MATERIALS AND METHODS

2.1 Mapping and genotyping

To isolate DNA for genotyping adult ear punches or extraembryonic tissue samples were incubated at 55°C in a Proteinase K solution (30 µg/mL Proteinase K in 1X PCR buffer) for 16-18 hours, the enzyme was then heat inactivated prior to use in PCR reactions. All PCR reactions were run with equal parts 2X PCR Mix (2X PCR buffer + 1.5 mM MgCl₂ + 400 µM of each dNTP) and a 1:200 dilution of DNA samples; 0.15 µL of Platinum-Taq (Roche) was added per 20 µL reaction and PCR was run according to standard procedures, varying the annealing temperature (55-62°C) as needed for each specific primer pair. After PCR, samples that required digestion by restriction enzymes were incubated with 0.33X of the appropriate buffer (1 µL) and 0.5 µL of enzyme in 30 µL reactions for 16-18 hours. DNA products were analyzed on 4% agarose gels in TBE.

2.1.1 Mouse strains

TOPGAL

Mice carrying the *TOPGAL* transgene (DasGupta and Fuchs, 1999) were provided by Dr. Elaine Fuchs (Rockefeller University) and were genotyped by

PCR using primers to detect bacterial β -galactosidase (F: 5'atactgtcgtcgtcccctcaaactg, R: 5'accacgctcatcgataatttcac).

Hex-GFP

Mice carrying the *Hex-GFP* transgene (Rodriguez et al., 2001) were provided by Dr. Terry Magnuson (The University of North Carolina at Chapel Hill) and were genotyped by PCR using primers to detect *GFP* (Jackson Labs; IMR872: 5'aagttcatctgcaccaccg, IMR873: 5'tgctcaggtagtggtgtcg).

Axin2^{canp}

Mice carrying the *Axin2^{canp}* mutation were isolated in our lab in a forward genetic screen (Qian et al., 2011) and were genotyped by PCR using primers to detect a BamHI RFLP, which was cleaved in the mutant but not the wild-type sequence (F: 5'gtttggtggactggaccttg, R: 5'agacgctctccctcacat).

APC^{Min/J}

Mice carrying the *APC^{Min/J}* mutation (Su et al., 1992) were purchased from The Jackson Laboratory (stock# 002020) and were genotyped by PCR using primers to detect the wild-type and nonsense alleles in a multiplex reaction (F: 5'ttctgagaaagacagaagtta, wild-type R: 5'gcatcccttcacgttag, Min/J R: 5'ttcactttggcataaggc).

Vangl2^{Lp}

Mice carrying the *Vangl2^{Lp}* mutation (Kibar et al., 2001b) were purchased

from The Jackson Laboratory (Stock # 00020) and were genotyped by PCR using primers to detect a MwoI RFLP, which was cleaved in the wild-type but not the mutant sequence (F: 5'cgttggctggccaaacagtgaggcttggtg, R: 5'tcacacagaggctctccgactgc).

***Cfl1*^{C5}**

Mice carrying the *Cfl1*^{C5} mutation were isolated in our lab in a forward genetic screen (Mahaffey et al., 2013) and were genotyped by PCR using primers to detect a BclI RFLP, which was cleaved in the mutant but not the wild-type sequence (F: 5'gtcaagatgctgccagacaa, R: 5'ccccacacctggaataatt).

***Cfl1*^{tm1Wit}**

Mice carrying the *Cfl1*^{tm1Wit} mutation (Gurniak et al., 2005) were provided by Dr. Walter Witke (Rheinische Friedrich-Wilhelms University) and were genotyped by PCR using primers to detect the wild-type and targeted alleles in a multiplex reaction (F: 5'cgctggaccagagcacgcggcatc, wild-type R: 5'ctggaagggtgttacaaccctgg, tm1Wit R: 5'catgaagggtcgcaagtcctcaac).

***Dstn*^{corn1}**

Mice carrying the *Dstn*^{corn1} mutation (Ikeda et al., 2003) were purchased from The Jackson Laboratory (stock# 001649) and were genotyped by PCR using primers to detect the wild-type and deletion alleles in a multiplex reaction (F: 5'gtcccatgaatgtgaattgc, wild-type R: 5'ccctggtgaccttccttctatc, corn1 R: 5'tggcactcctgctgtcac).

centrifugation. Half of the lysate was used to assay for β -galactosidase activity, and the other half was used to determine protein concentration. β -galactosidase activities were normalized to protein concentration, which was determined with BCA Protein Assay kit (Pierce). Samples for analysis contained extracts from one to three litters of cultured embryos.

For Western blotting, samples were lysed in 100 μ L Mad2 lysis buffer (50 mM Tris, pH 7.5 + 150 mM NaCl + 1% Nonidet P-40 + 10% glycerol + 2 mM EDTA) containing protease and phosphatase inhibitors (50 mM NaF + 0.1 mM orthovanadate + 15 mM phenylmethylsulfonyl fluoride + 15 mM 4-nitrophenyl phosphate) (Wassmann and Benezra, 1998), and the extracts were cleared by centrifugation. Samples for analysis contained extracts from one litter of cultured embryos, or the indicated number of wild-type or mutant embryos. ImageJ (NIH) was used to quantify protein levels from Western blots.

***In situ* probes**

The probes used for *in situ* hybridization were: *Brachyury* (*T*) (Herrmann, 1991), *Esrr β* (Luo et al., 1997), *Mash2* (Rossant et al., 1998), *Meox1* (Candia et al., 1992) and *Nodal* (Conlon et al., 1994).

Western blot antibodies

For all Western blots antibodies were diluted at the given concentration in TBST + 5% BSA. Axin1 (Cell Signaling) 1:5000, Cofilin (Sigma) 1:5000, phospho-Cofilin (Ser3; Cell Signaling) 1:5000, LRP6 (Cell Signaling) at 1:1000, phospho-LRP6 (Ser1490; Cell Signaling) 1:5000, α -tubulin (Sigma) at 1:10000,

β -catenin (BD Biosciences) at 1:10000, phospho- β -catenin (Ser33/37/Thr41; Cell Signaling) at 1:5000 and phospho- β -catenin (Thr41/Ser45; Cell Signaling) at 1:5000.

2.2.1 Immunofluorescence and microscopy

All dissections for protein immunofluorescence analysis were done in ice-cold PBS + 4% BSA and embryos were fixed for 60-90 minutes in PBS + 4% paraformaldehyde at 4°C. Immunofluorescence staining of cryosections was done according to previously established lab protocols (Lee et al., 2010). For whole mount staining, embryos were rinsed three times after fixation in PBS, and then blocked for 1-3 hours in IF buffer (PBS + 0.1% Triton-X100 + 1% heat-inactivated goat serum) at 4°C. Primary antibody was diluted in IF buffer and embryos incubated overnight at 4°C. The next day, embryos were washed three times for 15 minutes in IF buffer at 4°C, and then incubated 2-3 hours with Alexa-488- and/or Alexa-633-conjugated secondary antibodies (Sigma) diluted 1:400 in IF buffer at 4°C. Next, embryos were rinsed three times with PBS then incubated for 1-2 hours in with TRITC-conjugated phalloidin (Sigma) diluted 10 U/mL and DAPI (Sigma) diluted 1:400 in IF buffer at room temperature. Finally, embryos were rinsed with PBS, and then mounted for imaging. For neural plate, node and midline imaging, embryos were flat-mounted dorsal-side up on a slide, and mounted with a coverslip using 25-40 μ L VectaShield (Vector Labs). To flatten the embryos small cuts were made lateral to the node with a tungsten needle.

After mounting, slides were imaged with a LSM510 confocal microscope

(Carl Zeiss) or a DeltaVision microscope (Applied Precision). Images taken with the DeltaVision were deconvolved after imaging. Databases were analyzed using the Volocity software suite (Improvision) and ImageJ (NIH). Unless otherwise noted, all confocal images are single optical slices. The immunofluorescence data presented are representative images of at least three stained embryos per genotype or per drug treatment.

Samples for scanning electron microscopy (SEM) were dissected in ice-cold PBS and fixed overnight in PBS + 2.5% glutaraldehyde, then processed and observed according to standard procedures (Sulik et al., 1994) using a Supra-25 Field Emission Scanning Electron Microscope (Carl Zeiss).

Antibodies for immunofluorescence staining

For immunofluorescent staining, all antibodies were diluted at the given concentration in IF buffer. Arl13b antibody, produced in rabbits by Dr. Tamara Caspary in our lab (Caspary et al., 2007) was used at 1:800. Brachyury (T) antibody (Lee et al., 2010), a gift from Dr. Frank Conlon (The University of North Carolina at Chapel Hill), was used at 1:3200. Celsr1 antibody (Devenport and Fuchs, 2008), a gift from Dr. Elaine Fuchs (The Rockefeller University), was used at 1:800, and Vangl2 antibody (Montcouquiol et al., 2006), a gift from Dr. Mireille Montcouquiol (University of Bordeaux), was used at 1:800. Commercially available antibody dilutions were: Cofilin (Sigma) 1:1000, E-Cadherin (Sigma) 1:1000, EEA1 (Abcam) 1:800, Fibronectin (Sigma) 1:2500, GM-130 (BD Biosciences) 1:800, Par3 (Millipore) 1:1000, Pericentrin (Covance) 1:800, phospho-Myosin Light Chain 2 (Cell Signaling) 1:200, Rab5 (Cell Signaling)

1:400, Rab8 (BD Biosciences) 1:400, Rab11 (Cell Signaling) 1:400, Sox2 (BD Biosciences) 1:2000 and ZO-2 (BD Biosciences) 1:1000.

2.2.2 Embryo culture

Embryos for culture were dissected in 37°C DMEM/F12 + 10% rat serum. After dissection, embryos were transferred to a glass-bottomed culture dish. Static embryo cultures were performed in media containing 50% rat serum/50% DMEM/F12 and incubated at 37°C with 5% CO₂ for 4-18 hours (as indicated).

Pharmacological inhibitors

A stock of CHIR99021 (Stemgent) in DMSO was diluted in the culture medium to 1-40 µM (0.05-0.2% DMSO). A stock of jasplakinolide (Sigma) in DMSO was diluted in the culture medium to 10 nM (0.01% DMSO). A stock of IWP-2 (Sigma) in DMSO was diluted in the culture medium to 5-50 µM (0.1-1.0% DMSO). A stock of IWR-1 (Sigma) in DMSO was diluted in the culture medium to 50-100 µM (0.25-0.5% DMSO). A stock of MG132 (Sigma) was diluted in the culture medium to 10-30 µM (0.1-0.3% DMSO). A stock of nocodazole (Sigma) was diluted in the culture medium to 3 µM (0.033% DMSO). A stock of taxol (R&D) was diluted in the culture medium to 10 nM (0.01% DMSO). Control embryos were cultured in 0.1-1.0% DMSO (to match drug culture conditions).

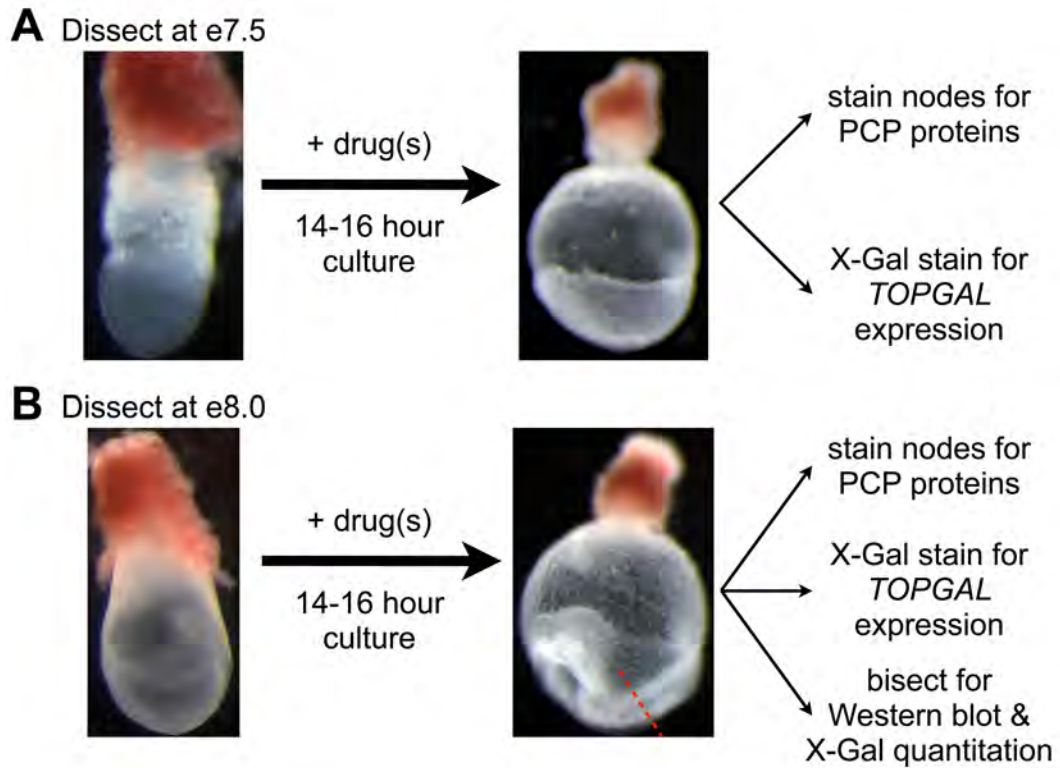


Figure 2.1: Embryo culture time-lines.

All embryos for culture were dissected in 37°C DMEM/F12 + 10% rat serum and transferred to a glass-bottomed culture dish with DMEM/F12 + 50% rat serum and incubated at 37°C with 5% CO₂. **(A)** To obtain mid/late headfold stage embryos after culture, wild-type embryos were dissected at e7.5. From these dissections the late streak and early bud stage embryos were put in static culture with drug or DMSO for 14-16 hours. The next day headfold stage embryos were removed from culture. For immunofluorescence staining, embryos were immediately fixed with 4% PFA on ice and antibody stained; alternatively embryos carrying the *TOPGAL* transgene were fixed with 2% Glutaraldehyde on ice and X-Gal stained. **(B)** To obtain embryos with 6-8 somites after culture, wild-type embryos were dissected at e8.0. From these dissections the late headfold and early somite stage embryos were put in static culture with drug or DMSO for 14-16 hours. The exceptions were embryos treated with the protease inhibitor, MG132, which were only cultured for 4-6 hours. After culture, embryos were fixed for immunofluorescence or X-Gal staining as above. To prepare protein lysate for Western blotting and β -Galactosidase quantitation, embryos with 6-8 somites after culture were bisected at the border of the most caudal somite and the presomitic mesoderm (dashed red line). The anterior halves of the embryos were pooled into the 'heads' and the posterior halves were pooled into the 'tails'.

2.2.3 Embryonic stem cell culture

E14 mouse embryonic stem (ES) cells (ATCC) were maintained in a pluripotent state with leukemia inhibitory factor (Millipore), diluted to 1250 U/mL in standard feeder-free mouse ES cell media (Tremml et al., 2008). Vectors containing the luciferase reporters *TOPFLASH*, *FOPFLASH* and *Renilla* were electroporated (250V, 500 μ F) into the cells, diluted 7×10^6 cells/mL in PBS, in a 4 mm electroporation cuvette (Bio-Rad). The cells were then replated in standard media for 2 hours prior to drug treatment. Wnt3a conditioned media was made by culturing L-cells expressing a *Wnt3a* construct in standard feeder-free ES cell media (minus leukemia inhibitory factor) for 48-72 hours, and then filtering the supernatant. *Luciferase* and *Renilla* expression was determined using the Dual-Luciferase Reporter Assay System (Promega).

2.3 Data analysis and statistics

All statistical analysis was performed using PRISM software (GraphPad); all values are shown as mean \pm s.d., and data were analyzed with one-way ANOVA followed by the Newman-Keuls post-test.

2.3.1 Image analysis

To determine the longest axis of the cell for *en face* images of the neural

plate, individual cells were outlined in ImageJ (NIH). The longest axis of the bounding rectangle was then overlaid onto the original image. From this data the angle of the longest axis with respect to the midline was determined, and these angles were plotted in a histogram.

To analyze the distribution of T-positive (T^+) notochordal plate cells, the Cell-Counter plugin for ImageJ (NIH) was used to count every T^+ nucleus in a row of the notochord. The number of rows counted was used to find the length of the tissue. Measurements of the stained tissue were made using the line draw feature of Volocity (Improvision); this was also used to determine the length to width ratio (LWR) of *Meox1-stained* somites. The midline width measurements are an average of ten equally spaced lines, ranging from the beginning to the end of the notochordal plate.

To determine the relative position of the basal body, cells from the central node region were outlined individual using ImageJ (NIH) and the length of the *x-axis* (parallel to the left-right axis of the embryo) and *y-axis* (parallel to the anterior-posterior axis of the embryo) was measured. The position of the basal body was determined by finding the center of mass of the Pericentrin signal, isolating a coordinate point within the cell. The *y*-value of this coordinate point was then divided by total length of the *y-axis*, such that a point on the anterior face of the cell would have a value of 1, and a point on the posterior face of the cell would have a value of 0. The same equation was applied to determine the relative position of the basal body along the *x-axis*; with 0 representing a basal body polarized the left side of the image (right side of the embryo) and 1

representing a basal body polarized to the right side of image (corresponding to the left side of the embryo). To delineate between the central pit and peripheral cells of the node, basal body localization was determined for 4-5 rows of node cells from the outside moving inward. This was repeated around the circumference of the node, and these cells were labeled as the periphery, the remaining cells were grouped as the central pit. This organization was a rough approximation of the results from lineage tracing experiments in the node (Hashimoto et al., 2010), and erred on the side of including central pit cells in the periphery group, not visa versa.

To quantify the degree of planar polarization of Celsr1 and Rab11, images containing Celsr1 or Rab11 and phalloidin staining were transformed into hyperstacks, such that the red and green channels of the images were treated as separate images within the same stack. The cell borders were then traced with individual lines along the phalloidin channel, and these lines were used to quantify the average pixel intensity for both the phalloidin and Celsr1/Rab11 staining. The Celsr1/Rab11 signal intensities were then normalized to the phalloidin signal. These data were organized according to the angle of the line that was drawn. For all images and quantification, the anterior of the embryo is toward the top. I measured the intensities from over 40 node cells per embryo, which totaled ~150 cell borders (owing to shared borders); at least two embryos per genotype were quantified.

CHAPTER THREE

3 AXIN PROMOTES CANONICAL WNT SIGNALING IN THE LATE PRIMITIVE STREAK

Axin2 is a potent negative regulator of the canonical Wnt pathway in all vertebrate cells, capable of reforming the β -catenin destruction complex after ligand induced pathway activation (Jho et al., 2002). *Axin2* expression is dependent upon active Wnt signaling and nuclear β -catenin, unlike *Axin1*, which is ubiquitously expressed (Aulehla et al., 2003; Li et al., 2012). As a Wnt target gene, *Axin2* is constitutively expressed in many cancer cell lines that have mutations in *APC* or N-terminal truncations in *β -catenin* (Lustig et al., 2002), but in these contexts it is unable to reconstitute an active destruction complex due to the initial oncogenic mutations. However, *Axin2* has been found to be epigenetically silenced in other colorectal patients, and in cell lines from these patients the addition of exogenous *Axin2* is capable of reducing Wnt signaling, slowing the growth potential of these cell *ex vivo* (Koinuma et al., 2006). These data demonstrate that like *Axin1*, *Axin2* is a tumor suppressor, highlighting the importance of the *Axin2* negative feedback loop in adult tissue homeostasis.

Axin2 is also expressed in response to active Wnt signaling in the mouse embryo; however, the *Axin2* negative feedback loop appears to be largely dispensable for normal development as *Axin2* null mice are viable and fertile, and have only subtle defects in skull morphogenesis and tooth development (Lammi

et al., 2004; Yu et al., 2005). Prior to the identification of the *Axin2^{canp}* allele, there was no data indicating that *Axin2* could promote Wnt signaling (Qian et al., 2011).

The discovery that the homozygous lethal *canp* mutation was an allele of *Axin2* suggested that this allele may be a gain of function mutation (Qian et al., 2011). The *Axin2^{canp}* mutation leads to a V26D substitution in an evolutionarily conserved N-terminal motif of *Axin2* and confers a 3-fold increase in the half-life of Axin2 protein (Figure 1.2). The N-terminal motif disrupted by the *canp* mutation is directly involved in the binding of Axin2 by Tankyrase (Morrone et al., 2012). Tankyrase is a member of the Poly-ADP-ribose polymerase (PARP) family of proteins, which catalyzes the transfer of ADP to target proteins (Schreiber et al., 2006). Tankyrase was originally identified as a factor required for telomere elongation (Smith and de Lange, 2000), but it was recently shown that poly-ADP-ribosylation of Axin by Tankyrase leads to its ubiquitination and proteasomal degradation (Huang et al., 2009). The Tankyrase-dependent degradation of Axin is distinct from the Wnt ligand-induced Axin degradation pathway as Axin degradation in response to Wnt ligand can occur in the absence of the N-terminal Tankyrase binding domain (Cselenyi et al., 2008); what regulates the Tankyrase-Axin interaction is unknown. Recently a class of small molecule inhibitors of the Wnt pathway was discovered based on their ability to reduce β -catenin activity in cancer cell lines. Two of these compounds target Tankyrase, stabilizing Axin1 and Axin2 in cultured cells (Chen et al., 2009; Huang et al., 2009).

Stabilized Axin2 protein in the *Axin2^{canp}* mutants is most likely due to the

mutation disrupting the motif that binds Tankyrase, and this N-terminal motif of Axin is not required for interactions with the other components of the β -catenin destruction complex, nor is it required for interactions with Dvl. This suggests that the overall function of Axin2 protein in the *Axin2^{canp}* mutant is not changed, and that the phenotypes associated with this mutation are due to the increased Axin2 levels alone. Therefore, I investigated the Axin/Tankyrase interaction in the context of wild type *Axin1* and *Axin2*, examining how Tankyrase inhibitors affect canonical Wnt activity in wild-type embryos. The aims of these experiments were twofold: first to confirm that the stabilization of Axin2 protein in the *Axin2^{canp}* embryos could be attributed to inhibiting the interaction between Axin and Tankyrase and second, to determine by independent means that stabilized Axin could promote canonical Wnt signaling in the late primitive streak. Through embryo culture experiments I showed that stabilized wild-type Axin1 and Axin2 promote Wnt signaling in the late primitive streak; I further showed that the positive role for Axin in the canonical Wnt transduction pathway is ligand and GSK3 β dependent. Together, these results suggest that Wnt signaling in the late primitive streak is more reliant on the activity of CK1 and GSK3 β at the membrane than any other cell type in the early embryo.

3.1 IWR-1-treated embryos phenocopy *Axin2^{canp}* mutants

Wnt signaling is required for the initiation and distal elongation of the primitive streak in the mouse embryo (Marikawa, 2006). During the early stages of gastrulation (e7.0-e7.5) expression of the Wnt reporter *TOPGAL* is uniformly

high in the posterior of the embryo, as almost every epiblast cell in this region is responding to Wnt ligands expressed in the primitive streak. One day later in development, the primitive streak is confined to the tailbud region of the embryo, and a smaller proportion of epiblast cells express the Wnt reporter (Figures 1.4A, C and 3.1A, C). Wnt signaling in the primitive streak at both of these stages is required for mesoderm induction, but the regulation of the pathway appears to be different, as homozygous *Axin2^{canp}* embryos had a decrease in Wnt signaling at e7.5 and an increase in Wnt signaling at e8.5 (Figure 1.4B, D).

To determine whether these two distinct effects on Wnt signaling were due solely to increased Axin2 levels, or if they revealed novel activities of the Axin2 protein in the *Axin2^{canp}* mutant, I tested how Tankyrase inhibitors affected canonical Wnt activity in wild-type embryos carrying the *TOPGAL* reporter. In initial experiments, both IWR-1 and XAV939 inhibited β -galactosidase (β -Gal), as revealed by X-Gal staining, expression in e7.5 embryos from the *TOPGAL* reporter, but IWR-1 gave stronger and more consistent results, as previously reported in explanted mouse kidneys (Karner et al., 2010); therefore IWR-1 was used in all subsequent experiments.

When bud-staged (e7.25) wild-type embryos were cultured for 14-18 hours in the presence of 100 μ M IWR-1, they showed an almost complete loss of X-Gal staining in the primitive streak compared with control embryos (Figure 3.1A-B); the reduction in *TOPGAL* expression at this stage was much stronger than that observed in *Axin2^{canp}* mutants (Figure 1.4A-B). When e8.0 wild-type embryos (late headfold-early somite stage) were cultured either in the presence

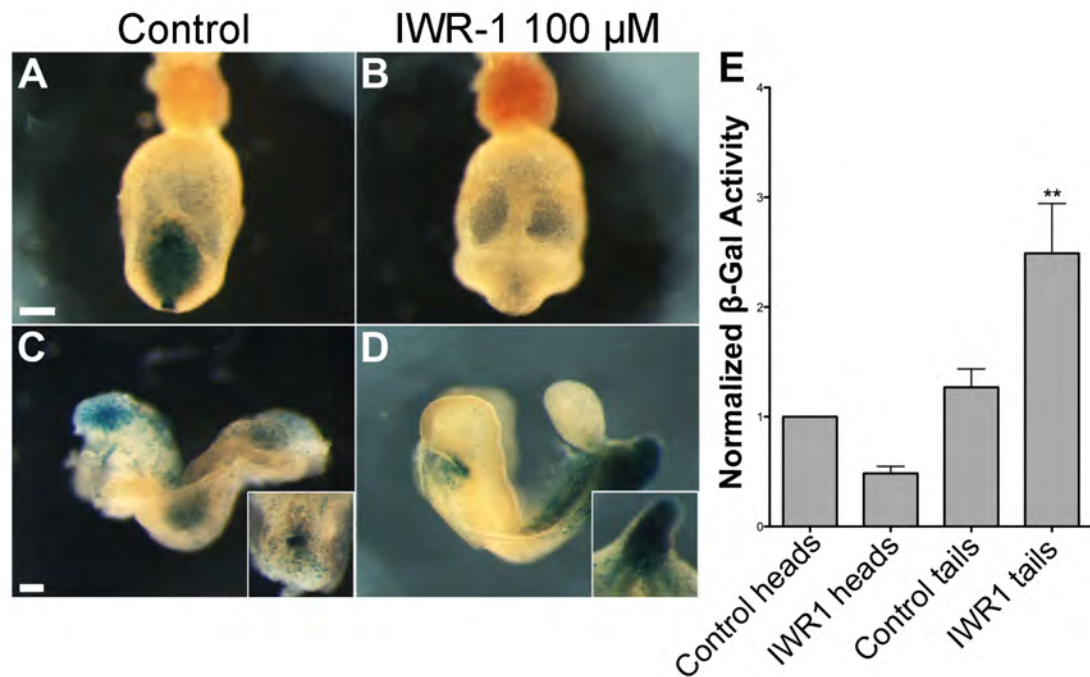


Figure 3.1: Tankyrase inhibition alters Wnt signaling in wild-type embryos.

(A–D) X-Gal stained wild-type embryos carrying one copy of the *TOPGAL* transgene, cultured with DMSO (A, C) and 100 μM IWR-1 (B, D). (A–B) Posterior views of late headfold embryos after 14–18 hours of culture, showing decreased expression of *TOPGAL* in the primitive streak of IWR-1-treated embryos. (C–D) Lateral views of 6-somite staged embryos after culture, showing reduced *TOPGAL* expression in the head, but increased expression in the primitive streak and PSM of IWR-1-treated embryos. Insets in C and D are dorsal and ventral views of the primitive streak, respectively. The unusual shape of the tail is characteristic of drug treated embryos. (E) β-Galactosidase activity in anterior (head) and posterior (tail) halves of control and IWR-1-treated 6-somite embryos, normalized to the activity in control heads. β-Galactosidase activity was measured in three independent experiments, with six to eight embryos per condition in each experiment. Scale bars: 100 μm.

or absence of 100 μ M IWR-1, they developed 6-10 somite pairs and had beating hearts after 14-18 hours in culture, suggesting that this concentration of IWR-1 did not disrupt overall embryo health and development. After culture, *TOPGAL* expression was diminished in the head and somite regions in embryos cultured in the presence of IWR-1 compared with controls (Figure 3.1C-D), as expected due to the increased level of Axin. In contrast to the inhibition of Wnt signaling in the anterior of the embryo, X-Gal staining appeared to be elevated in the primitive streak of early somite stage embryos cultured in the presence of IWR-1 (Figure 3.1C-D), similar to the phenotype of the *Axin2^{canp}* embryos at this stage (Figure 1.4C-D). To quantitate the TOPGAL expression at early somite stages, embryos were cut into anterior and posterior halves at the anterior border of the presomitic mesoderm (PSM) after culture and β -galactosidase activity in each lysate was assayed. β -gal activity in the anterior half of IWR-1-treated embryos was reduced by 52% compared to controls, similar to the results from *Axin2^{canp}* embryos (Figure 3.1E; Qian et al., 2011). In contrast, the β -galactosidase activity in the posterior half of IWR-1-treated embryos increased by 2.5-fold and 2.0-fold compared to the anterior or posterior regions of control embryos, respectively ($P < 0.01$), and was 5.0-fold greater than in the anterior half of drug-treated embryos ($P < 0.01$) (Figure 3.1E). Thus, inhibition of Tankyrase, like the *Axin2^{canp}* mutation, decreased canonical Wnt activity in the early primitive streak, as well as in the head and somites of older embryos, but increased Wnt activity in the late primitive streak.

3.1.1 Elevated Wnt signaling in response to IWR-1 is ligand dependent

The previous results, along with the data from *Axin2^{canp}* mutants, showed by two different means that stabilized Axin could promote Wnt signaling in the late primitive streak. It has been proposed that in addition to its role as a negative regulator of β -catenin, Axin may play a positive role in canonical Wnt signaling by recruiting the Axin/GSK3 β /CK1 complex to Wnt bound Fzd/LRP6 receptors at the membrane (Bilic et al., 2007; Li et al., 2012; Mao et al., 2001; Zeng et al., 2005; Zeng et al., 2008); in this model, the GSK3 β and CK1 dependent phosphorylation of LRP5/6 is important for the nuclear localization of β -catenin. I therefore assayed the level of phospho-LRP6 and other components of Wnt signaling in IWR-1-treated embryos. Because IWR-1 activated *TOPGAL* specifically in the late streak and PSM, and reduced the expression of the reporter in all anterior tissues, embryos were again bifurcated after culture at the anterior boundary of the PSM prior to lysis.

As expected, the level of Axin1 protein was elevated in both the anterior and posterior regions of embryos cultured in the presence of 100 μ M IWR-1 (Figure 3.2A). Quantifying the Axin1 levels from six independent experiments revealed that IWR-1 treatment resulted in a 1.9-fold and 2.5-fold increase of Axin1 protein in the anterior and posterior regions of the embryo, respectively, compared to DMSO controls, and these increases were both statistically significant ($P < 0.05$) (Figure 3.2B).

IWR-1 treatment increased the levels of phosphorylated LRP6 in the posterior half of the embryo, compared to either the anterior half of drug-treated

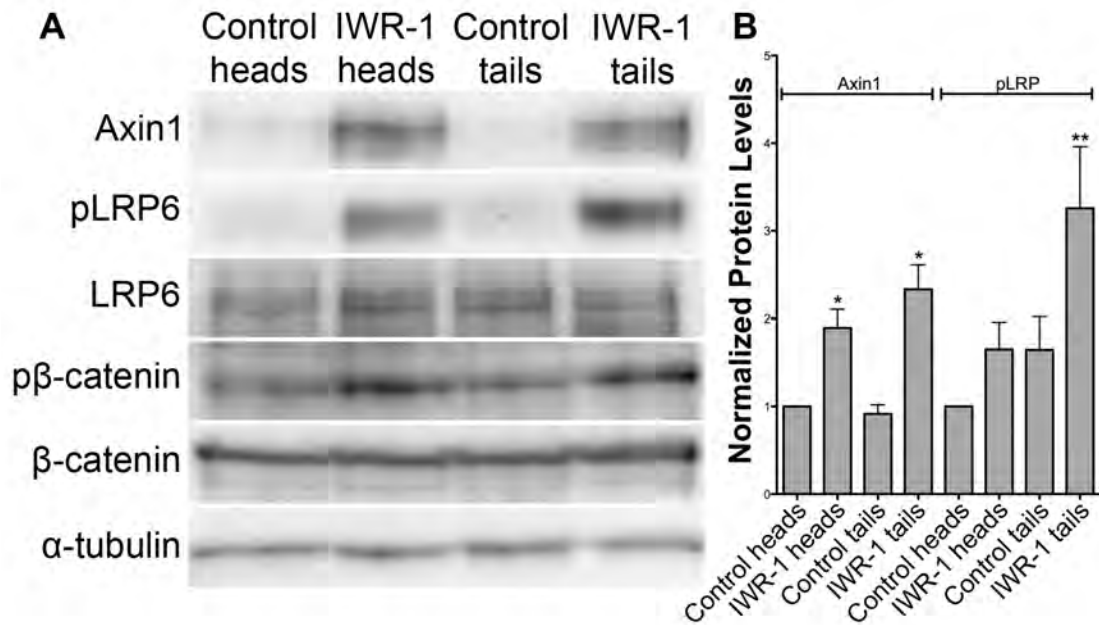


Figure 3.2: IWR-1 stabilizes Axin1 and increases LRP6 phosphorylation.

(A) Representative Western blots showing increased levels of Axin1 and N-terminal phosphorylation of β -Catenin at Ser33/37/Thr41 in 6-somite embryos treated with 100 μ M IWR-1 for 14 hours compared with DMSO controls. Embryos treated with IWR-1 also had a higher level of phosphorylated LRP6 in the tails. **(B)** Analysis of Western blot data from six independent experiments in which four to eight embryos were cultured per condition in each experiment. Protein levels were normalized to α -tubulin, and values were normalized to protein levels in DMSO-treated heads. Axin1 levels were increased 1.90-fold in IWR-1-treated heads ($P < 0.05$) and 2.33-fold in treated tails ($P < 0.05$). The change in phosphorylated LRP6 levels in treated heads was variable and not significant, whereas the 3.26-fold increase in IWR-1-treated tails was significant ($P < 0.01$).

embryos or the posterior half of control embryos (Figure 3.2A). Quantification of Western blots from six independent experiments showed a statistically significant ($P < 0.01$) 2.0-fold increase in the level of phosphorylated LRP6 in the caudal half of IWR-1-treated embryos compared to the same region in control embryos, and a 1.4-fold increase in the posterior versus anterior half of treated embryos ($P < 0.05$) (Figure 3.2B). While an increase in phospho-LRP6 was detected in the anterior half of IWR-1-treated embryos in some experiments (Figure 3.2A), this result was variable, and quantification revealed no significant difference in phospho-LRP6 in treated versus untreated heads (Figure 3.2B). The variability in the phospho-LRP6 signal in the anterior half of IWR-1-treated samples was likely due to the inclusion of some PSM tissue in the anterior lysate. Therefore, this data shows that elevated levels of phosphorylated LRP6 are only found in regions of the embryo with increased *TOPGAL* expression.

The primary role of Axin is to serve as a scaffold for the β -catenin destruction complex, and genetically *Axin1* is a negative regulator of Wnt signaling, as *Axin1* mutants have phenotypes consistent with ectopic Wnt signaling (Zeng et al., 1997). In addition, IWR-1 treatment caused a decrease in *TOPGAL* expression in the majority of embryonic tissues. Therefore, I also analyzed the activity of the β -catenin destruction complex in IWR-1-treated embryos. To assay for destruction complex activity, embryo lysates were probed with an antibody that recognizes phospho-Ser33/37/Thr41- β -catenin. These are the sites on β -catenin that are phosphorylated by GSK3 β , and therefore indicate CK1 α activity as well, as CK1 α is required to prime β -catenin for subsequent

GSK3 β phosphorylation (Amit et al., 2002; Hagen and Vidal-Puig, 2002). Despite decreased levels of *TOPGAL* only in the anterior half IWR-1-treated embryos, phospho-Ser33/37/Thr41- β -catenin levels were uniformly increased in both anterior and posterior embryo lysate (Figure 3.2A). Thus, Tankyrase inhibition increased the amount of destruction complex in all cells.

The previous results showed that the increased levels of Axin1 in IWR-1-treated embryos led to increased destruction complex activity in the entire embryo. However, in the late primitive streak elevated levels of Axin1 are also correlated with an increase in both phospho-LRP6 and active Wnt signaling. In other model systems, the phosphorylation of LRP6 by GSK3 β and CK1 γ requires Wnt ligand binding to Fzd and LRP (Zeng et al., 2008). To determine whether Wnt ligands were required for the elevated Wnt signaling in the late primitive streak of IWR-1-treated embryos, embryos were cultured in the presence of both IWR-1 and IWP-2, which inhibits Porcupine and stops the secretion of Wnt ligands (Biechele et al., 2011; Chen et al., 2009). In contrast to IWR-1, embryos treated with 25 μ M IWP-2 showed a uniform decrease in Wnt signaling in the entire embryo (Figure 3.3B-C), consistent with the role of Porcupine in Wnt ligand production. Embryos cultured with both IWR-1 and IWP-2 had the same expression pattern of *TOPGAL* as embryos treated with IWP-2 alone (Figure 3.3), suggesting that the increased expression of Wnt target genes in the late primitive streak in response to stabilized Axin requires Wnt ligands.

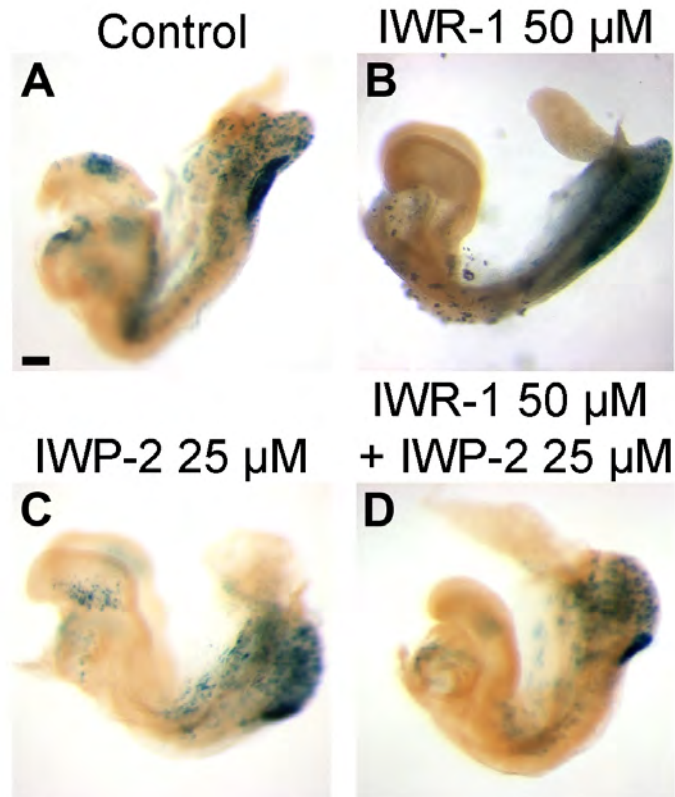


Figure 3.3: Stabilized Axin requires ligand to increase *TOPGAL* expression.

(A–D) Lateral views of 6-8-somite staged wild-type embryos carrying one copy of the *TOPGAL* transgene. All embryos were stained with X-Gal after 16-hour culture with DMSO (A), 50 μ M IWR-1 (B), 25 μ M IWP-2 (C) and the combination of 50 μ M IWR-1 and 25 μ M IWP-2 (D). Embryos treated with IWR-1 showed reduced *TOPGAL* expression in the head, and increased in the tail (B). In contrast, the Porcupine inhibitor reduced the Wnt reporter in all tissues compared to DMSO controls (A, C). As expected, embryos cultured with both IWR-1 and IWP-2 showed reduced Wnt signaling in the head and somites, but also showed reduced Wnt activity in the primitive streak, similar to embryos treated with IWP-2 alone (D). Scale bar: 100 μ m.

3.1.2 Wnt pathway regulation in embryonic stem cells

The late primitive streak is a population of progenitor cells that is required to supply mesodermal lineages to the growing embryo. One of the key Wnt ligands involved in maintaining the primitive streak at later stages is Wnt3a. While several Wnt ligands, including Wnt5a and Wnt11, are also expressed in the late streak, in the absence of Wnt3a there are no somites caudal to the forelimbs in e9.5 embryos, and at e12.5 there are no mesodermal structures caudal to the umbilicus (Takada et al., 1994); thus, Wnt3a is required to maintain the late primitive streak. Mouse embryonic stem (ES) cells also require Wnt pathway activation to maintain their pluripotency, and Wnt3a is capable of maintaining undifferentiated ES cells in culture (Berge et al., 2011). Because both the late primitive streak and ES cells are progenitor populations that respond to Wnt3a, I next tested whether IWR-1 could promote Wnt target gene expression in ES cells.

ES cells transfected with the Wnt reporter *TOPFLASH* were cultured with 10 and 20 μ M IWR-1 with or without Wnt3a conditioned media for 24 hours, then assayed for reporter expression. As a positive control, transfected ES cells were also treated with the 1.5 and 3 μ M CHIR99021 (CHIR), which is a GSK3 β inhibitor that has been shown to elevate β -catenin levels in ES cells (Bennett et al., 2002; Ying et al., 2008), and at these concentrations CHIR is used to maintain pluripotent ES cells in culture. Like the neural tube and somites, IWR-1-treated ES cells showed a reduction in the transcription of the Wnt reporter in the

presence of Wnt3a in the media, while no changes were observed in the absence of Wnt3a, where luciferase activity remained at background levels (Figure 3.4A). The reduction in *TOPFLASH* expression was accompanied by a 1.6-fold increase in β -catenin marked for proteasomal degradation (phospho-Ser33/37/Thr41- β -catenin), while only a nominal (less than 10%) increase in phospho-LRP6 was detected (Figure 3.4B). These data suggest that Tankyrase inhibition in ES cells promotes the formation of the destruction complex but not Fzd/LRP6 signaling complex at the membrane. Therefore, I conclude that increased Axin levels in ES cells inhibit canonical Wnt signaling; thus Wnt pathway regulation in ES cells is not similar to the late primitive streak.

3.2 GSK3 β is required to activate Wnt signaling in the late streak

Analysis of lysates from IWR-1-treated embryos established that stabilized Axin increased both the cytoplasmic destruction complex and the membrane Fzd/LRP6 complex in the late primitive streak. While these two complexes have antagonizing roles in β -catenin activation, the increased expression of *TOPGAL* in the late primitive streak suggested that the membrane-signaling complex overcame the increased levels of phospho-Ser33/37/Thr41- β -catenin, allowing β -catenin to activate the reporter transgene. The kinase activity of GSK3 β is required in both of these complexes, marking β -catenin for poly-ubiquitination in the destruction complex and, in response to Wnt ligands, phosphorylating the cytoplasmic tail of LRP5/6 at the membrane (Itoh et al., 1998; Zeng et al., 2005). The phosphorylation of LRP5/6 by GSK3 β promotes Wnt signaling, as

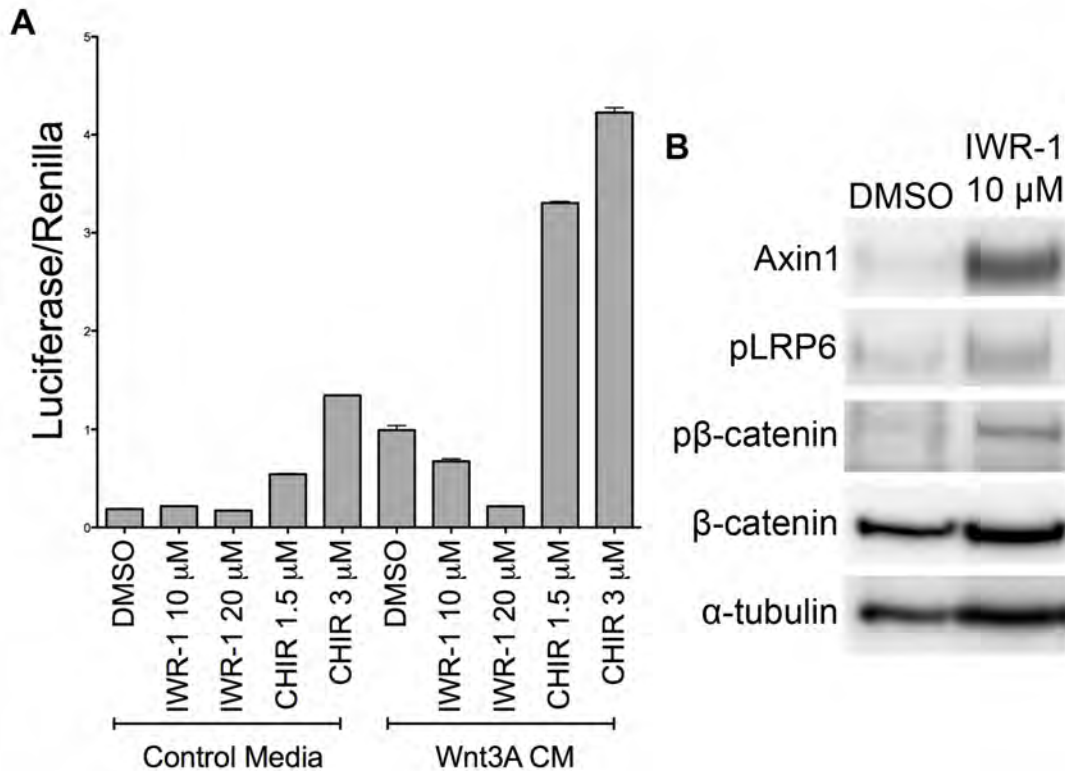


Figure 3.4: IWR-1 inhibits Wnt signaling in embryonic stem cells.

(A) *TOPFLASH* luciferase activity in E14-ES cells normalized to *FOPFLASH* and Renilla. There are only background levels of *TOPFLASH* expression in ES cells grown in control media, and this expression is unchanged by the treatment with 10 or 20 μ M IWR-1 for 24-hours, whereas GSK3 β inhibition by CHIR99021 (CHIR) increased luciferase activity in a dose dependent manner. Wnt3A conditioned media (CM) induced a 5-fold increase in reporter activity in control cells, and this activity was inhibited by IWR-1. The addition of 3 μ M CHIR to Wnt3A containing media produced a 4.2-fold increase in *TOPFLASH* expression compared to control cells. **(B)** 10 μ M IWR-1 stabilized Axin1 and increased phospho-Ser33/37/Thr41- β -catenin levels in ES cells, but did not significantly increase phospho-LRP6, as the observed increase was minor when normalized to the α -tubulin loading control.

phosphorylated LRP5/6 is both a competitive inhibitor of GSK3 β -mediated β -catenin phosphorylation and phospho-LRP5/6 can also recruit additional Axin to membrane (Piao et al., 2008; Zeng et al., 2008). The phosphorylation of LRP5/6 has been shown to be a common response to Wnt ligand, but the results from culturing embryos with IWR-1 suggested that GSK3 β activity at the membrane might be stronger in the late primitive streak than the rest of the embryo, as stabilized Axin promoted the activity of the membrane complex only in the late streak. To test this hypothesis I cultured embryos with the GSK3 β inhibitor CHIR99021 (CHIR) and assayed for *TOPGAL* expression.

Genetically, *GSK3 β* has been defined as a negative regulator of Wnt signaling, and CHIR has been shown to dramatically increase Wnt signaling by stabilizing cytoplasmic β -catenin (Bennett et al., 2002; Siegfried et al., 1990; Ying et al., 2008). In accordance with these published results, embryos cultured with 20 μ M CHIR showed elevated X-Gal staining in all anterior tissues compared to control embryos (Figure 3.5A-B). Increasing the dose of CHIR above 20 μ M had no qualitative effect on X-Gal staining in the anterior half of the embryo, so 20 μ M was considered the minimal effective dose, and was used for all subsequent experiments. There was no effect on *TOPGAL* expression when embryos were cultured with less than 15 μ M CHIR, and at 15 μ M, CHIR caused only a modest increase in reporter expression.

Unlike cells in the anterior half of the embryo (or any cell line that has been treated with CHIR), cells of the late primitive streak displayed a decrease in Wnt signaling when GSK3 β was inhibited (Figure 3.5B). CHIR99021 inhibition of

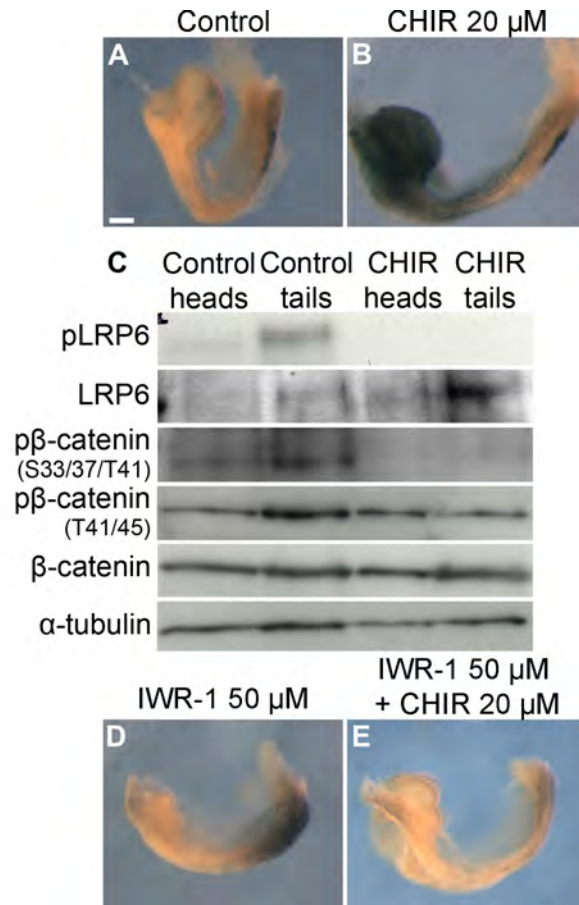


Figure 3.5: CHIR99021 inhibits Wnt signaling in the late primitive streak.

(A-B, D-E) X-Gal stained 6-8-somite staged wild-type embryos carrying one copy of the *TOPGAL* transgene, cultured with DMSO (A), 20 μM CHIR (B), 50 μM IWR-1 (D) and 50 μM IWR-1 + 20 μM CHIR (E). After an 18-hour culture with CHIR, X-Gal staining was elevated in the head and somites, but decreased in the late primitive streak compared to control embryos (A-B). (C) 20 μM CHIR inhibited GSK3β activity. Compared to control embryo lysate, phospho-Ser33/37/Thr41-β-catenin and phospho-Ser1490-LRP6 levels were dramatically decreased in embryos cultured with CHIR. CHIR did not affect overall β-catenin levels or CK1α activity in the destruction complex, as total- and phospho-Thr41/45-β-catenin were unchanged in treated lysate compared to controls. In these experimental conditions an increase in phospho-LRP6 was seen in control tails versus control heads. (D-E) Low levels of *TOPGAL* expression were seen in the head of IWR-1-treated and IWR-1+CHIR-treated embryos, but the increased *TOPGAL* expression in the primitive streak and PSM of IWR-1-treated embryos was abolished when GSK3β was also inhibited (n = 9). Scale bar: 100 μm.

GSK3 β kinase activity should repress β -catenin phosphorylation and degradation, and the stabilized β -catenin can then enter the nucleus and activate Wnt target gene expression. While *TOPGAL* expression suggests that this series of events occurs in the anterior tissues, in the late primitive streak GSK3 β inhibition did not yield the expected results.

To better understand the effects of CHIR in the embryo I analyzed components of the Wnt pathway in embryo lysates. Treatment with 20 μ M CHIR completely inhibited GSK3 β activity in both the anterior and posterior halves of the embryo, blocking the phosphorylation of β -catenin at Ser33/37/Thr41 and LRP6 at Ser1490 (Figure 3.5C). CHIR did not change overall β -catenin levels, but this was expected as the overwhelming majority of β -catenin in the embryo is at adherens junctions, and not involved in canonical Wnt signaling (Orsulic et al., 1999). Interestingly, these Western blots revealed that there was a significant increase in phospho-LRP6 in the posterior versus the anterior of control embryos, which was not detected in previous blots (compare pLRP6 in Figures 3.2A and 3.5C). This is likely due to the fact that in previous experiments control embryo lysate was run with IWR-1-treated lysate, and the strong pLRP6 signal in the treated embryos required short exposure times, which precluded the detection of the pLRP6 signal in the control embryos. These results show that while there is active Wnt signaling in both the anterior and posterior of the embryo, phospho-LRP6 levels are much higher in the late primitive streak, the cells is GSK3 β required for Wnt target gene expression.

The observed increase in Wnt signaling in IWR-1-treated embryos is

ligand dependent and is associated with increased levels of phospho-LRP6, which is GSK3 β dependent. I therefore tested whether stabilized Axin required GSK3 β activity to increase *TOPGAL* expression in the late primitive streak. Embryos cultured in the presence of both IWR-1 and CHIR showed reduced X-Gal staining in the late primitive streak compared to IWR-1 alone or control embryos (Figure 3.5A, D-E). Thus, the increased *TOPGAL* expression in IWR-1-treated embryos requires GSK3 β activity, presumably for the phosphorylation of LRP6 in the membrane-signaling complex. Unexpectedly, embryos cultured with IWR-1 and CHIR also showed reduced levels of Wnt reporter expression in the head compared to both control and CHIR-treated embryos (Figure 3.5A, B, E), suggesting that the increased level of nuclear β -catenin that results from GSK3 β inhibition is blocked by the presence of more Axin.

3.2.1 Proteasome inhibition promotes Wnt signaling in the late streak

The increased Wnt signaling seen in *GSK3 β* mutants, or CHIR-treated cells indicates that, in most cells, unless β -catenin is phosphorylated and degraded, it is capable of entering the nucleus and activating Wnt target genes (Figure 3.4A; Siegfried et al., 1990; Ying et al., 2008). This model is supported by the presence of *β -catenin* mutations in cancer patients and cancer cell lines that remove the N-terminal residues of β -catenin that are phosphorylated by GSK3 β (La Coste et al., 1998). These oncogenic mutations cause an ectopic activation of Wnt signaling because they shield β -catenin from CK1 α and/or GSK3 β phosphorylation. However, my data from CHIR-treated embryos suggests that

this dogma does not hold true in the late primitive streak. My data suggests that, in the late primitive streak, GSK3 β activity at the Fzd/LRP membrane complex is required for *TOPGAL* expression, regardless of β -catenin levels in the cytosol. I have also found that the IWR-1-mediated increase in Wnt target gene expression is correlated with increased activity of GSK3 β at the membrane, despite increased levels of β -catenin marked for degradation. Together, these data suggested that unlike any other tissue or cell line, Wnt pathway regulation in the late primitive streak is primarily dependent on GSK3 β activity at the membrane, not cytoplasmic β -catenin levels. I therefore, tested whether changing β -catenin levels without changing the normal ratio between GSK3 β in destruction complex and membrane signaling complex could increase *TOPGAL* expression in the late streak. If GSK3 β has a permissive role then increasing β -catenin should increase Wnt reporter transcription in the late streak and PSM, which display a higher level of phospho-LRP6 compared to anterior regions in control embryos (Figure 3.5C)

To modulate β -catenin levels without affecting GSK3 β or the destruction complex, I treated embryos with MG132. After phosphorylation and poly-ubiquitination, β -catenin is degraded by the proteasome. Treating cultured cells with proteasome inhibitor MG132 has been shown to activate the transcription of Wnt target genes, as cytoplasmic β -catenin are elevated in treated cells, despite presence of the destruction complex (Li et al., 2012). Thus, phosphorylated and poly-ubiquitinated β -catenin can activate transcription in the context of an inactive proteasome. To test how increased levels of cytoplasmic β -catenin affect Wnt

target gene transcription in the context of normal GSK3 β activity in the late streak I treated embryos with MG132. The toxicity of MG132 was a complication, as embryos could not be cultured for longer than 4-6 hours in MG132 without showing high levels of apoptosis. However, comparable levels of *Axin2* transcript were detected in HEK293T cells after 7-hour treatment with MG132 or Wnt ligand (Li et al., 2012), suggesting that MG132 can fully activate the pathway in this time period.

Embryos carrying one copy of the *TOPGAL* reporter cultured with 10 μ M MG132 for 4-hours did not have altered levels of X-Gal staining in the head, somites or primitive streak compared to controls (Figure 3.6A-B). However, there was increased *TOPGAL* expression in both the head and primitive streak in embryos cultured for 4-hours in the presence of 30 μ M MG132. This increased Wnt activity was only detected in area where Wnt ligand was expressed, and not in other tissues, as was seen in CHIR-treated embryos. This suggests that treatment with 30 μ M MG132 for 4hrs was only sufficient to enhance Wnt signaling in response to ligand, as it either did not generate enough cytoplasmic β -catenin to induce ectopic *TOPGAL* expression in 4-hours, or that increased *TOPGAL* expression depends on Wnt ligand expression, which promotes GSK3 β activity at the membrane.

3.3 Discussion

The *Axin2*^{canp} mutation causes a nonconservative Valine-to-Glutamate substitution that disrupts an N-terminal PRPPVPGEE motif, which is conserved

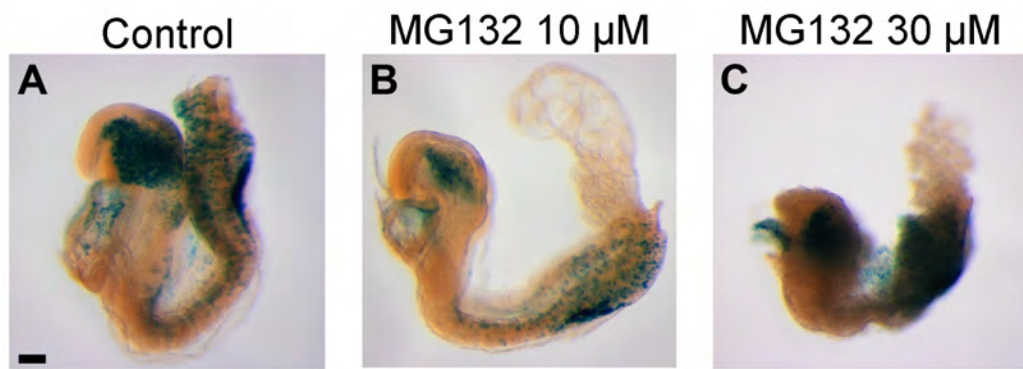


Figure 3.6: MG132 increases Wnt signaling in the primitive streak.

(A-C) X-Gal stained 6-8 somite staged wild-type embryos carrying one copy of the *TOPGAL* transgene, cultured with DMSO (A), 10 μ M MG132 (B) and 30 μ M MG132 (C). After 4-hour culture with 10 μ M MG132, there was no difference in X-Gal staining compared to control embryos (A-B). (C) Increasing the dose of MG132 to 30 μ M over the same time period caused an increase in *TOPGAL* expression in the rostral forebrain and primitive streak. No ectopic *TOPGAL* expression was detected, only an increase in expression in regions that are exposed to Wnt ligand. Scale bar: 100 μ m.

in all *Axin* family members, from *Drosophila* to humans. The initial characterization of this allele supported the importance of the N-terminal region of Axin, as a critical regulator of Axin2 stability. This motif has been named the Tankyrase-binding domain (TBD), as this domain can bind Tankyrase, an enzyme with poly-ADP ribosylation activity. Modification of Axin by Tankyrase leads to the ubiquitin-mediated, proteasomal degradation of Axin1 and Axin2 (Huang et al., 2009). The analysis of the effects of the *Axin2^{canp}* mutation confirms that this protein domain regulates Axin2 stability *in vivo* and that disruption of this domain of Axin led to a predicted reduction in canonical Wnt signaling in most tissues. This caused phenotypes seen in other mutants that lack Wnt signaling, such as *cardia bifida* and a shortened tail bud (Lickert et al., 2002; Takada et al., 1994). However, *TOPGAL* expression in the primitive streak of *Axin2^{canp}* mutants revealed a complex regulation of Wnt signaling in this tissue. All *Axin2^{canp}* mutants show decreased Wnt signaling in the early primitive streak, similar to the effect on Wnt signaling seen in other tissues. However, in contrast to the early loss of Wnt reporter activity, all *Axin2^{canp}* homozygous embryos showed elevated activity of the canonical Wnt reporter in the e8.5 primitive streak. Whereas mutants in other genes associated with decreased canonical Wnt signaling in the primitive streak arrest by e9.0 with reduced or absent mesodermal cell types (Takada et al., 1994), all *Axin2^{canp}* embryos differentiate a nearly normal number of somites at e9.5, which provides independent evidence that Wnt signaling is restored in the late *Axin2^{canp}* streak.

Inhibition of Axin1 and Axin2 turnover by the Tankyrase inhibitor IWR-1

has a similar tissue-specific effect in somite-stage embryos as *Axin2^{canp}*: canonical Wnt signaling is decreased in the anterior regions of the embryo and elevated in the late primitive streak. The increased *TOPGAL* activity in the posterior of IWR-1-treated embryos is greater than that in *Axin2^{canp}* embryos, which suggests that both Axin1 and Axin2 can activate Wnt signaling in the streak. Biochemical data showed that the IWR-1-stabilized Axin increased the activity of the β -catenin destruction complex throughout the embryo; however, in the late primitive streak, where there was an unexpected increase in Wnt signaling, I also detected an increase in phospho-LRP6. This suggests that stabilized Axin is capable of both forming the destruction complex and interacting with Fzd/Dvl/LRP at the membrane. Together, these results confirmed that the effects of the *Axin2^{canp}* mutation were due solely to increased Axin levels in the mutants, and the mutation in the TBD did not confer any other gain-of-function activities to Axin2, as stabilizing wild-type Axin could reproduce all *Axin2^{canp}* phenotypes.

Axin2 is a direct transcriptional target of β -catenin/TCF, and *Axin2^{canp}* embryos showed decreased Wnt activity in the e7.5 primitive streak. This predicts reduced levels of a negative regulator of Wnt signaling in these cells, which suggested a possible mechanism for the increased *TOPGAL* expression in the late streak of *Axin2^{canp}* mutants. However, it should be noted that the expression of *Axin2* in ligand receiving cells is a cell-intrinsic event, and the gastrulating epiblast cells in the e7.5 primitive streak are distinct from the cells responding to Wnt in the tail-bud. My experiments with IWR-1 also refuted this

possible model, as I was able to demonstrate that Axin promoted Wnt signaling in the late streak of wild-type embryos that had progressed through early streak development with no manipulation of the Wnt pathway, and thus, no changes in intracellular Axin levels prior to drug treatment.

While Western blots showed a uniform increase in phospho-Ser/33/37/41- β -catenin in the anterior and posterior halves of IWR-1-treated embryos, this might not reflect a uniform increase in the activity of the destruction complex. N-terminal phosphorylated β -catenin is subsequently poly-ubiquitinated and degraded by the proteasome. Therefore, concluding that the equivalent increase of phospho-Ser/33/37/41- β -catenin in embryo lysates from the anterior and posterior regions reflects a uniform increase in destruction complex activity assumes equal rates of ubiquitination proteasomal degradation in the anterior and posterior halves of the embryo. Therefore, it is possible that Axin may be differentially recruited to the destruction complex in the anterior or posterior of the embryo. This is the simplest model to explain my data; the ratio of cytoplasmic to membrane associated Axin predicts the expression of the *TOPGAL* reporter. To fully test this phospho-Ser/33/37/41- β -catenin levels could be checked in embryos treated with both IWR-1 and MG132; alternatively co-immunoprecipitation of Axin in IWR-1 treated embryos could reveal if Axin is predominantly associated with the destruction or the membrane complex in the anterior versus posterior halves of the embryo.

Axin, along with all the components of the destruction complex, can be recruited to the Fzd/LRP complex at the membrane in response to Wnt ligand (Li

et al., 2012). While there is active Wnt signaling in the both the anterior and posterior halves of the embryo, I found increased levels of phospho-LRP6 in the posterior half compared to the anterior half of control embryo lysates. This suggested two alternative models: first, there are simply higher levels of Wnt signaling in the posterior half of control embryos, and the increased exposure to Wnt ligand in the late streak promotes the association of Axin with Fzd/LRP or, second, that the specific combination of Wnt ligands and Wnt receptors in the late streak promotes the recruitment of Axin to the membrane to a greater degree than in the anterior half of the embryo. To test the first model, embryos could be cultured with media containing both Wnt3a and IWR-1, increasing the amount of available Wnt ligand and Axin to the entire embryo. If the amount of Wnt ligand determines the ratio of stabilized Axin in the destruction complex versus the membrane signaling complex, then increasing the amount of Wnt ligand in the anterior regions of IWR-1-treated embryos may increase *TOPGAL* expression in anterior tissues, as more Axin will be associated the Fzd/LRP complex.

Two lines of evidence suggest that this first model is not the reason for increased levels of Axin at the membrane in the late streak of IWR-1-treated embryos. First, β -galactosidase activity assays did not detect increased reporter expression when normalized to overall protein levels in the posterior half of control embryos (Figure 3.1E), and second, IWR-1-treatment decreased *TOPGAL* expression in the e7.5 primitive streak, which had higher levels of Wnt signaling than the late streak (Figure 3.1A-B). Therefore, I hypothesize that the second model is correct, and the specific components of the Wnt pathway that

are expressed in the late streak create an environment that promotes Axin recruitment to the membrane.

The increased levels of *TOPGAL* expression in late streak suggested that stabilized Axin1 is either preferentially recruited to the membrane or that the activity at the membrane is able to out compete the increased activity of the destruction complex in these cells. This result provides *in vivo* support for studies that suggested that Axin can play a positive role in canonical Wnt signaling through its interaction with activated LRP5/6 (Bilic et al., 2007; Zeng et al., 2005). In these models, binding of Wnt ligand leads to recruitment of the Axin/GSK3 β /CK1 complex to LRP5/6, which is subsequently phosphorylated by GSK3 β . Phosphorylated LRP5/6 can recruit additional Axin in a positive feedback loop that amplifies receptor phosphorylation (Zeng et al., 2008). The finding that phospho-LRP6 levels are higher in the late primitive streak in DMSO-treated embryos further support this model, as these initial asymmetries in phospho-LRP6 levels could be key to Axin promoting Wnt signaling only in the late streak.

LRP6 is phosphorylated by GSK3 β in response to Wnt ligand, and I found that both Wnt ligand and GSK3 β are required for the IWR-1-mediated increase in *TOPGAL* expression in the late streak (Figure 3.7). These data, along with the increased levels of phospho-LRP6 in the late streak of wild-type embryos, suggest that the unexpected increase in Wnt signaling in IWR1-treated embryos may be linked with the recruitment of Axin to the Fzd/Dvl/LRP signaling complex at the membrane. However, I was unable to directly show that Axin was preferentially recruited to membrane in the posterior half of IWR-1 treated

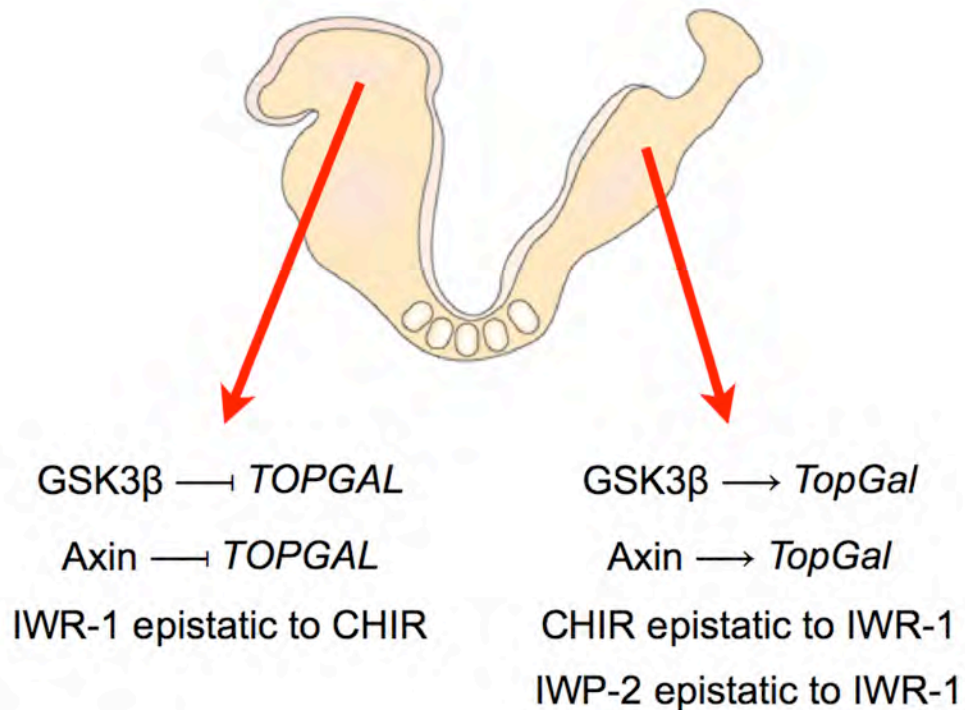


Figure 3.7: The tissue specific roles of Axin and GSK3β in the Wnt pathway.

Like mouse ES cells and other cell lines, in the anterior neural tube (forebrain) and somites IWR-1 and CHIR treatment showed that Axin and GSK3β inhibit canonical Wnt signaling. In addition, the increased *TOPGAL* expression seen in embryos treated with CHIR is suppressed by IWR-1 in these tissues. In contrast, Axin and GSK3β promote canonical Wnt signaling in the late primitive streak. The increased expression of *TOPGAL* in response to IWR-1 treatment requires both GSK3β activity and Wnt ligand secretion as demonstrated in by culturing embryos with IWR-1 and either CHIR or IWP-2.

embryos. I attempted to replicate the results from the late streak by treating ES cells grown in Wnt3a conditioned media with IWR-1, as this would provide a better system for biochemical analysis; however, Wnt signaling in ES cells was reduced upon IWR-1 treatment.

Culturing embryos with the GSK3 β inhibitor revealed two surprising results: first, I found that GSK3 β was required to activate Wnt signaling in the late streak, and, second, I found that increased *TOPGAL* expression in the anterior half of the embryo could be inhibited by Axin stabilization (Figure 3.7). This first result does not fit the current model of the Wnt signaling cascade, and I have not been able to precisely define the underlying mechanism. Previous reports have shown that phosphorylated LRP6 promotes Wnt signaling in two ways: first, the phosphorylated PPSPXS motifs in the cytoplasmic tail of LRP6 are potent inhibitors of GSK3 β , and can block the phosphorylation of β -catenin (Piao et al., 2008; Wu et al., 2009), and second, phospho-LRP6 enhances the membrane association of Axin, which may be a necessary step in the formation of Wnt 'signalsomes' at the membrane (Liu et al., 2003; Yokoyama et al., 2010). CHIR-treatment independently inhibits the phosphorylation of β -catenin by GSK3 β , so this activity of phospho-LRP6 is not what is required for Wnt signaling in the late streak. Therefore, I hypothesize that the aggregation of Axin and the destruction complex at the membrane is required for β -catenin/TCF transcription of the Wnt reporter in the late streak. Previous studies have concluded that the formation of Wnt signalsomes was a means to quickly and efficiently sequester the destruction complex away from newly translated β -catenin (Yokoyama et al.,

2010). Again, this activity is not required in CHIR-treated cells, which suggests that these supermolecular structures have a separate activity that promotes Wnt signaling, and the cells in the late primitive streak are uniquely dependent upon this activity. Increasing β -catenin levels in late streak by inhibiting the proteasome can lead to increased *TOPGAL* expression, but unlike CHIR treatment, MG132 presumably does not affect phospho-LRP levels. Comparing CHIR and MG132 treated embryos suggests that increased cytoplasmic β -catenin levels only lead to increased *TOPGAL* expression in the context of active GSK3 β at the membrane. However, one caveat to this experiment is that Wnt ligands can promote the proteasomal degradation of Axin. Therefore, MG132 treatment may have caused an increase in Axin as well as β -catenin. As I have previously shown that increased Axin in the late streak promotes signaling, I cannot rule out the possibility that the increased *TOPGAL* expression in the late streak of MG132-treated embryos was due solely to increased Axin levels.

It has been reported that Wnt ligands promote the association of the membrane bound signaling complex into multivesicular endosomes, and the isolation of GSK3 β from the cytoplasm can increase the half-life of many cellular proteins, not just β -catenin (Taelman et al., 2010). Perhaps one of the proteins that is stabilized by the sequestration of GSK3 β is also required for Wnt signaling downstream of β -catenin stabilization, for instance the nuclear import of β -catenin. To test this hypothesis, future experiments will need to check Wnt signaling in *Hrs* mutants, a gene required for the formation of early endosomes (Komada and Soriano, 1999; Taelman et al., 2010). To test if the incorporation of

the destruction complex is required for the increased *TOPGAL* expression in IWR-1-treated embryos, I would also want to treat *Hrs* mutants with IWR-1 to see if the increased Wnt signaling is abolished in these mutants.

While embryos treated with CHIR showed the expected increase in Wnt signaling in the anterior half of the embryo, culturing embryos in the presence of IWR-1 and CHIR reduced the anterior expression of *TOPGAL* below the levels observed in control embryos. Thus, stabilized Axin can overcome the effects of stabilized cytoplasmic β -catenin. The phosphorylation of β -catenin by GSK3 β not only marks β -catenin for degradation, it also makes the destruction complex processive, as APC binds phospho- β -catenin and shuttles it to the E3-ligase β TrCP (Ha et al., 2004). This frees Axin, allowing the destruction complex to capture another β -catenin molecule and repeat the phosphorylation and ubiquitination cycle (Lee et al., 2003). The reduction of Wnt signaling in the anterior half of IWR-1 + CHIR-treated embryos suggests that stabilized Axin increases the total number of destruction complexes, and while these are not processive and do not lead to β -catenin destruction, they are sufficient to inhibit the stabilized β -catenin from entering the nucleus and activating the Wnt reporter construct.

These experiments, along with the characterization of the *Axin2^{canp}* phenotype, have revealed that the canonical Wnt pathway is regulated by different mechanisms in head and somites compared to the late primitive streak (Figure 3.7). Unlike anterior embryonic tissues, ES cells or adult cancer cell lines, GSK3 β activity with the active Fzd complex at the membrane is paramount for

canonical Wnt signaling in the late primitive streak. Stabilized Axin in IWR-1 treated embryos may be preferentially recruited to this membrane complex, allowing for increased *TOPGAL* expression. The primary Wnt ligand that is expressed in the primitive streak changes from Wnt3 to Wnt3a around the time that stabilized Axin changes from inhibiting to promoting *TOPGAL* expression. While I have demonstrated that Wnt ligands in general are required for Axin to promote Wnt signaling in the late streak, future experiments will need to address whether the role of Axin as a Wnt agonist depends on the expression of specific Wnt ligands or reflects a unique environment in late streak, possibly due to cross-talk between other pathways that are active in this tissue.

CHAPTER FOUR

4 PLANAR POLARITY CONTROLS CONVERGENT EXTENSION AND LEFT-RIGHT PATTERNING IN THE EARLY MOUSE EMBRYO

All cells in an epithelial sheet have an inherent apical-basal polarity; the basal surface interacts with the basement membrane while the apical surface is exposed to the extracellular environment. This structural polarity is also defined molecularly by the asymmetric distribution of proteins; integrins are trafficked to basal side of the cell and adherens junction proteins are trafficked to the apical side. Most epithelial sheets are also polarized along the face of the sheet, orthogonal to the apical-basal axis, in what is termed planar cell polarity. This level of cellular organization is important for the delineation of common body axes to all cells within the sheet, and is manifest in the uniform orientation of cellular appendages such as the wing hairs in *Drosophila* (Figure 1.5).

A key regulator of planar polarity is the non-canonical Wnt/planar cell polarity (PCP) pathway, which, like apical-basal polarity, establishes the axis of polarity through the asymmetric trafficking of transmembrane proteins. Thus, planar cell polarity can be molecularly defined by the segregation of the Vang and Fzd complexes. Along with orienting cellular appendages, the PCP pathway is also important for the morphogenesis of embryonic structures. Mutations in *Vangl2*, as well as the other mouse core PCP genes, disrupt embryonic morphogenesis, affecting the shape of the somites, notochord and cochlea. A

hallmark of mouse PCP mutants is craniorachischisis, a failure to close the neural tube in all regions caudal to the midbrain (Copp et al., 2003).

Craniorachischisis in these mutants has been attributed to convergent extension (CE) defects in neural tube, a morphogenetic process that leads to mediolateral narrowing and anterior-posterior elongation through mediolateral intercalation (Keller, 2002). However, the cellular mechanisms of CE in the mammalian neural tube are unknown. Here, I present data that helps explain the underlying cell biology of CE during neural tube closure.

Despite the dramatic defect in neural tube closure in mouse single PCP mutants such as *Vangl2*, other aspects of CE, such as somite morphogenesis, are only mildly affected compared to *Xenopus* or zebrafish embryos lacking PCP signaling (Darken et al., 2002; Greene et al., 1998; Park and Moon, 2002; Wallingford and Harland, 2002) or in mouse *Vangl1 Vangl2* double mutants (Song et al., 2010). The stronger phenotypes of the *Vangl1 Vangl2* double mutants compared to single PCP mutants provide a tool to identify other proteins required for planar cell polarity. In the work presented here I utilized the ability to enhance the *Vangl2*^{L^p} phenotype to show that Cofilin1 plays a role in mammalian PCP. I analyzed the phenotypes of double mutants that lacked normal activity of both *Vangl2* and Cofilin1. Two aspects of PCP can be characterized quantitatively at cellular resolution in the early mouse embryo: elongation of the axial mesendoderm (the notochordal plate, or midline) and positioning of nodal cilia. My results show that actin dynamics participate in planar polarity signaling during mammalian development.

4.1 The cellular basis of neural tube closure

Craniorachischisis is a hallmark phenotype of mammalian planar cell polarity mutants, present in all mutants for the core PCP genes. The identification of mutants with neural tube closure defects has also led to the discovery of novel genes associated with planar cell polarity regulation such as *Scribble* and *Ptk7* (Lu et al., 2004; Murdoch et al., 2003). In *Xenopus* embryos, disruption of planar cell polarity signaling causes defects in CE in the neural plate, resulting in neural folds that are abnormally far apart, preventing fusion at the roof plate (Wallingford and Harland, 2002). While defects in CE are the proposed mechanism for craniorachischisis in mammalian PCP mutants, it has not been directly tested. There are also differences in the epithelial structure of the mouse neural plate and *Xenopus* neural folds, suggesting that the cell behaviors that drive CE in these tissues may operate via different methods. Therefore, I wanted to study the underlying cell biology of mouse neural tube closure to identify what processes were governed by planar polarity signaling.

Characterization of *Dvl1 Dvl2* double mutants showed that the overall length-to-width ratio of embryos lacking PCP signaling is reduced (Wang et al., 2006a), suggesting that the PCP pathway contributed to CE movements in the early mouse embryo. However, previous work in our lab has established that there are only minor defects in the morphogenesis of the somites (mesoderm lineage) and foregut (endoderm lineage) in *Vangl2^{Lp}* embryos. Therefore, it appears that Vangl2-mediated morphogenesis primarily affects the neural tube. Consistent with this hypothesis, it has been shown that chimeric embryos

containing wild-type and *Vangl2^{L-p}* cells have a higher proportion of wild-type cells in the central region of the neural tube and lateral domains that are predominantly comprised of mutant cells (Ybot-Gonzalez et al., 2007). This could suggest that in the neural tube, wild-type cells are migrating towards the midline and *Vangl2^{L-p}* cells are defective in this process. However, neural tube closure defects were not reported in these chimeric embryos, so it is unclear if the observed segregation of wild-type and mutant cells in the neural tube has an effect on morphogenesis.

In my experiments I sought to define the stage in development in which the head folds were undergoing convergent extension, as this had not been defined for mouse embryos. For these experiments, I sectioned wild-type and *Vangl2^{L-p}* mutant embryos from the early headfold stage to the 6-8-somite stage, and compared length of head folds. Between these stages the head folds drastically change their morphology, starting from a simple epithelium at the early head fold stages, then transitioning to a pseudo-stratified epithelium at the mid/late headfold stages, and finally forming medial- and dorsolateral-hinge points that are required for neural tube closure (Kibar et al., 2007a).

The neural tissue present in the early head fold-staged embryo will give rise to the cephalic neural tube, which does not require PCP signaling for closure. Consistent with this, I found no difference in the length of the neural plate between the wild type and *Vangl2^{L-p}* in the early or late head fold stages, suggesting that at these early stages there is no PCP-dependent morphogenesis in the rostral neural tube.

Neural tube closure in the trunk proceeds in a zipper like fashion, starting

around fourth somite and migrating rostrally and caudally along the anterior-posterior axis of the embryo. Sections of 6-somite-staged wild-type embryos revealed that there are dramatic changes in the architecture of the neural plate as it transitions from open to closed (Figure 4.1A-B). Serial sections separated by less than 50 μm reveal that the closed neural tube is remarkably shorter from the floor plate to the roof plate than the sections containing open neural tissue. It is unclear if this change was associated with a lengthening of the tissue, as classic convergent-extension models would predict, as the closed neural tube also appeared thicker, suggesting increased pseudo-stratification or cell-packing accompanies the shortening of the tissue. Sections from stage matched *Vangl2^{Lp}* embryos showed that the mutant neural plate failed to become shorter or thicker (increased pseudo-stratification), and at all levels appeared similar to the open sections of neural tissue in the wild type (Figure 4.1C-D). Together, these data show that the PCP-dependent morphogenesis of the neural plate appears to coincide specifically with neural tube closure in the trunk.

Next I examined the cellular architecture of the trunk neural tube in fixed embryos, focusing on regions adjacent to closed neural tube to address the mechanism of cell rearrangements during neural tube closure. The data from *Vangl2^{Lp}* chimeras suggested that there was a medial migration of wild-type cells in the neural tube (Ybot-Gonzalez et al., 2007), so I looked for patterns that could indicate the mechanism by which these cells were moving. If the cell rearrangement were occurring similar to the *Xenopus* neural tube, and there was directional mediolateral intercalation, the cells should be elongated perpendicular

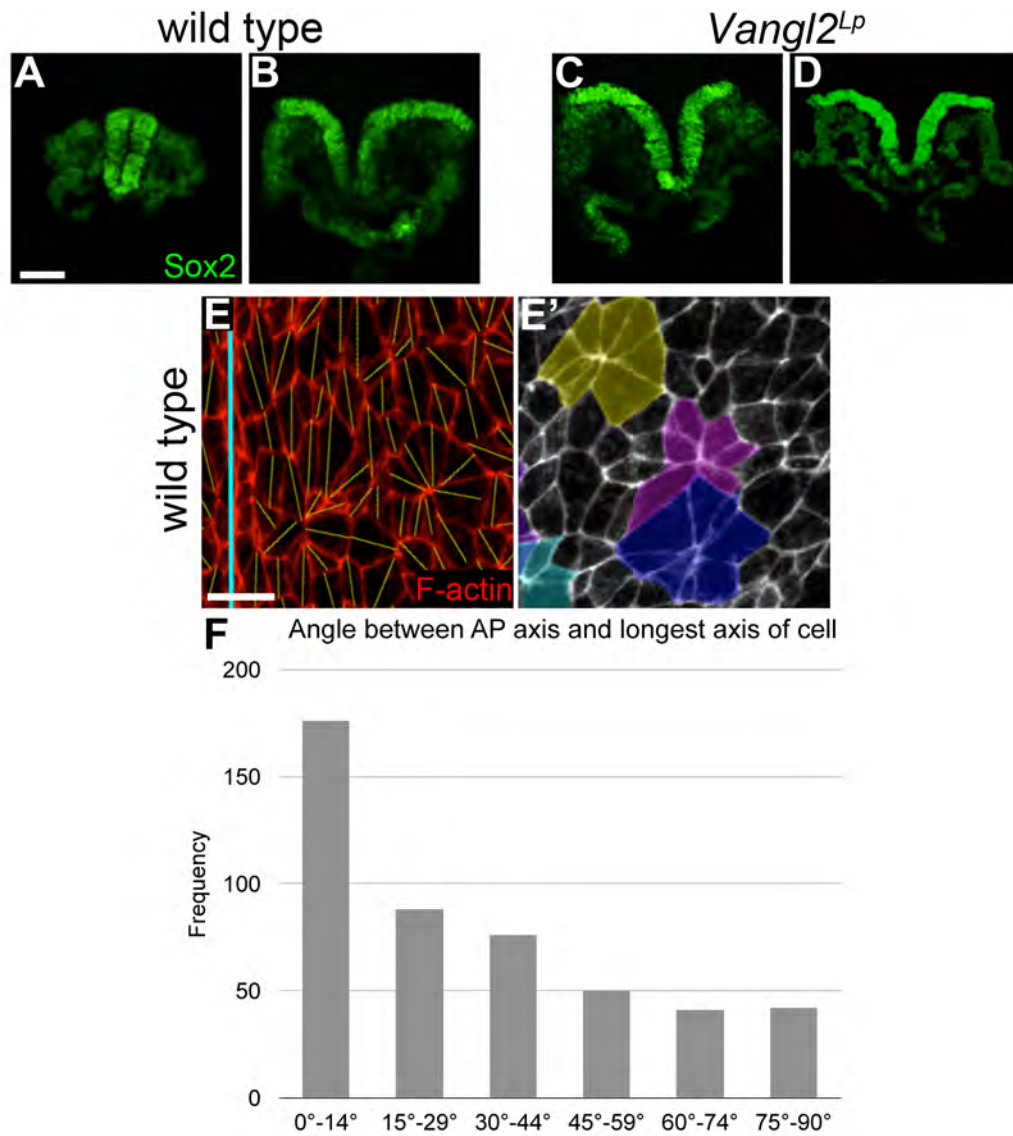


Figure 4.1: The changes in cellular architecture during neural tube closure.

(A-B) Transverse sections separated by 50 μm from a wild-type e8.5 embryo stained with Sox2 (green). The neural tube is shorter in the closed (A) versus open (B) neural tube. **(C-D)** The neural plate in e8.5 *Vangl2^{Lp}* mutants is similar to the open neural tube in wild-type embryos **(E-E')**. The axis of elongation overlaid on neural plate cells from a wild-type e7.75 embryo. Blue line marks the midline. Pseudo-coloring of rosette structures containing six or more cells with a common vertex. **(F)** Histogram of the angle between the longest cell axis and the AP axis of the embryo. Over 50% of the cells counted are elongated parallel to the AP axis. Scale bars: 50 μm (A-D); 10 μm (E).

to the midline, which serves as a marker for the anterior-posterior (AP) axis of the embryo. Conversely, if the cell rearrangements were taking place similar to *Drosophila* germ-band extension or the chick neural tube, there should be multicellular rosettes in the tissue (Blankenship et al., 2006; Nishimura et al., 2012). To address these two models I outlined each cell in a region of the neural tube and overlaid the longest side of the bounding rectangle on the cell, which served to mark the axis of elongation of the cell (Figure 4.1E). I then plotted the angle of the axis of elongation versus the embryonic AP axis on a histogram. From this data there was no evidence of mediolateral cell intercalation, as over 50% of the cells counted were elongated roughly parallel to the AP axis (Figure 4.1F). However, when the axis of elongation was overlaid on the cells there were many instances where a group of cells were all elongated towards a common vertex, suggesting that the cells were fixed while forming or resolving a multicellular rosette structure (Figure 4.1E'). However, when similar images were taken of the *Vangl2^{Lp}* neural plate, these same structures were found with approximately the same frequency. Therefore, without time-lapse imaging of the neural plate during neural tube closure I cannot conclude that these structures are playing a role in the PCP-dependent morphogenesis of this tissue.

4.2 *Cofilin1* enhances the *Vangl2^{Lp}* phenotype

Dynamic changes in the actin cytoskeleton accompany many cellular processes, several of which have been well documented such as cell migration and cytokinesis. However, actin dynamics have also been shown to play critical

functions in other aspects of basic cell biology as well, including cargo sorting in the Golgi and vesicle trafficking (Blume et al., 2011; Blume et al., 2009; Salvarezza et al., 2009). Cofilin is a key regulator of actin dynamics; known primarily for its role in severing existing actin filaments. Cofilin has two actin binding sites, one site is specific for filamentous actin (F-actin) while the second can bind either F-actin or actin monomers. When Cofilin molecules bind an existing F-actin filament with these two domains they induce a twist in the filament, ultimately causing it to sever. This activity suggests Cofilin is a negative regulator of actin dynamics, and in fact F-actin severing can lead to the disassembly of large actin filaments (McGough et al., 1997). However, Cofilin can also enhance actin polymerization, and Cofilin activity is required for the formation of branched actin structures, such as lamellipodia (Cai et al., 2007). This is due to the ability of the ARP2/3 complex to nucleate a branched actin structure, which can promote further actin polymerization, at the newly created plus-end after Cofilin-mediated actin severing (Rohatgi et al., 1999). Thus, Cofilin can act as both a positive and negative regulator of actin dynamics within the cell.

Cofilin activity is regulated through the phosphorylation of the N-terminal F-actin binding site, as the addition of a phosphate group to Serine 3 inhibits actin binding. The phosphorylation of Cofilin has been shown to be downstream of many different signaling pathways including Rho and its associated kinase ROCK as well as Rac and Cdc42 which activate LIM kinase (Klooster et al., 2006; Mouneimne et al., 2006). Cofilin is activated by the phosphatases

Slingshot and PP2A. The phosphatase activity of Slingshot is regulated through its association with 14-3-3, and many different signaling pathways have been shown to liberate, thus activating, Slingshot from 14-3-3, including PDGF and PI3 kinase (Maheswaranathan et al., 2011; Nishita et al., 2004). Slingshot appears to activate Cofilin by two mechanisms in some contexts, as it can also remove a phosphate group from, thus inactivating, LIM kinase (Soosairajah et al., 2005).

Many regulators of actin dynamics have been shown to be downstream effectors of PCP signaling in the *Drosophila* wing disc, including the GTPases RhoA, Rac1 and Cdc42, which in turn regulate the formation of the actin-based wing hair (Eaton et al., 1996; Matusek et al., 2006; Strutt et al., 1997; Winter et al., 2001). While these GTPases have been shown to directly regulate Cofilin activity in tissue culture cells, PCP phenotypes in the wing disc of *Cofilin* mutants were shown to be caused by a failure to localize Fzd and Fmi to the cell membrane, suggesting that Cofilin activity might be required both upstream of PCP signaling (Blair et al., 2006), as well as downstream of RhoA, Rac1 and Cdc42. Therefore, I tested whether *Cofilin* was similarly required for PCP signaling in the mouse embryo, and whether loss of *Cofilin* could enhance the *Vangl2*^{Lp} phenotype.

Cofilin1 (*Cfl1*) is one of three *Cofilin* family members in the mouse genome: *Cofilin1*, *Cofilin2* and *ADF* (*actin depolymerizing factor*, also known as *Destrin* (*Dstn*)). *Cfl1* is the only member of this family that has an embryonic phenotype when genetically ablated (Gurniak et al., 2005; Smith et al., 1996). Like *Cfl1*, *Dstn* is ubiquitously expressed in the early mouse embryo, while

Cofilin2 expression is restricted to muscles. Dstn protein is upregulated in *Cofilin1^{null}* embryos, and may partially compensate for the loss of Cofilin1 protein in the embryo as Dstn can rescue *Cfl1* knock-down in tissue culture cells (Hotulainen et al., 2005).

A strong missense allele of *Cofilin1*, the *C5* mutation, was isolated in a screen for recessive N-ethyl N-nitrosourea (ENU)-induced mutations that caused morphological defects in midgestation mouse embryos. *Cfl1^{C5}* mutants had an open cranial neural tube, a closed but wavy neural tube in the trunk, and defects in outflow tract development that caused pericardial edema (Figure 4.2B), similar to the phenotype of a null allele of *Cfl1* (Figure 4.3A; Gurniak et al., 2005). The newly discovered allele encodes a T to A transversion mutation at position 301 of the *Cfl1* protein coding sequence, and at e9.5, there was a significant decrease in the amount of Cfl1 protein in *Cfl1^{C5}* homozygous mutants (Figure 4.3F), suggesting that the resulting F101I substitution destabilized the protein. All Cofilin family proteins share a common protein structure, consisting of six α -helices surrounding a core of four anti-parallel β -sheets (Pope et al., 2004). The conservative amino acid substitution encoded by the *C5* allele changes a conserved phenylalanine in the third β -sheet, and this substitution reduced protein levels by 72% in the mutant embryos (Figure 4.3F). The phenotype of *Cfl1^{C5}* was identical to *Cfl1^{null}* embryos, suggesting that the remaining Cofilin1 protein detected by Western blot was inactive. The mutated residue in the mutant protein sits directly under the F- and G-actin binding site of Cofilin, leading me to believe that this allele encodes an inactive and unstable protein.

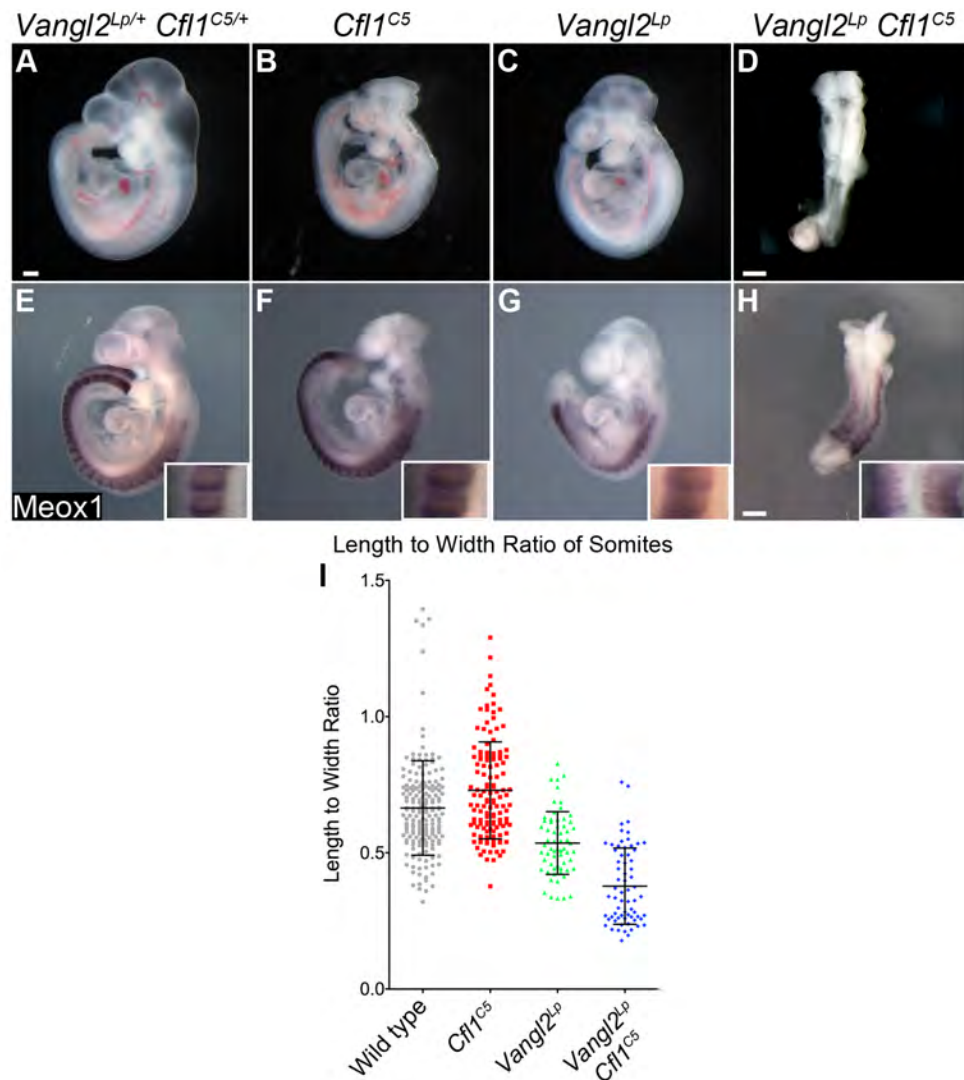


Figure 4.2: Genetic interaction between *Vangl2^{Lp}* and *Cfl1^{C5}* at e9.5.

(A) *Vangl2^{Lp/+} Cfl1^{C5/+}* embryo, indistinguishable from wild type. (B) *Cfl1^{C5}* homozygous mutants are exencephalic and die ~e11.0. (C) *Vangl2^{Lp}* homozygous mutant embryos have an open trunk neural tube (D) *Vangl2^{Lp} Cfl1^{C5}* double mutants have a completely open neural tube, a short body axis, and abnormal somites. (E-H) *Meox1* *in situ* hybridization highlights the somites. Insets are a 4X magnification. (I) The length to width ratio (LWR) of somites. Somites in *Vangl2^{Lp}* mutants are significantly shorter and wider than wild-type or *Cfl1^{C5}* embryos ($P < 0.001$). Somites in *Vangl2^{Lp} Cfl1^{C5}* double mutants have significantly reduced LWR compared to wild type or either single mutant ($P < 0.001$); *Vangl2^{Lp} Cfl1^{C5}* double mutants had 20-22 somite pairs and other genotypes had 22-28 at the stage analyzed. Scale bars: 250 μm .

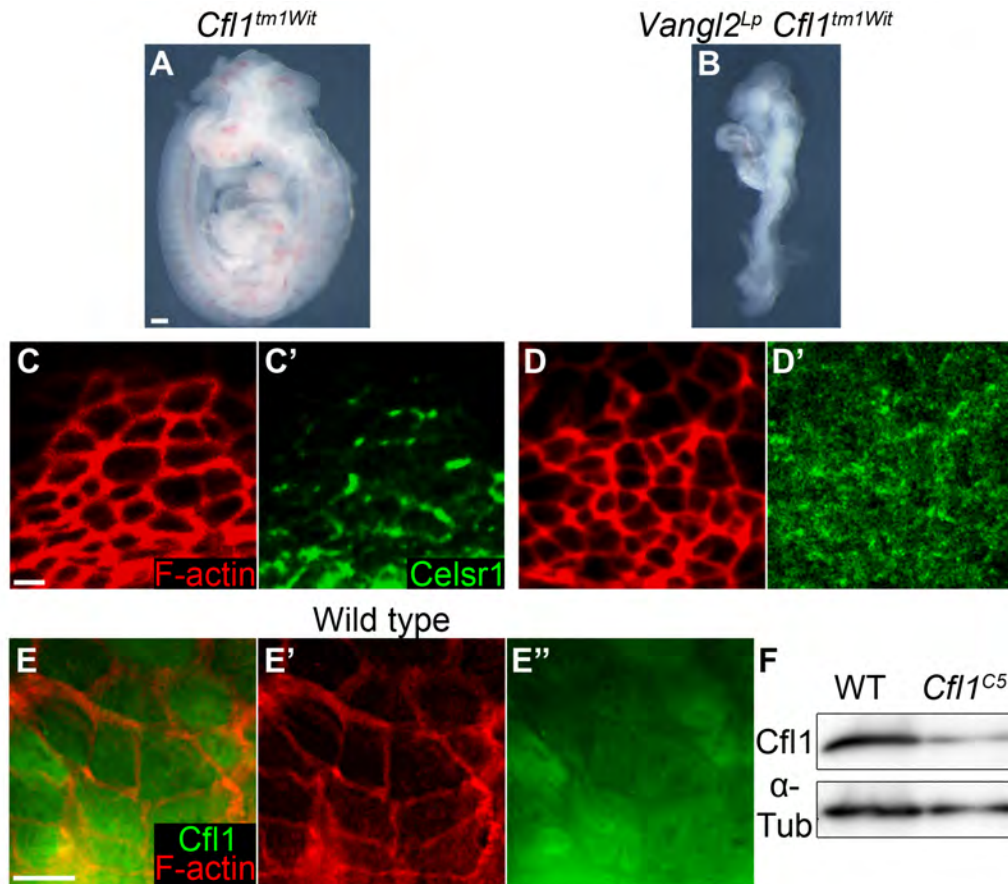


Figure 4.3: Planar polarity is disrupted in *Cfl1^{tm1wit} Vangl2^{Lp}* double mutants.

At e9.5, the phenotype of *Cfl1^{tm1wit}* homozygous embryos (A) is indistinguishable from that of *Cfl1^{C5}* homozygotes, including exencephaly, a wavy dorsal neural tube and heart defects. The *Vangl2^{Lp} Cfl1^{tm1wit}* double mutants (B) have the same appearance as *Vangl2^{Lp} Cfl1^{C5}* double mutants, with a shorter body axis, heart-looping defects and abnormal somites. As in *Cfl1^{C5}*, Celsr1 protein is localized to the apical membrane in the anterior and posterior faces of node cells in the e8.0 *Cfl1^{tm1wit}* mutants (C), and this membrane recruitment is lost in the *Vangl2^{Lp} Cfl1^{tm1wit}* double mutants (D). Cfl1 protein (green) is detected throughout the apical cytoplasm in node cells in wild-type e8.0 embryos (E-E''). (F) Western Blot of whole embryo lysate from a single e9.5 embryo shows a significant decrease in Cfl1 protein in *Cfl1^{C5}* mutants compared to wild-type littermates. Scale bars: (A-B) 250 μ m; (C-E) 2.5 μ m.

Despite the known role of Cofilin in the PCP pathway in *Drosophila* (Blair et al., 2006), *Cfl1*^{C5} mutants did not show hallmark PCP phenotypes. However, removal of another PCP protein can enhance the relatively weak phenotypes of *Vangl2* mutations (Song et al., 2010); therefore, to test whether Cofilin has a role in the mouse PCP pathway I generated *Vangl2*^{Lp} *Cfl1*^{C5} double mutants. The e9.5 *Vangl2*^{Lp} neural tube was open from the hindbrain to the tail (craniorachischisis) (Figure 4.2C), while the *Cfl1*^{C5} neural tube was closed caudal to the hindbrain. The e9.5 *Vangl2*^{Lp} *Cfl1*^{C5} double mutant embryos had a stronger phenotype than either single mutant: they were shorter, had an open neural tube along the entire axis of the embryo, failed to undergo embryonic turning and arrested at ~e9.5 (Figure 4.2D); a similar phenotype was seen in *Vangl2*^{Lp} *Cfl1*^{null} double mutants (Figure 4.3B).

The PCP pathway is required for the convergent extension movements that extend the anterior-posterior body axis of the vertebrate embryo. *Xenopus* morphants and zebrafish mutants that lack *Vangl2* or other core pathway components have short and wide somites, suggesting that convergent extension is required in the paraxial mesoderm for normal somite morphology (Park and Moon, 2002; Veeman et al., 2003). Somite shape in mouse *Vangl2*^{null} embryos suggest mild CE defects in this tissue, but *Vangl1* *Vangl2* double mutants have somites that are dramatically shorter along the anterior-posterior axis and wider mediolaterally (Song et al., 2010). *Vangl2*^{Lp} *Cfl1*^{C5} double mutant embryos also appeared to have wide somites. Therefore, I measured the length-to-width ratio (LWR) of the somites of *Meox1*-stained embryos (Figure 4.2E-H), where length is

the distance along the anterior-posterior axis, and width is the mediolateral distance. *Cfl1*^{C5} somites were similar in shape to those in wild-type littermates, with a LWR of 0.66 ± 0.17 in wild type and 0.73 ± 0.18 in the mutant. *Vangl2*^{Lp} somites were shorter and wider, with a LWR of 0.54 ± 0.11 ($P < 0.001$). The somites of *Vangl2*^{Lp} *Cfl1*^{C5} double mutants were significantly wider than *Vangl2*^{Lp} single mutants, with a LWR of 0.38 ± 0.14 ($P < 0.001$) (Figure 4.2I), similar to what was reported in *Vangl1 Vangl2* double mutants (Song et al., 2010). These data show that Cofilin1 genetically interacts with Vangl2, and together control the shape of somites in the mouse embryo.

4.2.1 Convergent extension of the midline

Previous observations based on histological analysis and *in situ* hybridization with midline markers suggested that the axial midline of *Vangl2*^{Lp} mutants is shorter and wider than that of wild-type embryos (Greene et al., 1998; Ybot-Gonzalez et al., 2007). To determine whether the morphogenetic defects in the *Vangl2*^{Lp} *Cfl1*^{C5} double mutants were due to true defects in CE, I analyzed the cellular organization of the axial midline. The notochordal plate of the 1-4 somite-stage embryo is a single layer epithelium that lies on the surface of the embryo, allowing imaging at a cellular resolution. At this stage, cells of the midline are quiescent (Bellomo et al., 1996), so cell division does not complicate the analysis of midline morphogenesis. 1-4 somite-stage *Vangl2*^{Lp} *Cfl1*^{C5} embryos were similar in size and global morphology to wild-type embryos; therefore, changes in the organization of the midline were likely to be a primary

defect. To visualize individual cells in the midline, I stained e8.0 embryos with an antibody against Brachyury (T), which specifically labels the nuclei of cells in the node and midline (Figure 4.4A-D').

Embryos of all four genotypes (wild type, *Vangl2*^{Lp}, *Cfl1*^{C5} and *Vangl2*^{Lp} *Cfl1*^{C5}) at the 1-4 somite stage had indistinguishable numbers of Brachyury-positive (T⁺) cells in the midline (wild type: 200 ± 14, *Vangl2*^{Lp}: 205 ± 22, *Cfl1*^{C5}: 199 ± 33 and *Vangl2*^{Lp} *Cfl1*^{C5}: 195 ± 24). The notochordal plate of wild-type embryos was 3.7 ± 0.3 cells in width and 54.7 ± 6.3 cells long (AP axis) (Figure 4.4A). The *Cfl1*^{C5} single mutant midline was not significantly different from wild type (3.7 ± 0.4 cells wide and 53.3 ± 9.5 cells long) (Figure 4.4B). The midline of *Vangl2*^{Lp} single mutants was significantly wider and shorter (4.6 ± 0.5 cells wide and 45.12 ± 7.1 cells long) (Figure 4.4C), confirming earlier histological observations (Greene et al., 1998; Wang et al., 2006a; Ybot-Gonzalez et al., 2007).

Vangl2^{Lp} *Cfl1*^{C5} double mutant embryos showed a stronger midline defect than *Vangl2*^{Lp} single mutants. The midline of double mutants was shorter and wider (6.21 ± 0.8 cells wide and 31.6 ± 4.4 cells long) than *Vangl2*^{Lp} or *Cfl1*^{C5} single mutants (Figure 4.4D). When calculated in terms of LWR, the *Vangl2*^{Lp} *Cfl1*^{C5} double mutant was three-fold shorter and wider than wild type and two-fold shorter and wider than *Vangl2*^{Lp} (LWR in wild type and *Cfl1*^{C5} embryos = 14-15; *Vangl2*^{Lp} = 10.3; *Vangl2*^{Lp} *Cfl1*^{C5} double mutant = 5.4) (Figure 4.4E). This phenotype was not due to changes in cell shape, as I measured similar decreases in the LWR in *Vangl2*^{Lp} mutants and *Vangl2*^{Lp} *Cfl1*^{C5} double mutants

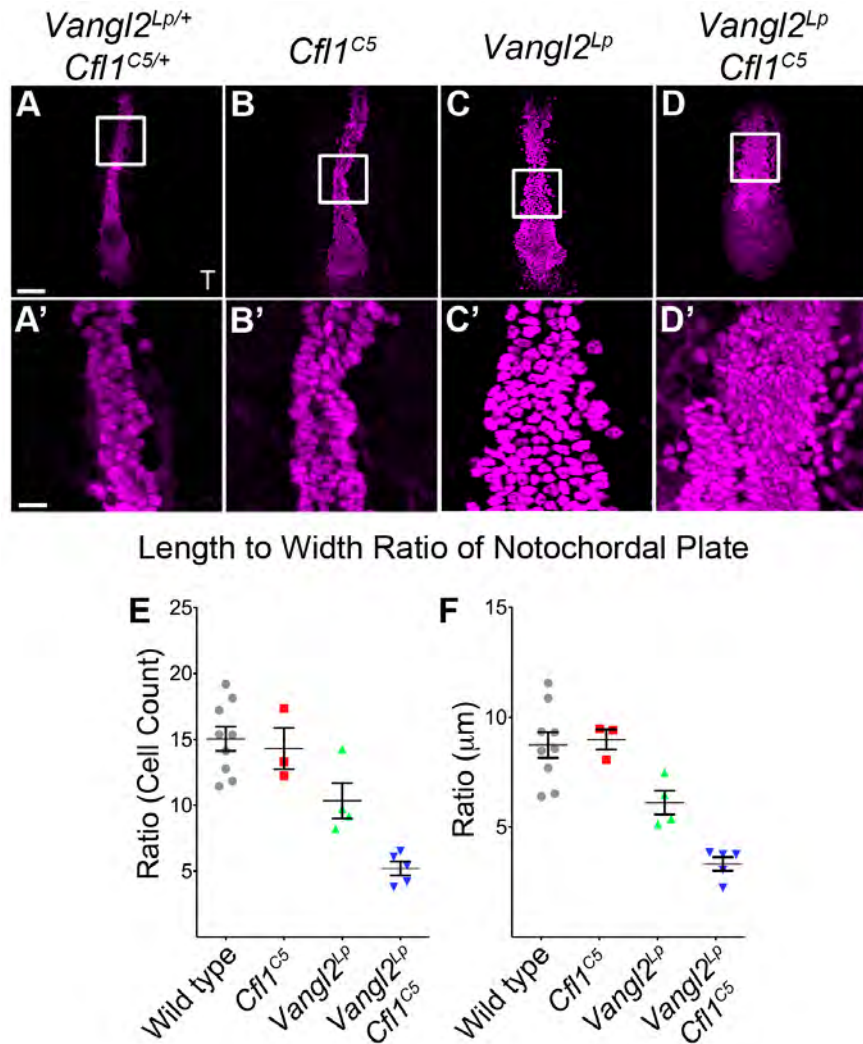


Figure 4.4: *Cfl1^{C5}* enhances the CE defect in the *Vangl2^{LP}* notochord.

(A-D) Projections of flat-mounted e8.0 embryos stained for Brachyury (T) (magenta). (A'-D') 4X magnifications of midline cells from boxed region of A-D highlight the arrangement of cells in each genotype. Wild type (A) and *Cfl1^{C5}* (B) have a similar arrangement of T⁺ cells in the midline, while the *Vangl2^{LP}* midline (C) is wider and shorter. The *Vangl2^{LP} Cfl1^{C5}* mutant midline (D) is wider and shorter than *Vangl2^{LP}*. (E-F) The LWR of the notochordal plate measured by the distribution of cells (E) or in microns (F). Scale bars: (A-D) 100 μm ; (A'-D') 25 μm .

(compared to wild type or *Cfl1^{C5}*) when the dimensions of the notochordal plate were measured in microns rather than cell number (Figure 4.4F). Thus, convergent extension of the axial midline depends on both *Vangl2* and *Cfl1*.

4.2.2 Cofilin1 and PCP signaling cooperate to orient nodal cilia

Of six *Vangl2^{Lp} Cfl1^{C5}* double mutants examined at e9.5, one embryo had a linear heart tube and two showed a left-right reversal of heart-looping, a phenotype not seen in either single mutant (Figure 4.5A-C). Like wild-type embryos, *Cfl1^{C5}* and *Vangl2^{Lp}* single mutants expressed the left-sided marker *Nodal* exclusively on the left side of the embryo in the lateral plate mesoderm at e8.5 and showed stronger expression of *Nodal* on the left side of the node at e8.0. In contrast, four of seven double mutant embryos examined showed either bilateral expression of the *Nodal* gene at e8.5 (Figure 4.5D-F') or stronger staining on the right side of the node at e8.0 (Figure 4.5G-I), indicating that the left-right embryonic axis is randomized in these double mutants.

The establishment of left-right asymmetry in the mouse embryo is dependent on two populations of ciliated cells in the ventral node; the cells in the central pit of node are required to generate leftward directed fluid flow, and the cells along the periphery are required as mechanosensors to detect the nodal flow. The cells in the central pit region of the node have a 9+0 microtubule doublet structure in the axoneme, an architecture that is normally associated with the non-motile primary cilia. Despite the lack of a central microtubule pair, cilia in the central pit of the node are motile and require a unique set of genes to

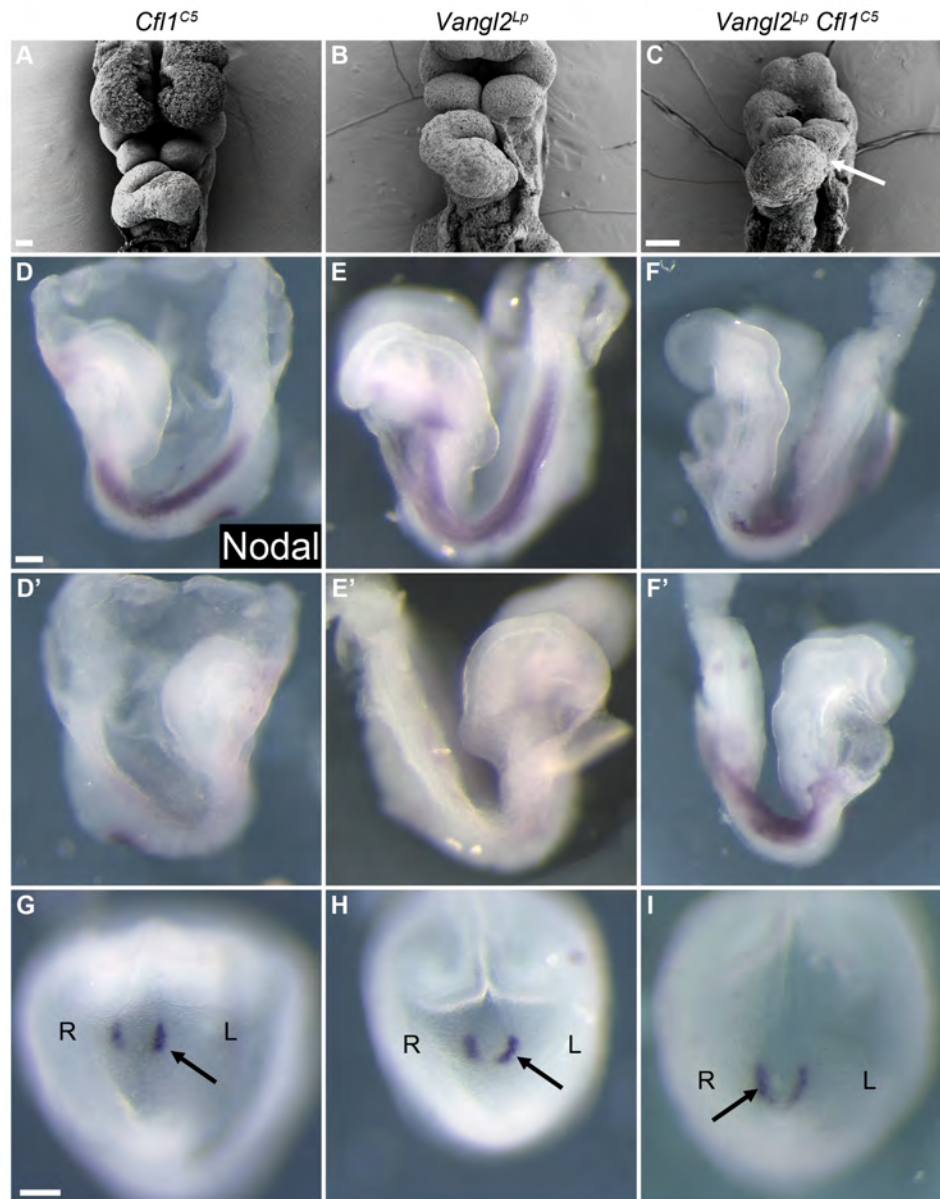


Figure 4.5: Left-right asymmetry defects in *Vangl2*^{Lp} *Cfl1*^{C5} double mutants.

A fraction of *Vangl2*^{Lp} *Cfl1*^{C5} double mutants examined at e9.5 showed reversed heart looping (arrow), a phenotype not seen in either single mutant (A-C). This phenotype is due to an earlier defect in left-right asymmetry, as some e8.5 double mutants express *Nodal* (purple) bilaterally in the lateral plate mesoderm and show increased *Nodal* expression on the right side of the node (D-I). Arrows (G-I) mark the side of the node with stronger *Nodal* expression at e8.0. Scale bars: 100µm.

generate fluid flow, including *dynein axonemal-heavy chain 11* (also known as *left right dynein*) and *Inversin* (McGrath et al., 2003; Nonaka et al., 1998; Sulik et al., 1994; Watanabe et al., 2003). Unlike the 9+2 containing motile cilia found in the kidney or ovary, which exhibit a unidirectional biphasic beating pattern, the lack of a central pair of microtubules in node cilia results in a beating pattern of concentric circles. This rotational beating should generate a vortex, not directional flow; however, cilia in the central pit of the node are polarized towards the posterior of the cell (Hashimoto et al., 2010; Nonaka et al., 2005). This establishes an efficient phase to the clockwise beating of node cilia, towards the left side of the embryo, and an inefficient phase towards the right side, when the cilia drags across the apical cell surface (Nonaka et al., 2005). Thus, planar polarity of node cilia in the central pit is critical for the establishment of the left-right body axis, and previous studies have shown that the cilia remain at the center of the cell in PCP compound mutants, which causes randomization of sidedness (Hashimoto et al., 2010; Song et al., 2010).

In SEM images of the central region of the node in wild-type, *Cfl1^{C5}* and *Vangl2^{Lp}* single mutant embryos, cilia pointed posteriorly and appeared to emanate from the posterior face of the cell (Figure 4.6A, C, E). SEM images of *Vangl2^{Lp} Cfl1^{C5}* double mutant nodes at the 2-somite stage showed that node cilia of normal length were present, but they did not point uniformly to the posterior and their position on the cell appeared more variable than in wild type or the single mutants (Figure 4.6G).

Images of whole mount embryos at 2-4 somite stage stained with

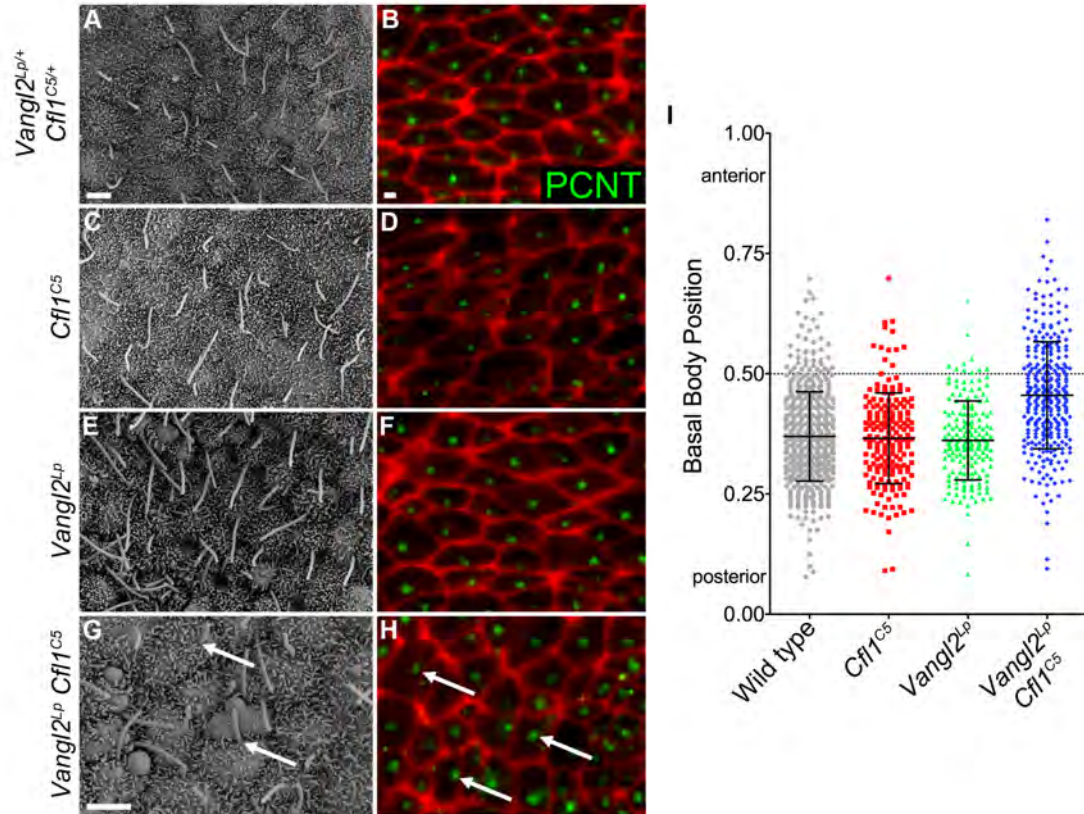


Figure 4.6: Nodal cilia are not polarized in *Vangl2^{Lp} Cfl1^{C5}* double mutants.

(A,C,E) Scanning electron microscope images of the e8.0 node show that cilia are polarized to the posterior of node cells in wild type, *Cfl1^{C5}* and *Vangl2^{Lp}* single mutants. (B,D,F) Basal bodies, visualized by the centrosomal protein Pericentrin (green), show a similar posterior position in the cells of wild type, *Cfl1^{C5}* and *Vangl2^{Lp}* single mutants. F-actin at the cell borders is highlighted with phalloidin (red). (G) In *Vangl2^{Lp} Cfl1^{C5}* double mutants, many cilia point anteriorly (arrows). (H) Many basal bodies are mislocalized to the anterior half of the cell in *Vangl2^{Lp} Cfl1^{C5}* double mutants (arrows). Anterior is towards the top in all images. (I) The relative localization of basal bodies in individual central node cells was quantified from immunofluorescence images from at least three e8.0 embryos per genotype. The graph shows that basal bodies in double mutants are not positioned on the posterior of cells; in addition, there is a greater variance in the placement of cilia compared with wild type or either single mutant. Data are mean \pm s.d. Scale bars: 2 μ m.

Pericentrin, a protein localized at the ciliary basal body, showed that the majority of the basal bodies in the central region of wild-type, *Vangl2^{Lp}* and *Cfl1^{C5}* node cells were polarized towards the posterior side of the cell (Figure 4.6B, D, F). In contrast, there were many cells in *Vangl2^{Lp} Cfl1^{C5}* double mutants where the Pericentrin staining was localized towards the anterior side of the cell (Figure 4.6H). I then used the immunofluorescence images to measure the relative position of the basal body along the y-axis (the posterior to the anterior face) of the cell. The position of the basal body was calculated by dividing the coordinate of the center of mass of the Pericentrin staining by the length of the cell along the y-axis, such that a basal body residing on the posterior face of the cell would have a value of zero, and one on the anterior face of the cell would have a value of one. The basal body was polarized to the posterior side of node cells in wild type and in both single mutants (the position was 0.37 ± 0.09 in wild type (n = 536); 0.37 ± 0.09 in *Cfl1^{C5}* (n = 193) and 0.36 ± 0.08 in *Vangl2^{Lp}* (n = 187)). In contrast, the basal bodies of *Vangl2^{Lp} Cfl1^{C5}* double mutants were located near the center of the cell (average basal body position = 0.46 ± 0.11 (n = 307)), significantly different from the other genotypes ($P < 0.001$) (Figure 4.6I). The variance of basal body position was also significantly increased in the double mutant ($P < 0.001$). Thus, the basal bodies in the *Vangl2^{Lp} Cfl1^{C5}* double mutants failed to polarize to the posterior of the cell and were localized randomly along anterior-posterior axis, causing the average basal body position to be approximately 0.5 in this assay.

The cells along the periphery of the node are also ciliated. Although these

cilia are non-motile (McGrath et al., 2003), recent studies have shown that they too are required for the establishment of the left-right body axis. Leftward fluid flow in the node is associated with increased Ca^+ signaling in the left-sided endoderm (McGrath et al., 2003). The calcium channel *Polycystin-2* (*Pkd2*) is expressed in all node cells, and *Pkd2* mutant mice exhibit *situs inversus*, despite the presence of normal leftward flow in the mutant nodes (McGrath et al., 2003; Pennekamp et al., 2002; Yoshida et al., 2012). Restricted expression of *Pkd2* in peripheral node cells can rescue left-right asymmetry defects in *Pkd2* mutant embryos, demonstrating that the Ca^+ release on the left side of the embryo depends on *Pkd2* activity solely in the peripheral node cilia.

While the central pit cells of the mouse node contain motile cilia that are planar polarized towards the posterior of the cell (Hashimoto et al., 2010; Nonaka et al., 2005), the cells along the periphery of node may not require planar polarity for their function in left-right asymmetry. To test this hypothesis I quantitated the position of the cilia basal body along the anterior-posterior axis of individual node cells in the central and peripheral regions of the ventral node in wild-type and *Vangl2^{Lp} Cfl1^{C5}* embryos. As previously shown, the basal bodies in the central pit region of the node are polarized towards the posterior of the cell in wild-type embryos, and this polarized placement is lost in *Vangl2^{Lp} Cfl1^{C5}* mutant embryos (Figures 4.6I, 4.7). However, when the same analysis was applied to cells on the periphery of the node I found that the Pericentrin staining was not polarized in wild-type embryos (average basal body position = 0.46 ± 0.11 (n = 290)) or *Vangl2^{Lp} Cfl1^{C5}* mutants (average basal body position = 0.46 ± 0.11 (n = 169)).

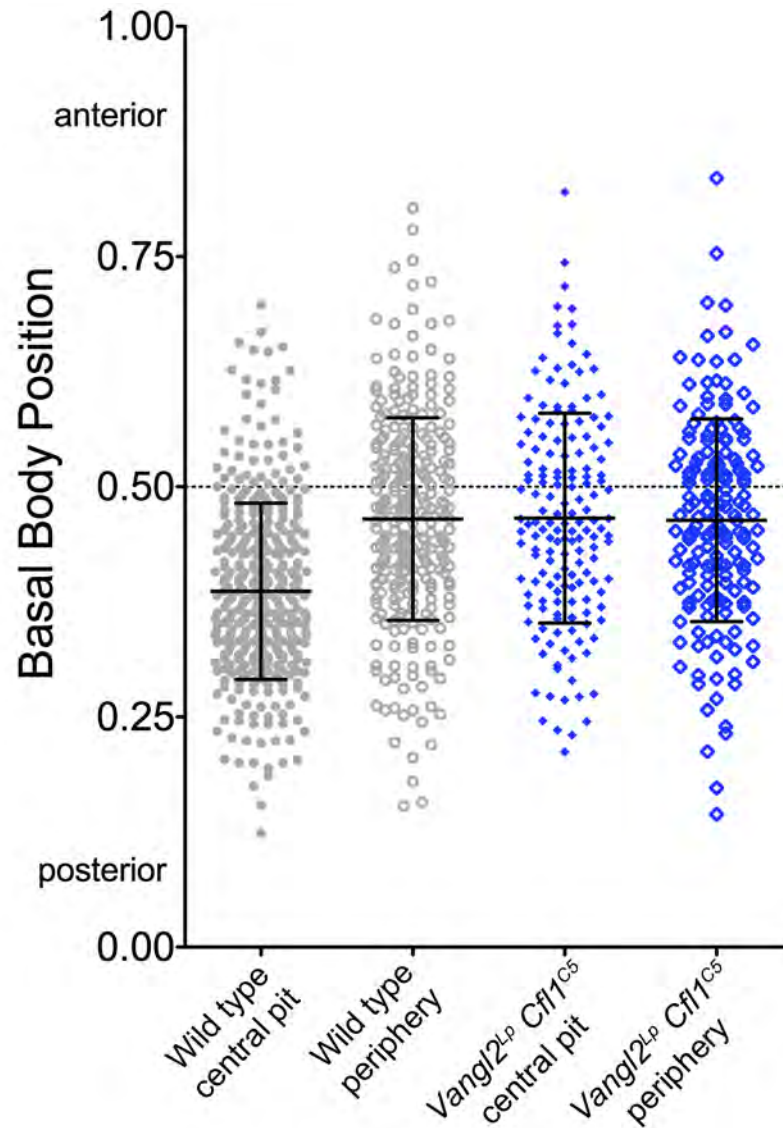


Figure 4.7: Peripheral node cilia are not planar polarized.

The relative localization of basal bodies in individual central and peripheral node cells was quantified from immunofluorescence images of Pericentrin stained wild-type and *Vangl2^{Lp} Cfl1^{C5}* e8.0 embryos. The graph shows that basal bodies in the periphery of the wild-type node are not positioned towards the posterior of cell, similar to both the central pit and periphery of mutant embryos. Data are mean \pm s.d.

These data were identical to the previous results for the central pit cells of the *Vangl2^{Lp} Cfl1^{C5}* mutants (Figure 4.7). Therefore, I conclude that the cilia in the peripheral region of the wild-type node are not planar polarized. Because the average position of basal bodies is the same in the central pit of *Vangl2^{Lp} Cfl1^{C5}* mutants and the periphery of wild type cells that do not polarize their cilia, I can further conclude that planar polarity signaling is completely lost in *Vangl2^{Lp} Cfl1^{C5}* mutant nodes.

I also determined the position of ciliary basal body along the x-axis in the *Vangl2^{Lp} Cfl1^{C5}* double mutants, as defects in wing hair and denticle placement along the axis that is orthogonal to the Vang/Fzd axis of polarity have been seen in *Drosophila* (Price et al., 2006; Strutt and Strutt, 2002). While there is no evidence that the PCP pathway directly controls planar polarity along the anterior-posterior axis in the wing disc or mediolateral polarity in the denticle belt, cells lacking PCP genes have defects in the placement of cellular appendages in all embryonic axes, which creates the classic swirling pattern in these mutants.

Similar to the y-axis data, the position of basal body along the x-axis was determined by dividing the coordinate of the center of mass of the Pericentrin staining by the length of the cell along the x-axis, such that a basal body residing on the leftward face of the cell would have a value of zero, and one on the rightward face of the cell would have a value of one. In wild-type embryos the average basal body position along the x-axis was 0.52 ± 0.01 (n = 380), demonstrating that nodal cilia are normally centered within the cell along this axis. However, unlike the denticles in PCP mutants in the *Drosophila* epidermis,

there was no significant change in basal body positioning along the mediolateral axis in the *Vangl2^{Lp} Cfl1^{C5}* double mutants, which also had Pericentrin staining in the middle of cell (0.56 ± 0.01 (n = 163)) (Figure 4.8). Importantly, there was no increase in the variance of these data, which confirms that unlike the positioning along anterior-posterior axis, basal bodies in the *Vangl2^{Lp} Cfl1^{C5}* double mutants are not randomly distributed along the mediolateral axis, causing the average position to be approximately 0.5 in this assay.

4.3 Discussion

The *Vangl2^{Lp}* mutation provides a sensitized background to identify additional genes required for mammalian PCP. I have shown that, as in *Vangl1 Vangl2* double null mutants, planar polarity appears to be abolished in *Vangl2^{Lp} Cfl1^{C5}* double mutants both in the convergent extension of the midline and the polarized positioning of node cilia, indicating that *Vangl2* and *Cofilin* act in pathways that converge on regulation of planar polarity in the mouse embryo. In both contexts, embryos lacking *Cofilin1* and *Vangl2* show a phenotype indistinguishable from that of the strongest combinations of core PCP mouse mutants that have been described (Hashimoto et al., 2010; Song et al., 2010).

It was described previously that the notochordal plate (midline mesendoderm) is wider in *Vangl2^{Lp}* mutants than in wild type embryos (Greene et al., 1998). Our data provide the first cellular analysis of mouse midline convergent extension and its dependence on planar cell polarity. At the 0-4 somite stage, there are approximately 200 Brachyury-expressing cells in the

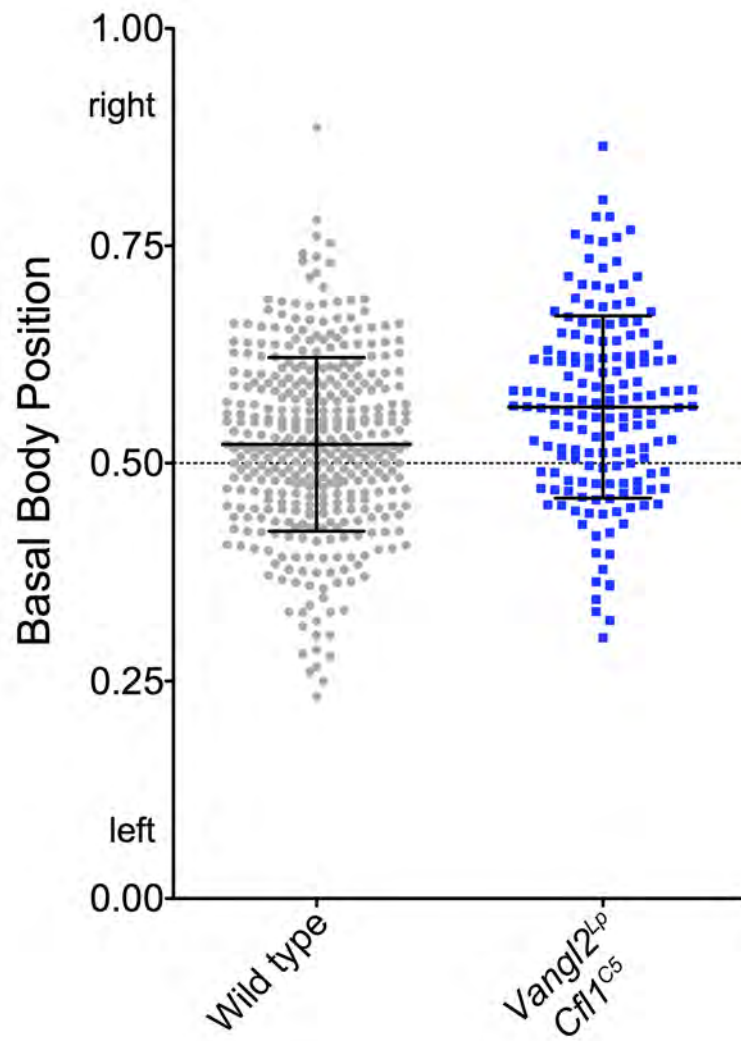


Figure 4.8: Node cilia are centered along the mediolateral axis of node cells.

The relative localization of basal bodies in individual central node cells was quantified from immunofluorescence images from at least two e8.0 embryos per genotype. The graph shows that basal bodies are positioned in the center of the cell along the mediolateral axis (x-axis) in both wild type and double mutants; in addition, there is no change in the variance in the placement of cilia in *Vangl2^{Lp} Cfl1^{C5}* double mutants.

midline, anterior to the node in all the genotypes examined, but the cellular arrangement of the T⁺ cells depended on the genotype. In wild-type and *Cfl1*^{C5} embryos, the midline cells were arranged in a narrow stripe, 3-4 cells wide and 55-60 cells long. Confirming previous impressions, the *Vangl2*^{Lp} midline was somewhat wider and shorter (4-5 cells wide and 40-50 cells long). The *Vangl2*^{Lp} *Cfl1*^{C5} midline was approximately twice as wide and half as long (6-7 cells wide and 30-35 cells long) as in the wild type, and significantly shorter and wider than that of *Vangl2*^{Lp} single mutants. The cells of the midline arise from the cells of the node (Hashimoto et al., 2010), and the number of cells across the width of the midline of the double mutants was the same as the number of cells at the anterior edge of the node, suggesting that convergent extension normally leads to a two-fold narrowing of the midline in wild type, a process that fails completely in the *Vangl2*^{Lp} *Cfl1*^{C5} double mutants.

In principle, *Cofilin1* could be required for convergent extension of the midline either upstream or downstream of planar polarity signals. Cofilin activity has been shown to be a key regulator of the actin cytoskeleton rearrangements that drive cell motility and morphogenesis in many contexts (Kim and Davidson, 2011; Zhang et al., 2011). However, Cofilin is also involved in cargo sorting and vesicle trafficking in tissue culture cells, and in *Drosophila*, *Cofilin* mutations are associated with a disruption in the membrane localization of PCP proteins, suggesting that Cofilin activity may be acting upstream of PCP signaling (Blair et al., 2006; Blume et al., 2009; Blume et al., 2011; Salvarezza et al., 2009).

It was recently demonstrated that the node contains two populations of

cells: a static central pit of cells with planar polarized cilia, which generate the fluid flow that determines left/right asymmetry, and a dynamic group of mobile cells derived from the anterior primitive streak that migrate around the central pit cells and exit the node at the anterior to form the notochordal plate (Hashimoto et al., 2010). While the defects in the migratory population of cells is consistent with Cofilin activity downstream of PCP signaling, I have also documented that cilia are randomized in position in *Vangl2^{Lp} Cfl1^{C5}* double mutants. This suggests that dynamic rearrangement of the actin cytoskeleton may be required for the establishment of PCP signaling in the mouse, as Cofilin has not been proposed to have a role in the positioning of cilia, which is a microtubule based organelle.

CHAPTER FIVE

5 ACTIN DYNAMICS ARE REQUIRED FOR PCP SIGNALING IN THE MOUSE EMBRYO

The enhancement of the *Vangl2*^{Lp} morphogenesis phenotypes by *Cfl1*^{C5} demonstrated that Cofilin1 and actin dynamics are involved in the PCP pathway during mouse embryogenesis. Additionally, the defects in establishing the left-right body axis in the double mutants suggested that there is a complete loss of non-canonical Wnt signaling in the double mutants, as they displayed a similar phenotype to embryos null for both *Vangl1* and *Vangl2* (Song et al., 2010). Together, this presented two alternative models for the role of Cofilin in the non-canonical Wnt pathway: Cofilin could be a downstream effector protein, regulated by, and necessary for PCP signaling, or Cofilin could be involved in the establishment of planar cell polarity. In the next set of experiments I tested these two models, and found that, as in the *Drosophila* wing disc, Cofilin is required for the membrane localization of the core PCP proteins. Using a small molecule inhibitor of actin dynamics, jasplakinolide, I showed that these defects are due to a disruption in the membrane association of Rab11⁺ vesicles, which caused *Vangl2* and *Celsr1* protein to accumulate in Early Endosome Antigen 1 (EEA1⁺) vesicles in the apical cytosol.

5.1 *Cofilin1* and *Vangl2* are required for the localization of *Celsr1*

As evidenced by the differences in somite morphology and cilia polarity in *Vangl2* single versus *Vangl1 Vangl2* double mutants (Song et al., 2010), there remains a low level of planar polarity signaling in the absence of *Vangl2*. Reducing Cofilin1 activity in *Vangl2^{Lp}* mutants is equivalent to *Vangl1* mutations, eliminating all PCP pathway activity. In the *Drosophila* wing disc planar polarity signaling is manifested by the asymmetric distribution of the Vang and Fzd complexes to the proximal and distal sides of the cell, respectively (Strutt and Strutt, 2009). The core PCP proteins are similarly restricted in their localization in the ventral node, only in this context to the anterior and posterior faces of the cell (Hashimoto et al., 2010; Song et al., 2010). Therefore, I examined the localization of the core PCP protein *Celsr1* in *Vang2^{Lp} Cfl1^{C5}* double mutant nodes. If the enhancement of the *Vang2^{Lp}* phenotype by *Cfl1^{C5}* was due disruption in actin dynamics downstream of PCP signaling, then there should be no difference in *Celsr1* localization in the nodes of *Vang2^{Lp}* and *Vang2^{Lp} Cfl1^{C5}* embryos. On the other hand, if Cofilin activity is required for the establishment of PCP signaling then I would expect to see altered *Celsr1* localization in the double mutant embryos.

As previously reported for *Vangl1*, *Vangl2* and GFP-tagged- *Dvl1* and - *Dvl2*, I observed that *Celsr1* (the Flamingo homologue) was highly enriched along the anterior/posterior borders of wild-type node cells and was excluded from the mediolateral faces of the cells. To quantitate the planar polarization of *Celsr1*, I measured the mean fluorescence intensity of the *Celsr1* signal along all

edges of cells within the ventral node. In wild-type embryos, there was a two-fold enrichment of Celsr1 on the anterior/posterior faces of the cell compared to the mediolateral sides (Figures 5.1A-B, 5.2A). The same degree of polarization of Celsr1 was seen in *Vangl2^{Lp}* and *Cfl1^{C5}* single mutants (Figures 5.1C-F, 5.2B-C). In contrast, Celsr1 was not enriched to any membrane of *Vangl2^{Lp} Cfl1^{C5}* double mutant node cells (Figures 5.1G-H, 5.2D) or *Vangl2^{Lp} Cfl1^{null}* double mutants (Figure 4.3D), indicating that Cofilin1 directly regulated PCP protein polarization.

The defect in Celsr1 localization in the double mutant embryos appeared to be specific to the PCP pathway, as I did not detect defects in other apically-localized proteins, including Par3, E-Cadherin and ZO2, or in the basal localization of Fibronectin (Figure 5.3). SEM analysis also indicated that every cell in the node had a single apical cilium, and Pericentrin staining showed that there were apically docked basal bodies in every cell (Figure 4.6G-H), consistent with normal apical-basal polarity in the *Vangl2^{Lp} Cfl1^{C5}* double mutant node cells.

5.1.1 Cofilin1 regulation in *Vangl2^{Lp}* embryos

The lack of membrane associated Celsr1 in the *Vangl2^{Lp} Cfl1^{C5}* double mutant node cells suggested that Cofilin activity was required for the establishment of planar cell polarity in the mouse. However, Rho, Rac and Cdc42, which have been shown to be downstream effectors of non-canonical Wnt signaling, also regulate Cofilin1 activity. Therefore, I assessed the phosphorylation status of Cfl1 in wild-type and *Vangl2^{Lp}* embryos lysate, which have reduced PCP signaling, and presumably altered levels GTP bound Rho,

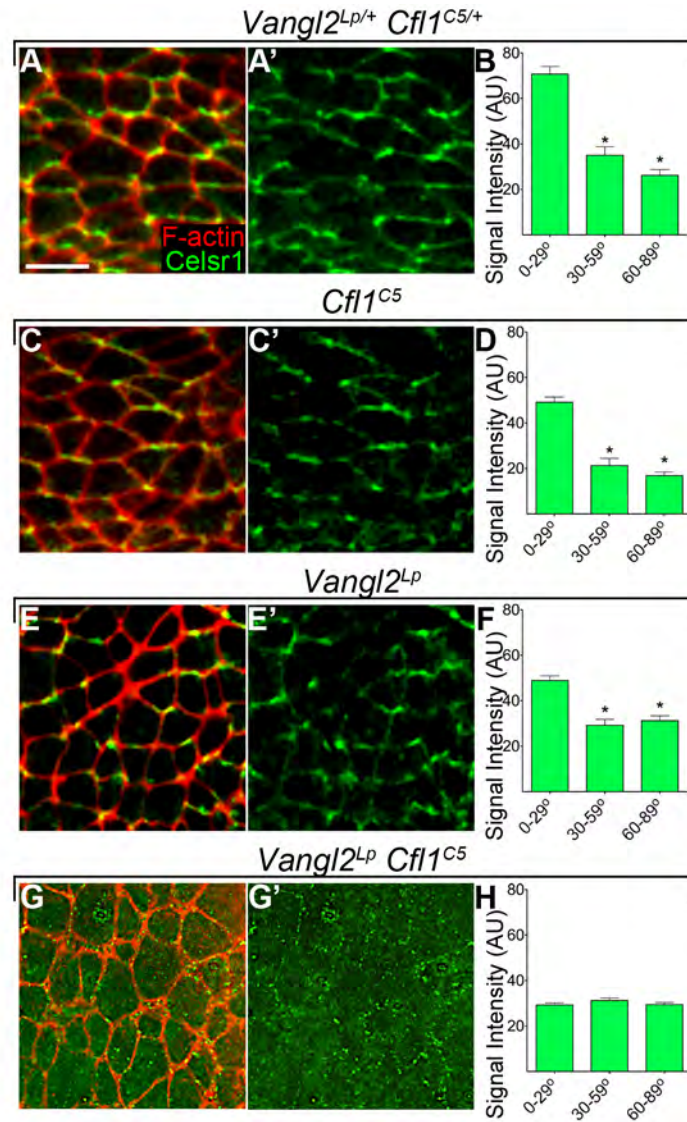


Figure 5.1: Celsr1 is not planar polarized in *Vangl2^{Lp} Cfl1^{C5}* double mutants.

Celsr1 (green) is enriched on the anterior/posterior faces of node cells in e8.0 wild-type embryos (A, B). Cell boundaries are highlighted by phalloidin (red), anterior towards the top. The anterior/posterior enrichment of Celsr1 is retained in *Cfl1^{C5}* (C, D) and *Vangl2^{Lp}* single mutants (E, F). In contrast, Celsr1 is not enriched at the apical membrane in *Vangl2^{Lp} Cfl1^{C5}* double mutants (G, H). (B, D, F, H) Graphs describe the mean intensity of Celsr1 staining normalized to phalloidin intensity along different edges of the cell. Celsr1 intensity was measured along individual cell borders and binned based on the angle with respect to the mediolateral axis of the embryo, such that 0-29° (horizontal) lines correspond to anterior/posterior faces of the cell, and 60-90° (vertical) lines correspond to mediolateral faces of the cell. Scale bar: 10 μ m.

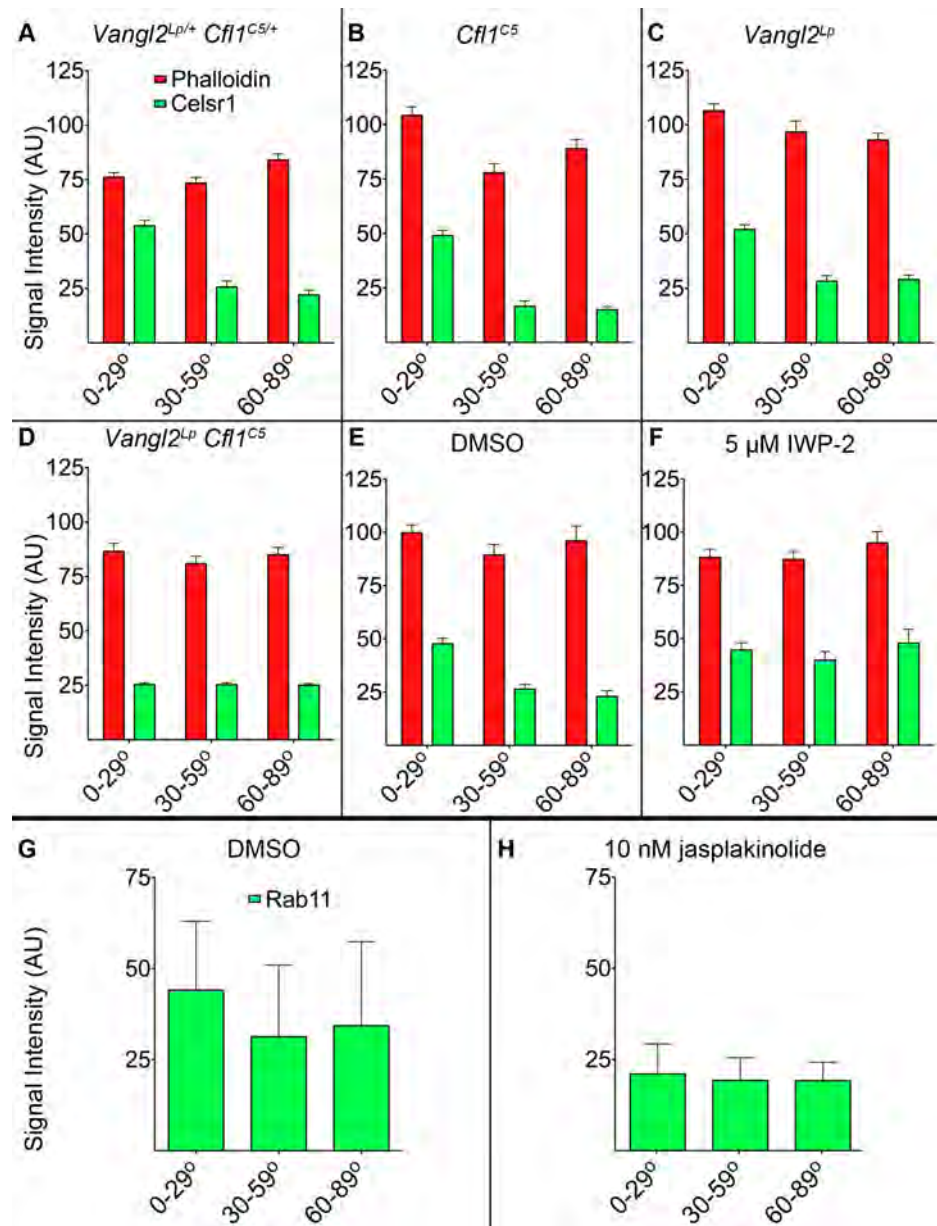


Figure 5.2: Membrane association of Celsr1 and Rab11

(A-F) Raw data for phalloidin and Celsr1 intensities from Figures 5.1 and 5.4. (G) Rab11 signal intensity at the apical membrane, normalized to the phalloidin intensity at the given angles. Although the mean signal intensity for Rab11 along the horizontal lines is greater than both 30-59° and 60-89°, the difference is not statistically significant. (H) The membrane association of Rab11 is lost after treatment with 10 nM jasplakinolide. These data have been normalized to the phalloidin intensity.

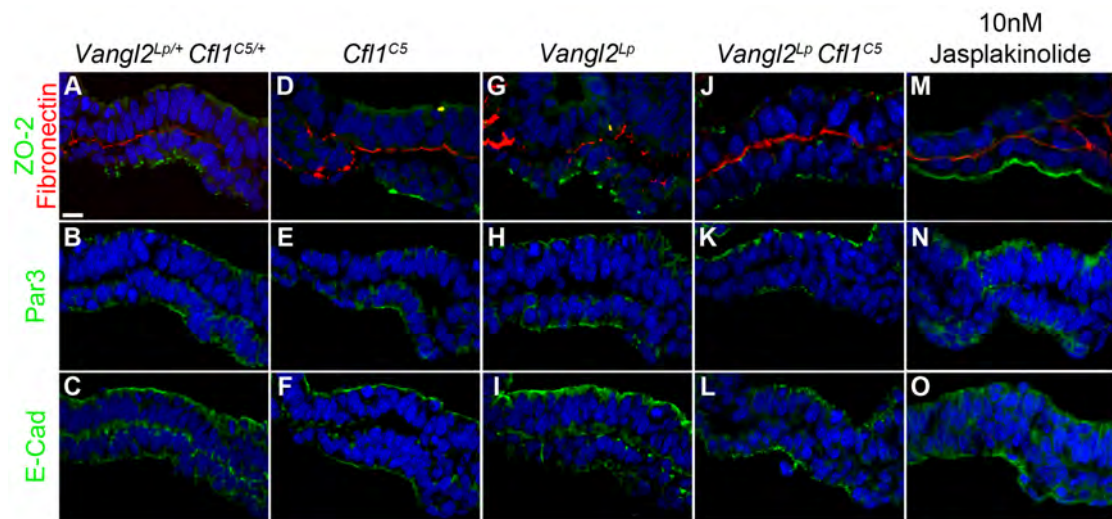


Figure 5.3: Apical-basal polarity in nodes with reduced Cofilin activity.

All images are sagittal sections of e8.0 embryos, the ventral node is the lower epithelium, and the apical membrane faces the bottom of the image. The apical markers ZO-2 (A, D, G, J, M), Par3 (B, E, H, K, N) and E-Cadherin (C, F, I, L, O) are localized correctly to the apical membrane of the node. The basal lamina component Fibronectin (red) (A, D, G, J, M) is localized correctly to the basal side of node cells in sections of wild type (A-C), *Cfl1*^{C5} (D-F) and *Vangl2*^{Lp} (G-I) single mutants as well as the compound mutants *Vangl2*^{Lp} *Cfl1*^{C5} (J-L). Apical-basal polarity is not disrupted in wild-type embryos after 14-18 hours of culture in 10 nM jasplakinolide (M-O). Scale bar: 10 μ m.

Rac and Cdc42. If Cofilin activity was required exclusively for the establishment of PCP signaling in the early mouse embryo, then there should be no changes in phospho-Cofilin levels in *Vangl2^{Lp}* embryos. However, if Cofilin were a downstream effector of PCP signaling then Cofilin regulation would be likewise altered in these mutants.

Serine 3 of Cofilin1 is an evolutionarily conserved residue in the N-terminal F-actin binding site, and the addition of a phosphate group to this residue by ROCK and LIM kinase interferes with actin binding, blocking the actin depolymerizing activity of Cofilin (Zebda et al., 2000). In lysate from single e9.5 *Vangl2^{Lp}* mutant embryos there was a strong decrease in the level of phospho-Ser3-Cofilin1 compared to wild-type embryo lysate (Figure 5.4A, D). In vertebrates, planar cell polarity signaling ultimately leads to the localized activation of Dvl, which in turn, remodels the actin cytoskeleton through the activation of the GTPases Rho and Rac (Park et al., 2005). Therefore, this result could be explained by an overactivation of Dvl in *Vangl2^{Lp}* mutant embryos at e9.5. However, my previous results showed that Celsr1 was not mislocalized in the node of *Vangl2^{Lp}* mutant embryos at e8.0. To reconcile these two findings, phospho-Ser3-Cofilin levels were assayed in lysates from e8.5 and e7.5 embryos. At these earlier time points there was only a slight decrease in phosphorylated Cofilin in *Vangl2^{Lp}* compared to wild type (Figure 5.4 B-D). The neural tube closure defects in *Vangl2^{Lp}* mutants begin to manifest at e8.0 and this coincided with the drop in phospho-Cofilin levels. At e9.5 *Vangl2^{Lp}* mutants have craniorachischisis, and the cells of the neural plate are noticeably less

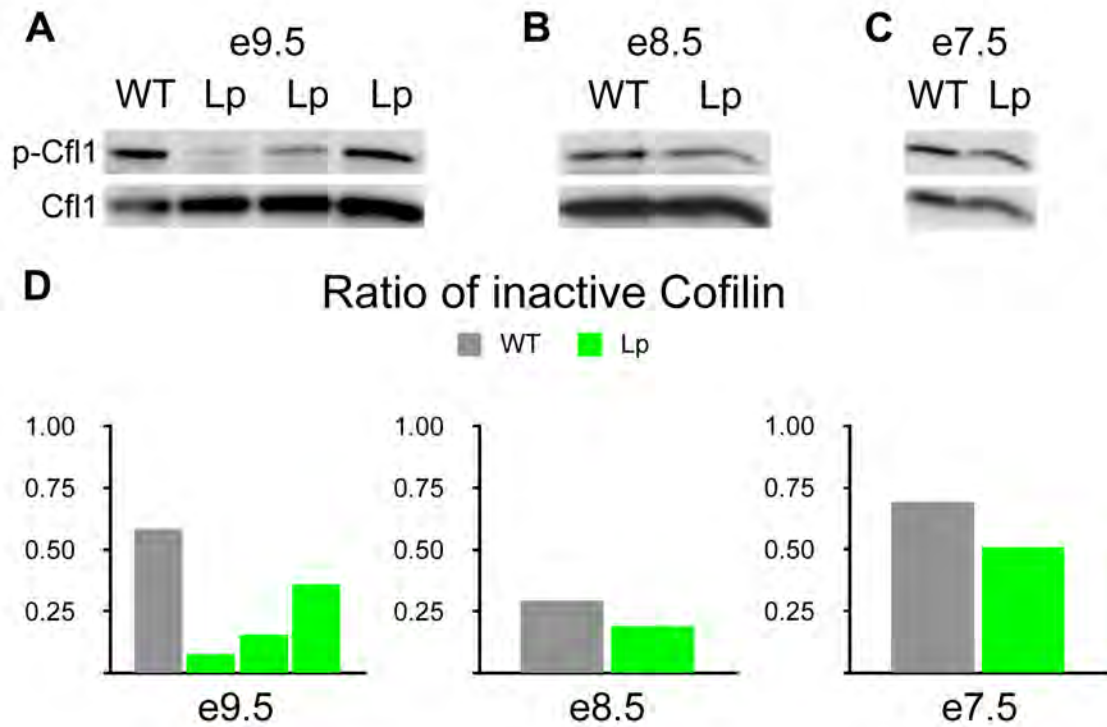


Figure 5.4. Cofilin1 regulation in *Vangl2^{Lp}* mutant embryos

(A-C) Western blots showing the levels of inactivated phospho-Ser3-Cofilin1 and total Cofilin1 from wild type (WT) and *Vangl2^{Lp}* (Lp) mutant embryos. Western blots were run with lysates from individual e9.5 embryos (A), three pooled e8.5 embryos (B) and five pooled e7.5 embryos. The strong reduction of phospho-Cofilin1 in mutant embryo lysate at e9.5 was not seen in earlier embryos. (D) Graphs of the Western blot data, showing the ratio of phospho-Cofilin1 to total Cofilin levels.

apically constricted than wild-type cells in the closed neural tube. Remodeling of the actin cytoskeleton is a critical event in apical constriction (Plageman et al., 2011), and specifically, Cofilin activity has been shown to be important for apical constriction that drives the morphogenesis of the chick otic vesicle (Sai and Ladher, 2008). Therefore, I suspect that the changes in Cofilin phosphorylation are secondary defects that arise from a failure to apically constrict neural plate cells in *Vangl2^{LP}* mutants, and do not result from direct changes in PCP signaling through Dvl and RhoA or Rac1.

5.1.2 Loss of cofilin activity is sufficient to disrupt planar polarity

There are three *Cofilin* genes in the mouse. *Cofilin2* is expressed specifically in muscle, while *Cfl1* and *Dstn* are broadly expressed throughout development (Gurniak et al., 2005). Animals homozygous for a deletion removing the *Dstn* locus, *Dstn^{corn1}*, are viable and fertile, but show a thickening of the cornea in adults (Smith et al., 1996). *Cfl1* and *Dstn* may overlap in function, as Destrin protein is up-regulated in *Cfl1* null mutants (Gurniak et al., 2005).

To test whether actin-severing activity is required for PCP signaling in the presence of wild-type *Vangl2*, I analyzed PCP protein localization in *Cfl1^{C5}* embryos with reduced *Dstn* activity. I was unable to recover *Cfl1^{C5} Dstn^{corn1}* double homozygotes at post-implantation stages, suggesting that actin severing is essential for preimplantation development. Although the majority of the *Cfl1^{C5} Dstn^{corn1/+}* embryos arrested prior to node formation, I recovered three embryos that developed nodes. In contrast to *Cfl1^{C5/+} Dstn^{corn1/+}* littermates, both *Celsr1*

and Vangl2 localized to cytoplasmic puncta that were dispersed throughout the apical cytoplasm in the *Cfl1^{C5} Dstn^{corn1/+}* mutant nodes, providing evidence that the stabilization of actin filaments is sufficient to prevent membrane association of PCP proteins (Figure 5.5A-B). Both Vangl2 and Celsr1 are transmembrane proteins; therefore, the presence of these proteins in cytoplasmic puncta suggested that they were retained in vesicles in the *Cfl1^{C5} Dstn^{corn1/+}* mutants, indicating that Cofilin activity is required for the trafficking of PCP vesicles.

Actin dynamics are required for the initiation, but not maintenance, of planar polarity

In an independent test of the role of actin dynamics in mouse PCP, I stabilized actin filaments pharmacologically using jasplakinolide, a small molecule that coats actin filaments and prevents their depolymerization (Bubb et al., 1994). Wild-type embryos were cultured in 10 nM jasplakinolide, a concentration that phenocopied the effects of a dominant negative Cofilin in the mouse yolk sac (Koike et al., 2009). At late-bud stage (e7.25), the node is not mature and Vangl1 and Vang2 are not yet planar polarized in the membrane (Song et al., 2010). When wild-type e7.25 embryos were cultured for 15 hours in DMSO alone, Celsr1 became planar polarized in node cells during the period of culture (Figures 5.6C-D, 5.2E). In contrast, when wild-type embryos at the same stage were cultured in the presence of jasplakinolide, Celsr1 and Vangl2 did not become enriched in the apical membrane in either the node or the midline (Figures 5.6B, 5.7B, 5.8B), while markers of apical-basal polarity were maintained (Figure 5.3M-O). As in *Vangl2^{Lp} Cfl1^{C5}* and *Cfl1^{C5} Dstn^{corn1/+}* mutants,

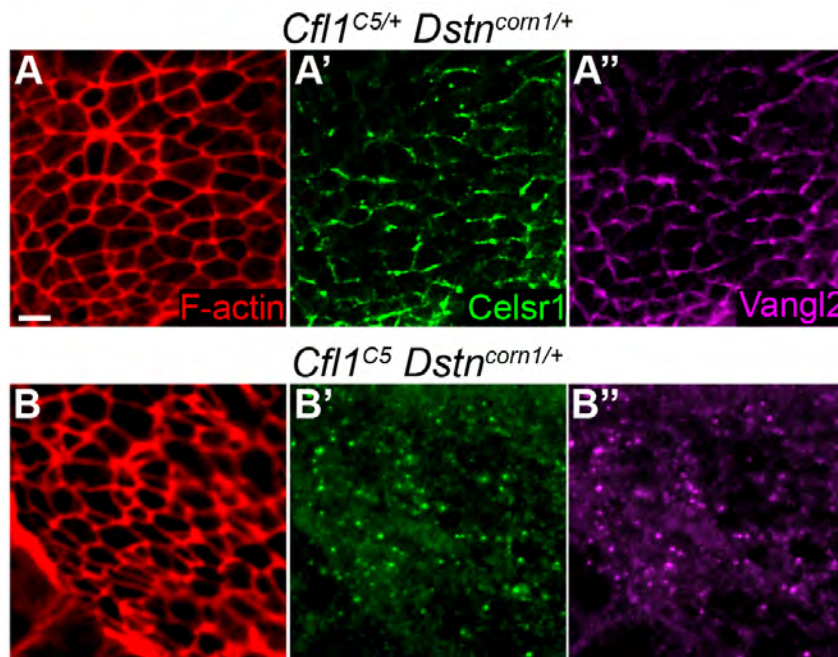


Figure 5.5: Vangl2 and Celsr1 localization in *Cfl1^{C5} Dstn^{corn1/+}* mutants.

(A) The PCP proteins Celsr1 (green) and Vangl2 (magenta) colocalize to the anterior/posterior faces of node cells in e7.5 wild-type embryos. **(B)** Celsr1 and Vangl2 colocalize in cytoplasmic puncta in the compound *Cfl1^{C5} Dstn^{corn1/+}* mutant. Scale bar: 10 μ m.

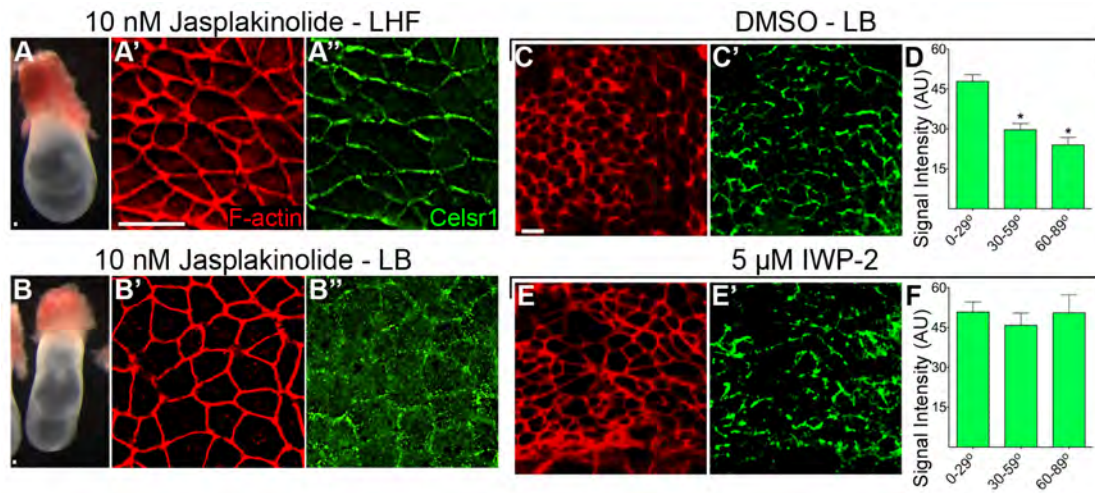


Figure 5.6: Jasplakinolide and IWP-2 disrupt planar polarity signaling.

(A-F) Effects of pharmacological inhibitors on the planar polarization of PCP proteins in cultured embryos. Late-headfold (LHF) stage embryos, shown before culture (A), show normal Celsr1 localization after 14-18 hours of culture in 10 nM jasplakinolide (A''). (B) When cultured in the presence of jasplakinolide in the same conditions, earlier embryos (late-bud stage, LB) phenocopy *Vangl2^{Lp} Cfl1^{C5}* and *Cfl1^{C5} Dstn^{corn1/+}*, as Celsr1 fails to become membrane localized (B''). (C) DMSO control for the late-bud stage culture. (E) Blocking Wnt ligand secretion does not prevent recruitment of Celsr1 to the membrane, as embryos cultured with 5 μM IWP-2 (an inhibitor of Wnt secretion) retain membrane-localized Celsr1, although Celsr1 is present on all faces of node cells. Quantification of the intensity of Celsr1 staining shows normal enrichment to the horizontal (anterior and posterior) edges of node cells in DMSO control (D), which is lost when embryos are cultured with IWP-2 (F) Scale bar: 10 μm.

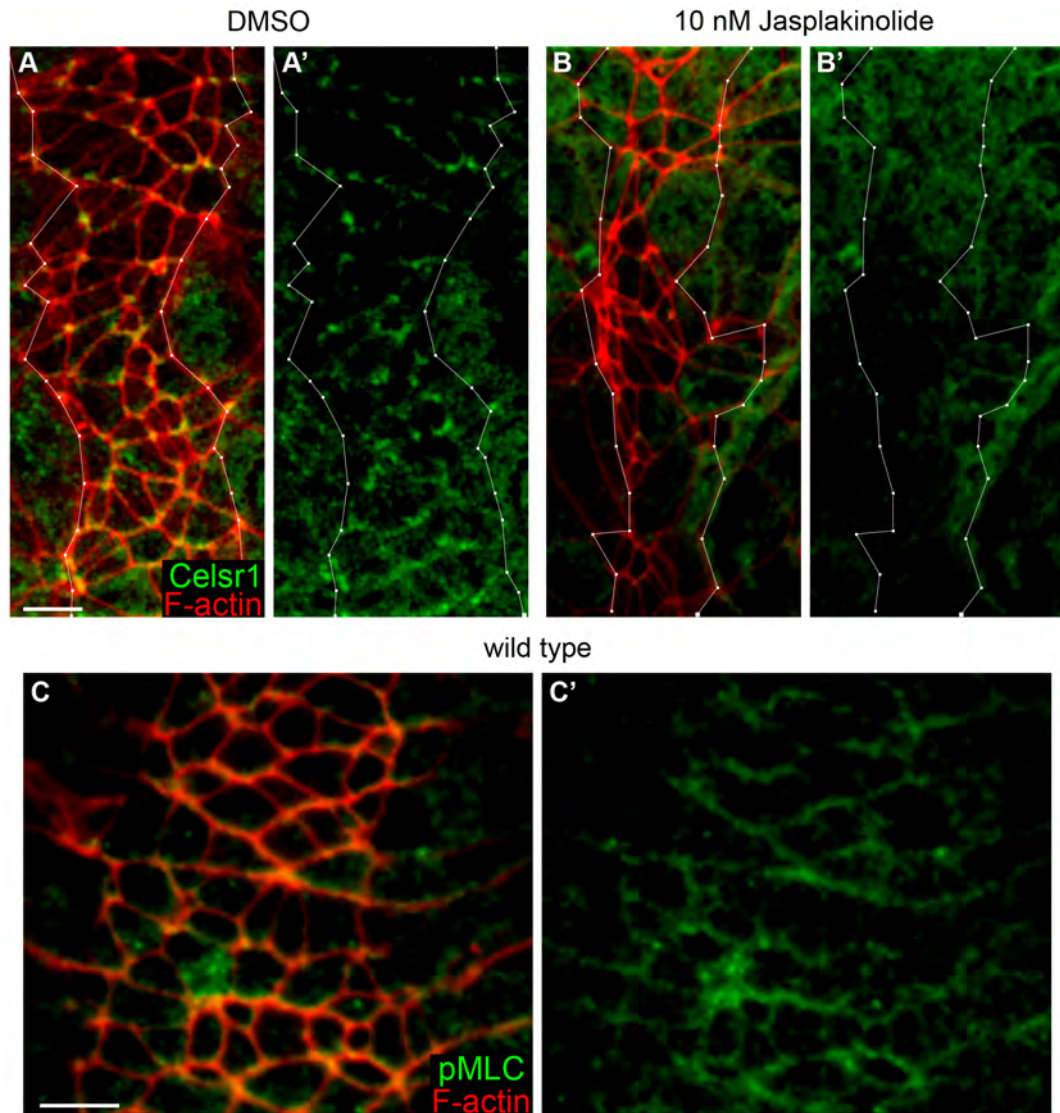


Figure 5.7: Celsr1 and pMLC2 are planar polarized in the axial midline. In wild-type embryos cultured for 14-18 hours in 0.1% DMSO (**A-A'**), Celsr1 (green) is planar polarized to the anterior/posterior faces in the apical membrane of cells in the midline (outlined in white). Membrane enrichment of Celsr1 is lost when wild-type embryos are cultured in the presence of 10 nM jasplakinolide (**B-B'**). (**C-C'**) In the midline of wild-type e8.0 embryos, phospho-Myosin Light Chain 2 (pMLC, green) is also planar polarized at the apical membrane to the anterior/posterior faces of the cell. Scale bar: 10 μ m.

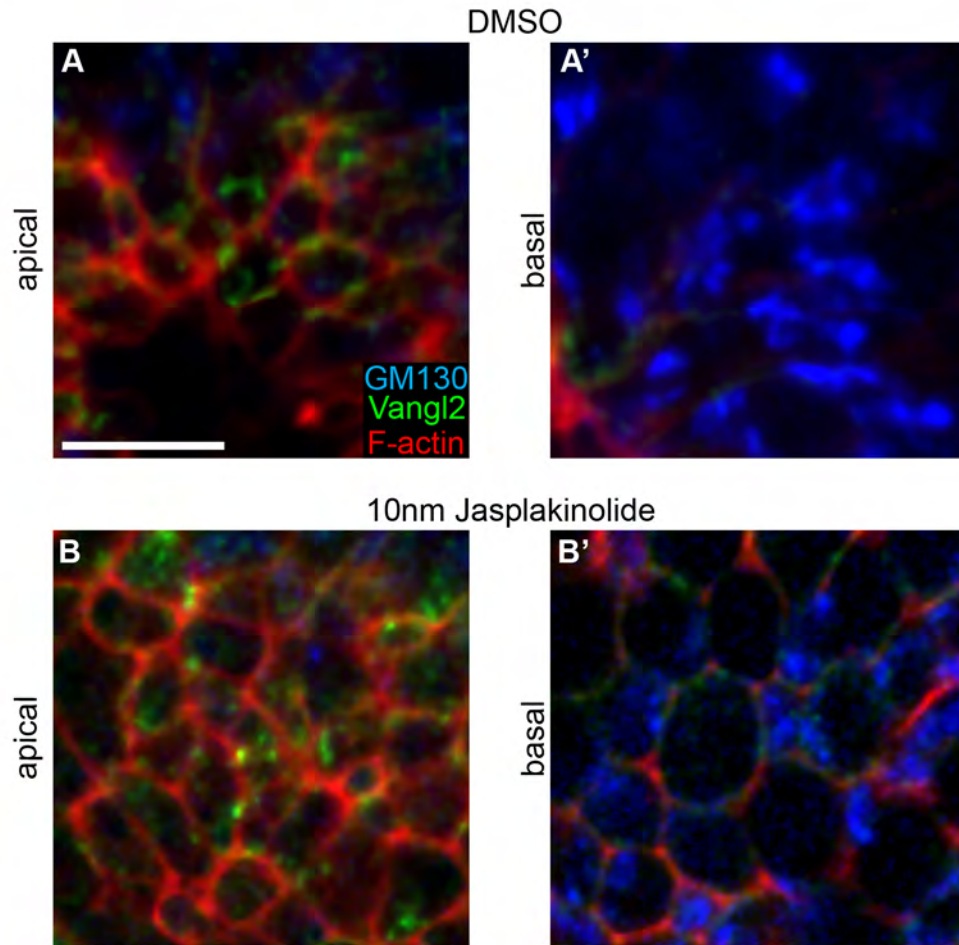


Figure 5.8: Jasplakinolide does not cause Vangl2 accumulation in the Golgi.

(A) Like Celsr1, Vangl2 (green) is planar polarized in the apical membrane of wild-type node cells, as seen in a 3 μm projection from a Z-stack of the apical domain of cells from the node of a wild-type embryo cultured in DMSO for 14-18 hours. In the same sample, GM130 (blue), a marker for the cis-Golgi network, is 4.5 μm below (basal to) the region where Celsr1 is enriched (A'). **(B)** After treatment with 10 nM jasplakinolide, Vangl2 is found in cytoplasmic puncta enriched in the apical domain. **(B')** These cytoplasmic puncta are apical to the Golgi, as GM130 is found 3.75 μm below the apical surface in this embryo. Note the increased phalloidin staining along the lateral membrane after treatment with 10 nM jasplakinolide. Scale bar: 10 μm .

Celsr1 and Vangl2 were present in cytoplasmic puncta in the apical domain of the cells. The puncta of Celsr1 and Vangl2 staining in these embryos appear to represent post-Golgi vesicles, as they were found apical to GM130, a marker of the cis-Golgi network (Figure 5.8B).

At a later stage, after formation of the node (~e7.75), culture in the presence of jasplakinolide did not affect the localization of Celsr1 in the node, which was planar polarized at the membrane in both treated embryos and controls (Figure 5.6A). This stage-dependent effect is likely responsible for the variability of Celsr1 staining in jasplakinolide-treated embryos (compare Figures 5.6B", 5.10B", 5.10D", 5.11B", 5.12B",). The findings indicate that Cofilin is required for the initiation, but not the maintenance, of planar polarity in the mouse node.

Celsr1 protein was also enriched on the anterior and posterior faces of cells in the notochordal plate of wild-type embryos (Figure 5.7A), which I have shown require PCP for convergent extension (Figure 4.4). As in the node, membrane association of Celsr1 was lost when actin remodeling was blocked by culture in the presence of jasplakinolide (Figure 5.7B). It was shown recently that the PCP pathway controls the morphogenetic movements required for neural tube closure in chick embryos by regulating the activation of Myosin (Nishimura et al., 2012). Similarly, I found that active phosphorylated-Myosin Light Chain 2 (pMLC2) was planar polarized to anterior/posterior faces of cells at the anterior border of the node and the midline (Figure 5.7C), the cells that are undergoing convergent extension morphogenesis as they exit the node and form the

notochordal plate. This planar polarization of pMLC2 was not detected in the central pit of the node, where active myosin was distributed uniformly around the circumference of the apically constricted cells. In contrast to the cells at the border of the node and midline, these cells are static, and are not involved in CE.

These two populations of cells highlight to dual roles of planar cell polarity signaling in the node. Planar polarized Vangl2 and Celsr1 is detected in all node cells, but cilia are polarized only in the central pit cells and randomly distributed in the cells along the periphery. However, pMLC2 is planar polarized in peripheral cells at the anterior border of the node, and evenly distributed in the central pit. Thus, PCP signaling defines the anterior-posterior body axis to all the cells in the node, but these two different groups of cells use these directional cues for distinct purposes.

Wnt ligands are required for planar cell polarity signaling

To test whether the loss of Celsr1 in the apical membrane was a consequence of the loss of PCP pathway activity, I compared the localization of Celsr1 in *Vangl2^{Lp} Cfl1^{C5}* double mutants to its localization in the absence of Wnt ligand. To block ligand production, I cultured e7.25 wild-type embryos in the presence of 5 μ M IWP-2, a small molecule inhibitor of the glycosyl-transferase Porcupine, which is required for secretion of Wnt ligands (Chen et al., 2009). After culture with IWP-2, Celsr1 was recruited to the apical membrane of node cells but planar polarity was disrupted: unlike DMSO control cultures, Celsr1 was no longer restricted solely to the anterior/posterior faces of node cells. Within the same node, Celsr1 was enriched on the medial/lateral faces (60-89°) in some

cells and anterior/posterior faces (0-30°) in other cells, demonstrating that Wnt ligand is not required for membrane localization or even restriction of Celsr1 to particular sides of the cell, but is required for coordinated planar polarization of Celsr1 throughout the cells in node (Figures 5.6E-F, 5.2F). I conclude that Cofilin activity is required for apical membrane association of PCP proteins, and Wnt ligands are required for their planar polarized asymmetric distribution.

PCP signaling in the node does not require the primary cilium

In *Drosophila*, *Inturned* and *Fuzzy* are downstream effectors of the PCP pathway that help implement polarized changes in the cytoskeleton during wing hair formation (Lee and Adler, 2002). However, mouse embryos lacking the homologues of either of these genes display phenotypes that are consistent with a defect in ciliogenesis, not planar cell polarity signaling (Gray et al., 2009; Zeng et al., 2010). This suggests that these proteins may reveal a link between the polarization of cytoskeleton and ciliogenesis. My experiments, along with other studies in the mouse have shown that cilia formation in the node is normal when the PCP pathway is genetically inactivated (Figure 4.6G-H; Song et al., 2010). In addition, it has been suggested that the primary cilium is required for normal PCP signaling. For example, mice lacking the Bardet-Biedl syndrome protein BBS4 have defects in neural tube closure and in the alignment of stereocilia in the cochlea (Ross et al., 2005), and conditional deletion of *Ift88*, a gene required for ciliogenesis, in the cochlea affects planar polarity of the actin-based stereocilia (Jones et al., 2008).

To test whether cilia play a role in PCP signaling in the node, I generated

e8.0 *Ift88* null embryos and stained them for Pericentrin, Celsr1 and Vangl2. In the *Ift88*^{-/-} embryos there were no defects in the positioning of the basal body compared to wild-type littermates. The average basal body position was 0.36 ± 0.09 in wild-type embryos and 0.38 ± 0.09 in *Ift88*^{-/-} mutant embryos, demonstrating that basal bodies were positioned towards the posterior side of the embryo even in the absence of cilia. Additionally, Celsr1 and Vangl2 proteins were apically enriched in the plasma membrane on the anterior and/or posterior faces of the cells in embryos lacking *Ift88*, as in wild-type littermates (Figure 5.9). I therefore conclude that the primary cilium is dispensable for the establishment of planar cell polarity in the e8.0 node, ruling out the possibility that misplaced cilia in the *Vangl2*^{Lp} *Cfl1*^{C5} node are responsible for the mislocalization of Celsr1 and Vangl2 in these cells.

5.2 Jasplakinolide inhibits vesicle trafficking of PCP proteins

The disruption of actin severing, either by the genetic reduction in the *Cfl1*^{C5} *Dstn*^{com1/+} compound mutants or treatment with jasplakinolide, blocked the localization of Vangl2 and Celsr1 to the plasma membrane. These proteins were not trapped inside the Golgi (Figure 5.8), rather were distributed throughout the apical cytoplasm in punctate structures. Because both Vangl2 and Celsr1 are transmembrane proteins I hypothesized that these puncta were vesicles that contain PCP proteins, suggesting that actin dynamics might be required for a specific step in vesicle trafficking that allows the incorporation of PCP proteins into the apical membrane.

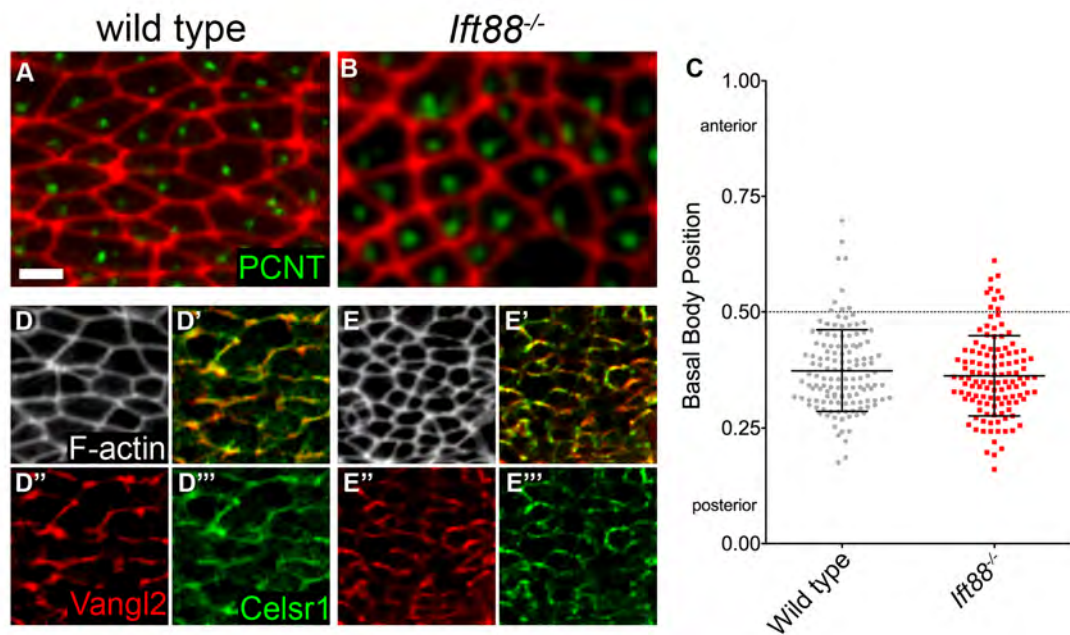


Figure 5.9: Planar cell polarity is normal in the node of *Ift88*^{-/-} mutant embryos. (A-C) Like wild-type embryos, Pericentrin (green) is posteriorly polarized in the central region of the node in *Ift88*^{-/-} mutants at e8.0. Phalloidin staining (red) outlines the cells. (D-E) Recruitment of Vangl2 and Celsr1 to the anterior and posterior faces of node cells is also normal in *Ift88*^{-/-} mutants. Scale bar: 5 μ m.

Little is known about the trafficking of PCP proteins, many of which contain transmembrane domains and thus are translated in the endoplasmic reticulum. The S464N substitution in the *Vangl2*^{Lp} allele specifically disrupts interactions with the COPII complex, inhibiting the trafficking of Vangl2 protein from the ER to the Golgi (Merte et al., 2010; Wansleben et al., 2010). Thus, PCP proteins are normally trafficked to the membrane via the Golgi in wild-type cells. Despite the roles for Cofilin that have been described in cargo sorting and vesicle budding from the Golgi (Blume et al., 2009; Blume et al., 2011; Salvarezza et al., 2009; Weisz and Rodriguez-Boulan, 2009), jasplakinolide treatment did not result in the accumulation of Vangl2 or Celsr1 in the Golgi in node cells (Figure 5.8). Therefore, I tested whether treatment of embryos with jasplakinolide affected the localization of any specific class of post-Golgi vesicles.

Transmembrane and secreted proteins can take a number of routes from the Golgi to the membrane; they can be directly trafficked from the Golgi or can stop first in early endosomes, where they are further modified and sorted before ultimately reaching the membrane (Stenmark, 2009). The asymmetric distribution of the PCP proteins in the anterior and posterior faces of node cells suggests that membrane trafficking of these proteins could involve an additional step, as proteins initially incorporated to lateral faces of the cell may be internalized and shuttled to a different membrane domain.

To test the first model, I examined the localization of Rab8, a marker associated with vesicles translocating from the Golgi directly to the apical membrane (Peränen, 2011). Jasplakinolide treatment did not cause a change in

the apical staining pattern of Rab8, nor was there an overlap between Celsr1 signal and Rab8 (Figure 5.10A-B”). From these data I conclude that actin dynamics do not affect Rab8 trafficking.

To test if Vangl2 and Celsr1 were enriched in endosomes I stained jasplakinolide treated embryos with the early endosome marker EEA1. I did not detect any change in the distribution of EEA1-associated vesicles in node cells after culture in the presence of jasplakinolide (Figures 5.11). However, 44% (n = 157) of the apical Celsr1⁺ puncta were marked by EEA1 in the presence, but not the absence, of jasplakinolide (Figure 5.11). The endosomal accumulation of PCP proteins in jasplakinolide-treated embryos is consistent with the model in which transmembrane proteins are trafficked from the Golgi to endosomes prior to being deposited in the plasma membrane. Alternatively, it could suggest that after incorporation in the membrane Vangl2 and Celsr1 are recycled from the membrane to endosomes. In either case, the accumulation of Celsr1 in the EEA1 compartment suggests that trafficking from the endosome to the membrane requires actin dynamics.

To test whether Celsr1 entered early endosomes after endocytosis, jasplakinolide-treated embryos were stained with Rab5, a marker of endocytic vesicles (Somsel Rodman and Wandinger-Ness, 2000). Jasplakinolide treatment did not cause a change in the apical staining pattern of Rab5, nor was there an overlap between Celsr1 signal and Rab5 (Figure 5.10A-B”), suggesting that the PCP⁺ endosomes were not coincident with the Rab5 compartment.

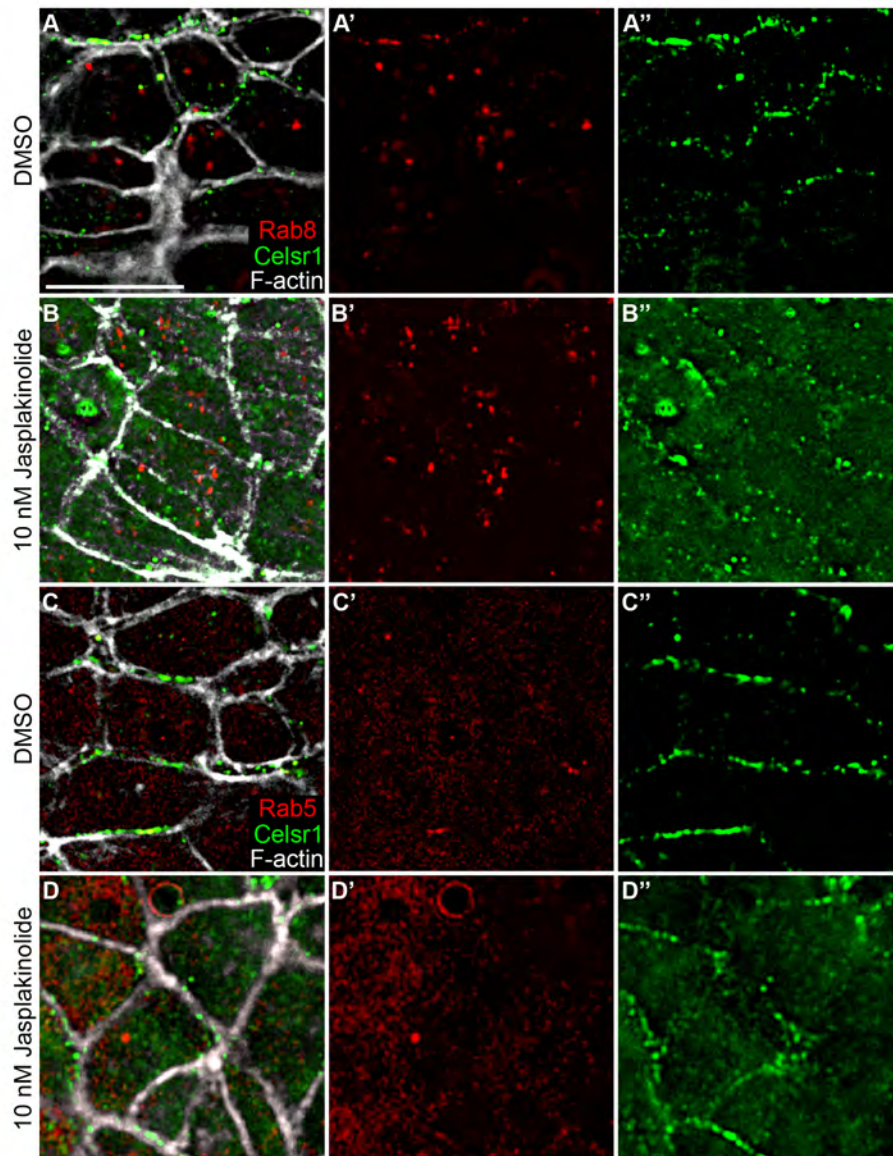


Figure 5.10: Vesicles containing Celsr1 do not colocalize with Rab8 or Rab5.

Wild-type embryos cultured for 14 hours in 0.1% DMSO have Celsr1 (green) enrichment in the apical membrane along the anterior/posterior faces of node cells (**A-A''**, **C-C''**). There is no colocalization between Celsr1 and Rab8 (**A-A''**) or Rab5 (**C-C''**) in these DMSO controls. Treatment with 10 nM jasplakinolide inhibits the membrane association of Celsr1 (**B-B''**, **D-D''**), which is now localized in cytoplasmic puncta. These cytoplasmic vesicles containing Celsr1 do not co-stain for Rab8 (**B-B''**) or Rab5 (**D-D''**). F-actin (white) is stained with phalloidin. Scale bar: 10 μ m.

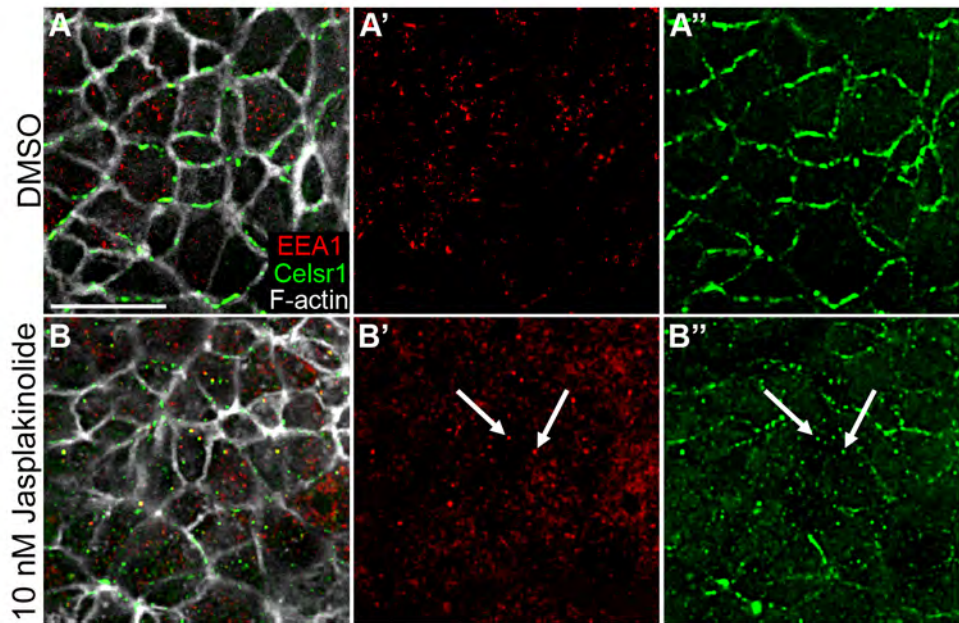


Figure 5.11: Jasplakinolide causes Celsr1 accumulation in endosomes.

(A-A'') In wild-type embryos cultured for 14 hours in DMSO, there is no colocalization between Celsr1 (green) and the early endosomal marker EEA1 (red). **(B-B'')** Treatment with 10 nM jasplakinolide does not change the distribution of EEA1, but inhibits plasma membrane association of Celsr1. In drug treated embryos 44% (n = 157) of the cytoplasmic Celsr1 puncta overlaps with EEA1 (arrows).

5.2.1 Actin severing is required for the coordinated localization of Rab11 and PCP proteins to the plasma membrane

The above data demonstrated that culturing embryos in the presence of jasplakinolide caused an accumulation of PCP proteins in early endosomes in the ventral node. However, it remained unclear what specific step in vesicle trafficking was affected by inhibiting actin dynamics, as the localization of Rab5, and EEA1 were unaffected in treated embryos. I next tested the hypothesis that there were defects in the trafficking of PCP proteins from the early/recycling endosomal compartment to the membrane by examining the localization of Rab11, a marker associated with membrane-bound vesicles and recycling endosomes (Wang et al., 2000).

Rab11 showed an interesting change in distribution in jasplakinolide treated embryos. In control embryos, Rab11 was present in both cytoplasmic apical vesicles and in vesicles immediately adjacent to the plasma membrane at the level of the adherens junctions. The membrane-associated Rab11 appeared to be more commonly associated with horizontal faces of cells where Celsr1 was localized (Figures 5.12A-A''); however, I did not detect membrane-associated Rab11 in every cell, so when the Rab11 signal intensity at the membrane was quantified this association with the anterior/posterior faces was not statistically significant (Figure 5.2G).

Inhibition of actin severing by jasplakinolide treatment caused a clear change in Rab11 distribution: cytoplasmic Rab11⁺ vesicles were still present, but

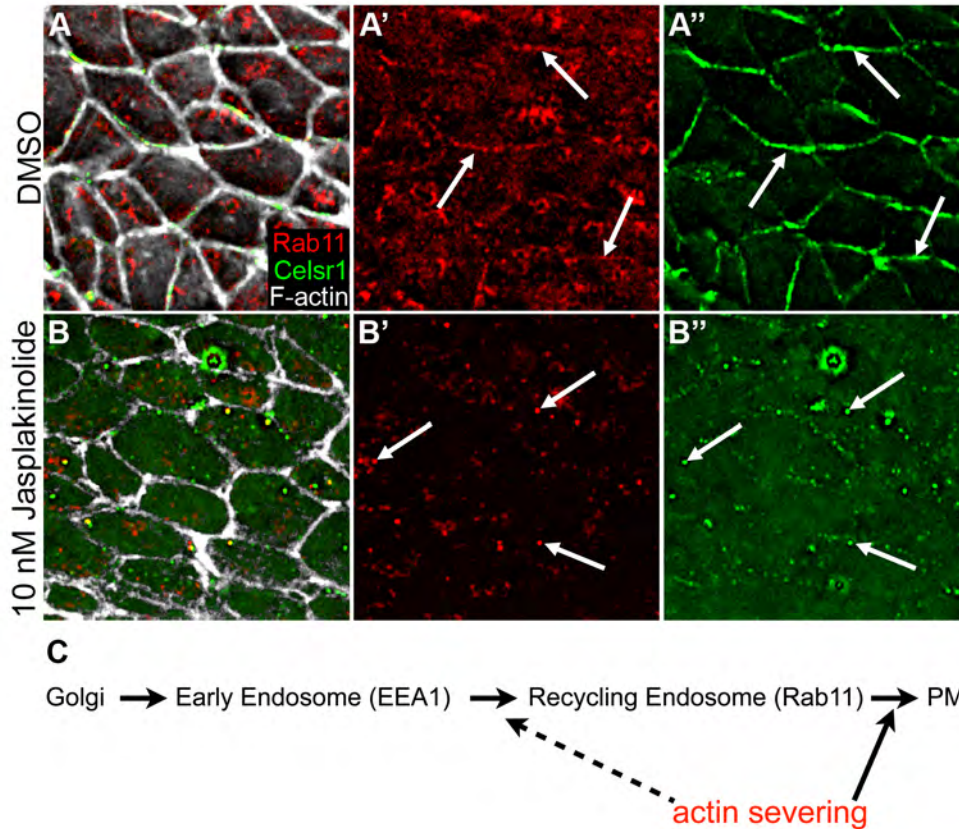


Figure 5.12: Membrane associated Rab11 and Celsr1 require dynamic actin.

(A-A'') In wild-type embryos cultured for 14 hours in DMSO, there is some overlap between Celsr1 (green) and Rab11 (red) adjacent to the plasma membrane (arrows).

(B-B'') In embryos treated with 10 nM jasplakinolide neither Rab11 nor Celsr1 localizes to the plasma membrane, and 31% (n = 187) of the cytoplasmic Celsr1 puncta overlaps with Rab11 (arrows). **(C)** Model for trafficking of PCP proteins. Celsr1 and Vangl2 traffic to EEA1⁺ endosomes then enter Rab11⁺ vesicles and are delivered to planar polarized complexes at the plasma membrane (PM) at the initiation of PCP in the node. Actin dynamics are required for this last step and possibly for the movement/transition of EEA1⁺ endosomes to the Rab11 compartment. Scale bar: 10 μm.

these vesicles were no longer adjacent to the plasma membrane (Figures 5.12B-B', 5.2H). Approximately 31% (n=187) of the *Celsr1*⁺ puncta were also positive for Rab11 in jasplakinolide-treated embryos (Figure 5.12B-B''). These data suggest that *Celsr1* normally moves to the membrane through EEA1 and Rab11-positive vesicles, and that inhibition of actin turnover prevents the fusion of the Rab11⁺ vesicles with the apical plasma membrane.

5.3 Discussion

The defects in convergent extension of the midline, and cilia polarity in the node that were presented in chapter four indicated that planar cell polarity signaling is abolished in *Vangl2*^{Lp} *Cfl1*^{C5} double mutants. The experiments outlined help define the mechanistic basis of the genetic interaction by demonstrating that *Vangl2* and *Cofilin* act in pathways that converge on membrane trafficking of *Celsr1*. While defects in membrane trafficking of *Celsr1* are not apparent in the *Cfl1*^{C5} single mutants, stronger disruptions of actin dynamics, caused either by loss-of-function mutations in two *Cofilin* genes or by a pharmacological inhibitor of actin severing, blocks membrane localization of PCP proteins. I hypothesize that there are subtle defects in trafficking of PCP vesicles to the membrane in *Cfl1*^{C5} single mutants, and when combined with *Vangl2* deficiency, the trafficking of PCP proteins to the membrane is abolished.

My data argue that dynamic rearrangement of F-actin filaments is required to target vesicles containing PCP proteins to the apical plasma membrane.

Cofilin has been implicated in several steps of vesicle trafficking. Disruption of

Cofilin by knockdown or overexpression has been shown to disrupt formation of vesicles from the trans-Golgi network (Salvarezza et al., 2009) or sorting of proteins in the Golgi (Blume et al., 2009). However, because *Celsr1* and *Vangl2* are found in cytoplasmic puncta in a domain apical to the Golgi in the node cells of *Cfl1^{C5} Dstn^{corn1/+}* compound mutants and jasplakinolide-treated embryos, I conclude that a later step in the vesicle trafficking pathway is disrupted in the mutants. Recent genetic experiments in the *C. elegans* intestine indicated that cofilin also regulates the apical distribution of Rab11⁺ vesicles (Winter et al., 2012). Consistent with those observations, I observed that loss of actin severing disrupts the association of Rab11⁺ vesicles with the plasma membrane and leads to accumulation of Rab11⁺ *Celsr1*⁺ vesicles in the apical domain of node cells, arguing that Rab11⁺ vesicles are critical targets of cofilin-regulated trafficking in PCP. It was previously shown that planar polarity is maintained through cell division by regulated internalization and retargeting of PCP proteins during mitosis, and more than 70% of the *Celsr1*⁺ vesicles are also Rab11⁺ in that context (Devenport et al., 2011). My results suggest that the initial targeting of PCP proteins to the cell surface also goes through a Rab11⁺ vesicle intermediate. Although Rab11 is important for dynamic relocalization of E-cadherin (Classen et al., 2005; Desclozeaux et al., 2008), E-cadherin localization is not affected in either *Vangl2^{Lp} Cfl1^{C5}* double mutants or jasplakinolide-treated embryos, indicating that the PCP proteins in the node are particularly sensitive to disruptions of this trafficking pathway.

The data show that actin stabilization causes a specific defect in the

trafficking or docking of Rab11⁺ vesicles containing PCP proteins to the apical membrane in the node. However, once established within a cell, these PCP complexes are unaffected by actin stabilization. After localization to the apical membrane, interactions among the cytoplasmic PCP proteins and trafficking along the microtubule cytoskeleton are important to maintain PCP proteins on opposite faces of the cell (Shimada et al., 2006). My data suggest that the initial targeting of PCP proteins depends on an F-actin-dependent pathway, either through direct targeting of Rab11⁺ PCP⁺ vesicles directly to the plasma membrane or by endocytosis of membrane-associated PCP proteins into a Rab11⁺ EEA1⁺ recycling endosome; in either scenario, dynamic reorganization of the apical F-actin cytoskeleton is required for the initial targeting of Rab11⁺ PCP⁺ vesicles to the plasma membrane, which ultimately allows planar polarized localization (Figure 5.12C).

The activity of Cofilin can be regulated by phosphorylation and is downstream of a variety of signals (Bernstein and Bamburg, 2010). The identification of Cofilin as a regulator of mammalian planar cell polarity suggests that planar polarity could be modulated through phosphorylation or dephosphorylation of Cofilin in response to tissue-specific signals during mammalian development.

CHAPTER SIX

6 PROTEIN VIRILIZER HOMOLOGUE

Dr. Kathryn Anderson identified the TO1 line in a forward genetic screen for N-ethyl N-nitrosourea (ENU)-induced recessive mutations that caused morphological defects in midgestation mouse embryos (García-García et al., 2005). Initially, homozygous TO1 mutant embryos were characterized by a severe developmental delay and underdeveloped derivatives of the polar trophoderm, the ectoplacental cone and extraembryonic ectoderm (Figure 6.1). Using Sanger sequencing, I subsequently found that the TO1 line harbored a single point mutation in the coding sequence of the *Protein virilizer-homologue* (*Pvh*, 1110037F02Rik) gene product, a previously uncharacterized gene in the mouse genome. *Pvh* is a homologue of the *Drosophila* gene *Virilizer*, a component of the RNA splicing machinery that is required for sex determination and X chromosome dosage compensation in females. *In situ* hybridization for *Brachyury* (*T*) expression revealed that TO1 mutants had gastrulation defects, and often a large gap in the primitive streak. Hex-GFP expression showed no defect in AVE migration, so it is unclear if these defects represent true axis duplication or defects in primitive streak formation. After cloning the mutated gene, we named this allele of *Pvh* *2-seam* (*2sm*), based on the similarity of the *Brachyury* expression in the TO1 mutants to a baseball gripped for throwing a 2-seam fastball (Figure 6.1).

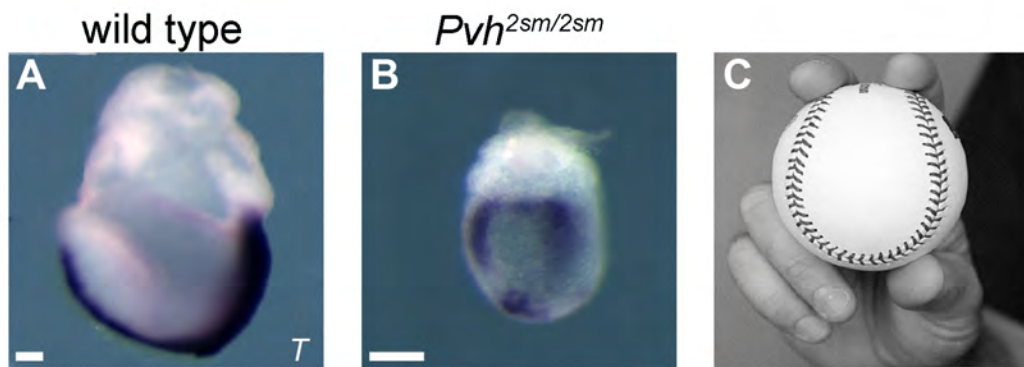


Figure 6.1: Embryonic phenotype of homozygous *Pvh*^{2sm} mutants.

(A-B) *Brachyury* (*T*) expression in wild type (A) and homozygous *Pvh*^{2sm} mutant (B) littermates at e7.5 shows the split primitive streak on the posterior side of the mutants. *Pvh*^{2sm} mutants are delayed and have growth defects in derivatives of the polar trophoblast. Scale bar: 100 μ m. (C) *T* expression in the mutants with the split streak phenotype is reminiscent of the seams of a baseball gripped for throwing a 2-seam fastball.

6.1 Introduction

As the first phenotype based screen for mutations that alter embryonic development taught us almost 40 years ago (Nüsslein-Volhard and Wieschaus, 1980), the best way to understand the function of a gene is to look at its loss-of-function phenotype. One approach to this paradigm is to remove a gene of interest and study the resulting phenotype. However, this strategy can be complicated when working with the mammalian genome, as there are multiple copies of many gene families in the genome, rendering some single mutant analysis ineffective. Our lab has taken an unbiased approach to this problem, isolating loss-of-function mutations based on embryonic phenotypes, and then finding the mutated gene. These forward genetic screens have yielded a plethora of novel mutations, affecting many different developmental processes, and have given us a platform to study the genetic regulation of signal transduction pathways required for normal development. The initial screens in the lab relied on isolating mutant lines based on morphological defects alone. Subsequently, we have begun to modify this approach by backcrossing our mutagenized mice to strains expressing transgenic reporters for important developmental processes. In one of these recent screens we used mice expressing GFP under control of the *Brachyury* promoter. Thus, mutants from this screen could be isolated by defects in gross morphology, and also by aberrant expression of a primitive streak marker. The TO1 line was a novel mutation isolated from this reporter-based screen.

6.1.1 ENU mutagenesis

Like the *Axin2*^{canp} and *Cfl1*^{C5} mutations that were previously discussed, the *Pvh*^{2sm} mutation was recovered from an ongoing phenotype-based forward genetic screen in our lab (Figure 6.2; García-García et al., 2005). In this screen male mice from the C57BL/6J background are mutagenized with N-ethyl N-nitrosourea (ENU). ENU is a DNA alkylating agent, most often generating point mutations, primarily A/T to T/A transversions and A/T to G/C transitions, in the genome (Balling, 2001). The C57BL/6J males are injected with a concentration of ENU that yields approximately one inactivating mutation per gene per 700 gametes (Balling, 2001); thus each haploid gamete from the injected male contains between 40 to 60 gene inactivating point mutations in the genome.

In order to isolate single phenotypes from these germline mutations, we first outcross the mutagenized males to the FVB/NJ background. This establishes individual F1 lines, each of which carries multiple mutations in the chromosomes inherited from the C57BL/6J strain. These F1 males are then again outcrossed the FVB/NJ background, generating a G2 population; 50% of these G2 animals will be carriers for a given mutation that is present in the F1 line. We isolate novel mutations by crossing these G2 females back to the F1 male. If the F1 male is carrying a mutation that causes mid-gestation lethality then we will isolate those mutants in 50% of these blind crosses (Figure 6.2).

After a few generations of backcrossing to the FVB/NJ background we then submit DNA from either embryos or carrier adults for whole genome single nucleotide polymorphism (SNP) mapping (Moran et al., 2006). This technology is

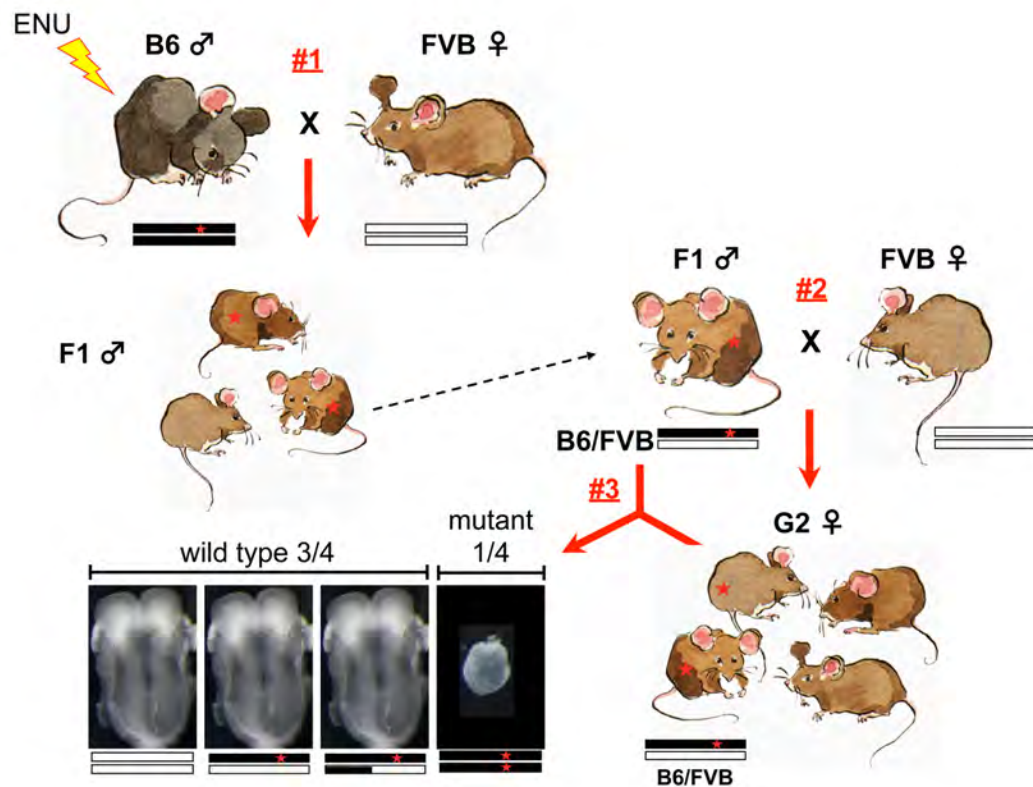


Figure 6.2: ENU mutagenesis screen.

ENU Mutations are induced in the germline of C57BL/6J (B6) males. These males are then backcrossed to the FVB/NJ (FVB) line (cross #1). The resulting F1 males have 40-60 inactivating mutations in the inherited B6 chromosomes. G2 females are produced by another round of backcrossing to FVB/NJ (cross #2). 50% of these G2 females will be carriers for a given mutation present in the F1 male. If the G2 female is a carrier for a recessive mutation that causes embryonic phenotypes, then 25% of the embryos from that F1 x G2 intercross (cross #3) will have a phenotype. Modified from García-García et al., 2005.

able to distinguish regions of the genome that are inherited from either the C57BL/6J or FVB/NJ strains based on single base-pair differences between these inbred strains. Because our mutations were induced in the C57BL/6J background, we look for regions of the genome that contain C57BL/6J markers in all our samples. This not only helps us map the location of the mutation within the genome, but also confirms that the phenotype we are following is the product of one genetic lesion, and not two independently segregating alleles.

6.1.2 Virilizer in *Drosophila*

The regulatory event that govern sex determination and dosage compensation for transcripts from the X chromosome vary greatly between different species, and appear to be one of most rapidly evolving genetic networks in biology (Gempe and Beye, 2011). Some organisms, such as the fruit fly, employ a chromosome counting mechanism that yields females from the presence of two X chromosomes. Other organism of the order Diptera use the presence or absence of a Y chromosome to generate males and females (e.g. the housefly), another variation on this process has been found in wasps, where unfertilized eggs develop into males and fertilized eggs develop into females. One hallmark of this process in Diptera is that all of these decisions appear to hinge on alternative splicing networks, which act as binary switch for sex determination and the expression of *transformer* (Salz, 2011).

The best genetically characterized sex determination pathway is from *Drosophila*, where alternative splice forms of the *Sex-lethal* (*Sxl*) transcript

govern the male/female decision. The full length *Sxl* transcript contains a translational terminating exon 3, which is removed by the U1 mRNA splicing complex only in females (Bopp et al., 1999). CHIP data has shown that the U1 splicing complex is assembled at the 5' end of the male exon (exon 3) of the *Sxl* transcript in both males and females (Johnson et al., 2010), suggesting that specific factors must be required to deactivate this complex only in female embryos and allow direct splicing from exon 2 to exon 4. When exon 3 is removed *Sxl* protein is made, and is sufficient to drive a positive feedback loop that generates the female specific isoform of *Sxl*, allowing the expression of *transformer*; however, the initial splicing of the *Sxl* mRNA requires factors that allow for the female specific splicing in the absence of *Sxl* protein (Horabin and Schedl, 1996).

Two gene products that were found to be required for this initial splicing of *Sxl* are *Virilizer* and *Female-lethal-2-D (Fl(2)d)* (Granadino et al., 1990; Hilfiker et al., 1995). When either of these genes is mutated only male embryos are generated. While the mechanism that allows expression of *Virilizer* and *Fl(2)d* only in XX eggs is unknown, these genes also act together in splicing of the *Ultrabithorax* mRNAs, later in the development of somatic tissues (Burnette et al., 1999). *Fl(2)D* is the *Drosophila* homologue of the *Wilms' tumor 1-associating protein (WTAP)* and physically interacts with *Wilms' tumor suppressor gene-1 (WT-1)* (Little et al., 2000). *WT-1* is a zinc finger containing protein that has multiple functions during development as well as acting a tumor suppressor in the kidney. There are many isoforms of *WT-1* and it has been shown to function

as a transcription factor, and regulate mRNA stability, Wnt signaling, and possibly apoptosis (Wagner et al., 2003).

6.2 The 2-seam mutation

Homozygous *Pvh*^{2sm} mutants, originally identified as the TO1 line from the 2006 screen, arrest prior to headfold formation at e7.5; at e8.5 the embryos are slightly larger in overall size compared to e7.5, but they remain arrested at streak stages (Figure 6.3). Although some mutant embryos were recovered at e9.5, most appear to be reabsorbed by nine days of embryonic development. Apart from the developmental delay, mutant embryos also have underdeveloped derivatives of the polar trophectoderm lineage and appear to lack embryonic mesoderm (Figure 6.3).

6.2.1 2-seam is an allele of *Protein virilizer homologue*

To isolate the mutated gene in the TO1 line we took advantage of our crossing scheme; the mutation would be present in DNA from the C57BL/6J strain and not the FVB/NJ strain that we used for outcrossing. To distinguish between DNA inherited from these two lines we used a whole genome single nucleotide polymorphism (SNP) array (Broad Institute; Moran et al., 2006). There are many SNPs between the C57BL/6J and FVB/NJ strains, and this technology can identify a locus as either C57BL/6J or FVB/NJ based on the single base pair differences. The array that was used contained one SNP every 4-10 megabases

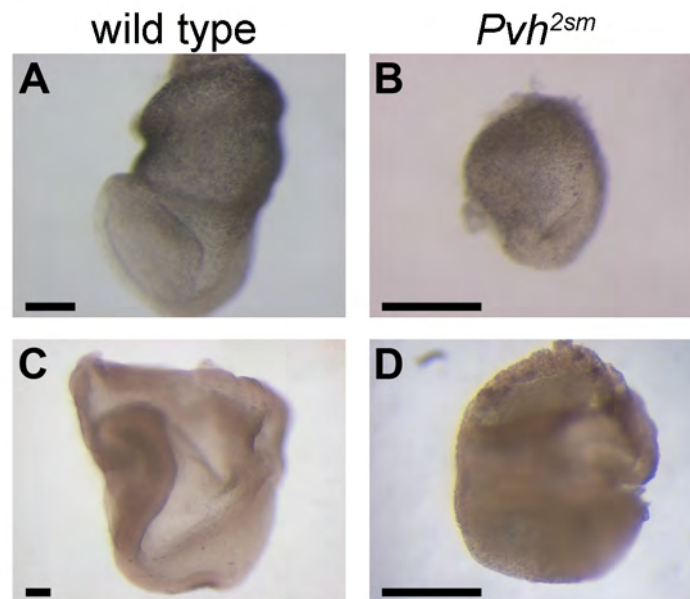


Figure 6.3: The 2-seam phenotype.

(A-D) Wild-type littermates (A, C) and 2-seam mutants (B, D) from e7.5 and 8.5 dissections. Embryos lacking Protein virilizer-homologue activity are delayed, but do still grow from e7.5 to e.85. The mutants appear to lack mesoderm, and while trace amounts of extraembryonic ectoderm are present, there are defects in the growth of this lineage. Scale bar: 100 μ m.

(Mb). Because the TO1 mutants were too small to obtain enough DNA for the SNP analysis, the array was performed using DNA from 10 confirmed carriers of the mutation. From this array we were looking for regions in which all 10 carriers were consistently heterozygous for C57BL/6J and FVB/NJ markers. From this initial analysis it was determined that the mutation was in the proximal 35.7 megabases (Mb) of chromosome 4, between the centromere and the SNP rs3703981 (Figure 6.4A).

Further backcrossing (448 recombination opportunities) to the FVB/NJ background mapped the mutation between the SNPs rs28261795 (10.33 Mb) and rs27715143 (11.66 Mb). Candidate genes from this interval were identified based on physical location in the Ensembl database. Genes that were expressed in the e7.5 embryo and whose knockout phenotype was unknown were sequenced from a cDNA library generated from a pool of six TO1 mutant embryos. From this pool of genes the only polymorphism identified by Sanger sequencing was the T to A transversion at nucleotide 2023 in *Protein virilizer-homologue* (*Pvh*, 1110037F02Rik; Figure 6.4B). This point mutation encodes a tyrosine to asparagine substitution at amino acid 675 in the protein.

There are three predicted splice variants of *Pvh*, and this mutation is present in all three isoforms of the transcript (Figure 6.4C). The full-length transcript of *Pvh*, which uniquely contains exon nine, would encode this mutation at nucleotide 2173, but my sequencing data suggests that this splice variant is not expressed at e7.5 because I never amplified a transcript containing exon nine from cDNA prepared from embryos.

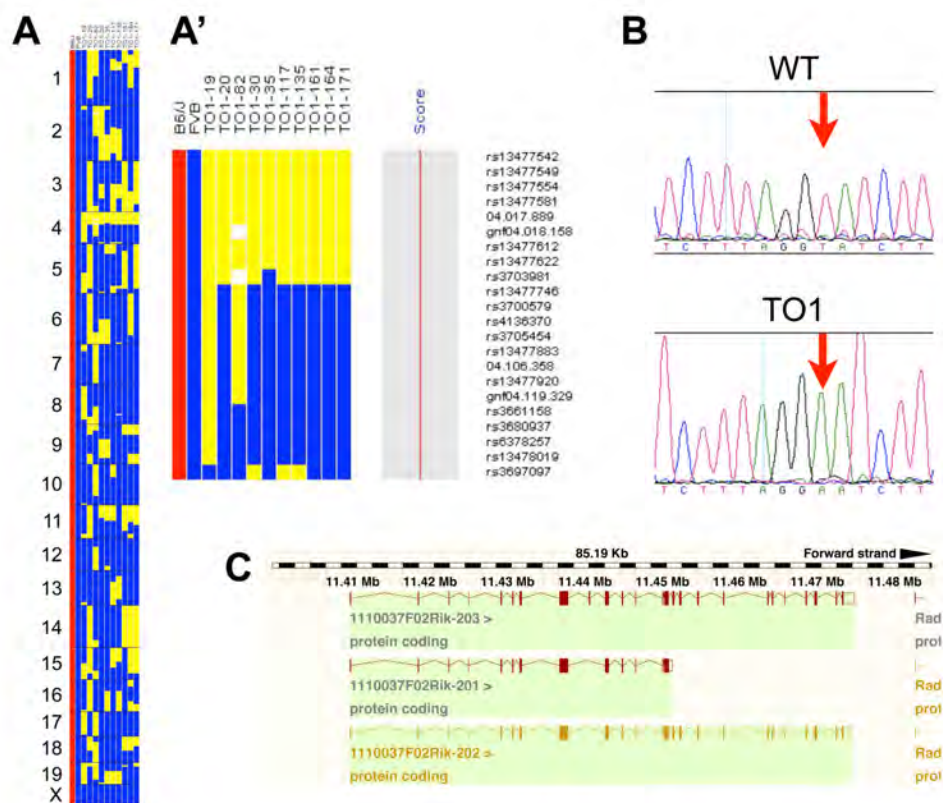


Figure 6.4: Mapping and cloning the TO1 allele.

(A-A') Data from the whole genome SNP array (518 SNPs) presented graphically. The SNP genotypes, C57BL/6J homozygous (red), FVB/NJ homozygous (blue), and heterozygous (yellow), from 10 carrier TO1 adults are shown. Numbers along the left indicate the chromosomal position of the SNPs. The proximal 34 Mb of chromosome 4 (A') is the only region in the genome that is heterozygous across all the samples. Data from Jennifer Moran, Broad Institute. (B) Sanger sequencing data from base pairs 2015-2028 of *Pvh* cDNA reveals a T to A transversion at nucleotide 2023 (red arrow). The TO1 sequencing was from a cDNA library generated from six pooled mutant embryos. (C) The *Pvh* genome locus (annotated by Ensembl Genome Browser; www.ensembl.org), shows three predicted splice variants. The point mutation in the TO1 line is present in all three predicted isoforms.

6.2.2 The 2-seam embryonic phenotype

The apparent lack of mesoderm in these mutants suggested defects in gastrulation; therefore, I first looked for the presence of a primitive streak in these mutants using both the transgene that expresses GFP from the *Brachyury* (*T*) promoter (Vigneau et al., 2007), and by analyzing *T* expression by RNA *in situ* hybridization. From the initial images of GFP expression in *2sm* mutants it appeared that there was a reduction in transgene expression, as no cells expressing comparable levels of GFP to streak cells in wild type littermates were found (Figure 6.5A, C). *Brachyury in situ* hybridization also showed lower levels of *T* transcript in the mutants compared to wild-type littermates (Figure 6.5B, D-E), supporting the previous results. From the *T in situ* it was clear that there were two classes of *2sm* mutants. The first class (9/32 embryos examined) had only a small spot of *T* expression in the presumptive posterior of the embryo, which did not elongate towards the distal tip of the embryo; the majority of these embryos also appeared to have a bulged primitive streak (6/9 embryos examined) (Figure 6.5D, F). The second class (23/32 embryos examined) had two bands of *T* expression separated by a patch of epiblast cells that did not express *T* (Figure 6.5E). These two primitive streaks were elongated towards the distal tip of the embryo, sometimes converging there (Figure 6.1B). Embryos of the second class were never found to have an obvious bulged streak.

The reduced levels of *Brachyury* expression, and the bulge of cells in the primitive streak of roughly a third of the *2-seam* mutant embryos suggested that

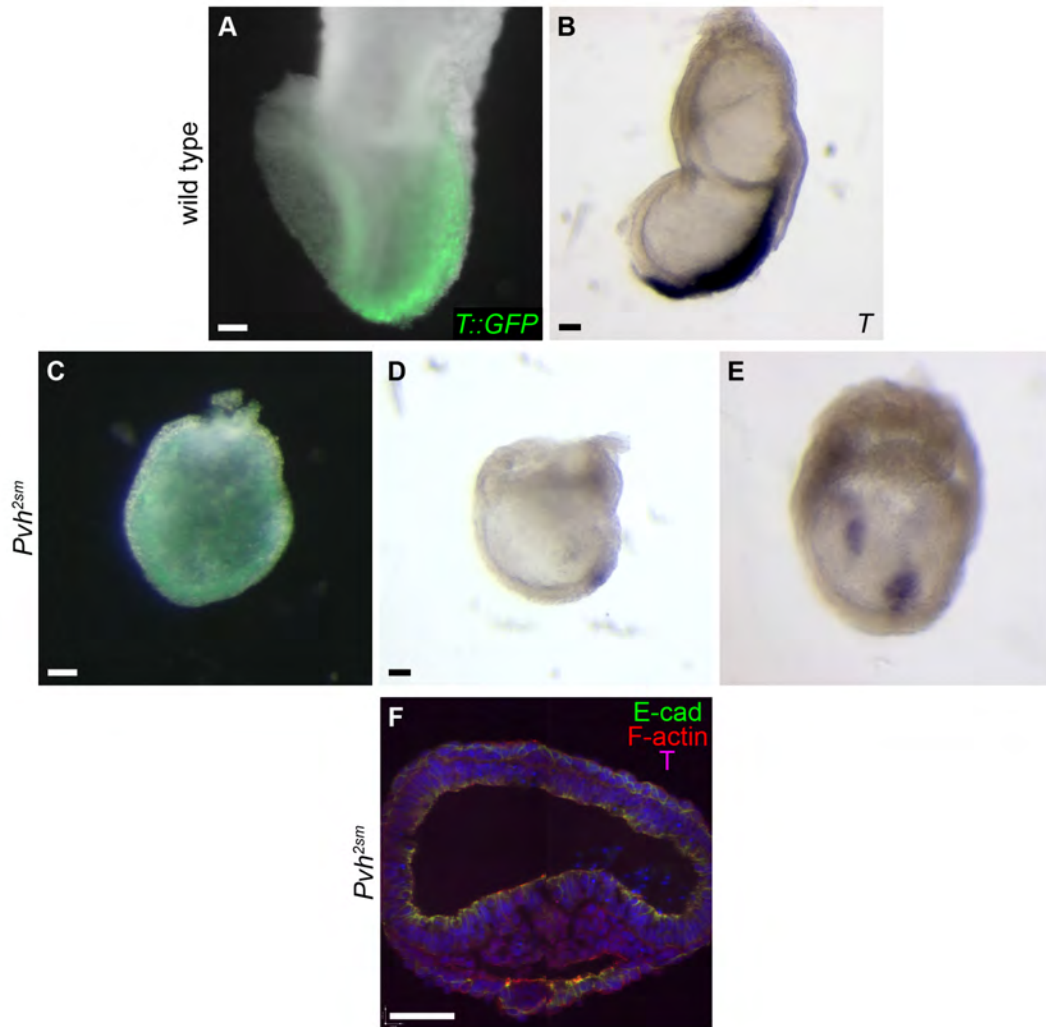


Figure 6.5: Primitive streak defects in 2-seam mutants.

(A-E) Whole mount images of *2sm* mutants (C-E) and wild-type littermates (A-B). Wild-type embryos expressed higher levels of *T::GFP* in the primitive streak than *2sm* mutants (A, C). *Brachyury in situ* hybridization shows lower levels of *T* transcript in the mutants compared to wild type (B, D-E), and also revealed two distinct phenotypes in the TO1 line at e7.5. The first class of embryos (D) had only a small spot of *T* expression in the posterior side of the embryo, and the second class (E) had two stripes of *T* expression separated by a patch of epiblast that does not express *T*. (F) Immunofluorescence staining for E-cadherin (green) and T (magenta) from a transverse section of a *2sm* mutant shows that gastrulating cells do not express E-cadherin, though they fail to migrate, forming a bulge at the streak. Scale bar: 100 μ m.

the lack of mesoderm in the *2sm* mutants might be due to mesoderm migration defects. One possible explanation of which could be a failure to down-regulate E-cadherin in gastrulating cells. However, immunofluorescence images from transverse sections of a *2sm* mutant with a bulged streak showed that E-cadherin was absent from Brachyury-positive cells in the primitive streak (Figure 6.5F).

I next examined *2sm* mutants at e6.5, and found that, like earlier stages, the mutants were delayed approximately 24-hours compared to wild-type littermates. E6.5 *2sm* mutants were much smaller than wild-type embryos and had no *T* expression (Figure 6.6A-B). Because roughly 66% of the *2sm* mutants had multiple streaks I next examined AVE migration in the mutants using the *Hex-GFP* transgene (Rodriguez et al., 2001). The multiple streaks in the *2sm* mutants do not resemble those in previously characterized mutants with axis duplication, e.g. *Nap1^{Khlo}* (Rakeman and Anderson, 2006), as the two streaks are in close proximity on the posterior side of the embryo, and I never observed a ring of *T* expression around the proximal portion of the *2sm* mutants. Nevertheless, I examined the position of *Hex-GFP⁺* cells in e6.5 *2sm* mutants. Due to the developmental delay, *2sm* mutants with complete AVE cell migration were only recovered from e7.0 dissection, so I could not compare them to wild-type littermates. However, at e7.0 there were *GFP⁺* cells at the embryonic/extraembryonic border only on the presumptive anterior side of the embryo in all (n=5) *2sm* mutants examined (Figure 6.6C). Therefore, the multiple streaks phenotype in the TO1 line does not appear to be a result of defects in

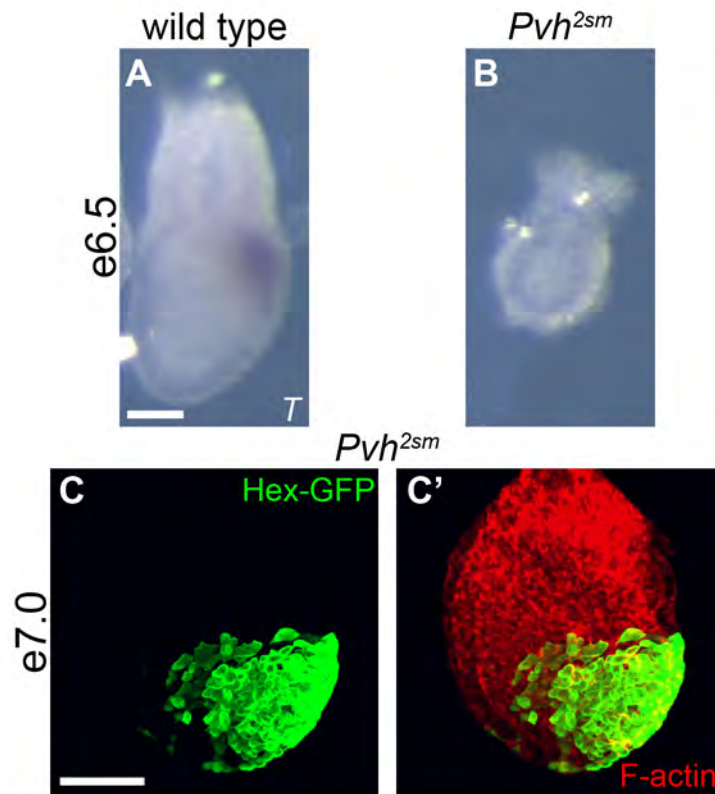


Figure 6.6: 2-seam phenotypes at e6.5.

(A-B) Whole mount images of wild type, and 2-seam mutant embryos at e6.5. Wild-type littermates are just beginning to express *T* in the primitive streak, while *T* expression is lacking in all 2sm mutants at this time point. (C-C') Immunofluorescence staining for Hex-GFP (green), marking anterior visceral endoderm cells, and F-actin (red) in a 2sm mutant dissected at e7.0. At this time point Hex-positive cells have migrated to the embryonic/extraembryonic border at the presumptive anterior side of the embryo. Scale bar: 50 μ m.

AVE migration.

The final phenotype that I investigated was the reduction in the derivatives of the polar trophoctoderm in the *2-seam* homozygous mutants. To verify that the polar trophoctoderm lineages were present, and properly positioned in the *2-seam* mutants I checked for the expression of the ectoplacental cone marker *Mash2* (Rossant et al., 1998), and the chorion (extraembryonic ectoderm) marker *Esrr β* (Luo et al., 1997). In wild-type e7.5 embryos *Mash2* is expressed at the proximal tip of the embryo, and *Esrr β* is expressed in cells just underlying the ectoplacental cone (Figure 6.7A, C). Despite the growth defects in these derivatives of the polar trophoctoderm in the *2sm* mutants, both markers were expressed, and their relative pattern of expression was also correct. This demonstrated that the derivatives of the polar trophoctoderm were present in embryos lacking Pvh activity, and suggests a specific defect in the growth of the ectoplacental cone and extraembryonic ectoderm lineages, not a defect in cell fate specification.

6.3 Discussion

Homozygous mutants from the TO1 line have growth defects in the derivatives of the polar trophoctoderm, and epiblast patterning defects that result in reduced *T* expression and split primitive streaks. Through linkage analysis of SNPs between the mutagenized C57BL/6J and the outcrossed FVB/NJ strains we mapped the ENU-induced mutation in this line to a 1.33 Mb interval in the proximal region of chromosome 4, subsequently identifying a T to A transversion

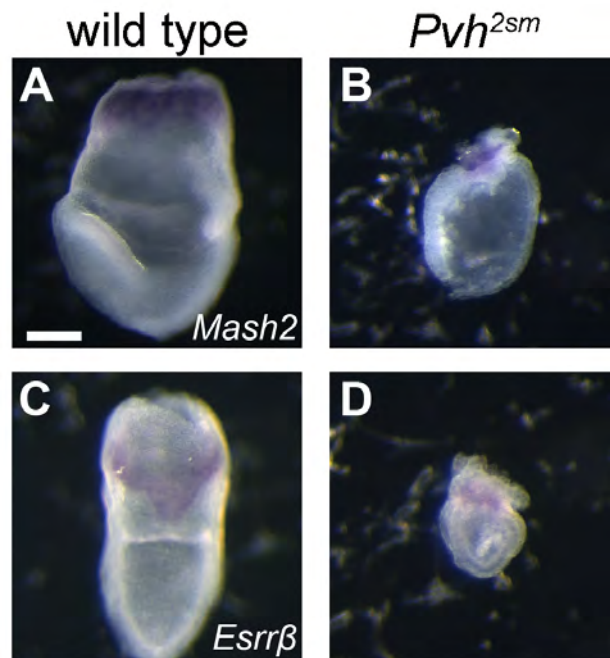


Figure 6.7: Extraembryonic ectoderm is present in 2-seam mutants.
(A-D) The expression pattern of *Mash2* (A-B) and *Esrrβ* (C-D) in e7.5 wild type (A, C) and 2-seam mutants (B, D). The 2sm mutants have growth defects in derivatives of the polar trophoctoderm, but the ectoplacental cone (B) and extraembryonic ectoderm (D) are specified, with *Mash2* at the proximal tip of the embryo, and *Esrrβ*, marking the chorion, underlying the ectoplacental cone. Scale bar: 100 μm.

in the coding region of *Pvh* only in the mutant embryos. While this was the only mutation I found in the coding region of genes expressed at e7.5 from this interval, we do not yet have independent confirmation that this allele of *Pvh* causes the TO1 phenotype. *Pvh* was a previously uncharacterized gene in the mouse, but recently the Wellcome Trust Sanger Institute reported germline transmission of a targeted knockout of *Pvh* as part of the National Institutes of Health Knockout Mouse Program, an effort to produce genome wide knockout alleles in the mouse (Skarnes et al., 2011). The most important step in the future of this project will be to obtain this targeted knockout allele and perform a complementation test, to verify that *Protein virilizer-homologue* is the mutated gene responsible for the TO1 phenotype.

While we do not yet have an independent allele of *Pvh*, other data suggest that the point mutation in *Pvh* is responsible for the TO1 phenotype. Embryos lacking *Wilms' tumor 1-associating protein (WTAP)* have a nearly identical phenotype to TO1 mutants, including an underdeveloped ectoplacental cone and extraembryonic ectoderm, and reduced *T* expression, despite having no defects in AVE migration (Fukusumi et al., 2008). WTAP was originally identified in mammalian cells as an interacting partner for WT-1 (Little et al., 2000), which is a critical regulator of genitourinary development. The *Drosophila* homologue of WTAP is fl(2)D, which like *virilizer*, is essential for generating the female specific splice variant of *Sxl* (Granadino et al., 1990). In *Drosophila*, fl(2)D and *virilizer* are both part of the female specific *Sxl* auto-regulatory splicing complex (Ortega et al., 2003). The similar observed phenotypes of WTAP and TO1 mutants, in

addition to the data showing that these two proteins physically interact in the fly, strongly suggests that the mutation in *Pvh* is responsible for the TO1 phenotype. If this were determined to be the case, it would demonstrate that the core of this mRNA splicing complex is conserved in mammals, where its activity is essential for embryogenesis.

There are two notable phenotypes in the TO1 line, the growth defect in the derivatives of the polar trophectoderm lineages and the split in the primitive streak along the posterior side of the embryo. It has been shown that the extraembryonic ectoderm secretes two proteases, Spc1 and Spc4, that are required for Nodal signaling and the formation of the AVE (Beck et al., 2002). While TO1 mutants have no defect in AVE specification or migration, Nodal is also required for mesoderm induction, and TO1 mutants have a severely reduced level of *T* expression in the posterior of the embryo. This suggests that the remnants of extraembryonic ectoderm in the *2sm* mutants allows for a level of Nodal signaling required for AVE induction, but not enough to properly specify the primitive streak. This phenotype has also been documented in another mouse mutant, *Elf5*, an *Ets* family transcription factor that was shown to be required for the maintenance of trophoblast stem cells (Donnison et al., 2005). Trophoblast stem cells are maintained by FGF signaling in culture and *in vivo* (Tanaka et al., 1998). FGF signaling is also required for the epithelial to mesenchymal transition during gastrulation, as embryos lacking *Fgf receptor-1* have a bulged primitive streak with mesoderm cells failing to down-regulate E-cadherin (Ciruna and Rossant, 2001). While TO1 mutant embryos did

successfully down-regulate E-cadherin, the common requirement for FGF signaling in the maintenance of trophoblast stem cells and gastrulation suggests that future studies on the *Pvh* mutants should focus on the role of mRNA processing in the response to FGF signaling.

The second phenotype of note in the TO1 line was the split primitive streak in the posterior half of the embryo. One possible explanation for this phenotype is again tied to FGF signaling. FGF is required for *Snail* expression (Ciruna and Rossant, 2001), and recently it was shown in the chick that *Snail2* and *Sox3* have a reciprocal repression relationship that defines the border of the epiblast and the primitive streak (Acloque et al., 2011). If TO1 mutants have reduced FGF signaling, and therefore less *Snail* expression, then excess *Sox3* in the surrounding epiblast may confine the border of the primitive streak to such a degree that a second streak is able to form from the available Wnt ligand produced in the posterior visceral endoderm.

An important question that needs to be addressed regarding this primitive streak phenotype is whether it is intrinsic to the *Pvh* mutant epiblast, or caused by defects in the extraembryonic lineages. In order to address these two models, we will take advantage of the targeted allele of *Pvh* generated by the Wellcome Trust Sanger Institute. This allele has inserted *loxP* sites flanking the second exon of *Pvh*. Therefore, this exon can be excised specifically from the epiblast using the *Sox2-Cre* (Hayashi et al., 2002); if the split streak phenotype is present in these epiblast-deleted *Pvh* mutants, we can conclude that this phenotype is a result of activity in the epiblast alone.

Finally, the major goal for this project is to uncover the mRNAs that are processed by the *Pvh* complex. In order to do this we will explore whole genome RNA sequencing technologies (Ng et al., 2009). We will focus on sequencing transcripts from a cDNA library produced from either *Pvh*^{2sm} mutants, or mutants from the epiblast deleted targeted allele. While the first approach will reveal all transcripts that are differentially processed between wild type and mutant embryos in all lineages, the downside to this approach is that the TO1 mutant embryos are small and do not yield a substantial amount of RNA. If the epiblast-deleted mutants are healthier this may aid in generating a library to interrogate with the RNA-Seq. This approach will definitively demonstrate the genes regulated by *Pvh* and help to understand the cause of the phenotypes from this mutant line.

CHAPTER SEVEN

7 SUMMARY AND FUTURE DIRECTIONS

The developmental processes that shape the radially symmetric e5.5 mouse embryo into a fully formed fetus at e15.5 require the specification and differentiation of a multitude of specific cell types; in addition these cells must undergo coordinated growth and morphogenesis in order to make functional organs and tissues for the adult animal. Despite these complexities, only a handful of signal transduction pathways, including Wnt, Hedgehog, TGF- β /BMP, RTK, Notch and JAK/STAT, regulate almost all of these steps (Pires-daSilva and Sommer, 2003). Many of these cell-cell signaling pathways are repeatedly used in different tissues and generate distinct cellular responses in different cell populations, demonstrating that the precise regulation of these signaling networks are critical for normal development.

Genetic screens in our lab have produced many mutations that have subsequently led to the discovery of novel regulatory components to these signaling cascades and provided models to study cell signaling in development. I have used two mutants from these screens, *Axin2^{canp}* and *Cfl1^{C5}*, to study the regulation of the two arms of the Wnt signaling pathway in early mouse development. I have also expanded upon the genetic characterization of these mutants by using small molecule inhibitors that mimic the effects of these mutations. Small molecule inhibitors are powerful tools to manipulate molecular

pathways during mouse development, as they can inhibit target proteins at a specific time in development; in addition comparing the effects of small molecule inhibitors to established mouse mutants serves as a good test for the *in vivo* efficacy of these drugs. Using these two approaches, I have shown that canonical Wnt signaling in the late primitive streak is uniquely dependent on the kinase activity of GSK3 β , presumably at the membrane Fzd/LRP complex. I have also shown that actin dynamics are required for the targeting of Rab11⁺ vesicles to the apical cell membrane in the ventral node, and that this step in vesicle trafficking is specifically required for the establishment of non-canonical Wnt signaling.

7.1 Canonical Wnt signaling

The initial characterization of the *Axin2*^{canp} phenotype revealed that the regulation of Wnt signaling in the late primitive streak was different than other regions of the embryo. My data confirmed that increased Axin levels led to a predictable reduction in Wnt signaling in the anterior half of the embryo as well as in the early streak, but through inhibiting the Tankyrase-dependent destruction of Axin pharmacologically, I observed the paradoxical increase of *TOPGAL* expression in the late primitive streak, similar to the *Axin2*^{canp} phenotype (Qian et al., 2011). IWR-1 treatment stabilizes both Axin1 and Axin2, and had a stronger effect than *Axin2*^{canp} in both the decrease of Wnt signaling in the anterior of the embryo and the increase in the late primitive streak. Thus, I can conclude the *Axin2*^{canp} mutation does not confer additional gain-of-function activities to the

protein, as both wild-type Axin1 and Axin2 are capable of acting as Wnt agonists in the late primitive streak.

The *TOPGAL* transgene is a commonly used Wnt reporter, and has been shown by many different groups to faithfully reveal areas of Wnt signaling during mouse development and adult tissue homeostasis (DasGupta and Fuchs, 1999; Davies et al., 2008). The increased expression of *TOPGAL* in the late primitive streak of both *Axin2^{canp}* homozygous mutants and wild-type embryos treated with IWR-1 are the first examples of Axin promoting Wnt signaling in any model organism; therefore the focus of my subsequent experiments was to determine the mechanism by which Axin acts as a Wnt agonist, as all previously described roles for Axin were to inhibit Wnt signaling (Fagotto et al., 1999; Salic et al., 2000; Zeng et al., 1997).

Wnt ligands have been shown to induce a supermolecular complex of Dvl, Fzd, LRP5/6 and Axin, and in these complexes GSK3 β phosphorylates LRP5/6, inhibiting the activity of the kinase on β -catenin (Wu et al., 2009; Yokoyama et al., 2010). Using pharmacological inhibitors of Porcupine, which blocks the secretion of Wnt ligands, and of GSK3 β , my data showed that both Wnt ligands and GSK3 β activity were required for Axin to act as a Wnt agonist in the late primitive streak. These data suggested that the increased Wnt signaling in the late primitive streak of IWR-1-treated embryos could be due to Axin being recruited into these supermolecular complexes, increasing the phosphorylation of LRP6 by GSK3 β .

The primary role of GSK3 β in the canonical Wnt pathway is as a negative

regulator of β -catenin stability. GSK3 β phosphorylates the N-terminus of β -catenin in the destruction complex, marking it for subsequent poly-ubiquitination by β TrCP (Liu et al., 1999a). GSK3 β also phosphorylates LRP6 in response to Wnt ligand (Zeng et al., 2005); however, the generation of phospho-LRP6 is not required for Wnt signaling in most cell types as evidenced by the transcription of Wnt target genes in cells treated with CHIR99021 (Bennett et al., 2002). Thus, previous data suggests that the phosphorylation of LRP6 promotes Wnt signaling under normal circumstances, but when β -catenin is stabilized either through mutation or GSK3 β inhibition, the membrane recruitment of Axin by phospho-LRP6 is not required for signaling. In accordance with these previous results, my data showed that *TOPGAL* expression was highly increased in all anterior tissues in embryos treated with CHIR. However, in the late primitive streak CHIR-treatment reduced Wnt signaling, demonstrating that in these cells inhibiting GSK3 β in the destruction complex was not sufficient to allow *TOPGAL* expression. At the molecular level, I found that N-terminally phosphorylated β -catenin was absent in both the anterior and posterior regions of embryos treated with 20 μ M CHIR. Phosphorylated LRP6 was also absent in CHIR treated embryos, suggesting that in the late streak, β -catenin can only promote *TOPGAL* expression in the presence of phospho-LRP6.

The data I have presented in this thesis has begun to define the differences in the regulation of the Wnt pathway between the late primitive streak and the cranial neural tube and somites, however, there are three major outstanding questions regarding this project that future experiments in the lab will

address. First, we need to further characterize the molecular interactions associated with Wnt signaling in the head and somites and compare them to the late primitive streak. Second, we will investigate the genetic/molecular differences between the late and early primitive streak that create the environment that causes stabilized Axin to promote Wnt signaling in the former, and repress the pathway in the latter. Finally, we will determine if there are adult tissues or cancer models where stabilized Axin promotes Wnt signaling as in the late primitive streak, rather than reforming the β -catenin destruction complex.

7.1.1 Localization of stabilized Axin in the head versus primitive streak

The data I have presented using IWR-1, IWP-2, and CHIR to modulate the Wnt pathway in the early embryo, strongly suggest that Axin is required to form the Fzd/LRP/GSK3 β signaling complex after stimulation by Wnt ligand in the late primitive streak. In contrast, in the cranial neural tube and somites all evidence suggests that Axin and GSK3 β only function in the β -catenin destruction complex. In the discussion of these results the effects of stabilized Axin have been referred to as increasing or decreasing Wnt signaling. However, my data show that there is not simply an increase in *TOPGAL* expression, rather, there are more cells expressing *TOPGAL* in the late streak of IWR-1-treated embryos than in controls. At the molecular level, IWR-1 increased the activity of GSK3 β in both the destruction complex and the membrane-signaling complex in the late streak. Therefore, it is important to view this data not in terms of cells going from the Wnt-off to the Wnt-on state, instead we should consider the balance between

Axin at the destruction complex and at the membrane, and at some point the activity at the membrane outweighs the activity of the destruction complex and allows for *TOPGAL* expression. To further elucidate the mechanism by which Axin acts as a Wnt agonist in the late streak will require assaying the proportion of Axin in these two complexes. Currently we are working towards developing a cell fractionation protocol that can separate the nuclear, membrane and cytosolic fractions from embryos lysates. This will allow us to quantitate the subcellular localization of Axin and β -catenin in the anterior and posterior halves of the embryo. This assay will prove powerful, not only to directly test whether Axin is preferentially recruited to the membrane in the late streak, but also to determine what factors are required for this activity.

In these experiments, prior to fractionation, we bisect the embryos after culture at the PSM. Then using centrifugation and sucrose gradients we can separate the cell lysates into nuclear, cytoplasmic and membrane fractions. If IWR-1 treatment is increasing *TOPGAL* expression in the late streak by increasing the amount of Axin in the Fzd/LRP complex then we should detect more Axin protein in the membrane fraction from the primitive streak. In contrast, from the anterior lysate fractions we would predict to find more Axin protein accumulation in the cytosolic fraction, corresponding the destruction complex. To support the data from cell fractionation experiments, we will also try to co-immunoprecipitate Axin from cell lysate from the head and tail regions of IWR-1 treated embryos. Data from *TOPGAL* expression suggests that in these experiments Axin will co-immunoprecipitate with LRP only in the lysate from

caudal half of the embryo, and not the rostral half.

The cell fractionation assay will also allow us to address the effects of these pharmacological inhibitors on β -catenin levels in the nucleus. Some of these experiments will be proof of principle, for example we would expect to see increased levels of β -catenin in the nucleus in IWR-1 treated primitive streak fractions and CHIR treated anterior fractions. However, this assay will be more informative for other treatments, for example CHIR treatment reduced *TOPGAL* expression in the late primitive streak, but was this accompanied by decreased levels of nuclear β -catenin? The kinase activity of GSK3 β is required for other signaling pathways including Notch and TGF β . If these experiments reveal that CHIR treatment does increase nuclear β -catenin levels in the late streak, but this does not lead to Wnt target gene expression, it would suggest that there is cross talk between the Wnt pathway and another pathway that requires GSK3 β in these cells.

7.1.2 The environment of late streak

There are many components of the Wnt signal transduction pathway, including *Wnt* ligands and *Frizzled* receptors, that are differentially expressed between the late primitive streak and the forebrain and somites. For example, at the early somite stage *Wnt1* and *Wnt2b* are expressed in the forebrain, while *Wnt3a*, *Wnt7a* and *Wnt11* are expressed in the late streak (Kispert et al., 1996; Liu and Joyner, 2001; Takada et al., 1994; Zakin et al., 1998). Similarly, *Fzd1*, *Fzd3*, *Fzd7* and *Fzd8* are all expressed in the forebrain and somites, while only

Fzd3 is expressed in the tailbud (Borello et al., 1999). My data suggests that the specific interactions between these receptors and ligands may promote Axin binding to Dvl and LRP6 at the membrane, enhancing *TOPGAL* expression in IWR-1 treated embryos in the late streak, but not in other tissues.

The canonical Wnt signal transduction pathway hinges on the ability to generate nuclear β -catenin; however, different Wnt ligands can generate different responses in the same cells. For example, presomitic mesoderm cells cultured *ex vivo* primarily express *Myf5* in response to Wnt1, while Wnt7a generates *MyoD* expression in the same cells (Tajbakhsh et al., 1998). This suggests that β -catenin accumulation in the nucleus is not the whole story for Wnt receiving cells, and that different ligands can generate unique transcriptional responses. Perhaps, these different responses are due to the amount of nuclear β -catenin, such that targets genes with lower affinity for the β -catenin/TCF are only expressed in cells that generate high levels of nuclear β -catenin levels. This model would suggest that some Wnt ligands only moderately repress the destruction complex, while others do so more efficiently. My data suggests that the combination of Wnt ligands in the late primitive streak strongly repress the destruction complex by generating a robust GSK3 β /LRP6 complex at the membrane, which fuels the feed-forward loop that is responsible for recruiting excess Axin in the IWR-1-treated embryos. To test this model, we are beginning to study genetic interactions between *Axin2*^{canp} and *Wnt3a* null mutants, as well as IWR-1-treatment of *Wnt3a* null embryos. This will test whether the presence of *Wnt3a* is specifically required for *Axin2* to act as an agonist of Wnt signaling in

the late streak.

Another possible explanation for the differential effects of stabilized Axin in the embryo is that there are different levels of Wnt ligands in the cranial neural tube and late primitive streak. My hypothesis for this model is that there is more Wnt ligand in the late streak, and this generates a more robust Fzd/LRP/GSK3 β feed-forward loop at the membrane. In this context increased levels of Axin further drive the formation of this complex, rather than reform the destruction complex. To test this model we will culture embryos in the presence of exogenous Wnt3a. If increased levels of ligand drive the formation of the membrane signaling complex, then adding Wnt3a to the culture media could promote this complex in the head and somites. If this is the case, then IWR-1 treatment along with the Wnt3a will increase *TOPGAL* expression in these tissues similar to what I have shown in the late primitive streak.

7.1.3 Adult tissue homeostasis

The increased Wnt signaling in the late primitive streak of embryos treated with IWR-1 raises questions about the efficacy of this small molecule as a therapeutic agent for patients with colorectal cancer. My data raises two concerns: first, will increased levels of Axin in malignant colorectal cells serve to promote the degradation of β -catenin or could it possibly enhance Wnt signaling in these cells, and second, if IWR-1 or another Tankyrase inhibitor is given to patients will there be an increase in Wnt signaling in another cell type that could lead to side effects. To address these issues in the mouse we have begun to

assess Wnt signaling in adult tissues using animals that are heterozygous for the *canp* mutation. Heterozygous *Axin2^{canp/+}* embryos displayed an intermediate phenotype compared to homozygous *Axin2^{canp}* and wild-type littermates, including a mild reduction of TOPGAL expression in the head and somites and a mild increase in the late primitive streak (Qian et al., 2011). Therefore, *Axin2^{canp/+}* mice are a suitable model to begin to study the effects of increased Axin levels in adult tissues. Our initial findings suggest that there is increased TOPGAL expression in the small intestines and mammary glands of *Axin2^{canp/+}* adult animals but this increase alone is not sufficient to promote tumor formation. Future studies will need to address whether increased Axin2 levels enhance tumor progression in *APC* mutant mice.

One drawback to using the *Axin2^{canp/+}* adults to study the effects of increased Axin on adult tissue homeostasis is that in these mice the stabilized Axin2 protein is only expressed in cells that normally respond to Wnt ligand. To fully address the possible outcomes from treating patients with Tankyrase inhibitors we will need to develop a model where Axin1 is stabilized in all adult cells. To achieve this, we are currently working to generate a mouse that expresses an allele of *Axin1* that harbors a similar mutation in the TBD as *canp* under an inducible promoter. This will allow us to drive expression of stabilized Axin1 in all cells. We will use these mice to address the effects of stabilized Axin on adult tissue homeostasis, and cross these mice to *APC* mutants to see whether stabilized Axin enhances or mitigates tumor progression *in vivo*.

7.2 Non-canonical Wnt signaling

Studies in *Xenopus* and zebrafish have shown that non-canonical Wnt signaling is required for the morphogenetic movements that lengthen the embryonic AP body axis (Jessen et al., 2002; Wallingford and Harland, 2001). However, mouse embryos lacking single PCP genes have milder phenotypes than the comparable mutations in other vertebrates (Greene et al., 1998; Wang et al., 2006a). Recently it has been shown that these mild single mutant phenotypes in the mouse can be enhanced by genetically ablating all of the family members of a core PCP protein in the mammalian genome (Hashimoto et al., 2010; Song et al., 2010). I used the classic mouse PCP mutant *Vangl2^{Lp}* as a sensitized background to demonstrate that *Cofilin1* is required for PCP signaling in the mouse embryo. *Vangl2^{Lp} Cfl1^{C5}* double mutants had a similar embryonic phenotype as *Vangl1 Vangl2* mutants, including convergent extension defects in the midline and somites, and left-right asymmetry defects; all of which suggested that the PCP signaling was abolished in my double mutants.

I next addressed the molecular mechanism of this genetic interaction, and showed that the role of actin dynamics was upstream of the establishment of PCP signaling. Using the actin stabilizing drug jasplakinolide, I showed that Cofilin activity was required for the targeting of the core PCP proteins Celsr1 and Vangl2 to the plasma membrane, but once these proteins were localized to the membrane stabilizing actin with the drug did not disrupt Celsr1 or Vangl2 subcellular localization. When actin dynamics were blocked, either genetically or pharmacologically, PCP proteins were trapped in endosomes and vesicles in the

apical cytoplasm. I also demonstrated that the trafficking of Rab11⁺ vesicles to the plasma membrane was disrupted when actin turnover was blocked. The cytoplasmic Rab11⁺ vesicles in jasplakinolide-treated embryos co-labeled with both Vangl2 and Celsr1, suggesting that Rab11 facilitates normal trafficking of PCP proteins from recycling endosomes to the apical surface. These experiments proved that Cofilin is required upstream of PCP establishment in the ventral node, and confirmed a role for PCP signaling in the morphogenesis of the axial mesoderm and in the polarized orientation of nodal cilia. The next steps in this project will require time-lapse imaging to further elucidate the how the PCP pathway governs these processes.

7.2.1 Trafficking core PCP proteins to the apical membrane

Remodeling of the actin cytoskeleton has been shown to play an important role in many aspects of intracellular protein trafficking. Cofilin specifically functions in Ca⁺ ion-mediated cargo sorting in the Golgi (Blume et al., 2009; Blume et al., 2011), and vesicle fission in the Golgi and endocytic pathways (Okreglak and Drubin, 2007; Salvarezza et al., 2009). My data suggest that Cofilin is also required for the membrane targeting of the core PCP proteins and Rab11. Recently, a RNAi screen in *C.elegans* showed that PAR-5, the 14-3-3ζ homologue, is required for proper membrane recruitment of Rab11 in intestinal cells (Winter et al., 2012). 14-3-3ζ directly regulates Cofilin activity, binding to phosphorylated Cofilin, and sequesters many other key regulators of actin dynamics including LIM Kinase and Slingshot (Bernstein and Bamburg, 2010).

These data also suggest that actin dynamics play a key role in Rab11 trafficking to the apical cell membrane.

Rab11 labels both apical recycling endosomes and vesicles carrying cargo from the endosomes destined for the apical membrane. When actin remodeling was blocked, both Rab11 and Celsr1 were colocalized in the apical cytoplasm, presumably in apical recycling endosomes or vesicles that were unable to fuse to the apical membrane. This suggests that the normal trafficking of PCP proteins to the apical membrane involves Rab11 coated vesicles shuttling from the apical recycling endosome to the apical membrane. What remains to be investigated is what step in PCP establishment requires Rab11. Are PCP proteins trafficked directly to recycling endosomes from the Golgi, then shuttled to the membrane, or are PCP proteins uniformly deposited on the apical surface initially, then as a means of refining the Vangl and Fz domains endocytosed and trafficked back to a specific domain? Distinguishing between these two models will require time-lapse imaging of fluorescently tagged PCP proteins during the establishment of PCP in the node. Additionally embryos could be cultured with Chlorpromazine, a small molecule that removes clathrin and AP-2 from the plasma membrane, inhibiting endocytosis. If Chlorpromazine treatment caused uniform membrane localization of PCP proteins and blocked planar polarity, then we would support a model where endocytosis and recycling of PCP proteins was required to establish the Vangl and Fzd domains in the apical membrane.

My experiments with jasplakinolide also showed that actin dynamics were only required for the establishment of the Vangl and Fzd domains, but after these

were established there were no defects associated with jasplakinolide treatment. This suggests that either PCP proteins remain in the membrane after the segregation of the two domains and no new proteins are incorporated, or that newly synthesized proteins are specifically trafficked to the proper domain after the establishment of PCP in a Rab11 independent process. To test these two models we could perform fluorescence recovery after photobleaching (FRAP) experiments on the embryos expressing fluorescently tagged PCP proteins. If there were no signal recovery after photobleaching, this would support the first model. Fluorescence recovery in these experiments would suggest that new protein is being incorporated into the membrane. To prove that this was a Rab11 independent process we could repeat the FRAP experiments on embryos treated with jasplakinolide. Fluorescence recovery in the presence of jasplakinolide would show that maintenance of PCP signaling in the node is independent of Rab11. This would suggest that the Rab11/recycling endosome trafficking pathway was specifically required during the establishment of the Vangl and Fzd domains, but after they were established the inhibitory interactions between Prickle and Diego directed the trafficking of newly synthesized proteins.

7.2.2 Planar cell polarity signaling and cilia orientation

The posterior polarization of nodal cilia has been shown to be important for the generation of leftward fluid flow in the node, which is required for left-right asymmetry in the embryo (Nonaka et al., 2005). The PCP pathway was an obvious candidate pathway to direct the polarity of nodal cilia as PCP signaling

serves as the cellular compass and directs the polarity of cellular appendages in other contexts (Strutt, 2001). My data, and recently published work from other groups (Hashimoto et al., 2010; Song et al., 2010), confirmed this hypothesis: compound mutants that abolish planar polarity have defects in left-right asymmetry and randomly positioned basal bodies and cilia in the node. While this data is congruous with the known functions of the PCP pathway, it remains unclear how the PCP pathway moves the basal body. Most of the known downstream effectors of the non-canonical Wnt pathway are regulators of actin dynamics (Seifert and Mlodzik, 2007), but the basal body is a modified centrosome, and is thought to still act as the microtubule organizing center, even when it is apically docked and producing a cilium (Bornens, 2008).

The first question that future studies will need to address is what controls the movement of the basal body in node cells, the actin cytoskeleton or microtubules. In the mouse node, the ciliary basal bodies are found in the center of cell at the early stages of node development, and then migrate to the posterior of the cell at the early somite stages, prior to cilia beating (Hashimoto et al., 2010). To determine what generates the force to move the basal bodies, embryos will be cultured from the late headfold stage with small molecules that disrupt actin dynamics or microtubules, and we will monitor basal body position in the 4-somite embryos after culture. I have shown that treatment with jasplakinolide prevents the establishment of PCP signaling, but afterwards, jasplakinolide treatment does not affect the pathway. Therefore, treating embryos at later stages will show if actin dynamics are required for basal body positioning,

and will not perturb PCP signaling. For the drugs that have not been previously used, we will also have to stain for PCP protein localization to make sure that these drugs do not disrupt non-canonical signaling during treatment.

The first candidate drug is jasplakinolide, as it freezes the actin cytoskeleton. However, the basal body may be moved by actin-myosin contractions that operate on existing actin filaments. If this is the case, then stabilizing F-actin filaments with jasplakinolide may not stop basal body migration. To address this, two drugs could be used: Cytochalasin D, which prevents actin polymerization or blebbistatin which inhibits non-muscle Myosin (Straight et al., 2003). If these small molecules do not prevent the posterior polarization of the basal body, then we will try small molecules that disrupt the microtubule cytoskeleton, taxol and nocodazole to stabilize and depolymerize the microtubules, respectively. Both of these treatments will affect cilia length, but we will focus on quantifying basal body positioning, not left sided marker expression. Once we have established how the PCP pathway moves the basal body, we will next investigate the molecular mechanism of this activity.

Dishevelled has been shown to be an important regulator of cilia polarity in the *Xenopus* epidermis (Park et al., 2008), but there are key differences between this system and cilia orientation in the node. The *Xenopus* epidermis is composed of two cell types: mucus-secreting goblet cells interspersed by multiciliated cells. Dvl is required for the docking of the preformed multiciliated structure to the apical membrane in the ciliated cells. This is not the case in node cells, which have a single primary cilium that forms in the apical domain even in

the absence of Dvl (Hashimoto et al., 2010). The second difference is that cilia polarity in the *Xenopus* epidermis is not related to the position of the cilia within the cell, rather the orientation of an individual cilium to the basal body from which it emanates. In wild-type *Xenopus* embryos all cilia have a common angle between the cilia rootlet, the centrosome and the cilia, resulting in uniform fluid flow upon cilia beating. In Dvl morphants this orientation is randomized, as is the subsequent fluid flow.

While there are differences between the functions of PCP signaling in the *Xenopus* epidermis and the mouse node, some of the lessons from *Xenopus* may apply to the mouse. It was shown in *Xenopus* that active Rho is localized to the centrosome both as the rootlet and cilia dock to the apical surface, and when the cilia become planar polarized with respect to the basal body after docking (Park et al., 2008). Unlike the multiciliated cells in *Xenopus*, the PCP pathway is not required for apical docking of the basal body or cilia formation (Hashimoto et al., 2010; Mahaffey et al., 2013; Song et al., 2010). Therefore, we could look for active RhoA GTPase (GTP bound RhoA) in node cells as the cilium becomes polarized. Many groups have been successful in demonstrating the localization of active Rho using a tagged protein domain from Rhotekin that specifically binds to active RhoA (Habas and He, 2006; Park et al., 2005). If active RhoA were found around the basal body, this would suggest that downstream effectors of RhoA, possibly through increasing actin polymerization and/or myosin activation, move the basal body. As there is more Dvl at the posterior side of the node cells (Hashimoto et al., 2010), this would suggest that these actin/myosin contractions

pull the basal body to the posterior side of the cell. Alternatively, Diaphanous, a downstream target of active Rho has been shown to stabilize microtubules at the leading edge of migrating fibroblasts (Zaoui et al., 2008). If active Rho is found primarily at the posterior membrane, where Dvl is localized in node cells, then perhaps the increased microtubule stability at this face of cell relative to the other apical surface draws the basal body towards the posterior side of cell.

7.2.3 Non-canonical Wnt signaling regulates convergent extension

The data I have presented in this thesis confirm that PCP signaling is required for the morphogenesis of the neural tube, axial mesoderm and somites in the mouse embryo. The next step in this arm of the project is to determine how the PCP pathway directs these morphogenetic movements. As my efforts to describe the underlying cell biology of neural tube closure were limited by the inability to take time-lapse images of this process, we will focus future efforts on CE of the midline. The axial mesoderm lies on the ventral surface of the embryo, and is a single layer epithelium; therefore, it is an ideal tissue for the time-lapse imaging that is required to study the cell intercalation events that drive midline CE. The first question that we will address is what are the cell behaviors that facilitate midline CE, and then we will investigate the source of the biomechanical forces that drive this process.

The PCP pathway has been shown to play a critical role in CE in other vertebrate systems, such as the *Xenopus* mesoderm and neural tube (Davidson and Keller, 1999; Wallingford and Harland, 2001), and the chick neural tube

(Nishimura et al., 2012). The previous work on these systems has provided evidence for two different models of cell intercalation. In *Xenopus*, CE is driven by mediolateral cell intercalation, a process that is characterized by cells producing monopolar lamellipodia and elongating in the mediolateral direction (Elul and Keller, 2000). The force generated by these changes causes the cells to intercalate orthogonal to the axis of elongation, producing a tissue that is longer along the AP axis and shorter along the mediolateral axis. In the developing chick neural plate there is a correlation between multicellular rosette formation and the elongation of the neural tube (Nishimura et al., 2012). This model of cell intercalation was first documented during convergent extension of *Drosophila* germband (Blankenship et al., 2006). During this process groups of cells, aligned along the mediolateral axis, constrict upon a central point, forming a multicellular rosette; the rosette then resolves along the AP axis, elongating and narrowing the tissue.

In the next set of experiments we will address whether there is evidence to support either of these two models of cell intercalation during notochordal plate morphogenesis by taking time-lapse images of this process. Like the chick neural tube, the mammalian midline is an epithelial sheet, while the *Xenopus* mesoderm and neural tube have a more mesenchymal character. Therefore, I hypothesize that midline CE will involve rosette formation and resolution, as this process has been found more often in epithelial sheets undergoing CE.

Once we have identified the mode of cell intercalation, we will investigate the source of the biomechanical force that drives this process, and how the PCP

pathway controls the force generation. My data showing that pMLC2 aligns along the anterior/posterior faces of cells exiting the node suggests a mechanism for multicellular rosette intermediate. If our time-lapse imaging studies support this mechanism of cell intercalation, then we will continue to describe the molecular events that drive this process with other immunofluorescence staining. We will look at the localization of Par3, E-cadherin and other markers of newly formed membrane; these would be predicted to be enriched in vertical lines in the node, corresponding to newly formed cell-cell contacts in resolving rosettes (Blankenship et al., 2006). We will also use the GTP-bound RhoA sensor to address where active RhoA is in the cells at the anterior border of the node. In the previous section I discussed using this construct to address active Rho signaling with regards to basal body localization. However, RhoA can activate myosin through its downstream effector ROCK. My immunofluorescence data showed that pMLC2 was localized uniformly around the apical surface in node cells, and only enriched to the anterior/posterior face of cells at the anterior of the node, where the node transitions into the midline. Therefore, it is possible that RhoA activates Myosin only in these cells to facilitate cell intercalation.

We must also investigate what regulates the different activities of the PCP pathway in the node: CE of the midline and basal body positioning. Perhaps different Rho GEFs associate with Rho at the membrane to direct these different activities. One way to address this would be to genetically ablate different Rho GEFs in the embryo, and see if some cause CE defects but do not affect basal body positioning or visa versa.

REFERENCES

- Acloque, H., Ocaña, O. H., Matheu, A., Rizzoti, K., Wise, C., Lovell-Badge, R. and Nieto, M. A.** (2011). Reciprocal repression between Sox3 and snail transcription factors defines embryonic territories at gastrulation. *Dev Cell* **21**, 546–558.
- Adler, P. N., Charlton, J. and Liu, J.** (1998). Mutations in the cadherin superfamily member gene *dachsous* cause a tissue polarity phenotype by altering frizzled signaling. *Development* **125**, 959–968.
- Adler, P. N., Krasnow, R. E. and Liu, J.** (1997). Tissue polarity points from cells that have higher Frizzled levels towards cells that have lower Frizzled levels. *Curr Biol* **7**, 940–949.
- Aigouy, B., Farhadifar, R., Staple, D. B., Sagner, A., Röper, J.-C., Jülicher, F. and Eaton, S.** (2010). Cell flow reorients the axis of planar polarity in the wing epithelium of *Drosophila*. *Cell* **142**, 773–786.
- Amit, S., Hatzubai, A., Birman, Y., Andersen, J. S., Ben-Shushan, E., Mann, M., Ben-Neriah, Y. and Alkalay, I.** (2002). Axin-mediated CKI phosphorylation of beta-catenin at Ser 45: a molecular switch for the Wnt pathway. *Genes Dev.* **16**, 1066–1076.
- Arce, L., Yokoyama, N. N. and Waterman, M. L.** (2006). Diversity of LEF/TCF action in development and disease. *Oncogene* **25**, 7492–7504.
- Aulehla, A., Wehrle, C., Brand-Saberi, B., Kemler, R., Gossler, A., Kanzler, B. and Herrmann, B. G.** (2003). Wnt3a plays a major role in the segmentation clock controlling somitogenesis. *Dev Cell* **4**, 395–406.
- Axelrod, J. D.** (2001). Unipolar membrane association of Dishevelled mediates Frizzled planar cell polarity signaling. *Genes Dev.* **15**, 1182–1187.
- Balling, R.** (2001). ENU mutagenesis: analyzing gene function in mice. *Annu Rev Genomics Hum Genet* **2**, 463–492.
- Barker, N., Hurlstone, A., Musisi, H., Miles, A., Bienz, M. and Clevers, H.** (2001). The chromatin remodelling factor Brg-1 interacts with beta-catenin to promote target gene activation. *EMBO J* **20**, 4935–4943.
- Bastock, R., Strutt, H. and Strutt, D.** (2003). Strabismus is asymmetrically localised and binds to Prickle and Dishevelled during *Drosophila* planar polarity patterning. *Development* **130**, 3007–3014.

- Beck, S., Le Good, J. A., Guzman, M., Ben Haim, N., Roy, K., Beermann, F. and Constam, D. B.** (2002). Extraembryonic proteases regulate Nodal signalling during gastrulation. *Nat. Cell Biol.* **4**, 981–985.
- Bellomo, D., Lander, A., Harragan, I. and Brown, N. A.** (1996). Cell proliferation in mammalian gastrulation: the ventral node and notochord are relatively quiescent. *Dev Dyn* **205**, 471–485.
- Bennett, C. N., Ross, S. E., Longo, K. A., Bajnok, L., Hemati, N., Johnson, K. W., Harrison, S. D. and MacDougald, O. A.** (2002). Regulation of Wnt signaling during adipogenesis. *J. Biol. Chem.* **277**, 30998–31004.
- Berge, Ten, D., Kurek, D., Blauwkamp, T., Koole, W., Maas, A., Eroglu, E., Siu, R. K. and Nusse, R.** (2011). Embryonic stem cells require Wnt proteins to prevent differentiation to epiblast stem cells. *Nature Publishing Group* **13**, 1070–1075.
- Bernstein, B. W. and Bamburg, J. R.** (2010). ADF/cofilin: a functional node in cell biology. *Trends Cell Biol.* **20**, 187–195.
- Bhanot, P., Brink, M., Samos, C. H., Hsieh, J. C., Wang, Y., Macke, J. P., Andrew, D., Nathans, J. and Nusse, R.** (1996). A new member of the frizzled family from *Drosophila* functions as a Wingless receptor. *Nature* **382**, 225–230.
- Biechele, S., Cox, B. J. and Rossant, J.** (2011). Porcupine homolog is required for canonical Wnt signaling and gastrulation in mouse embryos. *Dev Biol* **355**, 275–285.
- Bilic, J., Huang, Y.-L., Davidson, G., Zimmermann, T., Cruciat, C.-M., Bienz, M. and Niehrs, C.** (2007). Wnt induces LRP6 signalosomes and promotes dishevelled-dependent LRP6 phosphorylation. *Science* **316**, 1619–1622.
- Blair, A., Tomlinson, A., Pham, H., Gunsalus, K. C., Goldberg, M. L. and Laski, F. A.** (2006). Twinstar, the *Drosophila* homolog of cofilin/ADF, is required for planar cell polarity patterning. *Development* **133**, 1789–1797.
- Blankenship, J. T., Backovic, S. T., Sanny, J. S. P., Weitz, O. and Zallen, J. A.** (2006). Multicellular rosette formation links planar cell polarity to tissue morphogenesis. *Dev Cell* **11**, 459–470.
- Bloomekatz, J., Grego-Bessa, J., Migeotte, I. and Anderson, K. V.** (2012). Pten regulates collective cell migration during specification of the anterior-posterior axis of the mouse embryo. *Dev Biol* **364**, 192–201.
- Blume, von, J., Alleaume, A.-M., Cantero-Recasens, G., Curwin, A., Carreras-Sureda, A., Zimmermann, T., van Galen, J., Wakana, Y., Valverde, M. A. and Malhotra, V.** (2011). ADF/cofilin regulates secretory

cargo sorting at the TGN via the Ca²⁺ ATPase SPCA1. *Dev Cell* **20**, 652–662.

Blume, von, J., Duran, J. M., Forlanelli, E., Alleaume, A.-M., Egorov, M., Polishchuk, R., Molina, H. and Malhotra, V. (2009). Actin remodeling by ADF/cofilin is required for cargo sorting at the trans-Golgi network. *J Cell Biol* **187**, 1055–1069.

Bopp, D., Schütt, C., Puro, J., Huang, H. and Nöthiger, R. (1999). Recombination and disjunction in female germ cells of *Drosophila* depend on the germline activity of the gene *sex-lethal*. *Development* **126**, 5785–5794.

Borello, U., Buffa, V., Sonnino, C., Melchionna, R., Vivarelli, E. and Cossu, G. (1999). Differential expression of the Wnt putative receptors Frizzled during mouse somitogenesis. *Mech Dev* **89**, 173–177.

Bornens, M. (2008). Organelle positioning and cell polarity. *Nat Rev Mol Cell Biol* **9**, 874–886.

Boulet, A. M. and Capecchi, M. R. (2012). Signaling by FGF4 and FGF8 is required for axial elongation of the mouse embryo. *Dev Biol* **371**, 235–245.

Brennan, K., Gonzalez-Sancho, J. M., Castelo-Soccio, L. A., Howe, L. R. and Brown, A. M. C. (2004). Truncated mutants of the putative Wnt receptor LRP6/Arrow can stabilize beta-catenin independently of Frizzled proteins. *Oncogene* **23**, 4873–4884.

Brunner, E., Peter, O., Schweizer, L. and Basler, K. (1997). *pangolin* encodes a Lef-1 homologue that acts downstream of Armadillo to transduce the Wingless signal in *Drosophila*. *Nature* **385**, 829–833.

Bryja, V., Andersson, E. R., Schambony, A., Esner, M., Bryjová, L., Biris, K. K., Hall, A. C., Kraft, B., Cajanek, L., Yamaguchi, T. P., et al. (2009). The extracellular domain of Lrp5/6 inhibits noncanonical Wnt signaling in vivo. *Mol Biol Cell* **20**, 924–936.

Bubb, M. R., Senderowicz, A. M., Sausville, E. A., Duncan, K. L. and Korn, E. D. (1994). Jasplakinolide, a cytotoxic natural product, induces actin polymerization and competitively inhibits the binding of phalloidin to F-actin. *J. Biol. Chem.* **269**, 14869–14871.

Burnette, J. M., Hatton, A. R. and Lopez, A. J. (1999). Trans-acting factors required for inclusion of regulated exons in the Ultrabithorax mRNAs of *Drosophila melanogaster*. *Genetics* **151**, 1517–1529.

Cai, L., Marshall, T. W., Uetrecht, A. C., Schafer, D. A. and Bear, J. E. (2007). Coronin 1B coordinates Arp2/3 complex and cofilin activities at the leading edge. *Cell* **128**, 915–929.

- Candia, A. F., Hu, J., Crosby, J., Lalley, P. A., Noden, D., Nadeau, J. H. and Wright, C. V.** (1992). Mox-1 and Mox-2 define a novel homeobox gene subfamily and are differentially expressed during early mesodermal patterning in mouse embryos. *Development* **116**, 1123–1136.
- Casal, J., Lawrence, P. A. and Struhl, G.** (2006). Two separate molecular systems, Dachshous/Fat and Starry night/Frizzled, act independently to confer planar cell polarity. *Development* **133**, 4561–4572.
- Caspary, T., Larkins, C. E. and Anderson, K. V.** (2007). The graded response to Sonic Hedgehog depends on cilia architecture. *Dev Cell* **12**, 767–778.
- Cavallo, R. A., Cox, R. T., Moline, M. M., Roose, J., Polevoy, G. A., Clevers, H., Peifer, M. and Bejsovec, A.** (1998). Drosophila Tcf and Groucho interact to repress Wingless signalling activity. *Nature* **395**, 604–608.
- Chae, J., Kim, M. J., Goo, J. H., Collier, S., Gubb, D., Charlton, J., Adler, P. N. and Park, W. J.** (1999). The Drosophila tissue polarity gene starry night encodes a member of the protocadherin family. *Development* **126**, 5421–5429.
- Chakrabarti, A., Matthews, G., Colman, A. and Dale, L.** (1992). Secretory and inductive properties of Drosophila wingless protein in Xenopus oocytes and embryos. *Development* **115**, 355–369.
- Chen, B., Dodge, M. E., Tang, W., Lu, J., Ma, Z., Fan, C.-W., Wei, S., Hao, W., Kilgore, J., Williams, N. S., et al.** (2009). Small molecule-mediated disruption of Wnt-dependent signaling in tissue regeneration and cancer. *Nat. Chem. Biol.* **5**, 100–107.
- Chen, C. M. and Struhl, G.** (1999). Wingless transduction by the Frizzled and Frizzled2 proteins of Drosophila. *Development* **126**, 5441–5452.
- Chen, G., Fernandez, J., Mische, S. and Courey, A. J.** (1999). A functional interaction between the histone deacetylase Rpd3 and the corepressor groucho in Drosophila development. *Genes Dev.* **13**, 2218–2230.
- Chen, W.-S., Antic, D., Matis, M., Logan, C. Y., Povelones, M., Anderson, G. A., Nusse, R. and Axelrod, J. D.** (2008). Asymmetric homotypic interactions of the atypical cadherin flamingo mediate intercellular polarity signaling. *Cell* **133**, 1093–1105.
- Chia, I. V. and Costantini, F.** (2005). Mouse axin and axin2/conductin proteins are functionally equivalent in vivo. *Mol. Cell. Biol.* **25**, 4371–4376.
- Ciruna, B. and Rossant, J.** (2001). FGF signaling regulates mesoderm cell fate specification and morphogenetic movement at the primitive streak. *Dev Cell* **1**, 37–49.

- Classen, A.-K., Anderson, K. I., Marois, E. and Eaton, S.** (2005). Hexagonal packing of *Drosophila* wing epithelial cells by the planar cell polarity pathway. *Dev Cell* **9**, 805–817.
- Conlon, F. L., Lyons, K. M., Takaesu, N., Barth, K. S., Kispert, A., Herrmann, B. and Robertson, E. J.** (1994). A primary requirement for nodal in the formation and maintenance of the primitive streak in the mouse. *Development* **120**, 1919–1928.
- Copp, A. J., Greene, N. D. E. and Murdoch, J. N.** (2003). The genetic basis of mammalian neurulation. *Nat Rev Genet* **4**, 784–793.
- Crabtree, M., Sieber, O. M., Lipton, L., Hodgson, S. V., Lamlum, H., Thomas, H. J. W., Neale, K., Phillips, R. K. S., Heinemann, K. and Tomlinson, I. P. M.** (2003). Refining the relation between 'first hits' and 'second hits' at the APC locus: the "loose fit" model and evidence for differences in somatic mutation spectra among patients. *Oncogene* **22**, 4257–4265.
- Cselenyi, C. S., Jernigan, K. K., Tahinci, E., Thorne, C. A., Lee, L. A. and Lee, E.** (2008). LRP6 transduces a canonical Wnt signal independently of Axin degradation by inhibiting GSK3's phosphorylation of beta-catenin. *Proc Natl Acad Sci U S A* **105**, 8032–8037.
- Curtin, J. A., Quint, E., Tsipouri, V., Arkell, R. M., Cattanach, B., Copp, A. J., Henderson, D. J., Spurr, N., Stanier, P., Fisher, E. M., et al.** (2003). Mutation of *Celsr1* disrupts planar polarity of inner ear hair cells and causes severe neural tube defects in the mouse. *Curr Biol* **13**, 1129–1133.
- Dajani, R., Fraser, E., Roe, S. M., Yeo, M., Good, V. M., Thompson, V., Dale, T. C. and Pearl, L. H.** (2003). Structural basis for recruitment of glycogen synthase kinase 3beta to the axin-APC scaffold complex. *EMBO J* **22**, 494–501.
- Dao, D. Y., Yang, X., Flick, L. M., Chen, D., Hilton, M. J. and O'Keefe, R. J.** (2010). Axin2 regulates chondrocyte maturation and axial skeletal development. *J. Orthop. Res.* **28**, 89–95.
- Darken, R. S., Scola, A. M., Rakeman, A. S., Das, G., Mlodzik, M. and Wilson, P. A.** (2002). The planar polarity gene *strabismus* regulates convergent extension movements in *Xenopus*. *EMBO J* **21**, 976–985.
- Das, G., Jenny, A., Klein, T. J., Eaton, S. and Mlodzik, M.** (2004). Diego interacts with Prickle and Strabismus/Van Gogh to localize planar cell polarity complexes. *Development* **131**, 4467–4476.
- Das, G., Reynolds-Kenneally, J. and Mlodzik, M.** (2002). The atypical cadherin Flamingo links Frizzled and Notch signaling in planar polarity establishment in the *Drosophila* eye. *Dev Cell* **2**, 655–666.

- DasGupta, R. and Fuchs, E.** (1999). Multiple roles for activated LEF/TCF transcription complexes during hair follicle development and differentiation. *Development* **126**, 4557–4568.
- Davidson, G., Wu, W., Shen, J., Bilic, J., Fenger, U., Stannek, P., Glinka, A. and Niehrs, C.** (2005). Casein kinase 1 gamma couples Wnt receptor activation to cytoplasmic signal transduction. *Nature* **438**, 867–872.
- Davidson, L. A. and Keller, R. E.** (1999). Neural tube closure in *Xenopus laevis* involves medial migration, directed protrusive activity, cell intercalation and convergent extension. *Development* **126**, 4547–4556.
- Davies, P. S., Dismuke, A. D., Powell, A. E., Carroll, K. H. and Wong, M. H.** (2008). Wnt-reporter expression pattern in the mouse intestine during homeostasis. *BMC Gastroenterol* **8**, 57.
- Dawes-Hoang, R. E., Parmar, K. M., Christiansen, A. E., Phelps, C. B., Brand, A. H. and Wieschaus, E. F.** (2005). folded gastrulation, cell shape change and the control of myosin localization. *Development* **132**, 4165–4178.
- Desclozeaux, M., Venturato, J., Wylie, F. G., Kay, J. G., Joseph, S. R., Le, H. T. and Stow, J. L.** (2008). Active Rab11 and functional recycling endosome are required for E-cadherin trafficking and lumen formation during epithelial morphogenesis. *Am. J. Physiol., Cell Physiol.* **295**, C545–56.
- Devenport, D. and Fuchs, E.** (2008). Planar polarization in embryonic epidermis orchestrates global asymmetric morphogenesis of hair follicles. *Nat. Cell Biol.* **10**, 1257–1268.
- Devenport, D., Oristian, D., Heller, E. and Fuchs, E.** (2011). Mitotic internalization of planar cell polarity proteins preserves tissue polarity. *Nature Publishing Group* **13**, 893–902.
- Donnison, M., Beaton, A., Davey, H. W., Broadhurst, R., L'Huillier, P. and Pfeffer, P. L.** (2005). Loss of the extraembryonic ectoderm in *Elf5* mutants leads to defects in embryonic patterning. *Development* **132**, 2299–2308.
- Donoughe, S. and DiNardo, S.** (2011). *dachsous* and *frizzled* contribute separately to planar polarity in the *Drosophila* ventral epidermis. *Development* **138**, 2751–2759.
- Eaton, S., Wepf, R. and Simons, K.** (1996). Roles for Rac1 and Cdc42 in planar polarization and hair outgrowth in the wing of *Drosophila*. *J Cell Biol* **135**, 1277–1289.
- Eggenschwiler, J. T. and Anderson, K. V.** (2000). Dorsal and lateral fates in the mouse neural tube require the cell-autonomous activity of the open brain gene. *Dev Biol* **227**, 648–660.

- Eklof Spink, K., Fridman, S. G. and Weis, W. I.** (2001). Molecular mechanisms of beta-catenin recognition by adenomatous polyposis coli revealed by the structure of an APC-beta-catenin complex. *EMBO J* **20**, 6203–6212.
- Elul, T. and Keller, R.** (2000). Monopolar protrusive activity: a new morphogenic cell behavior in the neural plate dependent on vertical interactions with the mesoderm in *Xenopus*. *Dev Biol* **224**, 3–19.
- Elul, T., Koehl, M. A. and Keller, R.** (1997). Cellular mechanism underlying neural convergent extension in *Xenopus laevis* embryos. *Dev Biol* **191**, 243–258.
- Fagotto, F., Jho, E. H., Zeng, L., Kurth, T., Joos, T., Kaufmann, C. and Costantini, F.** (1999). Domains of axin involved in protein-protein interactions, Wnt pathway inhibition, and intracellular localization. *J Cell Biol* **145**, 741–756.
- Feigun, F., Hannus, M., Mlodzik, M. and Eaton, S.** (2001). The ankyrin repeat protein Diego mediates Frizzled-dependent planar polarization. *Dev Cell* **1**, 93–101.
- Filali, M., Cheng, N., Abbott, D., Leontiev, V. and Engelhardt, J. F.** (2002). Wnt-3A/beta-catenin signaling induces transcription from the LEF-1 promoter. *J. Biol. Chem.* **277**, 33398–33410.
- Fischer, E., Legue, E., Doyen, A., Nato, F., Nicolas, J.-F., Torres, V., Yaniv, M. and Pontoglio, M.** (2006). Defective planar cell polarity in polycystic kidney disease. *Nat Genet* **38**, 21–23.
- Fukui, A., Kishida, S., Kikuchi, A. and Asashima, M.** (2000). Effects of rat Axin domains on axis formation in *Xenopus* embryos. *Dev. Growth Differ.* **42**, 489–498.
- Fukusumi, Y., Naruse, C. and Asano, M.** (2008). Wtap is required for differentiation of endoderm and mesoderm in the mouse embryo. *Dev Dyn* **237**, 618–629.
- Gao, B., Song, H., Bishop, K., Elliot, G., Garrett, L., English, M. A., Andre, P., Robinson, J., Sood, R., Minami, Y., et al.** (2011). Wnt signaling gradients establish planar cell polarity by inducing Vangl2 phosphorylation through Ror2. *Dev Cell* **20**, 163–176.
- García-García, M. J., Eggenschwiler, J. T., Caspary, T., Alcorn, H. L., Wyler, M. R., Huangfu, D., Rakeman, A. S., Lee, J. D., Feinberg, E. H., Timmer, J. R., et al.** (2005). Analysis of mouse embryonic patterning and morphogenesis by forward genetics. *Proc Natl Acad Sci U S A* **102**, 5913–5919.

- Gardner, R. L.** (1982). Investigation of cell lineage and differentiation in the extraembryonic endoderm of the mouse embryo. *J. Emb. Exper. Morph.* **68**, 175–198.
- Gempe, T. and Beye, M.** (2011). Function and evolution of sex determination mechanisms, genes and pathways in insects. *Bioessays* **33**, 52–60.
- Goetz, S. C. and Anderson, K. V.** (2010). The primary cilium: a signalling centre during vertebrate development. *Nat Rev Genet* **11**, 331–344.
- Granadino, B., Campuzano, S. and Sánchez, L.** (1990). The *Drosophila melanogaster* fl(2)d gene is needed for the female-specific splicing of Sex-lethal RNA. *EMBO J* **9**, 2597–2602.
- Gray, R. S., Abitua, P. B., Wlodarczyk, B. J., Szabo-Rogers, H. L., Blanchard, O., Lee, I., Weiss, G. S., Liu, K. J., Marcotte, E. M., Wallingford, J. B., et al.** (2009). The planar cell polarity effector Fuz is essential for targeted membrane trafficking, ciliogenesis and mouse embryonic development. *Nat. Cell Biol.* **11**, 1225–1232.
- Greene, N. D., Gerrelli, D., Van Straaten, H. W. and Copp, A. J.** (1998). Abnormalities of floor plate, notochord and somite differentiation in the loop-tail (Lp) mouse: a model of severe neural tube defects. *Mech Dev* **73**, 59–72.
- Guirao, B., Meunier, A., Mortaud, S., Aguilar, A., Corsi, J.-M., Strehl, L., Hirota, Y., Desoeuvre, A., Boutin, C., Han, Y.-G., et al.** (2010). Coupling between hydrodynamic forces and planar cell polarity orients mammalian motile cilia. *Nat. Cell Biol.* **12**, 341–350.
- Guo, N., Hawkins, C. and Nathans, J.** (2004). Frizzled6 controls hair patterning in mice. *Proc Natl Acad Sci U S A* **101**, 9277–9281.
- Gurniak, C. B., Perlas, E. and Witke, W.** (2005). The actin depolymerizing factor n-cofilin is essential for neural tube morphogenesis and neural crest cell migration. *Dev Biol* **278**, 231–241.
- Ha, N.-C., Tonzuka, T., Stamos, J. L., Choi, H.-J. and Weis, W. I.** (2004). Mechanism of phosphorylation-dependent binding of APC to beta-catenin and its role in beta-catenin degradation. *Mol Cell* **15**, 511–521.
- Habas, R. and He, X.** (2006). Activation of Rho and Rac by Wnt/frizzled signaling. *Methods in Enzymology* **406**, 500–511.
- Hagen, T. and Vidal-Puig, A.** (2002). Characterisation of the phosphorylation of beta-catenin at the GSK-3 priming site Ser45. *Biochem Biophys Res Commun* **294**, 324–328.
- Hamblet, N. S., Lijam, N., Ruiz-Lozano, P., Wang, J., Yang, Y., Luo, Z., Mei,**

- L., Chien, K. R., Sussman, D. J. and Wynshaw-Boris, A.** (2002). Dishevelled 2 is essential for cardiac outflow tract development, somite segmentation and neural tube closure. *Development* **129**, 5827–5838.
- Harumoto, T., Ito, M., Shimada, Y., Kobayashi, T. J., Ueda, H. R., Lu, B. and Uemura, T.** (2010). Atypical cadherins Dachsous and Fat control dynamics of noncentrosomal microtubules in planar cell polarity. *Dev Cell* **19**, 389–401.
- Hashimoto, M., Shinohara, K., Wang, J., Ikeuchi, S., Yoshida, S., Meno, C., Nonaka, S., Takada, S., Hatta, K., Wynshaw-Boris, A., et al.** (2010). Planar polarization of node cells determines the rotational axis of node cilia. *Nature Publishing Group* **12**, 170–176.
- Hatzis, P., van der Flier, L. G., van Driel, M. A., Guryev, V., Nielsen, F., Denissov, S., Nijman, I. J., Koster, J., Santo, E. E., Welboren, W., et al.** (2008). Genome-wide pattern of TCF7L2/TCF4 chromatin occupancy in colorectal cancer cells. *Mol. Cell. Biol.* **28**, 2732–2744.
- Hayashi, S., Lewis, P., Pevny, L. and McMahon, A. P.** (2002). Efficient gene modulation in mouse epiblast using a Sox2Cre transgenic mouse strain. *Mech Dev* **119 Suppl 1**, S97–S101.
- Haycraft, C. J., Zhang, Q., Song, B., Jackson, W. S., Detloff, P. J., Serra, R. and Yoder, B. K.** (2007). Intraflagellar transport is essential for endochondral bone formation. *Development* **134**, 307–316.
- He, F., Xiong, W., Yu, X., Espinoza-Lewis, R., Liu, C., Gu, S., Nishita, M., Suzuki, K., Yamada, G., Minami, Y., et al.** (2008). Wnt5a regulates directional cell migration and cell proliferation via Ror2-mediated noncanonical pathway in mammalian palate development. *Development* **135**, 3871–3879.
- Herrmann, B. G.** (1991). Expression pattern of the Brachyury gene in whole-mount TWis/TWis mutant embryos. *Development* **113**, 913–917.
- Hilfiker, A., Amrein, H., Dübendorfer, A., Schneiter, R. and Nöthiger, R.** (1995). The gene virilizer is required for female-specific splicing controlled by Sxl, the master gene for sexual development in *Drosophila*. *Development* **121**, 4017–4026.
- Hirota, Y., Meunier, A., Huang, S., Shimosawa, T., Yamada, O., Kida, Y. S., Inoue, M., Ito, T., Kato, H., Sakaguchi, M., et al.** (2010). Planar polarity of multiciliated ependymal cells involves the anterior migration of basal bodies regulated by non-muscle myosin II. *Development* **137**, 3037–3046.
- Horabin, J. I. and Schedl, P.** (1996). Splicing of the *Drosophila* Sex-lethal early transcripts involves exon skipping that is independent of Sex-lethal protein. *RNA* **2**, 1–10.

- Hotulainen, P., Paunola, E., Vartiainen, M. K. and Lappalainen, P.** (2005). Actin-depolymerizing factor and cofilin-1 play overlapping roles in promoting rapid F-actin depolymerization in mammalian nonmuscle cells. *Mol Biol Cell* **16**, 649–664.
- Huang, S.-M. A., Mishina, Y. M., Liu, S., Cheung, A., Stegmeier, F., Michaud, G. A., Charlat, O., Wiellette, E., Zhang, Y., Wiessner, S., et al.** (2009). Tankyrase inhibition stabilizes axin and antagonizes Wnt signalling. *Nature* **461**, 614–620.
- Huelsken, J., Vogel, R., Brinkmann, V., Erdmann, B., Birchmeier, C. and Birchmeier, W.** (2000). Requirement for beta-catenin in anterior-posterior axis formation in mice. *J Cell Biol* **148**, 567–578.
- Ikeda, S., Cunningham, L. A., Boggess, D., Hawes, N., Hobson, C. D., Sundberg, J. P., Naggert, J. K., Smith, R. S. and Nishina, P. M.** (2003). Aberrant actin cytoskeleton leads to accelerated proliferation of corneal epithelial cells in mice deficient for destrin (actin depolymerizing factor). *Hum Mol Genet* **12**, 1029–1037.
- Ishitani, T., Ninomiya-Tsuji, J., Nagai, S., Nishita, M., Meneghini, M., Barker, N., Waterman, M., Bowerman, B., Clevers, H., Shibuya, H., et al.** (1999). The TAK1-NLK-MAPK-related pathway antagonizes signalling between beta-catenin and transcription factor TCF. *Nature* **399**, 798–802.
- Itoh, K., Krupnik, V. E. and Sokol, S. Y.** (1998). Axis determination in *Xenopus* involves biochemical interactions of axin, glycogen synthase kinase 3 and beta-catenin. *Curr Biol* **8**, 591–594.
- Janda, C. Y., Waghray, D., Levin, A. M., Thomas, C. and Garcia, K. C.** (2012). Structural basis of Wnt recognition by Frizzled. *Science* **337**, 59–64.
- Jenny, A., Darken, R. S., Wilson, P. A. and Mlodzik, M.** (2003). Prickle and Strabismus form a functional complex to generate a correct axis during planar cell polarity signaling. *EMBO J* **22**, 4409–4420.
- Jenny, A., Reynolds-Kenneally, J., Das, G., Burnett, M. and Mlodzik, M.** (2005). Diego and Prickle regulate Frizzled planar cell polarity signalling by competing for Dishevelled binding. *Nat. Cell Biol.* **7**, 691–697.
- Jessen, J. R., Topczewski, J., Bingham, S., Sepich, D. S., Marlow, F., Chandrasekhar, A. and Solnica-Krezel, L.** (2002). Zebrafish trilobite identifies new roles for Strabismus in gastrulation and neuronal movements. *Nat. Cell Biol.* **4**, 610–615.
- Jho, E.-H., Zhang, T., Domon, C., Joo, C.-K., Freund, J.-N. and Costantini, F.** (2002). Wnt/beta-catenin/Tcf signaling induces the transcription of Axin2, a negative regulator of the signaling pathway. *Mol. Cell. Biol.* **22**, 1172–1183.

- Johnson, M. L., Nagengast, A. A. and Salz, H. K.** (2010). PPS, a large multidomain protein, functions with sex-lethal to regulate alternative splicing in *Drosophila*. *PLoS Genet* **6**, e1000872.
- Jones, C., Roper, V. C., Foucher, I., Qian, D., Banizs, B., Petit, C., Yoder, B. K. and Chen, P.** (2008). Ciliary proteins link basal body polarization to planar cell polarity regulation. *Nat Genet* **40**, 69–77.
- Jue, S. F., Bradley, R. S., Rudnicki, J. A., Varmus, H. E. and Brown, A. M.** (1992). The mouse Wnt-1 gene can act via a paracrine mechanism in transformation of mammary epithelial cells. *Mol. Cell. Biol.* **12**, 321–328.
- Julius, M. A., Schelbert, B., Hsu, W., Fitzpatrick, E., Jho, E., Fagotto, F., Costantini, F. and Kitajewski, J.** (2000). Domains of axin and disheveled required for interaction and function in wnt signaling. *Biochem Biophys Res Commun* **276**, 1162–1169.
- Karner, C. M., Chirumamilla, R., Aoki, S., Igarashi, P., Wallingford, J. B. and Carroll, T. J.** (2009). Wnt9b signaling regulates planar cell polarity and kidney tubule morphogenesis. *Nat Genet* **41**, 793–799.
- Karner, C. M., Merkel, C. E., Dodge, M., Ma, Z., Lu, J., Chen, C., Lum, L. and Carroll, T. J.** (2010). Tankyrase is necessary for canonical Wnt signaling during kidney development. *Dev Dyn* **239**, 2014–2023.
- Kato, M., Patel, M. S., Levasseur, R., Lobov, I., Chang, B. H.-J., Glass, D. A., Hartmann, C., Li, L., Hwang, T.-H., Brayton, C. F., et al.** (2002). Cbfa1-independent decrease in osteoblast proliferation, osteopenia, and persistent embryonic eye vascularization in mice deficient in Lrp5, a Wnt coreceptor. *J Cell Biol* **157**, 303–314.
- Keller, R.** (2002). Shaping the vertebrate body plan by polarized embryonic cell movements. *Science* **298**, 1950–1954.
- Kelly, G. M., Erezyilmaz, D. F. and Moon, R. T.** (1995). Induction of a secondary embryonic axis in zebrafish occurs following the overexpression of beta-catenin. *Mech Dev* **53**, 261–273.
- Kelly, O. G., Pinson, K. I. and Skarnes, W. C.** (2004). The Wnt co-receptors Lrp5 and Lrp6 are essential for gastrulation in mice. *Development* **131**, 2803–2815.
- Kemler, R., Hierholzer, A., Kanzler, B., Kuppig, S., Hansen, K., Taketo, M. M., de Vries, W. N., Knowles, B. B. and Solter, D.** (2004). Stabilization of beta-catenin in the mouse zygote leads to premature epithelial-mesenchymal transition in the epiblast. *Development* **131**, 5817–5824.
- Kemp, C., Willems, E., Abdo, S., Lambiv, L. and Leyns, L.** (2005). Expression

of all Wnt genes and their secreted antagonists during mouse blastocyst and postimplantation development. *Dev Dyn* **233**, 1064–1075.

- Kibar, Z., Capra, V. and Gros, P.** (2007a). Toward understanding the genetic basis of neural tube defects. *Clin. Genet.* **71**, 295–310.
- Kibar, Z., Gauthier, S., Lee, S.-H., Vidal, S. and Gros, P.** (2003). Rescue of the neural tube defect of loop-tail mice by a BAC clone containing the *Ltap* gene. *Genomics* **82**, 397–400.
- Kibar, Z., Torban, E., McDearmid, J. R., Reynolds, A., Berghout, J., Mathieu, M., Kirillova, I., De Marco, P., Merello, E., Hayes, J. M., et al.** (2007b). Mutations in *VANGL1* associated with neural-tube defects. *N. Engl. J. Med.* **356**, 1432–1437.
- Kibar, Z., Underhill, D. A., Canonne-Hergaux, F., Gauthier, S., Justice, M. J. and Gros, P.** (2001a). Identification of a new chemically induced allele (*Lp(m1Jus)*) at the loop-tail locus: morphology, histology, and genetic mapping. *Genomics* **72**, 331–337.
- Kibar, Z., Vogan, K. J., Groulx, N., Justice, M. J., Underhill, D. A. and Gros, P.** (2001b). *Ltap*, a mammalian homolog of *Drosophila Strabismus/Van Gogh*, is altered in the mouse neural tube mutant Loop-tail. *Nat Genet* **28**, 251–255.
- Kim, H. Y. and Davidson, L. A.** (2011). Punctuated actin contractions during convergent extension and their permissive regulation by the non-canonical Wnt-signaling pathway. *J Cell Sci* **124**, 635–646.
- Kimura-Yoshida, C., Nakano, H., Okamura, D., Nakao, K., Yonemura, S., Belo, J. A., Aizawa, S., Matsui, Y. and Matsuo, I.** (2005). Canonical Wnt signaling and its antagonist regulate anterior-posterior axis polarization by guiding cell migration in mouse visceral endoderm. *Dev Cell* **9**, 639–650.
- Kishida, S., Yamamoto, H., Hino, S., Ikeda, S., Kishida, M. and Kikuchi, A.** (1999). DIX domains of *Dvl* and axin are necessary for protein interactions and their ability to regulate beta-catenin stability. *Mol. Cell. Biol.* **19**, 4414–4422.
- Kispert, A., Vainio, S., Shen, L., Rowitch, D. H. and McMahon, A. P.** (1996). Proteoglycans are required for maintenance of Wnt-11 expression in the ureter tips. *Development* **122**, 3627–3637.
- Klooster, Ten, J. P., Evers, E. E., Janssen, L., Machesky, L. M., Michiels, F., Hordijk, P. and Collard, J. G.** (2006). Interaction between Tiam1 and the Arp2/3 complex links activation of Rac to actin polymerization. *Biochem J* **397**, 39–45.

- Koike, S., Keino-Masu, K., Ohto, T., Sugiyama, F., Takahashi, S. and Masu, M.** (2009). Autotaxin/lysophospholipase D-mediated lysophosphatidic acid signaling is required to form distinctive large lysosomes in the visceral endoderm cells of the mouse yolk sac. *J. Biol. Chem.* **284**, 33561–33570.
- Koinuma, K., Yamashita, Y., Liu, W., Hatanaka, H., Kurashina, K., Wada, T., Takada, S., Kaneda, R., Choi, Y. L., Fujiwara, S.-I., et al.** (2006). Epigenetic silencing of AXIN2 in colorectal carcinoma with microsatellite instability. *Oncogene* **25**, 139–146.
- Komada, M. and Soriano, P.** (1999). Hrs, a FYVE finger protein localized to early endosomes, is implicated in vesicular traffic and required for ventral folding morphogenesis. *Genes Dev.* **13**, 1475–1485.
- Komekado, H., Yamamoto, H., Chiba, T. and Kikuchi, A.** (2007). Glycosylation and palmitoylation of Wnt-3a are coupled to produce an active form of Wnt-3a. *Genes Cells* **12**, 521–534.
- Korinek, V., Barker, N., Moerer, P., van Donselaar, E., Huls, G., Peters, P. J. and Clevers, H.** (1998). Depletion of epithelial stem-cell compartments in the small intestine of mice lacking Tcf-4. *Nat Genet* **19**, 379–383.
- Krasnow, R. E. and Adler, P. N.** (1994). A single frizzled protein has a dual function in tissue polarity. *Development* **120**, 1883–1893.
- Kwon, G. S., Viotti, M. and Hadjantonakis, A.-K.** (2008). The endoderm of the mouse embryo arises by dynamic widespread intercalation of embryonic and extraembryonic lineages. *Dev Cell* **15**, 509–520.
- La Coste, de, A., Romagnolo, B., Billuart, P., Renard, C. A., Buendia, M. A., Soubrane, O., Fabre, M., Chelly, J., Beldjord, C., Kahn, A., et al.** (1998). Somatic mutations of the beta-catenin gene are frequent in mouse and human hepatocellular carcinomas. *Proc Natl Acad Sci U S A* **95**, 8847–8851.
- Lammi, L., Arte, S., Somer, M., Jarvinen, H., Lahermo, P., Thesleff, I., Pirinen, S. and Nieminen, P.** (2004). Mutations in AXIN2 cause familial tooth agenesis and predispose to colorectal cancer. *Am. J. Hum. Genet.* **74**, 1043–1050.
- Lee, E., Salic, A., Krüger, R., Heinrich, R. and Kirschner, M. W.** (2003). The Roles of APC and Axin Derived from Experimental and Theoretical Analysis of the Wnt Pathway. *PLoS Biol* **1**, e10.
- Lee, H. and Adler, P. N.** (2002). The function of the frizzled pathway in the *Drosophila* wing is dependent on inturnd and fuzzy. *Genetics* **160**, 1535–1547.
- Lee, J. D., Migeotte, I. and Anderson, K. V.** (2010). Left-right patterning in the

- mouse requires Epb4.115-dependent morphogenesis of the node and midline. *Dev Biol* **346**, 237–246.
- Levine, A. J. and Brivanlou, A. H.** (2007). Proposal of a model of mammalian neural induction. *Dev Biol* **308**, 247–256.
- Li, V. S. W., Ng, S. S., Boersema, P. J., Low, T. Y., Karthaus, W. R., Gerlach, J. P., Mohammed, S., Heck, A. J. R., Maurice, M. M., Mahmoudi, T., et al.** (2012). Wnt Signaling through Inhibition of β -Catenin Degradation in an Intact Axin1 Complex. *Cell* **149**, 1245–1256.
- Lickert, H., Kutsch, S., Kanzler, B., Tamai, Y., Taketo, M. M. and Kemler, R.** (2002). Formation of multiple hearts in mice following deletion of beta-catenin in the embryonic endoderm. *Dev Cell* **3**, 171–181.
- Little, N. A., Hastie, N. D. and Davies, R. C.** (2000). Identification of WTAP, a novel Wilms' tumour 1-associating protein. *Hum Mol Genet* **9**, 2231–2239.
- Liu, A. and Joyner, A. L.** (2001). EN and GBX2 play essential roles downstream of FGF8 in patterning the mouse mid/hindbrain region. *Development* **128**, 181–191.
- Liu, C., Kato, Y., Zhang, Z., Do, V. M., Yankner, B. A. and He, X.** (1999a). beta-Trcp couples beta-catenin phosphorylation-degradation and regulates Xenopus axis formation. *Proc Natl Acad Sci U S A* **96**, 6273–6278.
- Liu, C., Li, Y., Semenov, M., Han, C., Baeg, G. H., Tan, Y., Zhang, Z., Lin, X. and He, X.** (2002). Control of beta-catenin phosphorylation/degradation by a dual-kinase mechanism. *Cell* **108**, 837–847.
- Liu, G., Bafico, A., Harris, V. K. and Aaronson, S. A.** (2003). A novel mechanism for Wnt activation of canonical signaling through the LRP6 receptor. *Mol. Cell. Biol.* **23**, 5825–5835.
- Liu, P., Wakamiya, M., Shea, M. J., Albrecht, U., Behringer, R. R. and Bradley, A.** (1999b). Requirement for Wnt3 in vertebrate axis formation. *Nat Genet* **22**, 361–365.
- Liu, T., DeCostanzo, A. J., Liu, X., Wang Hy, Hallagan, S., Moon, R. T. and Malbon, C. C.** (2001). G protein signaling from activated rat frizzled-1 to the beta-catenin-Lef-Tcf pathway. *Science* **292**, 1718–1722.
- Liu, X., Rubin, J. S. and Kimmel, A. R.** (2005). Rapid, Wnt-induced changes in GSK3beta associations that regulate beta-catenin stabilization are mediated by Galpha proteins. *Curr Biol* **15**, 1989–1997.
- Logan, C. Y. and Nusse, R.** (2004). The Wnt signaling pathway in development and disease. *Annu. Rev. Cell Dev. Biol.* **20**, 781–810.

- Lu, C. C., Brennan, J. and Robertson, E. J.** (2001). From fertilization to gastrulation: axis formation in the mouse embryo. *Curr. Opin. Genet. Dev.* **11**, 384–392.
- Lu, X., Borchers, A. G. M., Jolicoeur, C., Rayburn, H., Baker, J. C. and Tessier-Lavigne, M.** (2004). PTK7/CCK-4 is a novel regulator of planar cell polarity in vertebrates. *Nature* **430**, 93–98.
- Luo, J., Sladek, R., Bader, J. A., Matthyssen, A., Rossant, J. and Giguère, V.** (1997). Placental abnormalities in mouse embryos lacking the orphan nuclear receptor ERR-beta. *Nature* **388**, 778–782.
- Lustig, B., Jerchow, B., Sachs, M., Weiler, S., Pietsch, T., Karsten, U., van de Wetering, M., Clevers, H., Schlag, P. M., Birchmeier, W., et al.** (2002). Negative feedback loop of Wnt signaling through upregulation of conductin/axin2 in colorectal and liver tumors. *Mol. Cell. Biol.* **22**, 1184–1193.
- MacDonald, B. T., Tamai, K. and He, X.** (2009). Wnt/beta-catenin signaling: components, mechanisms, and diseases. *Dev Cell* **17**, 9–26.
- Mahaffey, J. P., Grego-Bessa, J., Liem, K. F. and Anderson, K. V.** (2013). Cofilin and Vangl2 cooperate in the initiation of planar cell polarity in the mouse embryo. *Development* **140**, 1262–1271. Copyright 2013.
- Maheswaranathan, M., Gole, H. K. A., Fernandez, I., Lassègue, B., Griending, K. K. and San Martín, A.** (2011). Platelet-derived growth factor (PDGF) regulates Slingshot phosphatase activity via Nox1-dependent auto-dephosphorylation of serine 834 in vascular smooth muscle cells. *J. Biol. Chem.* **286**, 35430–35437.
- Manoukian, A. S., Yoffe, K. B., Wilder, E. L. and Perrimon, N.** (1995). The porcupine gene is required for wingless autoregulation in *Drosophila*. *Development* **121**, 4037–4044.
- Mao, J., Wang, J., Liu, B., Pan, W., Farr, G. H., Flynn, C., Yuan, H., Takada, S., Kimelman, D., Li, L., et al.** (2001). Low-density lipoprotein receptor-related protein-5 binds to Axin and regulates the canonical Wnt signaling pathway. *Mol Cell* **7**, 801–809.
- Mao, Y., Mulvaney, J., Zakaria, S., Yu, T., Morgan, K. M., Allen, S., Basson, M. A., Francis-West, P. and Irvine, K. D.** (2011). Characterization of a *Dchs1* mutant mouse reveals requirements for *Dchs1*-*Fat4* signaling during mammalian development. *Development* **138**, 947–957.
- Marikawa, Y.** (2006). Wnt/beta-catenin signaling and body plan formation in mouse embryos. *Semin Cell Dev Biol* **17**, 175–184.
- Marlow, F., Topczewski, J., Sepich, D. and Solnica-Krezel, L.** (2002).

Zebrafish Rho kinase 2 acts downstream of Wnt11 to mediate cell polarity and effective convergence and extension movements. *Curr Biol* **12**, 876–884.

Matusek, T., Djiane, A., Jankovics, F., Brunner, D., Mlodzik, M. and Mihály, J. (2006). The *Drosophila* formin DAAM regulates the tracheal cuticle pattern through organizing the actin cytoskeleton. *Development* **133**, 957–966.

McGough, A., Pope, B., Chiu, W. and Weeds, A. (1997). Cofilin changes the twist of F-actin: implications for actin filament dynamics and cellular function. *J Cell Biol* **138**, 771–781.

McGrath, J., Somlo, S., Makova, S., Tian, X. and Brueckner, M. (2003). Two populations of node monocilia initiate left-right asymmetry in the mouse. *Cell* **114**, 61–73.

McMahon, A. P. and Moon, R. T. (1989). Ectopic expression of the proto-oncogene *int-1* in *Xenopus* embryos leads to duplication of the embryonic axis. *Cell* **58**, 1075–1084.

Meneghini, M. D., Ishitani, T., Carter, J. C., Hisamoto, N., Ninomiya-Tsuji, J., Thorpe, C. J., Hamill, D. R., Matsumoto, K. and Bowerman, B. (1999). MAP kinase and Wnt pathways converge to downregulate an HMG-domain repressor in *Caenorhabditis elegans*. *Nature* **399**, 793–797.

Merte, J., Jensen, D., Wright, K., Sarsfield, S., Wang, Y., Schekman, R. and Ginty, D. D. (2010). *Sec24b* selectively sorts *Vangl2* to regulate planar cell polarity during neural tube closure. *Nat. Cell Biol.* **12**, 41–6; sup pp 1–8.

Mikels, A. J. and Nusse, R. (2006). Purified Wnt5a protein activates or inhibits beta-catenin-TCF signaling depending on receptor context. *PLoS Biol* **4**, e115.

Miyoshi, Y., Ando, H., Nagase, H., Nishisho, I., Horii, A., Miki, Y., Mori, T., Utsunomiya, J., Baba, S. and Petersen, G. (1992). Germ-line mutations of the APC gene in 53 familial adenomatous polyposis patients. *Proc Natl Acad Sci U S A* **89**, 4452–4456.

Molenaar, M., van de Wetering, M., Oosterwegel, M., Peterson-Maduro, J., Godsave, S., Korinek, V., Roose, J., Destree, O. and Clevers, H. (1996). XTcf-3 transcription factor mediates beta-catenin-induced axis formation in *Xenopus* embryos. *Cell* **86**, 391–399.

Montcouquiol, M., Rachel, R. A., Lanford, P. J., Copeland, N. G., Jenkins, N. A. and Kelley, M. W. (2003). Identification of *Vangl2* and *Scrb1* as planar polarity genes in mammals. *Nature* **423**, 173–177.

Montcouquiol, M., Sans, N., Huss, D., Kach, J., Dickman, J. D., Forge, A., Rachel, R. A., Copeland, N. G., Jenkins, N. A., Bogani, D., et al. (2006).

Asymmetric localization of Vangl2 and Fz3 indicate novel mechanisms for planar cell polarity in mammals. *J Neurosci* **26**, 5265–5275.

Moran, J. L., Bolton, A. D., Tran, P. V., Brown, A., Dwyer, N. D., Manning, D. K., Bjork, B. C., Li, C., Montgomery, K., Siepka, S. M., et al. (2006).

Utilization of a whole genome SNP panel for efficient genetic mapping in the mouse. *Genome Res.* **16**, 436–440.

Morkel, M., Huelsken, J., Wakamiya, M., Ding, J., van de Wetering, M., Clevers, H., Taketo, M. M., Behringer, R. R., Shen, M. M. and Birchmeier, W. (2003). Beta-catenin regulates Cripto- and Wnt3-dependent gene expression programs in mouse axis and mesoderm formation. *Development* **130**, 6283–6294.

Morrone, S., Cheng, Z., Moon, R. T., Cong, F. and Xu, W. (2012). Crystal structure of a Tankyrase-Axin complex and its implications for Axin turnover and Tankyrase substrate recruitment. *Proc Natl Acad Sci U S A* **109**, 1500–1505.

Mottola, G., Classen, A.-K., González-Gaitán, M., Eaton, S. and Zerial, M. (2010). A novel function for the Rab5 effector Rabenosyn-5 in planar cell polarity. *Development* **137**, 2353–2364.

Mouneimne, G., DesMarais, V., Sidani, M., Scemes, E., Wang, W., Song, X., Eddy, R. and Condeelis, J. (2006). Spatial and temporal control of cofilin activity is required for directional sensing during chemotaxis. *Curr Biol* **16**, 2193–2205.

Murdoch, J. N., Doudney, K., Paternotte, C., Copp, A. J. and Stanier, P. (2001). Severe neural tube defects in the loop-tail mouse result from mutation of *Lpp1*, a novel gene involved in floor plate specification. *Hum Mol Genet* **10**, 2593–2601.

Murdoch, J. N., Henderson, D. J., Doudney, K., Gaston-Massuet, C., Phillips, H. M., Paternotte, C., Arkell, R., Stanier, P. and Copp, A. J. (2003). Disruption of scribble (*Scrb1*) causes severe neural tube defects in the circletail mouse. *Hum Mol Genet* **12**, 87–98.

Musci, T. S. and Mullen, R. J. (1990). All-or-none craniorachischisis in Loop-tail mutant mouse chimeras. *Development* **110**, 229–237.

Nam, J.-S., Turcotte, T. J., Smith, P. F., Choi, S. and Yoon, J. K. (2006). Mouse cristin/R-spondin family proteins are novel ligands for the Frizzled 8 and LRP6 receptors and activate beta-catenin-dependent gene expression. *J. Biol. Chem.* **281**, 13247–13257.

Narimatsu, M., Bose, R., Pye, M., Zhang, L., Miller, B., Ching, P., Sakuma, R., Luga, V., Roncari, L., Attisano, L., et al. (2009). Regulation of planar cell

- polarity by Smurf ubiquitin ligases. *Cell* **137**, 295–307.
- Ng, S. B., Turner, E. H., Robertson, P. D., Flygare, S. D., Bigham, A. W., Lee, C., Shaffer, T., Wong, M., Bhattacharjee, A., Eichler, E. E., et al.** (2009). Targeted capture and massively parallel sequencing of 12 human exomes. *Nature* **461**, 272–276.
- Nishimura, T., Honda, H. and Takeichi, M.** (2012). Planar cell polarity links axes of spatial dynamics in neural-tube closure. *Cell* **149**, 1084–1097.
- Nishita, M., Wang, Y., Tomizawa, C., Suzuki, A., Niwa, R., Uemura, T. and Mizuno, K.** (2004). Phosphoinositide 3-kinase-mediated activation of cofilin phosphatase Slingshot and its role for insulin-induced membrane protrusion. *J. Biol. Chem.* **279**, 7193–7198.
- Nonaka, S., Shiratori, H., Saijoh, Y. and Hamada, H.** (2002). Determination of left-right patterning of the mouse embryo by artificial nodal flow. *Nature* **418**, 96–99.
- Nonaka, S., Tanaka, Y., Okada, Y., Takeda, S., Harada, A., Kanai, Y., Kido, M. and Hirokawa, N.** (1998). Randomization of left-right asymmetry due to loss of nodal cilia generating leftward flow of extraembryonic fluid in mice lacking KIF3B motor protein. *Cell* **95**, 829–837.
- Nonaka, S., Yoshida, S., Watanabe, D., Ikeuchi, S., Goto, T., Marshall, W. F. and Hamada, H.** (2005). De novo formation of left-right asymmetry by posterior tilt of nodal cilia. *PLoS Biol* **3**, e268.
- Nüsslein-Volhard, C. and Wieschaus, E.** (1980). Mutations affecting segment number and polarity in *Drosophila*. *Nature* **287**, 795–801.
- Okreglak, V. and Drubin, D. G.** (2007). Cofilin recruitment and function during actin-mediated endocytosis dictated by actin nucleotide state. *J Cell Biol* **178**, 1251–1264.
- Orsulic, S., Huber, O., Aberle, H., Arnold, S. and Kemler, R.** (1999). E-cadherin binding prevents beta-catenin nuclear localization and beta-catenin/LEF-1-mediated transactivation. *J Cell Sci* **112 (Pt 8)**, 1237–1245.
- Ortega, A., Niksic, M., Bachi, A., Wilm, M., Sánchez, L., Hastie, N. and Valcárcel, J.** (2003). Biochemical function of female-lethal (2)D/Wilms' tumor suppressor-1-associated proteins in alternative pre-mRNA splicing. *J. Biol. Chem.* **278**, 3040–3047.
- Park, M. and Moon, R. T.** (2002). The planar cell-polarity gene *stbm* regulates cell behaviour and cell fate in vertebrate embryos. *Nat. Cell Biol.* **4**, 20–25.
- Park, T. J., Gray, R. S., Sato, A., Habas, R. and Wallingford, J. B.** (2005).

- Subcellular localization and signaling properties of dishevelled in developing vertebrate embryos. *Curr Biol* **15**, 1039–1044.
- Park, T. J., Mitchell, B. J., Abitua, P. B., Kintner, C. and Wallingford, J. B.** (2008). Dishevelled controls apical docking and planar polarization of basal bodies in ciliated epithelial cells. *Nat Genet* **40**, 871–879.
- Peifer, M., Rauskolb, C., Williams, M., Riggelman, B. and Wieschaus, E.** (1991). The segment polarity gene armadillo interacts with the wingless signaling pathway in both embryonic and adult pattern formation. *Development* **111**, 1029–1043.
- Pennekamp, P., Karcher, C., Fischer, A., Schweickert, A., Skryabin, B., Horst, J., Blum, M. and Dworniczak, B.** (2002). The ion channel polycystin-2 is required for left-right axis determination in mice. *Curr Biol* **12**, 938–943.
- Peränen, J.** (2011). Rab8 GTPase as a regulator of cell shape. *Cytoskeleton (Hoboken)* **68**, 527–539.
- Piao, S., Lee, S.-H., Kim, H., Yum, S., Stamos, J. L., Xu, Y., Lee, S.-J., Lee, J., Oh, S., Han, J.-K., et al.** (2008). Direct inhibition of GSK3beta by the phosphorylated cytoplasmic domain of LRP6 in Wnt/beta-catenin signaling. *PLoS ONE* **3**, e4046.
- Pinson, K. I., Brennan, J., Monkley, S., Avery, B. J. and Skarnes, W. C.** (2000). An LDL-receptor-related protein mediates Wnt signalling in mice. *Nature* **407**, 535–538.
- Pires-daSilva, A. and Sommer, R. J.** (2003). The evolution of signalling pathways in animal development. *Nat Rev Genet* **4**, 39–49.
- Plageman, T. F., Chauhan, B. K., Yang, C., Jaudon, F., Shang, X., Zheng, Y., Lou, M., Debant, A., Hildebrand, J. D. and Lang, R. A.** (2011). A Trio-RhoA-Shroom3 pathway is required for apical constriction and epithelial invagination. *Development* **138**, 5177–5188.
- Polakis, P.** (2007). The many ways of Wnt in cancer. *Curr. Opin. Genet. Dev.* **17**, 45–51.
- Pope, B. J., Zierler-Gould, K. M., Kühne, R., Weeds, A. G. and Ball, L. J.** (2004). Solution structure of human cofilin: actin binding, pH sensitivity, and relationship to actin-depolymerizing factor. *J. Biol. Chem.* **279**, 4840–4848.
- Price, M. H., Roberts, D. M., McCartney, B. M., Jezuit, E. and Peifer, M.** (2006). Cytoskeletal dynamics and cell signaling during planar polarity establishment in the Drosophila embryonic denticle. *J Cell Sci* **119**, 403–415.
- Qian, D., Jones, C., Rzadzinska, A., Mark, S., Zhang, X., Steel, K. P., Dai, X.**

- and Chen, P.** (2007). Wnt5a functions in planar cell polarity regulation in mice. *Dev Biol* **306**, 121–133.
- Qian, L., Mahaffey, J. P., Alcorn, H. L. and Anderson, K. V.** (2011). Tissue-specific roles of Axin2 in the inhibition and activation of Wnt signaling in the mouse embryo. *Proc Natl Acad Sci U S A* **108**, 8692–8697. Copyright 2011.
- Rakeman, A. S. and Anderson, K. V.** (2006). Axis specification and morphogenesis in the mouse embryo require Nap1, a regulator of WAVE-mediated actin branching. *Development* **133**, 3075–3083.
- Ratcliffe, M. J., Itoh, K. and Sokol, S. Y.** (2000). A positive role for the PP2A catalytic subunit in Wnt signal transduction. *J. Biol. Chem.* **275**, 35680–35683.
- Reya, T., Duncan, A. W., Ailles, L., Domen, J., Scherer, D. C., Willert, K., Hintz, L., Nusse, R. and Weissman, I. L.** (2003). A role for Wnt signalling in self-renewal of haematopoietic stem cells. *Nature* **423**, 409–414.
- Rivera-Pérez, J. A. and Magnuson, T.** (2005). Primitive streak formation in mice is preceded by localized activation of Brachyury and Wnt3. *Dev Biol* **288**, 363–371.
- Rodriguez, T. A., Casey, E. S., Harland, R. M., Smith, J. C. and Beddington, R. S.** (2001). Distinct enhancer elements control Hex expression during gastrulation and early organogenesis. *Dev Biol* **234**, 304–316.
- Rohatgi, R., Ma, L., Miki, H., Lopez, M., Kirchhausen, T., Takenawa, T. and Kirschner, M. W.** (1999). The interaction between N-WASP and the Arp2/3 complex links Cdc42-dependent signals to actin assembly. *Cell* **97**, 221–231.
- Ross, A. J., May-Simera, H., Eichers, E. R., Kai, M., Hill, J., Jagger, D. J., Leitch, C. C., Chapple, J. P., Munro, P. M., Fisher, S., et al.** (2005). Disruption of Bardet-Biedl syndrome ciliary proteins perturbs planar cell polarity in vertebrates. *Nat Genet* **37**, 1135–1140.
- Rossant, J. and Tam, P. P. L.** (2009). Blastocyst lineage formation, early embryonic asymmetries and axis patterning in the mouse. *Development* **136**, 701–713.
- Rossant, J., Guillemot, F., Tanaka, M., Latham, K., Gertenstein, M. and Nagy, A.** (1998). Mash2 is expressed in oogenesis and preimplantation development but is not required for blastocyst formation. *Mech Dev* **73**, 183–191.
- Rothbächer, U., Laurent, M. N., Deardorff, M. A., Klein, P. S., Cho, K. W. and Fraser, S. E.** (2000). Dishevelled phosphorylation, subcellular localization and multimerization regulate its role in early embryogenesis. *EMBO J* **19**,

1010–1022.

- Rowan, A. J., Lamlum, H., Ilyas, M., Wheeler, J., Straub, J., Papadopoulou, A., Bicknell, D., Bodmer, W. F. and Tomlinson, I. P.** (2000). APC mutations in sporadic colorectal tumors: A mutational "hotspot" and interdependence of the "two hits". *Proc Natl Acad Sci U S A* **97**, 3352–3357.
- Sai, X. and Ladher, R. K.** (2008). FGF signaling regulates cytoskeletal remodeling during epithelial morphogenesis. *Curr Biol* **18**, 976–981.
- Salic, A., Lee, E., Mayer, L. and Kirschner, M. W.** (2000). Control of beta-catenin stability: reconstitution of the cytoplasmic steps of the wnt pathway in *Xenopus* egg extracts. *Mol Cell* **5**, 523–532.
- Salvarezza, S. B., Deborde, S., Schreiner, R., Campagne, F., Kessels, M. M., Qualmann, B., Caceres, A., Kreitzer, G. and Rodriguez-Boulan, E.** (2009). LIM kinase 1 and cofilin regulate actin filament population required for dynamin-dependent apical carrier fission from the trans-Golgi network. *Mol Biol Cell* **20**, 438–451.
- Salz, H. K.** (2011). Sex determination in insects: a binary decision based on alternative splicing. *Curr. Opin. Genet. Dev.* **21**, 395–400.
- Schneider, S., Steinbeisser, H., Warga, R. M. and Hausen, P.** (1996). Beta-catenin translocation into nuclei demarcates the dorsalizing centers in frog and fish embryos. *Mech Dev* **57**, 191–198.
- Schreiber, V., Dantzer, F., Ame, J.-C. and de Murcia, G.** (2006). Poly(ADP-ribose): novel functions for an old molecule. *Nat Rev Mol Cell Biol* **7**, 517–528.
- Seifert, J. R. K. and Mlodzik, M.** (2007). Frizzled/PCP signalling: a conserved mechanism regulating cell polarity and directed motility. *Nat Rev Genet* **8**, 126–138.
- Shimada, Y., Usui, T., Yanagawa, S.-I., Takeichi, M. and Uemura, T.** (2001). Asymmetric colocalization of Flamingo, a seven-pass transmembrane cadherin, and Dishevelled in planar cell polarization. *Curr Biol* **11**, 859–863.
- Shimada, Y., Yonemura, S., Ohkura, H., Strutt, D. and Uemura, T.** (2006). Polarized Transport of Frizzled along the Planar Microtubule Arrays in *Drosophila* Wing Epithelium. *Dev Cell* **10**, 209–222.
- Shinohara, K., Kawasumi, A., Takamatsu, A., Yoshida, S., Botilde, Y., Motoyama, N., Reith, W., Durand, B., Shiratori, H. and Hamada, H.** (2012). Two rotating cilia in the node cavity are sufficient to break left-right symmetry in the mouse embryo. *Nat Commun* **3**, 622.

- Siegfried, E., Perkins, L. A., Capaci, T. M. and Perrimon, N.** (1990). Putative protein kinase product of the *Drosophila* segment-polarity gene *zeste-white3*. *Nature* **345**, 825–829.
- Skarnes, W. C., Rosen, B., West, A. P., Koutsourakis, M., Bushell, W., Iyer, V., Mujica, A. O., Thomas, M., Harrow, J., Cox, T., et al.** (2011). A conditional knockout resource for the genome-wide study of mouse gene function. *Nature* **474**, 337–342.
- Smith, R. S., Hawes, N. L., Kuhlmann, S. D., Heckenlively, J. R., Chang, B., Roderick, T. H. and Sundberg, J. P.** (1996). *Corn1*: a mouse model for corneal surface disease and neovascularization. *Invest. Ophthalmol. Vis. Sci.* **37**, 397–404.
- Smith, S. and de Lange, T.** (2000). Tankyrase promotes telomere elongation in human cells. *Curr Biol* **10**, 1299–1302.
- Smolich, B. D., McMahon, J. A., McMahon, A. P. and Papkoff, J.** (1993). Wnt family proteins are secreted and associated with the cell surface. *Mol Biol Cell* **4**, 1267–1275.
- Sobrado, P., Jedlicki, A., Bustos, V. H., Allende, C. C. and Allende, J. E.** (2005). Basic region of residues 228–231 of protein kinase CK1 α is involved in its interaction with axin: binding to axin does not affect the kinase activity. *J. Cell. Biochem.* **94**, 217–224.
- Sokol, S. Y.** (2011). Maintaining embryonic stem cell pluripotency with Wnt signaling. *Development* **138**, 4341–4350.
- Somsel Rodman, J. and Wandinger-Ness, A.** (2000). Rab GTPases coordinate endocytosis. *J Cell Sci* **113 Pt 2**, 183–192.
- Song, H., Hu, J., Chen, W., Elliott, G., Andre, P., Gao, B. and Yang, Y.** (2010). Planar cell polarity breaks bilateral symmetry by controlling ciliary positioning. *Nature* **466**, 378–382.
- Soosairajah, J., Maiti, S., Wiggan, O., Sarmiere, P., Moussi, N., Sarcevic, B., Sampath, R., Bamburg, J. R. and Bernard, O.** (2005). Interplay between components of a novel LIM kinase-slingshot phosphatase complex regulates cofilin. *EMBO J* **24**, 473–486.
- Spink, K. E., Polakis, P. and Weis, W. I.** (2000). Structural basis of the Axin-adenomatous polyposis coli interaction. *EMBO J* **19**, 2270–2279.
- Srinivas, S., Rodriguez, T., Clements, M., Smith, J. C. and Beddington, R. S. P.** (2004). Active cell migration drives the unilateral movements of the anterior visceral endoderm. *Development* **131**, 1157–1164.

- Stenmark, H.** (2009). Rab GTPases as coordinators of vesicle traffic. *Nat Rev Mol Cell Biol* **10**, 513–525.
- Straight, A. F., Cheung, A., Limouze, J., Chen, I., Westwood, N. J., Sellers, J. R. and Mitchison, T. J.** (2003). Dissecting temporal and spatial control of cytokinesis with a myosin II Inhibitor. *Science* **299**, 1743–1747.
- Strutt, D. and Strutt, H.** (2007). Differential activities of the core planar polarity proteins during *Drosophila* wing patterning. *Dev Biol* **302**, 181–194.
- Strutt, D. I.** (2001). Asymmetric localization of frizzled and the establishment of cell polarity in the *Drosophila* wing. *Mol Cell* **7**, 367–375.
- Strutt, D. I.** (2002). The asymmetric subcellular localisation of components of the planar polarity pathway. *Semin Cell Dev Biol* **13**, 225–231.
- Strutt, D. I., Weber, U. and Mlodzik, M.** (1997). The role of RhoA in tissue polarity and Frizzled signalling. *Nature* **387**, 292–295.
- Strutt, H. and Strutt, D.** (2002). Nonautonomous planar polarity patterning in *Drosophila*: dishevelled-independent functions of frizzled. *Dev Cell* **3**, 851–863.
- Strutt, H. and Strutt, D.** (2005). Long-range coordination of planar polarity in *Drosophila*. *Bioessays* **27**, 1218–1227.
- Strutt, H. and Strutt, D.** (2008). Differential stability of flamingo protein complexes underlies the establishment of planar polarity. *Curr Biol* **18**, 1555–1564.
- Strutt, H. and Strutt, D.** (2009). Asymmetric localisation of planar polarity proteins: Mechanisms and consequences. *Semin Cell Dev Biol* **20**, 957–963.
- Su, L. K., Kinzler, K. W., Vogelstein, B., Preisinger, A. C., Moser, A. R., Luongo, C., Gould, K. A. and Dove, W. F.** (1992). Multiple intestinal neoplasia caused by a mutation in the murine homolog of the APC gene. *Science* **256**, 668–670.
- Su, Y., Fu, C., Ishikawa, S., Stella, A., Kojima, M., Shitoh, K., Schreiber, E. M., Day, B. W. and Liu, B.** (2008). APC is essential for targeting phosphorylated beta-catenin to the SCFbeta-TrCP ubiquitin ligase. *Mol Cell* **32**, 652–661.
- Sulik, K., Dehart, D. B., Iangaki, T., Carson, J. L., Vrablic, T., Gesteland, K. and Schoenwolf, G. C.** (1994). Morphogenesis of the murine node and notochordal plate. *Dev Dyn* **201**, 260–278.
- Taelman, V. F., Dobrowolski, R., Plouhinec, J.-L., Fuentealba, L. C.,**

- Vorwald, P. P., Gumper, I., Sabatini, D. D. and De Robertis, E. M.** (2010). Wnt signaling requires sequestration of glycogen synthase kinase 3 inside multivesicular endosomes. *Cell* **143**, 1136–1148.
- Tajbakhsh, S., Borello, U., Vivarelli, E., Kelly, R., Papkoff, J., Duprez, D., Buckingham, M. and Cossu, G.** (1998). Differential activation of Myf5 and MyoD by different Wnts in explants of mouse paraxial mesoderm and the later activation of myogenesis in the absence of Myf5. *Development* **125**, 4155–4162.
- Takada, S., Stark, K. L., Shea, M. J., Vassileva, G., McMahon, J. A. and McMahon, A. P.** (1994). Wnt-3a regulates somite and tailbud formation in the mouse embryo. *Genes Dev.* **8**, 174–189.
- Takemaru, K. I. and Moon, R. T.** (2000). The transcriptional coactivator CBP interacts with beta-catenin to activate gene expression. *J Cell Biol* **149**, 249–254.
- Tamai, K., Semenov, M., Kato, Y., Spokony, R., Liu, C., Katsuyama, Y., Hess, F., Saint-Jeannet, J. P. and He, X.** (2000). LDL-receptor-related proteins in Wnt signal transduction. *Nature* **407**, 530–535.
- Tanaka, S., Kunath, T., Hadjantonakis, A. K., Nagy, A. and Rossant, J.** (1998). Promotion of trophoblast stem cell proliferation by FGF4. *Science* **282**, 2072–2075.
- Tanaka, Y., Okada, Y. and Hirokawa, N.** (2005). FGF-induced vesicular release of Sonic hedgehog and retinoic acid in leftward nodal flow is critical for left-right determination. *Nature* **435**, 172–177.
- Taniguchi, K., Roberts, L. R., Aderca, I. N., Dong, X., Qian, C., Murphy, L. M., Nagorney, D. M., Burgart, L. J., Roche, P. C., Smith, D. I., et al.** (2002). Mutational spectrum of beta-catenin, AXIN1, and AXIN2 in hepatocellular carcinomas and hepatoblastomas. *Oncogene* **21**, 4863–4871.
- Taylor, J., Abramova, N., Charlton, J. and Adler, P. N.** (1998). Van Gogh: a new *Drosophila* tissue polarity gene. *Genetics* **150**, 199–210.
- Theisen, H., Purcell, J., Bennett, M., Kansagara, D., Syed, A. and Marsh, J. L.** (1994). *dishevelled* is required during wingless signaling to establish both cell polarity and cell identity. *Development* **120**, 347–360.
- Tolwinski, N. S., Wehrli, M., Rives, A., Erdeniz, N., DiNardo, S. and Wieschaus, E.** (2003). Wg/Wnt signal can be transmitted through arrow/LRP5,6 and Axin independently of Zw3/Gsk3beta activity. *Dev Cell* **4**, 407–418.
- Torban, E., Wang, H.-J., Groulx, N. and Gros, P.** (2004). Independent

- mutations in mouse *Vangl2* that cause neural tube defects in looptail mice impair interaction with members of the Dishevelled family. *J. Biol. Chem.* **279**, 52703–52713.
- Tree, D. R. P., Shulman, J. M., Rousset, R., Scott, M. P., Gubb, D. and Axelrod, J. D.** (2002). Prickle mediates feedback amplification to generate asymmetric planar cell polarity signaling. *Cell* **109**, 371–381.
- Tremml, G., Singer, M. and Malavarca, R.** (2008). Culture of mouse embryonic stem cells. *Curr Protoc Stem Cell Biol Chapter 1*, Unit 1C.4.
- Umbhauer, M., Djiane, A., Goisset, C., Penzo-Méndez, A., Riou, J. F., Boucaut, J. C. and Shi, D. L.** (2000). The C-terminal cytoplasmic Lys-thr-X-X-X-Trp motif in frizzled receptors mediates Wnt/beta-catenin signalling. *EMBO J* **19**, 4944–4954.
- Usui, T., Shima, Y., Shimada, Y., Hirano, S., Burgess, R. W., Schwarz, T. L., Takeichi, M. and Uemura, T.** (1999). Flamingo, a seven-pass transmembrane cadherin, regulates planar cell polarity under the control of Frizzled. *Cell* **98**, 585–595.
- van de Wetering, M., Cavallo, R., Dooijes, D., van Beest, M., van Es, J., Loureiro, J., Ypma, A., Hursh, D., Jones, T., Bejsovec, A., et al.** (1997). Armadillo coactivates transcription driven by the product of the *Drosophila* segment polarity gene *dTCF*. *Cell* **88**, 789–799.
- van den Heuvel, M., Harryman-Samos, C., Klingensmith, J., Perrimon, N. and Nusse, R.** (1993). Mutations in the segment polarity genes *wingless* and *porcupine* impair secretion of the *wingless* protein. *EMBO J* **12**, 5293–5302.
- Varlet, I., Collignon, J. and Robertson, E. J.** (1997). nodal expression in the primitive endoderm is required for specification of the anterior axis during mouse gastrulation. *Development* **124**, 1033–1044.
- Veeman, M. T., Slusarski, D. C., Kaykas, A., Louie, S. H. and Moon, R. T.** (2003). Zebrafish prickle, a modulator of noncanonical Wnt/Fz signaling, regulates gastrulation movements. *Curr Biol* **13**, 680–685.
- Vigneau, C., Polgar, K., Striker, G., Elliott, J., Hyink, D., Weber, O., Fehling, H.-J., Keller, G., Burrow, C. and Wilson, P.** (2007). Mouse embryonic stem cell-derived embryoid bodies generate progenitors that integrate long term into renal proximal tubules in vivo. *J. Am. Soc. Nephrol.* **18**, 1709–1720.
- Vinson, C. R. and Adler, P. N.** (1987). Directional non-cell autonomy and the transmission of polarity information by the frizzled gene of *Drosophila*. *Nature* **329**, 549–551.
- Viotti, M., Niu, L., Shi, S.-H. and Hadjantonakis, A.-K.** (2012). Role of the gut

- endoderm in relaying left-right patterning in mice. *PLoS Biol* **10**, e1001276.
- Wagner, K.-D., Wagner, N. and Schedl, A.** (2003). The complex life of WT1. *J Cell Sci* **116**, 1653–1658.
- Wagstaff, L. J., Bellett, G., Mogensen, M. M. and Münsterberg, A.** (2008). Multicellular rosette formation during cell ingression in the avian primitive streak. *Dev Dyn* **237**, 91–96.
- Wallingford, J. B.** (2005). Neural tube closure and neural tube defects: studies in animal models reveal known knowns and known unknowns. *American journal of medical genetics Part C, Seminars in medical genetics* **135C**, 59–68.
- Wallingford, J. B. and Harland, R. M.** (2001). *Xenopus* Dishevelled signaling regulates both neural and mesodermal convergent extension: parallel forces elongating the body axis. *Development* **128**, 2581–2592.
- Wallingford, J. B. and Harland, R. M.** (2002). Neural tube closure requires Dishevelled-dependent convergent extension of the midline. *Development* **129**, 5815–5825.
- Wallingford, J. B., Rowning, B. A., Vogeli, K. M., Rothbächer, U., Fraser, S. E. and Harland, R. M.** (2000). Dishevelled controls cell polarity during *Xenopus* gastrulation. *Nature* **405**, 81–85.
- Wallingford, J. B., Vogeli, K. M. and Harland, R. M.** (2001). Regulation of convergent extension in *Xenopus* by Wnt5a and Frizzled-8 is independent of the canonical Wnt pathway. *Int. J. Dev. Biol.* **45**, 225–227.
- Walters, J. W., Dilks, S. A. and DiNardo, S.** (2006). Planar polarization of the denticle field in the *Drosophila* embryo: roles for Myosin II (zipper) and fringe. *Dev Biol* **297**, 323–339.
- Wang, J., Hamblet, N. S., Mark, S., Dickinson, M. E., Brinkman, B. C., Segil, N., Fraser, S. E., Chen, P., Wallingford, J. B. and Wynshaw-Boris, A.** (2006a). Dishevelled genes mediate a conserved mammalian PCP pathway to regulate convergent extension during neurulation. *Development* **133**, 1767–1778.
- Wang, J., Mark, S., Zhang, X., Qian, D., Yoo, S.-J., Radde-Gallwitz, K., Zhang, Y., Lin, X., Collazo, A., Wynshaw-Boris, A., et al.** (2005). Regulation of polarized extension and planar cell polarity in the cochlea by the vertebrate PCP pathway. *Nat Genet* **37**, 980–985.
- Wang, Q. T., Piotrowska, K., Ciemerych, M. A., Milenkovic, L., Scott, M. P., Davis, R. W. and Zernicka-Goetz, M.** (2004). A genome-wide study of gene activity reveals developmental signaling pathways in the preimplantation

- mouse embryo. *Dev Cell* **6**, 133–144.
- Wang, X., Kumar, R., Navarre, J., Casanova, J. E. and Goldenring, J. R.** (2000). Regulation of vesicle trafficking in madin-darby canine kidney cells by Rab11a and Rab25. *J. Biol. Chem.* **275**, 29138–29146.
- Wang, Y., Guo, N. and Nathans, J.** (2006b). The role of Frizzled3 and Frizzled6 in neural tube closure and in the planar polarity of inner-ear sensory hair cells. *J Neurosci* **26**, 2147–2156.
- Wansleben, C., Feitsma, H., Montcouquiol, M., Kroon, C., Cuppen, E. and Meijlink, F.** (2010). Planar cell polarity defects and defective Vangl2 trafficking in mutants for the COPII gene Sec24b. *Development* **137**, 1067–1073.
- Wassmann, K. and Benezra, R.** (1998). Mad2 transiently associates with an APC/p55Cdc complex during mitosis. *Proc Natl Acad Sci U S A* **95**, 11193–11198.
- Watanabe, D., Saijoh, Y., Nonaka, S., Sasaki, G., Ikawa, Y., Yokoyama, T. and Hamada, H.** (2003). The left-right determinant Inversin is a component of node monocilia and other 9+0 cilia. *Development* **130**, 1725–1734.
- Wehrli, M., Dougan, S. T., Caldwell, K., O'Keefe, L., Schwartz, S., Vaizel-Ohayon, D., Schejter, E., Tomlinson, A. and DiNardo, S.** (2000). arrow encodes an LDL-receptor-related protein essential for Wingless signalling. *Nature* **407**, 527–530.
- Weisz, O. A. and Rodriguez-Boulan, E.** (2009). Apical trafficking in epithelial cells: signals, clusters and motors. *J Cell Sci* **122**, 4253–4266.
- Willert, K., Brown, J. D., Danenberg, E., Duncan, A. W., Weissman, I. L., Reya, T., Yates, J. R. and Nusse, R.** (2003). Wnt proteins are lipid-modified and can act as stem cell growth factors. *Nature* **423**, 448–452.
- Winter, C. G., Wang, B., Ballew, A., Royou, A., Karess, R., Axelrod, J. D. and Luo, L.** (2001). Drosophila Rho-associated kinase (Drok) links Frizzled-mediated planar cell polarity signaling to the actin cytoskeleton. *Cell* **105**, 81–91.
- Winter, J. F., Höpfner, S., Korn, K., Farnung, B. O., Bradshaw, C. R., Marsico, G., Volkmer, M., Habermann, B. and Zerial, M.** (2012). Caenorhabditis elegans screen reveals role of PAR-5 in RAB-11-recycling endosome positioning and apicobasal cell polarity. *Nature Publishing Group* **14**, 666–676.
- Wolff, T. and Rubin, G. M.** (1998). Strabismus, a novel gene that regulates tissue polarity and cell fate decisions in Drosophila. *Development* **125**, 1149–

1159.

- Wong, H.-C., Bourdelas, A., Krauss, A., Lee, H.-J., Shao, Y., Wu, D., Mlodzik, M., Shi, D.-L. and Zheng, J.** (2003). Direct binding of the PDZ domain of Dishevelled to a conserved internal sequence in the C-terminal region of Frizzled. *Mol Cell* **12**, 1251–1260.
- Wray, J., Kalkan, T., Gomez-Lopez, S., Eckardt, D., Cook, A., Kemler, R. and Smith, A.** (2011). Inhibition of glycogen synthase kinase-3 alleviates Tcf3 repression of the pluripotency network and increases embryonic stem cell resistance to differentiation. *Nature Publishing Group* **13**, 838–845.
- Wu, C.-H. and Nusse, R.** (2002). Ligand receptor interactions in the Wnt signaling pathway in *Drosophila*. *J. Biol. Chem.* **277**, 41762–41769.
- Wu, G., Huang, H., Garcia Abreu, J. and He, X.** (2009). Inhibition of GSK3 phosphorylation of beta-catenin via phosphorylated PPPSPXS motifs of Wnt coreceptor LRP6. *PLoS ONE* **4**, e4926.
- Wu, J. and Mlodzik, M.** (2008). The frizzled extracellular domain is a ligand for Van Gogh/Stbm during nonautonomous planar cell polarity signaling. *Dev Cell* **15**, 462–469.
- Xing, Y., Clements, W. K., Kimelman, D. and Xu, W.** (2003). Crystal structure of a beta-catenin/axin complex suggests a mechanism for the beta-catenin destruction complex. *Genes Dev.* **17**, 2753–2764.
- Xu, Q., Wang, Y., Dabdoub, A., Smallwood, P. M., Williams, J., Woods, C., Kelley, M. W., Jiang, L., Tasman, W., Zhang, K., et al.** (2004). Vascular development in the retina and inner ear: control by Norrin and Frizzled-4, a high-affinity ligand-receptor pair. *Cell* **116**, 883–895.
- Yamaguchi, T. P.** (2001). Heads or tails: Wnts and anterior-posterior patterning. *Curr Biol* **11**, R713–24.
- Yang, C.-H., Axelrod, J. D. and Simon, M. A.** (2002). Regulation of Frizzled by fat-like cadherins during planar polarity signaling in the *Drosophila* compound eye. *Cell* **108**, 675–688.
- Ybot-Gonzalez, P., Savery, D., Gerrelli, D., Signore, M., Mitchell, C. E., Faux, C. H., Greene, N. D. E. and Copp, A. J.** (2007). Convergent extension, planar-cell-polarity signalling and initiation of mouse neural tube closure. *Development* **134**, 789–799.
- Ying, Q.-L., Wray, J., Nichols, J., Batlle-Morera, L., Doble, B., Woodgett, J., Cohen, P. and Smith, A.** (2008). The ground state of embryonic stem cell self-renewal. *Nature* **453**, 519–523.

- Yokoyama, N., Golebiewska, U., Wang, H.-Y. and Malbon, C. C.** (2010). Wnt-dependent assembly of supermolecular Dishevelled-3-based complexes. *J Cell Sci* **123**, 3693–3702.
- Yoshida, S., Shiratori, H., Kuo, I. Y., Kawasumi, A., Shinohara, K., Nonaka, S., Asai, Y., Sasaki, G., Belo, J. A., Sasaki, H., et al.** (2012). Cilia at the node of mouse embryos sense fluid flow for left-right determination via Pkd2. *Science* **338**, 226–231.
- Yost, C., Torres, M., Miller, J. R., Huang, E., Kimelman, D. and Moon, R. T.** (1996). The axis-inducing activity, stability, and subcellular distribution of beta-catenin is regulated in *Xenopus* embryos by glycogen synthase kinase 3. *Genes Dev.* **10**, 1443–1454.
- Yu, H.-M. I., Jerchow, B., Sheu, T.-J., Liu, B., Costantini, F., Puzas, J. E., Birchmeier, W. and Hsu, W.** (2005). The role of Axin2 in calvarial morphogenesis and craniosynostosis. *Development* **132**, 1995–2005.
- Zakin, L. D., Mazan, S., Maury, M., Martin, N., Guénet, J. L. and Brulet, P.** (1998). Structure and expression of Wnt13, a novel mouse Wnt2 related gene. *Mech Dev* **73**, 107–116.
- Zakin, L., Reversade, B., Virlon, B., Rusniok, C., Glaser, P., Elalouf, J. M. and Brulet, P.** (2000). Gene expression profiles in normal and *Otx2*^{-/-} early gastrulating mouse embryos. *Proc Natl Acad Sci U S A* **97**, 14388–14393.
- Zaoui, K., Honoré, S., Isnardon, D., Braguer, D. and Badache, A.** (2008). Memo-RhoA-mDia1 signaling controls microtubules, the actin network, and adhesion site formation in migrating cells. *J Cell Biol* **183**, 401–408.
- Zebda, N., Bernard, O., Bailly, M., Welti, S., Lawrence, D. S. and Condeelis, J. S.** (2000). Phosphorylation of ADF/cofilin abolishes EGF-induced actin nucleation at the leading edge and subsequent lamellipod extension. *J Cell Biol* **151**, 1119–1128.
- Zeng, H., Hoover, A. N. and Liu, A.** (2010). PCP effector gene *Inturned* is an important regulator of cilia formation and embryonic development in mammals. *Dev Biol* **339**, 418–428.
- Zeng, L., Fagotto, F., Zhang, T., Hsu, W., Vasicek, T. J., Perry, W. L., Lee, J. J., Tilghman, S. M., Gumbiner, B. M. and Costantini, F.** (1997). The mouse *Fused* locus encodes Axin, an inhibitor of the Wnt signaling pathway that regulates embryonic axis formation. *Cell* **90**, 181–192.
- Zeng, X., Huang, H., Tamai, K., Zhang, X., Harada, Y., Yokota, C., Almeida, K., Wang, J., Doble, B., Woodgett, J., et al.** (2008). Initiation of Wnt signaling: control of Wnt coreceptor Lrp6 phosphorylation/activation via frizzled, dishevelled and axin functions. *Development* **135**, 367–375.

Zeng, X., Tamai, K., Doble, B., Li, S., Huang, H., Habas, R., Okamura, H., Woodgett, J. and He, X. (2005). A dual-kinase mechanism for Wnt co-receptor phosphorylation and activation. *Nature* **438**, 873–877.

Zhang, L., Luo, J., Wan, P., Wu, J., Laski, F. and Chen, J. (2011). Regulation of cofilin phosphorylation and asymmetry in collective cell migration during morphogenesis. *Development* **138**, 455–464.

Zhang, W., Yang, J., Liu, Y., Chen, X., Yu, T., Jia, J. and Liu, C. (2009). PR55 alpha, a regulatory subunit of PP2A, specifically regulates PP2A-mediated beta-catenin dephosphorylation. *J. Biol. Chem.* **284**, 22649–22656.